FGF AND TGFBETA SIGNALLING IN AN IN-VITRO MODEL OF CRANIOSYNOSTOSIS

Kingyin Michael Arthur Lee

李敬賢

BEng (1st class Hons)

Developmental Biology Unit

Institute of Child Health

University College London

30 Guilford Street

London WC1N 1EH

A thesis submitted for the degree of Doctor of Philosophy

University College London

February 2009

Abstract

Fibroblast Growth Factor (FGF) and Transforming Growth Factor beta (TGFbeta) are key regulators of bone development. Constitutively activating mutations of FGF Receptors (FGFR) 1-3 result in craniosynostosis, premature fusion of cranial sutures. The aim of this thesis was to determine how FGF signalling is impaired in osteoblasts with the mutation FGFR2-C278F, known to induce craniosnostosis and investigate possible interactions with TGFbeta signalling.

To this purpose MC3T3-E1 osteoblasts (derived from newborn mouse calvaria) that had been stably transfected with human FGFR2 (wild type *FGFR2-WT* or mutated *FGFR2-C278F)* were used as an *in-vitro* model and these cell lines were named R2-WT and R2-C278F. These cell lines were characterised at the cellular and molecular level to define the craniosynostotic phenotype. Gene expression was assessed with real time PCR, proliferation using both fluorescence activated cell sorting (FACS) and the methylene blue assay and protein expression by FACS, immunocytochemistry and Western blotting. Cell proliferation was reduced and apoptosis increased in the R2-C278F mutant and differentiation increased, as shown by reduced expression of differentiation marker *osteopontin* and an increase in *osteocalcin*. The effect of FGF signalling on cell growth was demonstrated by using FGFR inhibitor SU5402. This study suggested that FGFR2-C278F decreases the level of FGFR signalling.

FGFR2-C278F impairs TGFbeta signalling as shown by: i) reduced *Tgfbeta1* and -3 expression in R2-C278F cells; ii) maximal reduction of cell growth only in R2-C278F cells following TGFbeta inhibition using SB431542 (1μM); iii) the inability of exogenous TGFbeta1 to induce proliferation in R2-C278F cells. This suggests that exogenous TGFbeta1 cannot rescue the impaired TGFbeta signalling caused by FGFR2-C278F mutation. Fgf and Tgfbeta signalling may converge to affect osteoblast proliferation via extracellular related kinase 1/2 (Erk1/2). Analysis of the Erk1/2 protein expression in R2-C278F cells showed that Erk1 isoform had increased relative to Erk2. This change has been associated with growth arrest in osteoblasts, fibroblasts and hepatocytes and therefore it is likely to underlie the defect in proliferative response to Fgf and Tgfbeta signalling in R2-C278F cells.

In summary FGFR2-C278F in MC3T3 cells impairs Fgf and Tgfbeta signalling, resulting in a proliferation defect for which increased differentiation is implicated as a secondary effect. A key convergence between FGFR2-C278F and Tgfbeta appears to be via impaired Erk1/2 signal transduction. These findings provide a valuable basis for future investigations of other Erk1/2 upstream pathways and their contribution to the craniosynostotic osteoblast phenotype.

I, Kingyin Michael Arthur Lee, confirm that the work presented in this thesis is my own. Where information has been derived from other sources, I confirm that this has been indicated in the thesis.

Dedication

I dedicate my thesis to my parents, Michael and Helen Lee (李惠綿 and 李呂笑蘭) for nurturing me into the person I am and giving me one of the best opportunities in life for myself and to help others through their love, devotion, teaching and sacrifice.

Table of Contents

Abbreviations

3T3	3-day transfer, inoculum 3 x 10^6 cells
7AAD	7 Aminoactinomycin D
Aa	Amino acid
aFGF	Acidic Fibroblast Growth Factor (FGF1)
bFGF	Basic Fibroblast Growth Factor (FGF2)
BHLH	Basic Helix-Loop-Helix
BrdU	5-bromo-2-deoxyuridine
BSA	Bovine Serum Albumin
BSP	Bone Sialoprotein / BSPII / Integrin-binding Bone Sialoprotein (IBSP)
CICD	Caspase Independent Cell Death
CNC	Cranial Neural Crest
COL1	Collagen 1
DAB	3,3-Diaminobenzidine
DEPC	Diethylpyrocarbonate
dH_2O	Distilled water
DIC	Days In Culture
dNTP	Deoxyribonucleotide triphosphate
EDTA	Ethylenediaminetetra-acetic acid
ELISA	Enzyme Linked Immunosorbent Assay
EFNB1	Ephrin-B1
ERK	Extracellular signal-related Kinase
FACS	Fluorescent Activated Cell Sorting
FBS	Fetal Bovine Serum
FGF	Fibroblast Growth Factor
FGFR	Fibroblast Growth Factor Receptor
FGFR2IIIc	FGFR2 (BEK)
GAPDH	Glyceraldehyde 3 Phosphate Dehydrogenase
GJIC	Gap junction intercellular communication
HRP	Horse Radish Peroxidase
ICC	Immunocytochemistry
JNK	c-jun N-terminal Kinase
LICA	Ligand Independent Constitutively Activated
MSX	Muscle Segment homeobox

mTOR	Mammalian Target of Rapamycin
MTT	3-(4,5-dimethyl-2-yl)-2,5diphenyltetrazolium
NC	Neural Crest
NSAID	Non-Steroidal Anti-Inflammatory Drug
OC	Osteocalcin
OP	Osteopontin
OPD	O-phenylenediamine
OPN	Osteopontin / Secreted Phosphoprotein 1 (SPP1) / Bone Sialoprotein I (BSPI)
PBS	Phosphate buffered saline
PCNA	Proliferating Cell Nuclear Antigen
PFA	Paraformaldehyde
pH3	Phospho-Histone 3
PI3-K	Phosphatidylinositol 3-kinase
PKB	Protein Kinase B / AKT
PKC	Protein Kinase C
PLC-γ	Phospholipase C γ
PMA	Phorbol 12-myristate 13-acetate
RNA	Ribonucleic acid
Rpm	Rotations per minute
rRNA	Ribosomal ribonucleic acid
RT-PCR	Reverse Transcription Polymerase Chain Reaction
RUNX2	Runt Related Transcription Factor 2 / CBFA1 / OSF / Pebp2alphaA / Aml3
SMAD	Small Mothers Against Decapentaplegic homolog
SU5402	3-{[3-(2-carboxyethyl)-4-methylpyrrol-2-yl]methylene}-2-indolinone
TGFBeta	Transforming Growth Factor Beta
TK	Tyrosine Kinase
TUNEL	Terminal deoxynucleotidyl Transferase Biotin-dUTP Nick End Labeling
WB	Western Blot

List of figures

List of tables

Acknowledgements

First and foremost I would like to thank my supervisor Patrizia for her guidance and support throughout my PhD. I also thank my second supervisor Alan for his advice and introducing me to ICH. I am very grateful to my teachers Leonor and Pati, who have taught me the essentials to my project. From my arrival, I thank Joel and Yannis for their warm welcome and assistance to the end. I also thank Jane, Soo, Sigrun, Steffi, Jörn, Michael and Nabila for all their support. It has been a pleasure to work with and teach Pong and Sebastiano in my last year. In addition, I would also like to acknowledge the BSc students Mark, Raphael, Yury, Sheryl and Anushka, all of whom through multiple questions have encouraged me to become a better lab teacher.

For administration help, I thank Shane, Lucie and Anna. Special thanks goes to Diane and Matt for their support in maintaining the lab and autoclaving reagents, and recognising urgency even through difficult and memorable times in the lab, such as the powercuts, the bombing, liquid nitrogen explosion, the release of phenols, CO_2 and camping gas! In addition to the help from my teachers, my lab work would have been achieved without the help of others at UCL to help in methodology. I thank Meng from the Eastman Dental and Yin for help in real time PCR and accurate RNA measurement. For FACS, I would like to thank Jo and Joao for their guidance. In DNA sequencing and analysis I am very grateful to James and Aya. For improvement of the methylene blue assay, I thank Yury. I am very grateful to Sebastiano and Yvonne for their proof reading during my write up. I would also like to thank the members of NDU, NPU, MIU, MMU, IDM and the units of the Camelia Botnar laboratories to whom at some stage of the work I have come to for help. It has been a delight to have met many of the staff and students of ICH in both social and scientific contexts.

I thank my mum and dad for their love and support. Last, but not least I would like to thank Su Lynn for her support, encouragement and dedication from the MBPhD application process on the “biscuit”, through the best and the worst times of my PhD and inspiring me to learn the guitar.

Chapter 1 Introduction

1.1 Anatomy of the Cranium

The human cranium (skull) is the essential supporting structure for organs of the head to function. It protects the brain, the brain stem, eyes, cranial nerves and assists muscle movement in stereo vision, facial expression, breathing and verbal communication. The size, morphology and composition of the skull may affect the function of any of these organs and also the social interactions of the individual with society.

The entire skull consists of many bone plates that are grouped (with various nomenclature) into two main regions:

1. **Cranial (Skull) Vault / Neurocranium –** bones that encase the brain
2. **Facial Skeleton / Viscerocranium / Orognathofacial Complex / Splanchnocranium** - jaw and facial bones.

These are coloured in Figure 1.1. The cranial vault can be subdivided into two further regions:

1. **Calvarium** / **Desmocranium** – the superior and lateral casing of the brain
2. **Cranial Base** / **Chondrocranium** – the inferior brain casing

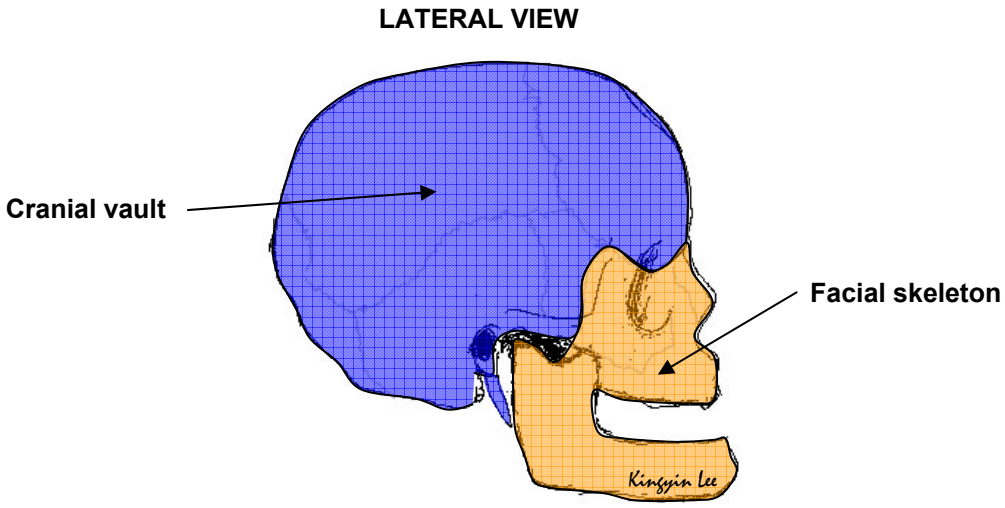

Figure 1.1 Side view illustration of an adult skull
The skull is composed of the cranial vault (blue area) and the facial skeleton (orange area).

1.1.1 The calvarium at birth

The calvarium is dome-shaped and consists of the frontal, parietal, occipital and part of the temporal bone (see Figure 1.2, temporal bone not shown). Between the bones lie fibrous joints called sutures. In new born humans there are membranous areas that resemble suture tissue called fontanelles. The fontanelles will usually disappear by the 2nd year after birth.

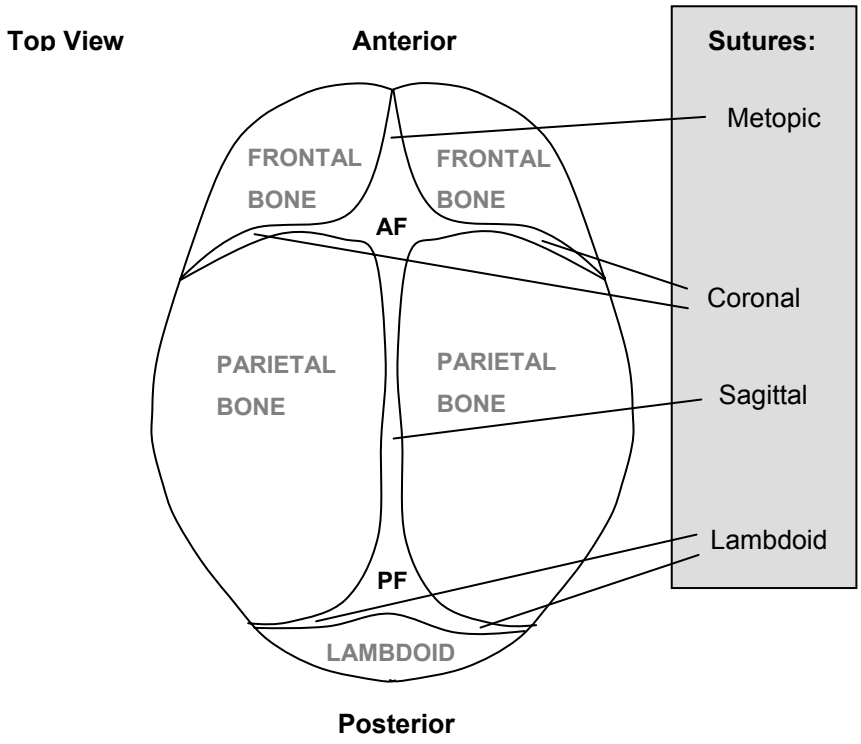

Figure 1.2 Human Newborn skull vault.

Superior view of the bones and sutures of the skull. Annotations show the sutures. **AF**: Anterior Fontanelle. **PF**: Posterior Fontanelle. Adapted from Grants Anatomy Atlas (Agur and Lee, 1999).

1.2 Craniofacial bone and sutures

Bone may be classified as endochondral and membranous, based upon its mode of formation. Membranous bone forms from direct ossification and is mainly protective in function. Endochondral bone varies in shape, grows from preformed cartilage, which differentiates into bone and allows weight bearing and skeletal movement. Craniofacial bones constitute the cranium and most are membranous except for the chondrocranium and the ossicles (bones of the ear), which are derived from Meckel's cartilage during development. The mandible is largely membranous, but forms from the mesenchyme that surrounds Meckel's cartilage (Sadler, 2004).

1.2.1 Origins of Craniofacial bone

Craniofacial bone is formed from mesenchymal tissue. The mesenchyme derives from two embryonic cell populations: cranial neural crest and head paraxial mesoderm (Jiang et al., 2002). In the embryo, the neural plate folds to create the neural tube between the 3rd and 8th week of gestation. The neural crest is formed from neuroepithelial cells that undergo epithelial to mesenchymal transition (EMT) at the neural plate border, between surface ectoderm and the neural plate, along most of the vertebral axis (Trainor, 2005). Paraxial mesoderm first arises at the lateral edges of the primitive node and cranial end of the primitive streak (Sadler, 2004; Opperman, 2000). Both neural crest and paraxial mesoderm lie lateral to the neural tube (Figure 1.3). In the avian and mammalian skull, neural crest-derived mesenchyme populates the facial skeleton and the frontal bone, whereas paraxial mesoderm-derived mesenchyme forms the parietal and occipital bone structures (Morriss-Kay and Wilkie, 2005).

1.2.2 Development and growth of craniofacial bone and sutures

The bones of the human skull vault form around the 8th week of foetal development. Studies on the mandibular, maxillary and frontal bone development have shown that an epithelial-mesenchyme interaction induces the neural crest-derived mesenchymal cells to commit to an osteogenic lineage (Dunlop and Hall, 1995; Tyler and McCobb, 1980; Tyler, 1983). A report by Opperman has suggested that tissue-tissue interactions with the underlying dura mater might also induce bone formation in the parietal and occipital regions, where paraxial mesoderm-derived mesenchyme is found (Opperman, 2000). Interestingly, epithelial-mesenchymal interactions do not induce bone formation in mesenchyme that is normally non-osteogenic, such as trunk neural crest (Hall, 1981). This may suggest that differences in permissiveness to bone formation exist, depending on the type of neural crest cell.

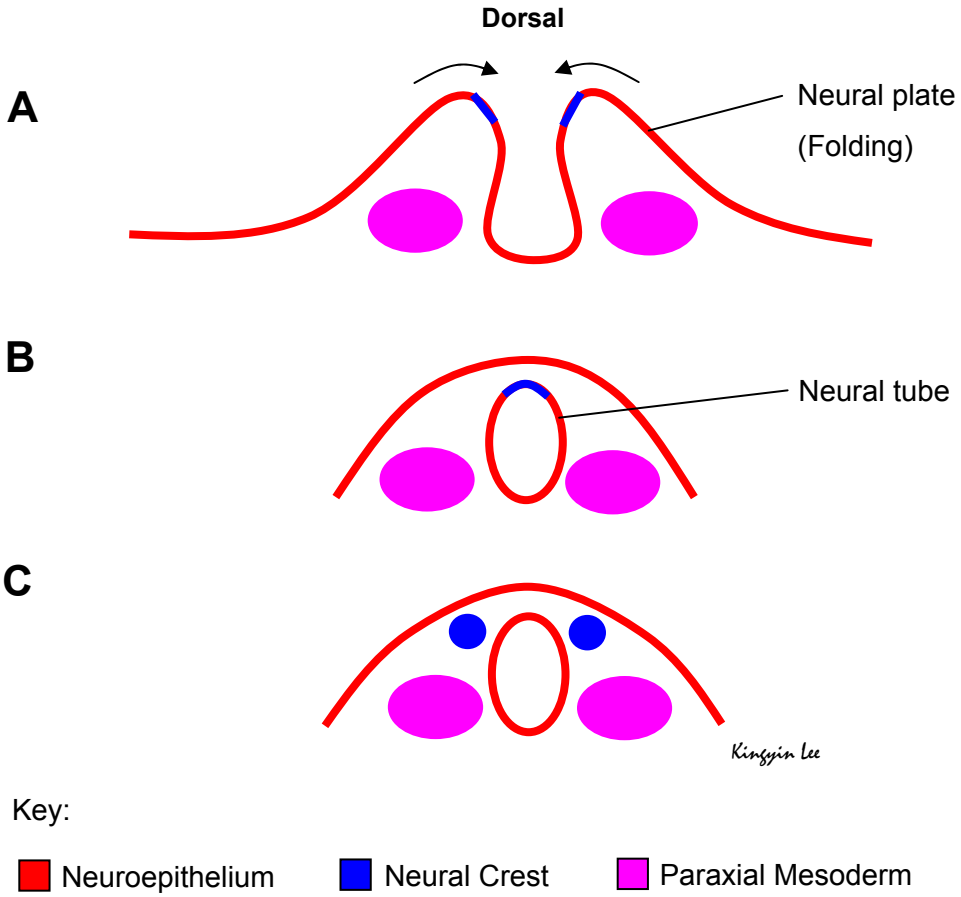

Figure 1.3 Cross-sections of the stages of neural tube formation

The neural plate (A) folds onto itself to form the neural tube (B) between the 3rd and 8th week of gestation. Neural crest (blue) is found on the crest of the folding neural plate and undergoes epithelial-mesenchymal transition as it leaves the neuroepithelium (C). The paraxial mesoderm is found just lateral to the neural tube.

Once osteogenic commitment is induced, no further signals are required to maintain the cell lineage. Immature osteogenic cells condense into clusters. This initiates differentiation into mature osteoblasts, which are responsible for bone matrix formation (Dunlop and Hall, 1995). As the bone matrix formation continues, it will form nodules, which will later fuse together to create a bone plate. The bone plate is covered by periosteum; a layer of osteogenic cells and an outer fibrous layer. The major sites of main bone formation occur at the edges of opposing bone plates known as bone fronts.

The bone front consists of several layers of osteogenic cells at different stages of differentiation: These range from the most differentiated osteoblasts that form mature bone, which lie next to

the newly formed bone, to the least differentiated osteoprogenitor cells that have just differentiated from the mesenchyme. The growth of the bone fronts occurs mainly by osteoprogenitor proliferation with a small contribution of mesenchymal cells recruited into an osteogenic fate (Lana-Elola et al., 2007).

1.2.3 Suture formation, stability and fate

When two bone fronts approach each other, a presumptive suture is formed, comprising of undifferentiated mesenchymal tissue. During this process there remain a few wide regions of mesenchymal tissue known as fontanelles. Sutures may be overlapping or butt ended in morphology (Figure 1.4). The formation, growth and maintenance of the craniofacial bone and sutures depend upon many factors. These may be cell autonomous, local (within a particular tissue) and paracrine interactions between the tissue of the bone front, suture and dura. It is thought that the mechanism underlying suture formation is a gradient of growth factor signalling between the bone fronts (Opperman et al., 1993; Roth et al., 1996).

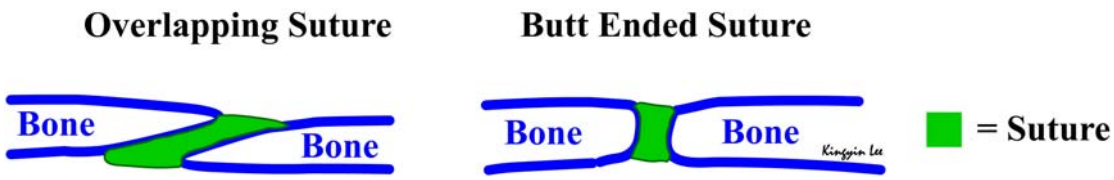

Figure 1.4 Cross section of a suture
Overlapping sutures include the lambdoid and parietal sutures. The sagittal suture is a butt ended suture.

Once the suture has begun to form, the dura is essential for its initial stability, otherwise the suture will fuse (Opperman et al., 1993). In the presumptive (forming) suture, the dura sends osteogenic signals causing the joint (suture and bone fronts) to thicken. As the suture tissue matures, it is thought that the suture sends osteo-inhibitory signals to the dura to cease osteogenic signalling, which leads to reduction in suture thickness (Opperman, 2000). The dura may play a role in controlling suture fate. In rats, the frontal suture remains patent and the sagittal fuses when the frontal (metopic) and sagittal suture positions are switched, such that the frontal suture overlies dura that normally interacts with the sagittal suture and vice versa (Levine et al., 1998). Furthermore, blocking the interactions between the dura and the frontal suture delays the time of suture fusion (Roth et al., 1996). Collectively, these reports indicate that the dura promotes suture patency or fusion depending on the region of the dura. When a suture has matured at the postnatal stage, it no longer requires the dura for maintenance (Kim et al., 1998).

As mentioned, the fate of a suture is either to fuse (obliterate) or remain patent (non-fused). When a suture fuses, the mesenchyme is replaced by bone, forming a continuous layer of bone between the bone plates. The timing of fusion differs according to the suture. In humans, about 90 % of metopic sutures fuse between the 2nd and 5th year after birth (Cohen, 1986). However coronal, sagittal and lambdoid sutures remain patent (open), allowing further growth of the cranial vault. The time for fusion of these sutures ranges from 20 to 60 years (Sahni et al., 2005; Perizonius, 1984). A similar pattern of suture fate occurs in rats: the posterior frontal suture (analogous to the metopic suture) fuses between 12 and 20 days postnatally, whereas coronal, sagittal and lambdoid sutures remain patent (Moss, 1958). In mice, only the posterior frontal cranial suture fuses, starting anteriorly between 25 and 29 days and fusing by 39 and 45 days postnatally (Bradley et al., 1996).

1.2.4 Differentiation at the bone fronts

As bone fronts approach each other, there is tight regulation of molecular signalling that causes cells in the suture to differentiate in a controlled manner. Within the suture, a mesenchymal cell will differentiate into an osteoprogenitor cell, then pre-osteoblast and later an osteoblast secreting bone matrix that mineralises and extends the bone front. Some osteoblasts may further differentiate into osteocytes when they are incorporated into the bone matrix.

Runt-related transcription factor (*Runx2*) is a key gene required for maturation of osteoprogenitors into osteoblasts and is expressed when mesenchymal cells differentiate into osteoprogenitors (Otto et al., 1997; Prince et al., 2001). Its expression is essential for bone maturation and mineralisation, as *Runx2* null mutants do not show ossification (Otto et al., 1997). In patients, many loss of function mutations in Runx2 leads to an autosomal dominant condition known as cleidocranial dysplasia in which the clinical features include a lack of ossification and delayed suture fusion (Lou et al., 2008). Runx2 is a transcription factor that contains a runt domain, which binds to promoters of osteoblast differentiation marker genes such as *Collagen type1* (*COL1*), *Alkaline Phosphatase* (*ALP*), *Osteopontin* (*OPN*) and *Osteocalcin* (OC) (Ducy et al., 1997; Harada et al., 1999; Karsenty et al., 1999). These Runx2 target molecules may be used to help classify the stage of differentiation of bone according to whether they are expressed and the level of their expression (Figure 1.5). Twist is another marker of osteoblast differentiation; its expression decreases during maturation of the suture (Johnson et al., 2000). The expression patterns and relative levels of expression of the bone markers are listed in Table 1.1.

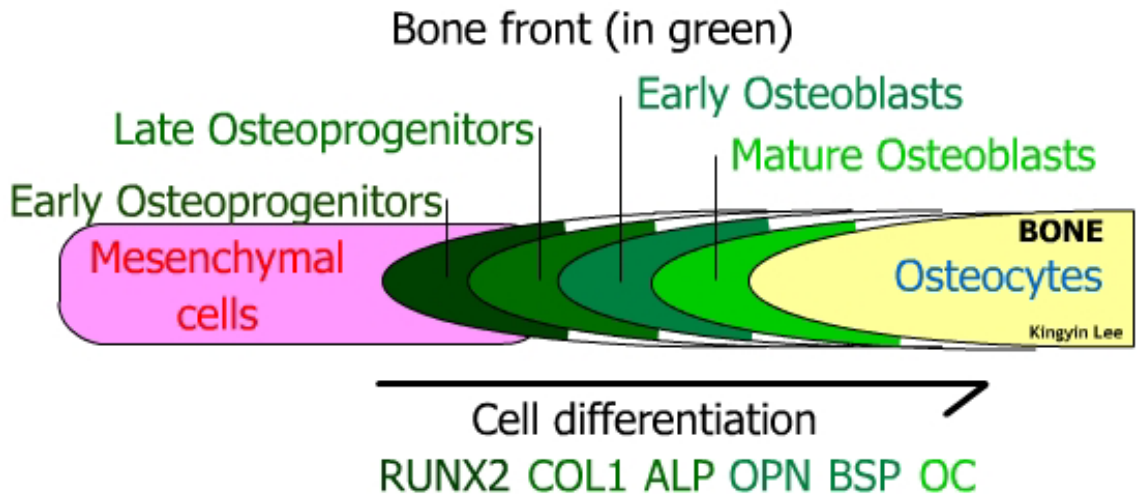

Figure 1.5 Markers of differentiation in osteogenic cells

Bone formation is mainly due to proliferation and differentiation of the bone front (green), with a small contribution from mesenchymal cells (pink) which differentiate into osteogenic cells (green). The stage at which each gene is first expressed may mark the stage of differentiation as indicated from left to right, though it is important to note that expressions of each gene tend to continue once started and overlap with one another.

Table 1.1 Differentiation marker expressions in osteogenic cells

Marker	Osteoprogenitor	Pre-osteoblast	Mature osteoblast
Runx2	Present	Present, amount unknown	Moderate
Collagen1	Low	Moderate	Moderate
Twist	High	Moderate	Low
Opn	None to low	None to low	None to High
Bsp	None to low	None to high	None to High
Oc	Undetectable	Undetectable	None to High

Adapted from (Aubin, 2001; Lee et al., 1999)

1.2.5 Signalling molecules in sutures and bones

Many molecules are involved in both suture and bone formation and maintenance. Fibroblast growth factor (FGF), transforming growth factor beta (TGFbeta), bone morphogenic protein (BMP) and Wnt are some of the main cell signalling molecules known to regulate bone formation.

1.3 Fibroblast Growth Factor (FGF)

The FGFs are a family of structurally related polypeptides, identified by a highly homologous central core of 140 amino acids and a strong affinity for heparin and heparin-like glycosaminoglycans (HLGAG) (Burgess and Maciag, 1989; Ornitz and Itoh, 2001). In addition to bone formation, FGFs are involved in development, repair, regeneration, tumourgenesis and degeneration (Powers et al., 2000; Jackson et al., 2006; Partanen, 2007; Grothe and Timmer, 2007). There are currently 25 known FGFs, of which 22 have been found in human (FGF1-23 except for FGF15 in mouse) (Katoh and Katoh, 2005; Reuss and Bohlen und, 2003).

A typical *FGF* gene such as *FGF1, -2, -4* or *-9* has three exons and is transcribed from a methionine (AUG) codon (Ornitz and Itoh, 2001), but a number of Fgfs also contain alternative CUG starting codons in the 5' sequence (upstream of AUG), which allow transcription of other higher molelcular weight isoforms (Arnaud et al., 1999; Kiefer et al., 1994). Examples include FGF2, which can vary from 17 to 34 kDa (Yu et al., 2007). Alternative isoforms can also be generated from splicing of exon 1, as shown with FGF8 (MacArthur et al., 1995). FGFs have been reported to initiate intracellular and extracellular signalling and their ability to do this is due in part to the existence of these isoforms.

1.3.1 Extracellular FGF signalling

Extracellular signalling occurs when extracellular FGFs, for example FGF1 and -2 complex with cell surface membrane FGFRs and heparan sulphate proteoglycans (HSPGs). FGF1 and -2 lack the classical signal peptide; however they are still exocytosed via non-ER-Golgi mechanisms, such as heat shock protein (Mignatti et al., 1992; Jackson et al., 1992; Piotrowicz et al., 1997).

There are four FGF receptors (FGFRs). Each has three immunoglobulin-like (Ig-like) extracellular domains and two intracellular tyrosine kinase (TK) domains (Figure 1.6). The Ig-like domain II and III form the FGF binding sites. FGFR1-3 have splice variants in IgIII labeled "b" and "c", which confer specificities to particular FGFs (Table 1.2). FGFs may bind in a 1:1 ratio to FGFRs (Figure 1.7) and the ligand-receptor complex dimerises to initiate signalling, a process mediated by heparan or heparin induced FGF oligomerization (Harmer, 2006; Spivak-Kroizman et al., 1994). FGFR dimerisation brings the TK domains close enough for autophosphorylation and activate downstream signalling. The order of FGF, FGFR and HSPG

binding before activation is still under debate, however some of the models suggest that the FGF to FGFR binding is stabilised by HSPG to allow dimerisation (Powers et al., 2000).

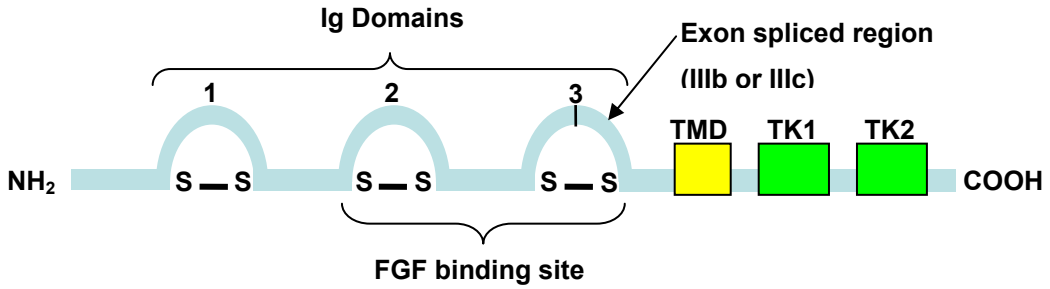

Figure 1.6 The general structure for FGFR.

FGFRs have three Ig-like domains, one transmembrane domain (TMD) and two tyrosine kinase domains (TK1 and TK2). Splice variants "b" and "c" are found in the third Ig-like domain (arrow).

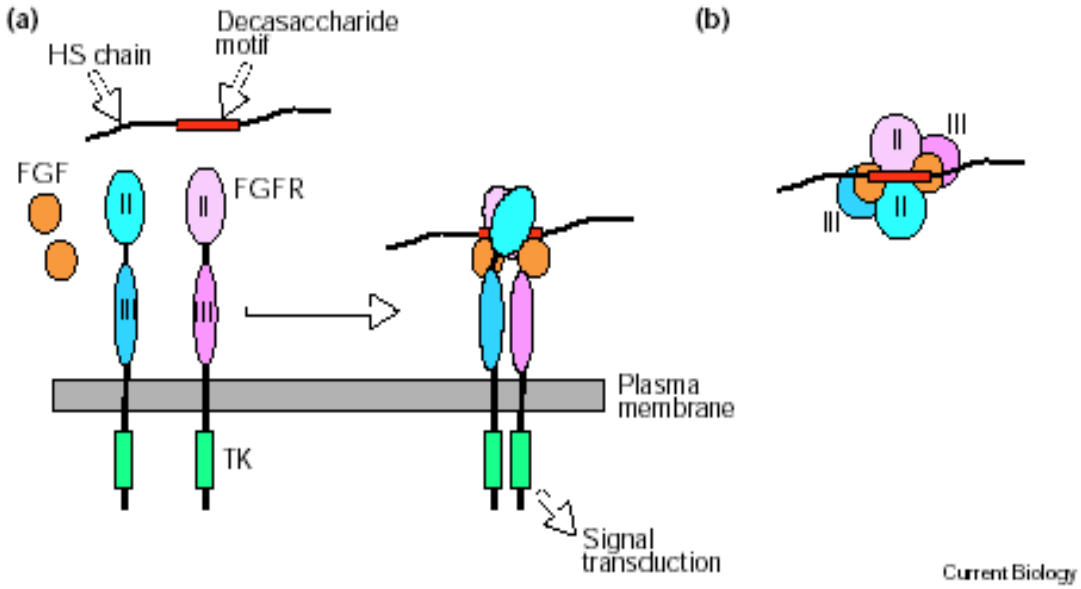

Figure 1.7 Interactions between FGF and FGFR for signalling (Guimond and Turnbull, 1999)

In order for FGFR signalling to occur, FGF binds to FGFR and this complex dimerises with another FGF-FGFR complex. This process requires heparan, which is bound to the FGF-FGFR. FGFR signalling is then initiated.

Table 1.2 Ligand specificities of FGFR isoforms (Eswarakumar et al., 2005)	
Isoform	**Ligand specificity**
FGFR1IIIb	FGF1, -2, -3 and -10
FGFR1IIIc	FGF1, -2, -4, -5 and -6
FGFR2IIIb	FGF1, -3, -7, -10, -22
FGFR2IIIc	FGF1, -2, -4, -6, -8, -9, -17 and -18
FGFR3IIIb	FGF1, and -9
FGFR3IIIc	FGF1, -2, -4, -8, -9, -17, -18 and -23
FGFR4	FGF1, -2, -4, -6, -8, -9, -16, -17, -18, -19

Note: FGF8 also included in binding to FGFR2IIIc (Ornitz et al., 1996).

Following FGFR signalling, the complexes are then endocytosed and either degraded or translocated to the cytosol and nucleus. The C-terminus of the FGFR may determine this fate, as shown in COS-1 cells (derived from African green monkey kidney), where FGF1 complexed with either FGFR1 or FGFR4 is translocated to the cytosol and nucleus, whereas FGFR2 or -3 (that have a different C-terminus to FGFR1 and FGFR4) are degraded after complexing with FGF1 (Sorensen et al., 2006b). Both ligand and receptor may translocate to different parts of the nucleus, for example FGF2 and FGFR1, where it is thought that they play different roles to each other and extracellular FGF-FGFR signalling (Reilly et al., 2004).

1.3.2 Intracellular FGF signalling

The intracellular FGFs include FGF 11, 12 13, and 14; these are known respectively as FGF Homologous Factors (FHFs) 3, 1, 2, and 4 (Schoorlemmer and Goldfarb, 2001). Unlike other FGFs, FHFs do not interact with any of the FGFRs even when added exogenously, but bind to intracellular proteins such as mitogen activated protein kinase (MAPK) scaffold protein Islet Brain-2 (IB2) (Olsen et al., 2003). Intracellular FGFs also include FGF1, -2 and -3, which are found intracellular and extracellularly (Sorensen et al., 2006a). Although FGF3 intracellularly has a signal peptide for extracellular signalling, it competes with a nuclear localisation signal on the protein, resulting in a significant level of intracellular localisation and signalling (Kiefer et al., 1994). Binding targets for these non-FHF ligands such as FGF2 may include intracellular proteins such as FGF interacting Factor (FIF) (Van den et al., 2000).

Some forms of FGFR exist intracellularly and do not reach the cell surface membrane. Evidence of nuclear localisation and transcriptional regulation by FGFR1 suggests that intracellular

signalling may be initiated by FGFRs, although it is not clear this is dependent on the FGF ligand (Stachowiak et al., 2003). The summary of initiation sites are given in Figure 1.8.

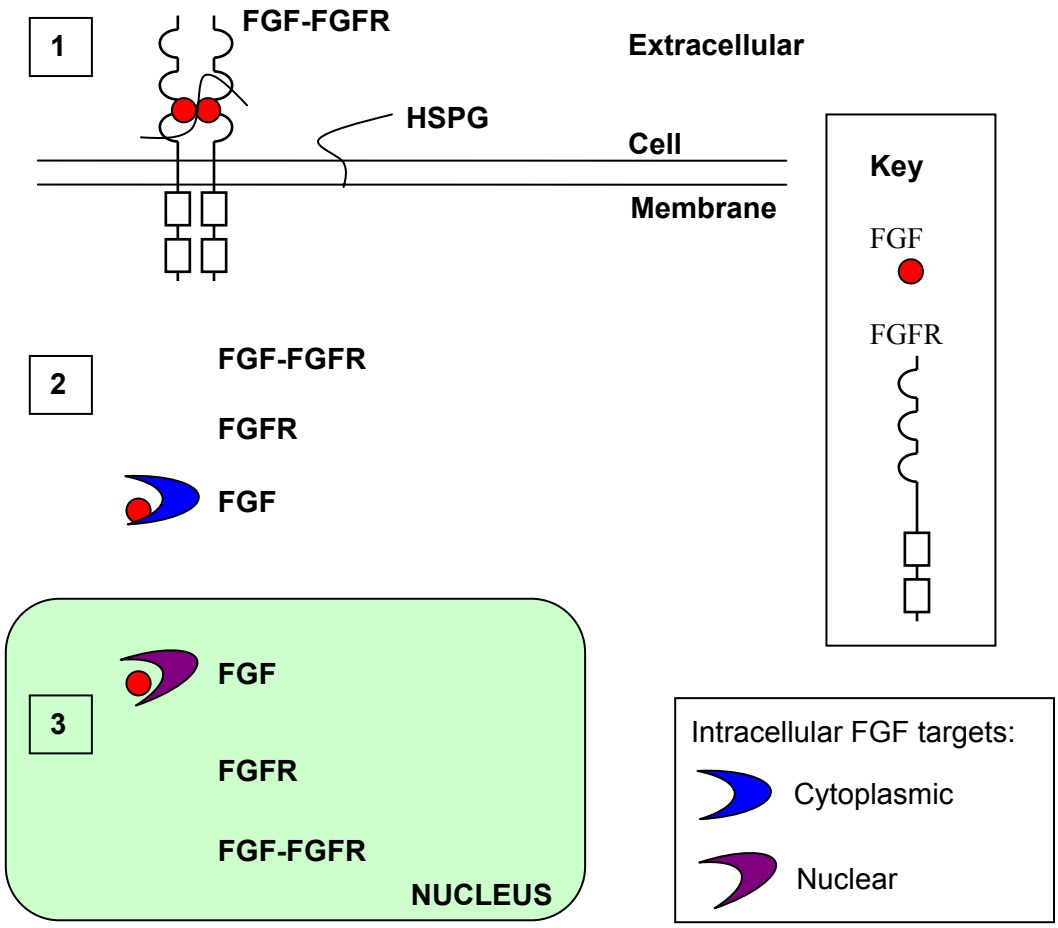

Figure 1.8 Sites where FGF signalling may be initiated and the likely complexes formed
1: Cell surface FGF signalling is brought about by formation of the FGF-FGFR complex in association with HSPG. **2** & **3:** Intracellular activation. Activation may occur by target proteins being bound to FGF, FGFR or with the FGF-FGFR complex.

1.3.3 The roles of FGFRs in craniofacial bone

All four FGFRs are present in craniofacial bone (Britto et al., 2001; Chan and Thorogood, 1999; Cool et al., 2002; Rice et al., 2003). Analysis of normal and mutated receptor expression patterns have helped to define some roles for FGFR1-3, which are the isoforms associated with developmental defects such as craniosynostosis. FGFR4's role in bone is not clear as mutation studies in this receptor have not revealed any specific function in bone and osteoblast development (Gaudenz et al., 1998), which may suggest redundancy of its function or that it has other roles as yet unknown.

Fgfr1 is positively upregulated in differentiated mouse osteoblasts (Kitching et al., 2002), but downregulated as osteoblasts mature and express osteopontin (Iseki et al., 1999). This indicates a role for Fgfr1 in osteoblast differentiation.

In human embryonic craniofacial bone, FGFR2IIIc is the predominant isoform of FGFR2 (Chan and Thorogood, 1999). In mouse calvaria, Fgfr2IIIc induces bone formation (Eswarakumar et al., 2002). On a cellular level, Fgfr2 may positively regulate proliferation in osteoprogenitors, because its gene expression is down regulated upon differentiation into osteoblasts (Iseki et al., 1999). This view is supported by a study showing that expression of dominant-negative Fgfr2 results in reduced osteoblast proliferation (Ratisoontorn et al., 2003). Conditional inactivation of Fgfr2 has revealed that differentiation markers were still present, suggesting that Fgfr2 may not be required for differentiation (Yu et al., 2003). Interestingly the expression patterns of *Fgfr2* and differentiation marker *Opn* are mutually exclusive (Iseki et al., 1997), indicating that osteoblast proliferation induced by Fgfr2 signalling precedes differentiation regulated by Opn.

Fgfr3 is expressed predominantly in the cartilaginous regions of the skull such as the synchondrosis of the cranial base and the mandibular condyle (Rice et al., 2003). Chondrocyte proliferation is negatively regulated by Fgfr3 (Sahni et al., 1999). It is also suggested to increase osteoblast differentiation (Funato et al., 2001). $Fgfr3^{-/-}$ mutations increase osteoblast number and activity in mouse tibia and femur, indicating a negative role for Fgfr3 in osteoblast proliferation; In addition, as Fgfr3 plays a positive role in long bone mineralisation, its role may be similar in craniofacial bone (Valverde-Franco et al., 2004).

In summary, of the four FGFR isoforms in osteoblasts, only FGFR2IIIc has been shown to be positively essential for osteoblast proliferation, whereas FGFR3 is a negative regulator. FGFR1 and -3 positively regulate differentiation. FGFR4 is not essential for either proliferation or differentiation.

1.3.4 Roles of FGFs in craniofacial bone

Fgf1 is expressed in embryonic rat dura and is replaced at the postnatal stage by *Fgf2* (Ogle et al., 2004). The addition of exogenous FGF1 increases proliferation in the immature mouse osteoblast (OB1) cell line (Mansukhani et al., 2000), whereas in the mature MG63 human osteoblast cell line it causes an increase in apoptosis (Chang et al., 2005).

FGF2 is of importance in craniofacial bone development, as indicated by up-regulation of its mRNA in normally fusing sutures and by exogenous Fgf2 treatment resulting in suture fusion (Gosain et al., 2004; Moursi et al., 2002; Moursi et al., 2002). FGF2 is known to have varied effects on osteoblast behaviour, such as increasing proliferation slightly in immature osteoblasts, and increase differentiation in mature osteoblasts (Debiais et al., 1998). The effect of FGF2 induced differentiation may be mediated by altering the expression patterns of Fgfr1 and -2, as *Fgfr1* up-regulation and *Fgfr2* down-regulation is observed in mouse sutures treated with FGF2 beads in vivo (Iseki et al., 1999). The effects of FGF2 are concentration dependent. Blocking FGF2 with a single bead soaked in neutralising antibody in chick cranial vault increased proliferation, however when several beads were used to block FGF2, both differentiation and proliferation were blocked (Moore et al., 2002). FGF2 interacts with other growth factors, such as BMP and TGFbeta, which are also involved in bone growth and development. FGF2 can significantly increase the transcription of *Tgfbeta1* for 24 hours after treatment (Mathy et al., 2003). *Bmp* expression is also upregulated by FGF2 stimulation (Choi et al., 2005). Nuclear translocalisation of FGF2 is necessary for the proliferative response (Sorensen et al., 2006a).

Fgf18 is found in mesenchyme and differentiating osteoblasts and it is required for osteoblast proliferation and differentiation (Ohbayashi et al., 2002). A lack of *Fgf18* expression results in delayed ossification and delayed suture fusion (Liu et al., 2002; Ohbayashi et al., 2002). FGF18 is most homologous to FGF8 and FGF17 (Itoh and Ornitz, 2004).

Both FGF6 and FGF17 can bind FGFR2IIIc, but in terms of bone development there has been no clear role and only FGF17 has been associated with costal cartilage development (Xu et al., 1999). FGF8 is known to stimulate osteogenesis in bone marrow cells (Valta et al., 2006), though its role in skull vault development has not been characterised. FGF9 has been reported to induce endochondral ossification in craniofacial bone and is therefore significant, though of lesser interest in intramembranous ossification (Govindarajan and Overbeek, 2006). In summary, the main FGFs that have been characterised for calvarial growth are FGF1, -2 and -18.

1.3.5 Mediators of downstream FGFR signalling

FGFR signalling in the cytosol activates downstream pathways that include mitogen activated protein kinase (MAPK), protein kinase C (PKC), phospholipase C-gamma (PLC-γ), phosphatidylinositol 3-kinase (PI3-K) and other pathways that are activated by less well characterised molecules such as Crk, Src and Shc (Dailey et al., 2005; Klint and Claesson-Welsh, 1999; Spector et al., 2005). Signalling in pathways are initiated by phosphorylation of specific tyrosine residues in the Tyrosine Kinase (TK) domain of FGFR. The local conformational structure around these residues allows proteins that contain PTB or SH2 domains to bind to them. Examples of these proteins are PLC-γ, PI3-K, Crk, Src and Shc, which are shown in Figure 1.9.

MAPK pathway involves a cascade of four kinases. The range of MAPK pathways includes Extracellular Related Kinase 1/2 (ERK1/2), p38 and c-jun N-terminal Kinase (JNK), each of which has their own specific molecules along their cascades. The RAS/RAF/MEK/ERK signalling cascade was the first to be discovered. As implied, the RAS molecule of the MAPK pathway is not directly activated by the TK domain of FGFR, but activated by the guanine exchange factor Son of Sevenless (SOS), which is complexed to Grb2, Shc and FRS2α (Dailey et al., 2005). FRSα directly binds to FGFR and is involved in ERK stimulation as overexpression of FRS results in prolonged FGF induced ERK activation (Hadari et al., 2001). RAS is a g-protein that lies on the cytoplasmic surface of the cell membrane. SOS dissociates GDP from RAS, resulting in an association of GTP with RAS. The resulting conformational change allows RAS to bind to effector proteins such as RAF. RAF may also be activated by Protein Kinase C (PKC) pathways (Grammer and Blenis, 1997).

In osteoblasts FGFR activates RAS/RAF/MEK/ERK pathway via SOS, but not via a PI3-K mechanism. However, if initiated by PDGF-BB, PI3-K may also activate RAS/RAF/MEK/ERK in this cell type (Chaudhary and Hruska, 2001). MEK1 may be activated independently of RAF (b-RAF) by autophosphorylation by PAK, which is associated with cell adhesion molecules such as Fibronectin (Park et al., 2007). This suggests that downstream pathways have complex interconnections that depend on the upstream signal. ERK MAPK signalling may be inhibited by the non-competitive MEK inhibitor U0126 (Suzuki et al., 2002a).

ERK1/2 controls proliferation in osteoblasts (Chambard et al., 2007; Fremin et al., 2007; Suzuki et al., 1999). In addition it is important for differentiation (Lai et al., 2001; Spector et al., 2005). In MC3T3 cells the JNK pathway mediates FGF2 induced release of VEGF, which important

for stimulating vascular endothelial growth. The p38 MAPK is involved in differentiation, as it positively regulates ALP expression in osetoblasts (Suzuki et al., 2002a). It also positively regulates the expression of PKC-eta (Lampasso et al., 2006). However p38 is not associated with FGF2-induced osteoblast apoptosis (Debiais et al., 2004).

PKC plays a role in cell proliferation (Kozawa et al., 1989; Sabatini et al., 1996; Uht et al., 2006; Villa et al., 2003) and is associated in differentiation. There are many isoforms of PKC. PKC-δ mediates FGF2 induced Runx2 activation and expression (Kim et al., 2006; Kim et al., 2003). It binds to and directly phosphorylates Runx2. It is also associated with FGFR and BMP induced osteoblast apoptosis (Fromigue et al., 2005; Lemonnier et al., 2001). PLC-γ is thought to activate PKC (Tang et al., 2007).

PI3-K positively mediates osteoblast cell survival induced by FGF2 (Debiais et al., 2004). It may be activated directly by FGFR or via Grb2 complexed to FRS2 (Hatch et al., 2006). Downstream of PI3-K is Akt, which is required for osteoblast cell survival, as disruption of the Akt gene in MC3T3 cells leads to increased susceptibility to mitochondria-dependent apoptosis (Kawamura et al., 2007). However a number of studies indicate that FGFR activated PI3-K may lead to variation in Akt activation in osteoblasts. In subconfluent MC3T3 cells and immortalised human neonatal calvarial (INHC) osteoblasts cells, Akt is either not activated or activated at very low levels by PI3-K (Chaudhary and Hruska, 2001; Debiais et al., 2004). FGF1 treatment in immature mouse osteoblasts (OB1) leads to low levels of Akt activation, whereas in the more mature OB5 osteoblasts the level of Akt activation appears to increase slightly (Raucci et al., 2008). Differentiation in OB1 and OB5 osteoblasts is enhanced by increasing the level of active Akt. Runx2 dependent osteoblast differentiation has been shown to require PI3-K-Akt signalling, in particular to allow Runx2-Akt interactions (Fujita et al., 2004). Together, this suggests a role for PI3-K and Akt in survival and differentiation in osteoblasts.

Synthetic inhibitors have been generated for FGF signalling such as SU5402. SU5402 binds to the adenine pocket of the ATP binding site of the FGFR tyrosine kinase and the substituted groups at the R1 position bound to the hydrophobic pocket of the ATP binding site, thus inhibiting the TK activity (Li et al., 2006).

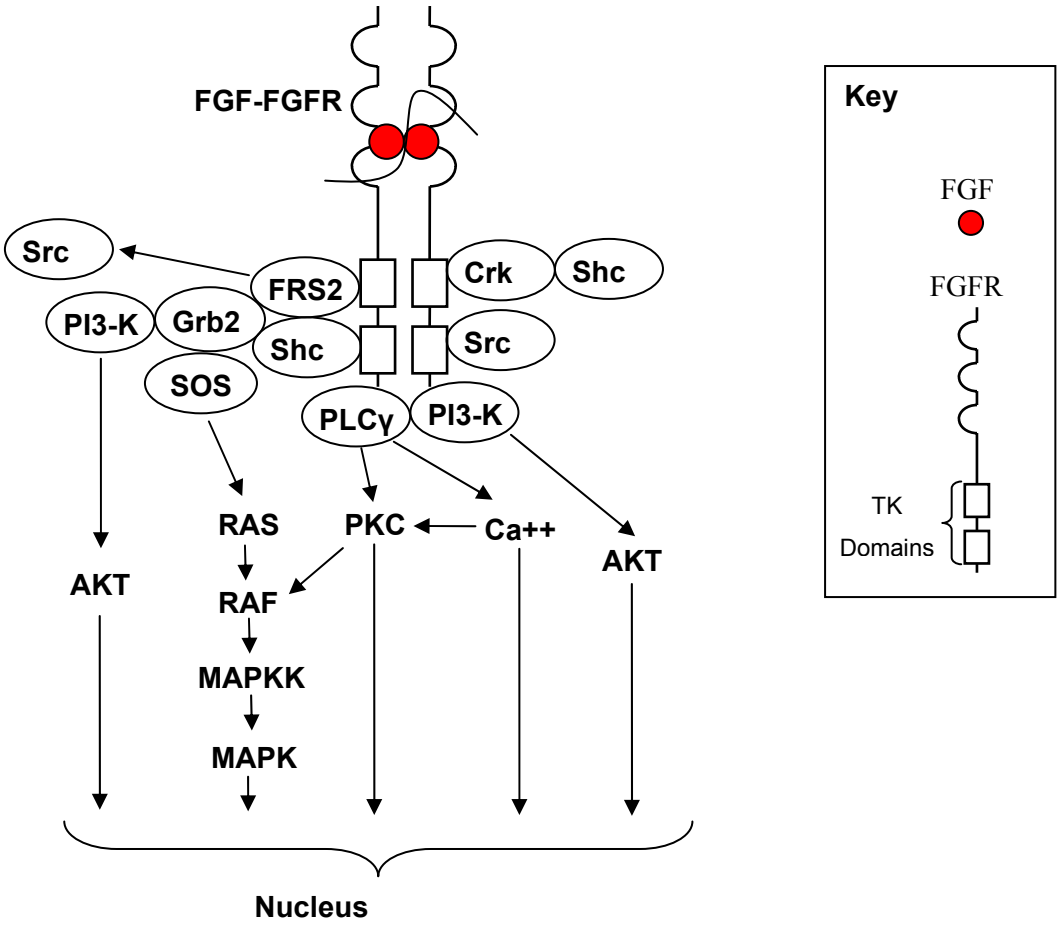

Figure 1.9 Downstream signals of the FGF-FGFR complex

In the Tyrosine Kinase domains of FGFR there are tyrosine residues, which are binding sites for proteins that contain Phosphotyrosine-binding (PTB) or Src Homology 2 (SH2) domains (Pawson 1993). The circled molecules shown in this figure either bind directly, because they contain PTB or SH2 domains, or they are adapter proteins. There are a number of downstream pathways of FGF signalling, which include MAPK, PKC, PLC-γ and PI3-K. The effects of these signal pathways involve the nucleus to produce cellular responses. Activation of MAPK requires a complex formation. FRS2 (Fibroblast growth factor receptor substrate 2) contains PTB domains to bind to FGFR. It binds to Shp and Grb2 (Growth factor receptor-bound protein 2), which is complexed to the Ras activator SOS (Son of Sevenless). SOS is one of the main initiators of MAPK signalling, however MAPK signalling may also be initiated by PKC. PI3-K may also be activated by Grb2 in addition to direct activation by FGFR. Adapted from Dailey et al, 2005, Nishizuka, 1988 and Hatch 2006.

1.4 Transforming growth factor beta (TGFbeta)

TGFbetas are part of the TGFbeta superfamily, a large group of structurally related dimeric cytokines (Janssens et al., 2005). The superfamily includes bone morphogenic proteins (BMPs) (Ito and Miyazono, 2003). Aside from bone formation, TGFbetas play roles in cancer and in the development of body structures including the blood vessels, eyes, lungs, heart and spine (Chai et al., 2003; Dubrovska et al., 2005). To date, there are three isoforms of TGFbeta in mammals (Schmierer and Hill, 2007). TGFbetas are homodimeric existence and must be activated before they can signal, by latency-associated peptide bound to TGFbeta based on studies of TGFbeta1 (Rawlins and Opperman, 2008; Shi and Massague, 2003).

1.4.1 TGFbeta signalling

The TGFbetas are ligands that bind to TGFbeta receptors I and –II (TβRs), which are serine/threonine kinase receptors. For signalling to initiate, TGFbeta binds to a homodimer of TβRII, which permits a TβRI homodimer to bind to the complex (Zuniga et al., 2005). This results in the formation of a heterotetrameric receptor complex of TGFbeta:TβRI:TβRII (ten Dijke and Hill, 2004). Unlike FGFRs, one of the receptors (TβRII) is constitutively active and phosphorylates TβRI on formation of the complex (Janssens et al., 2005).

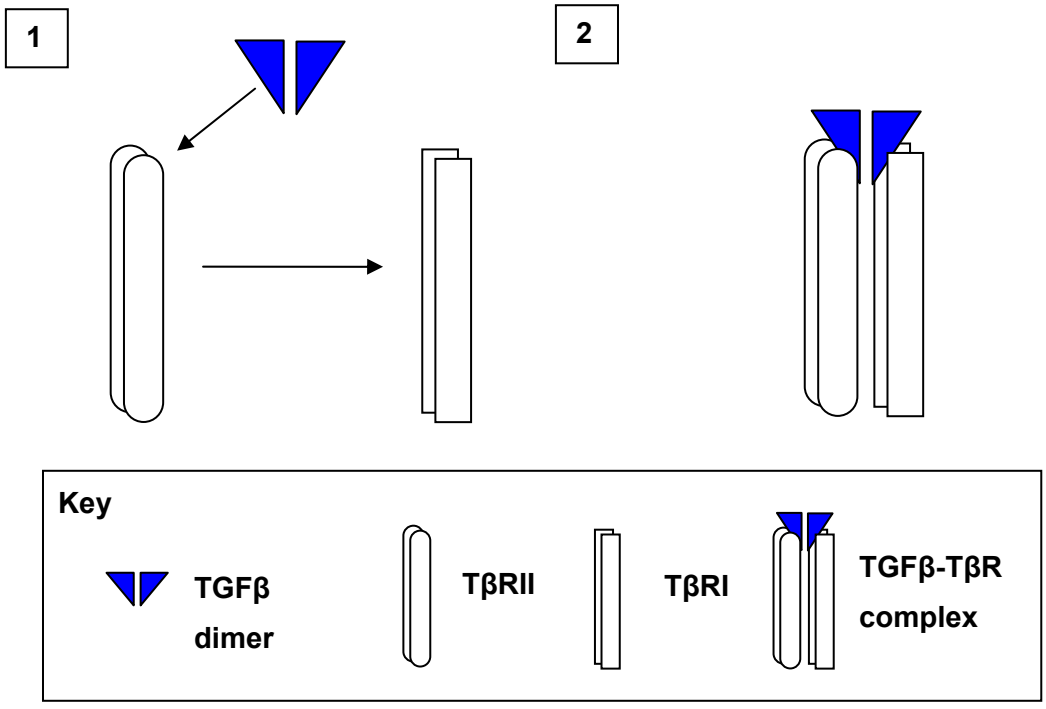

Figure 1.10 TGFbeta signal initiation

TGFbeta binds to a dimer of TβRII, which enables binding of this complex to TβRI. This completes the complex and allows TβRII to phosphorylate and activate TβRI, which initiates signalling.

1.4.2 The roles of TGFbetas in bone

In general, TGFbeta1, -2 and -3 are able to increase proliferation in osteoblasts, depending on experimental conditions and the stage of osteoblast maturation. These are mainly based on studies in mouse. *Tgfbeta1*, -2 and *-3* mRNA are expressed at the bone fronts and in the dura (Opperman et al., 1997). *Tgfbeta1* is also expressed in sutural mesenchyme, at higher levels in the rat posterior frontal suture and dura compared to the sagittal suture (Gosain et al., 2004). *Tgfbeta1* and *-3* are expressed in osteogenic bone fronts of presumptive sutures. *Tgfbeta1* and *-2* expression is found in fusing sutures (Opperman, 2000). During posterior frontal suture fusion, *TβRI* is upregulated relative to the brain (Gosain et al., 2004).

Of the many phenotypes that disrupted TGFbeta signalling may produce, a common feature is an osteopetrosis phenotype, where there is increased bone thickness. *In-vivo* mouse models have shown that inactivated TGFbeta1, dominant negative mutations of TβRII and TGF-beta binding protein (Ltbp)-3 null mutations in mice lead to increased bone mass with decreased osteoclast activity, but no change to the rate of bone deposition (Dabovic et al., 2005; Filvaroff et al., 1999). This indicates that TGFbeta signalling is also important for osteoclast activity and therefore bone remodelling. In bone, truncated TβRII mutations lead to a decrease in the osteocyte density (Filvaroff et al., 1999), whereas in TGFbeta2 overexpression mutants there is an increase in the number of osteocytes in bone (Erlebacher and Derynck, 1996; Erlebacher et al., 1998). This suggests that TGFbeta signalling is required for differentiation of osteoblasts into osteocytes.

Most of the current literature suggest that TGFbeta1 increases proliferation, particularly in less mature mouse osteoblasts (Bosetti et al., 2007; Centrella et al., 1994; Chung et al., 1999; Ghayor et al., 2005; Janssens et al., 2005; Reyes-Botella et al., 2002). In osteoblasts at postconfluence, TGFbeta1 does not affect proliferation (Chung et al., 1999). TGFbeta1 decreases proliferation in rat osteosarcoma cells and in MC3T3 at high passage (>60), or in serum free medium (Cabiling et al., 2007; Centrella et al., 1994; Chung et al., 1999). Runx2 is activated in UMR rat osteoblasts following by TGFbeta1 treatment (Selvamurugan et al., 2004), indicating that it may push differentiation. However, TGFbeta1 treatment decreases expression of late differentiation marker *Oc*, an effect that is abrogated by cycloheximide, indicating an indirect transcriptional control of *Oc* by TGFbeta1 (Noda, 1989). TGFbeta1 also inhibits BMP2-induced bone mineralization (Spinella-Jaegle et al., 2001). TGFbeta1 has not been reported to alter apoptosis, as demonstrated in E18 mouse osteoblasts cultured in differentiating medium after 2 days of TGFbeta1 treatment (Cabiling et al., 2007). Overall, TGFbeta1 is

suggested to increase early proliferation and block late stage differentiation and mineralization in osteoblasts (Alliston et al., 2001; Centrella et al., 1994).

TGFbeta2 generally increases proliferation in osteoblasts (Bosetti et al., 2007; Centrella et al., 1994; Opperman et al., 2000); although in rat osteosarcoma cells TGFbeta2 treatment leads to decreased proliferation (Centrella et al., 1994). TGFbeta2 also increases apoptosis in calvarial explants (Opperman et al., 2000). However this effect may depend on experimental conditions as in tibial bone *in-vivo*, osteoblast apoptosis is blocked by TGFbeta2 treatment (Dufour et al., 2008). Tgfbeta2 has a positive role in suture fusion, which involves induction of proliferation and signalling along the Erk1/2 pathway (Opperman et al., 2000; Opperman et al., 2006). In TGFbeta2-null mice at stage E18.5 there is a reduction in calvarial bone size and ossification with enlarged fontanelles (Sanford et al., 1997). In contrast, overexpression of TGFbeta2 in mice leads to lower bone mass through greater bone resorption (Erlebacher and Derynck, 1996). This suggests that TGFbeta2 is positively involved in osteoblast proliferation, differentiation and bone remodelling and plays a role in osteoblast apoptosis.

TGFbeta3 treatment increases proliferation in primary fetal rat bone cells and in primary human osteoblasts grown without differentiation factors (Bosetti et al., 2007; Centrella et al., 1994). In rat osteosarcoma cells, 0% serum culture conditions and calvarial explants, proliferation is decreased by TGFbeta3 treatment (Cabiling et al., 2007; Centrella et al., 1994; Opperman et al., 2000). TGFbeta3 may also increase apoptosis in osteoblasts (Cabiling et al., 2007; Opperman et al., 2000). TGFbeta3-induced apoptosis and inhibited proliferation is thought to contribute to suture patency and the delay of suture fusion (Opperman et al., 2000; Opperman et al., 2002a; Opperman et al., 2002b). Together this suggests that TGFbeta3 increases osteoblast proliferation in immature osteoblasts, but may decrease proliferation in more mature cells and in the absence of serum. Apoptosis is positively regulated by TGFbeta3.

TβRII is involved in regulating CNC cell populations for form frontal bone and development of the caudal region of the skull (Hosokawa et al., 2007; Sasaki et al., 2006). TGFbeta has differential functions, not only on osteoblasts, but in other cell types such as fibroblasts. For example, dermal fibroblasts have a higher hyaluronan (HA) expression compared to oral mucosal fibroblasts, which results in increased proliferation in dermal fibroblasts in response to TGFbeta1, whereas oral fibroblasts respond to TGFbeta1 by a reduction in proliferation (Meran et al., 2008). Interestingly, this effect is dependent on the downstream molecule Smad3, described in the next section.

1.4.3 Mediators of TGFbeta signalling

TGFbetas signal directly via Small Mothers Against Decapentaplegic homologue (SMAD) transcription factors (Sekelsky et al., 1995; Savage et al., 1996) and also via MAPKs such as ERK1/2 (Lee et al., 2006). PI3-K and PKC may also be activated by TGFbeta, however it is not clear if they are directly activated by the TGFbeta receptor complex.

The are eight SMADs, of which SMAD6-7 are inhibitory (Clarke and Liu, 2008). TGFbetas are best known to signal via SMAD2 and -3 by binding to TβRI (ALK5), but they can also signal via SMAD1 and -5 via a different TβRI (ALK1). In contrast, BMPs signal via SMAD1, -5 and 8 (Miyazawa et al., 2002). In addition, these SMADs associate with SMAD4 (the common mediator SMAD) in order to confer the downstream signalling. These TGFbeta-SMAD configurations are shown in Figure 1.11. The actions of these SMADs are blocked by inhibitory SMAD6 and -7. In mice, Smad2 and -3 play important roles in the normal development of the skull, as Smad2 may rescue cleft palate in TGFbeta3 null mice (Cui et al., 2005) and Smad3 mediates TGFbeta induced of downregulation of *Runx2* and *Osteocalcin* expression, thus inhibiting osteoblast differentiation (Alliston et al., 2001). There are also some direct interactions between Smad3 and Runx3, and Runx2 acts synergistically with Smad1 and -5 to regulate bone specific genes (Ito and Miyazono, 2003).

TGFbeta signalling may also activate MAPK by directly activating ShcA, which has been shown to result in ERK1/2 activation (Lee et al., 2007). TGFbeta may also activate prostaglandins, which activate PKC, which in turn activate the ERK1/2 pathway, leading to proliferation (Ghayor et al., 2005). Erk1/2 pathway signalling is required for processes such as TGFbeta2 induced suture fusion (Opperman et al., 2006). The p38 MAPK mediates a number of TGFbeta's functions with respect to differentiation (Karsdal et al., 2001; Lee et al., 2002; Selvamurugan et al., 2004; Sowa et al., 2002). Examples include the convergence of Smad and p38 pathways to regulate *Runx2* expression (Lee et al., 2002), and osteoblast elongation mediated by p38 following TGFbeta treatment (Karsdal et al., 2001). Interestingly, the effect of p38 may depend on the upstream signal. For example, p38 mediated TGFbeta signalling decreases *osteocalcin* expression, whereas p38 mediated BMP increases *osteocalcin* expression (Lai and Cheng, 2002). JNK and p38 have been shown not to be involved in TGFbeta mediated MC3T3 cell proliferation, whereas ERK1/2 has been shown to be essential (Ghayor et al., 2005). JNK and ERK1/2 play a role in differentiation by mediating TGFbeta inhibition of ALP expression and mineralisation (Tokuda et al., 2003).

TGFbeta influences cell survival by TGFbeta-PI3-K and Smad3-Akt interactions (Conery et al., 2004; Dufour et al., 2008; Song et al., 2006). TGFbeta can activate PI3-K, leading to increased osteoblast survival. Conversely, TGFbeta-Smad3 signalling can induce osteoblast apoptosis, which is inhibited by Smad3-Akt binding, as this sequesters Smad3 (Conery et al., 2004). Interestingly, TGFbeta induced Akt activation in mesenchymal cells is dependent on p38 (Horowitz et al., 2004).

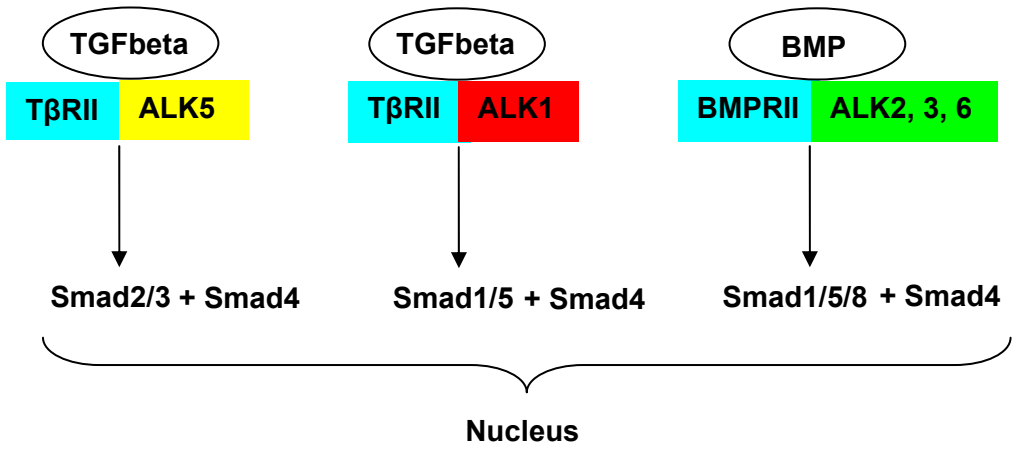

Figure 1.11 Receptor-Ligand complexes in TGFbeta and BMPs and associated SMAD signals
TβRII and BMPRII are common to TGFbeta and BMPs respectively, whereas the TβRI and BMPRI receptors (also known as ALK) determine which SMADs are activated. In TGFbeta signalling, ALK5 induces SMAD2/3 activation, whereas ALK1 induces SMAD1/5 activation. BMPs activate SMAD1/5/8 via ALK2, -3 or -6. All of these SMADs bind to the SMAD4 (a Co-SMAD), resulting in regulation of transcription. Adapted from Miyazawa, 2002.

SB431542 is a synthetic inhibitor of TGFbeta signalling. It inhibits ALK4, -5 and -7, but not ALK-1, -2, -3, and -6; hence it does not affect BMP signalling (Laping et al., 2002; Inman et al., 2002).

1.5 *In-vitro* model of bone development with MC3T3-E1

MC3T3-E1 is an osteogenic cell line derived from a clone derived from newborn mouse calvaria, established under 3-day transfer, inoculum 3 x 10^6 cells (3T3) culture conditions (Kodama et al., 1981). The 3T3 protocol was first described by Todaro and Green in 1963, where 3 x 10^6 cells were plated onto 50mm diameter (20cm^2) petri dishes, however in practice only the 3 day transfer is conserved, as differences in cells such as doubling time affect the number of cells needed to inoculate the culture plate (Todaro and Green, 1963). MC3T3-E1 cells resemble osteoprogenitors (Sudo et al., 1983), based on their fibroblastic appearance and

low ALP activity in the early stages of culture. The doubling time of MC3T3 was reported to be approximately 18 hours (Sudo et al., 1983).

MC3T3-E1 is a useful model for intramembranous bone formation as cultures have characteristics that are similar to developing bone *in-vivo*, such as the stages of differentiation from osteoprogenitors to osteoblasts and osteocytes. Although a number of bone cell lines exist, only few originate from calvaria, such as OB cells (Mansukhani et al., 2000). MC3T3 cultures are able to mineralise bone matrix if cultured with both ascorbic acid and beta-glycerophosphate to form periosteum and bone nodules (Petiot, 2001). The timing of these differentiation processes is associated with the initial cell density. Morphologically, fibroblastic-like cells are found at 2 days in culture (2 DIC), whereas cuboidal cells are found at 4 DIC, based on a seeding of 50,000 cells on a 35 mm culture plate (about 5200 cells per cm^2) (Sudo et al., 1983). The basic description of the osteoblast morphology is summarised in Table 1.3.

Table 1.3 MC3T3 maturity and morphology. Adapted from (Sudo et al., 1983)

Cell	Appearance	Day observed
Osteoprogenitor	Fibroblastic	2
Osteoblast precursor*	Lysozome rich cells	2
Osteoblast	Cuboidal cells	4
Osteocyte	Cell surrounded by bone	21

*Could be described as late osteoprogenitor or early osteoblast

A comparison of early and late passage MC3T3-E1 (<20 and >65 respectively) revealed marked changes in cell morphology and a reduction in both proliferation and cellular responses to TGFbeta1 and BMP2 (Chung et al., 1999). A study of MC3T3-E1 cell morphology, 7 days after seeding at 5000 cells/cm^2 showed that most were cuboidal in early passaged cells, whereas at late passage (>65), cells were spindle shaped (Chung et al., 1999). Exogenous TGFbeta1 treatment increased proliferation in early passage, but decreased proliferation in late passage cells. BMP2 did not have any significant effect on proliferation in either cell group. In another study of MC3T3, although cell population doubling had decreased slightly in passage 42 compared to passage 25, no significant difference in cell number was found until a few days post confluence (Peterson et al., 2004).

These studies indicate that cell morphology, passage number and response to TGFbeta1 should be monitored and that cells should be excluded from experimentation for passage numbers above 65 or when MC3T3 cells no longer respond to TGFbeta1.

1.6 Craniosynostosis

Craniosynostosis is a disease characterised by the premature fusion of one or more sutures leading to skull dysmorphologies. The incidence is approximately 1 in 2500 live births (Hollway et al., 1995). Bone growth is reduced at the site of suture fusion, which reduces the intracranial volume, as shown in rabbits with craniosynostosis (Cooper et al., 2006).

1.6.1 Clinical and genetic background

The key clinical features of craniosynostosis are the deformities at the prematurely fused suture(s) and also the compensatory growth in other areas of the skull to give head shapes described in Table 1.4. An example of sagittal suture fusion is given in Figure 1.12. Craniosyostosis is classically diagnosed according to the skull morphology around 2-3 weeks postnatally, to allow for normal skulls to return to their natural shape after deformation that may occur through the birth canal (Table 1.4). A direct defect in ossification leading to premature suture fusion is known as a primary craniosynostosis. These include syndromic craniosynostoses, which are categorised according to other cranial and extracranial features and specific genetic mutations (Table 1.6-1.6). For example, in Crouzon's syndrome, hypoplasia of the maxilla and hypertelorism (wide spacing) of the eyes are observed and this is associated with FGFR2 mutations. A secondary craniosynostosis occurs as a result of other primary defects and disorders (Table 1.7).

Table 1.4 Clinical classifications of craniosynostosis based on suture

Clinical Description	Suture involvement	Head shape
Scaphocephaly Syndolichocephaly	Sagittal	Elongated (anterior – posterior)
Plagiocephaly	Unicoronal	Asymmetric forehead flattening
Trigonocephaly	Metopic	Pointed triangular forehead
Posterior plagiocephaly	Lambdoid	Asymmetric occipital flattening
Brachycephaly	Bicoronal	Spherical
Acrocephaly Synoxycephaly**	Bicoronal/multiple	Pointed, tower

** The term turricephaly is also sometimes used to describe the tower-shaped deformity

Adapted from Clinical Management of Craniosynostosis (2004)

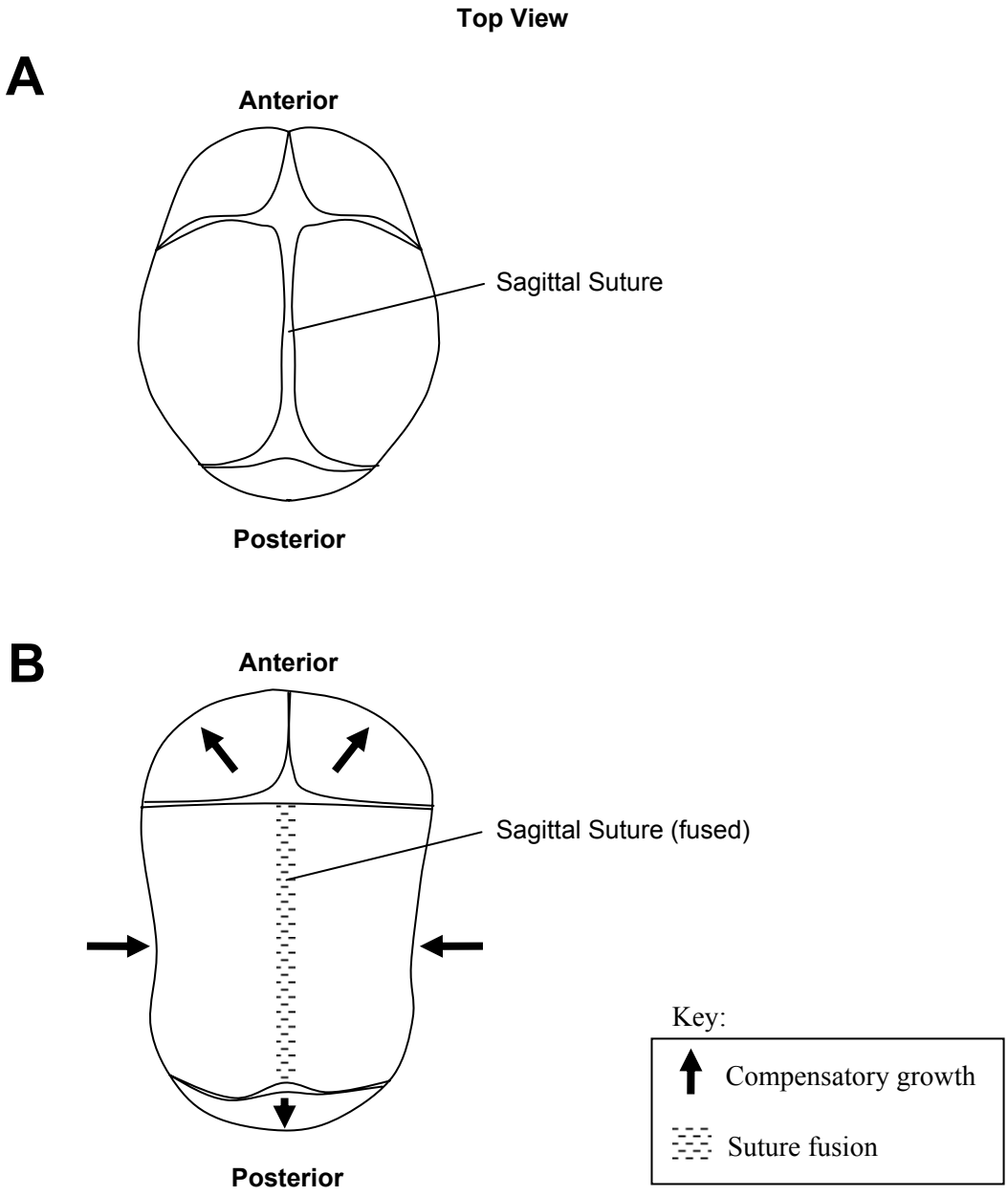

Figure 1.12 Dysmorphology in sagittal suture

A: Normal Skull at brith with all sutures patent. **B:** The premature fusion of the sagittal suture results in a lack of bone growth at this site. Bone growth is compensated at the remaining patent sutures, giving rise to anterior posterior skull enlongation and narrowing of the lateral aspects of the skull.

Approximately 40% (1:6250) of craniosynostoses are syndromic; the common ones include Apert, Crouzon, Pfeiffer, Muenke, and Saethre-Chotzen syndrome (Lajeunie et al., 2006). They are diagnosed by the clinical features and confirmed by genetic testing and skull imaging, for example X-rays, computer aided tomography (CT) and / or magnetic resonance imaging (MRI).

Crouzon syndrome is one of the most common syndromes, occuring in 1:25,000 births (Renier et al., 2000). In 1912, Crouzon described the syndrome's features: synostosis, hypertelorism (widely spaced eyes), exophthalmos (protrusion of the eyes), parrot-beaked nose, short upper lip (maxillary hypoplasia) and relative mandibular prognathism (forward positioned mandible) (Carinci et al., 2005). A bicoronal synostosis is often present, but other sutures may be involved or a unicoronal suture may exist (Hoefkens et al., 2004; Sher et al., 2008). Sutures are not always fused at birth, but progress to fusion within a few years of birth, delaying clinical diagnosis in some cases. Crouzon syndrome does not have clinically abnormal extracranial features, unlike other syndromes, which is useful in excluding Apert or Pfeiffer syndrome in the differential diagnosis (Renier et al., 2000).

Pfeiffer syndrome occurs in 1:100,000 births and features described by Pfeiffer in 1964 included coronal synostosis (with or without sagittal involvement) with turribrachycephaly, maxillary hypoplasia, hypertelorism, proptosis, low nasal bridge, choanal stenosis or atresia, partial syndactyly (Vogels and Fryns, 2006; Pfeiffer, 1964). Furthermore, Pfeiffer syndrome has extracranial features of broad thumbs and toes, that are useful in differentiating it from Apert syndrome (Cohen, Jr., 1993; Pfeiffer, 1964; Renier et al., 2000; Vogels and Fryns, 2006). Interestingly, a number of point mutations for Pfeiffer syndrome are also shared with Crouzon syndrome, such as FGFR2-C278F and FGFR2-C342Y (Ornitz and Marie, 2002). Pfeiffer syndrome is also clinically divided into 3 types, which exhibit additional features and prognoses. Type 1 is associated with normal neurological function and development with a good prognosis (Vogels and Fryns, 2006). Type 2 displays a trilobated skull deformity (cloverleaf skull), more extreme proptosis, elbow ankylosis or stenosis, respiratory difficulties, developmental delay and neurological complications, which carries a poorer prognosis for early survival. Type 3 is similar to type 2, but without the cloverleaf skull.

Craniosynostosis is associated with an increased risk of raised intracranial pressure (ICP); single suture synostosis carries a 15-20% risk, whereas syndromic cranioynostoses 30-40% (Tamburrini et al., 2005). Contributing factors for ICP include smaller skull volume following craniosynostosis, raised ICP results in compression of the brain in the cranial vault and underlying nerves such as the optic nerve. This may impair or result in loss of visual, cognitive

and motor function and development, therefore monitoring ICP and treatment to reduce raised ICP is of primary concern (Bannink et al., 2008). The development of ICP can be a slow insidious process, therefore regular ophthalmological monitoring is advised (Marucci et al., 2008; Renier et al., 2000; Tuite et al., 1996). It is currently debated whether primary defects in brain development independent ICP causing mental impairment exist (Raybaud and Di Rocco, 2007).

Management of craniosynostosis is surgical in order to correct skull dysmorphologies and to relieve high ICP, as damage to visual and mental development may occur if untreated. The surgical techniques are dependent on severity, the suture(s) and other cranial features present.

Table 1.5 Example surgical treatments for craniosynostosis

Clinical Description	**Surgery**
Scaphocephaly Syndolichocephaly	Complete reconstruction Simple craniectomy
Plagiocephaly	Forehead reconstruction
Trigonocephaly	Forehead reconstruction
Brachycephaly	Floating forehead advancement

Adapted from Renier et al, 2000

Table 1.6 Genetic and phenotypic classification of syndromic craniosynostosis						
Syndrome	**Cranial defects**	**Non-cranial defects**	**Locus**	**Gene**	**Mechanism**	**Reference**
Adelaide	Frontal bossing, Mid-face hypoplasia	Phalangeal hypoplasia, coned epiphyses, carpal bone malsegmentation,	4p16	*potentiall yFGFR3, MSX1*	Not established. Shares only cranial features with Jackson-Weiss	(Hollway et al., 1995)
Apert	Coronal, wide midline defect, acrocephaly, midface hypoplasia	Bony and cutaneous syndactyly hands and feet	10q26	*FGFR2*	Loss of ligand specificity	(Wilkie et al., 1995)
Beare-Stevenson	Cloverleaf skull	Furrowed skin disorder of cutis gyrata	10p26	*FGFR2*	Constitutive activation	(Przylepa et al., 1996)
Boston type	Cloverleaf skull, forehead retrusion	Short first metatarsals	5q34	*MSX2*	Gain of function	(Jabs et al., 1993)
Carpenter	Metopic, sagittal, cloverleaf skull	Hand brachydactyly, obesity, feet polysyndactyly	6p12.1-q12	*RAB23*	Predicted loss of function	(Jenkins et al., 2007)
Crouzon	Coronal, proptosis, hypertelorism		10q26	*FGFR2*	Constitutive activation	(Reardon et al., 1994)
Crouzon & acanthosis nigricans	Hypertelorism, Midface hypoplasia, proptosis	acanthosis nigricans	4p16.3	*FGFR3*	Constitutive activation	(Meyers et al., 1995)
Craniofrontonasal	Coronal, hypertelorism, grooved nasal tip,	Partial cutaneous syndactyly	Xq12, Xq22	*EFNB1*	Predicted loss of function	(Twigg et al., 2006; Wieland et al., 2004)

Genetic and phenotypic classification of syndromic craniosynostosis (continued)						
Syndrome	**Cranial defects**	**Non-cranial defects**	**Locus**	**Gene**	**Mechanism**	**Reference**
Jackson-Weiss	Frontal bossing, Midface hypoplasia hypertelorism,	Tarsal/metatarsal fusion, broad great toes	10q26	*FGFR2*	Constitutive activation	(Jabs et al., 1994)
Loeys-Dietz type 1	hypertelorism, cleft palate, blue sclera,	Arterial aneurisms and tortuosity	9q22 3p22	*TGFBR1* *TGFBR2*	Predicted gain of function	(Johnson et al., 2007; Loeys et al., 2005)
Muenke	Macrocephaly, midface hypoplasia	Carpel/tarsal fusion, short hands/feet, coned epiphyses	4p16.3	*FGFR3*	Constitutive activation	(Muenke et al., 1997)
Pfeiffer	Cloverleaf skull, midface hypoplasia	Broad thumb and great toes, cutaneous syndactyly	8p11.2 10q26	*FGFR1,* *FGFR2*	Constitutive activation	(Muenke et al., 1997; Webster and Donoghue, 1997)
Saethre-Chotzen	Coronal	Syndactyly, hallucial duplication, brachydactyly	7p21	*TWIST*	Haploinsufficiency	(de Heer et al., 2005)
Shprintzen-Goldberg	Sagittal & lambdoid Exopthalmos,	arachnodactyly	15q21.1	*FBN1*	Structural disruption	(Sood et al., 1996)
Thanatophoric dysplasia	Cloverleaf skull	Straight femur, short stature, shortened limbs, short ribs	4p16.3	*FGFR3*	Constitutive activation	(Tavormina et al., 1995)

Table 1.7 Secondary Craniosynostoses	
Primary condition	**Examples**
Chromosomal disorders	Del (1q), dup (3q), del (7p), dup(7p), triploidy, tetrasomy 14q
Metabolic Disorders	Hyperthyroidism, Rickets
Mucopolysaccharidoses	Hurler syndrome, Morquio syndrome
Haematological Disorders	Thalassaemias, Sickle Cell Anaemia, Congenital Haemolytic Icterus, Polycythaemia Vera
Teratogens	Aminopterin, Diphenylhydantoin, Retinoic acid, Valproic acid
Malformations	Microcephaly, Encephalocoele, Holoprosencephaly, Hydrocephalus

Adapted from (Cohen, Jr., 1993)

1.7 FGFR mutations

FGF signalling plays an important role in bone differentiation and proliferation. As shown previously in Table 1.6, many of the syndromes are caused by single point mutations in fibroblast growth factor receptors (FGFR) 1-3. FGFR2 is the most commonly reported mutated receptor in 90% of craniosynostosis patients with Apert, Crouzon, Pfeiffer and Jackson-Weiss syndromes (Passos-Bueno et al., 2008). FGFR2IIIc is of particular importance because it is the main isoform in craniofacial bone and is expressed in the paraxial and lateral mesoderm (Orr-Urtreger et al., 1993) that later forms the mesenchyme (Sadler, 2004), and is a positive regulator of bone formation. FGFR2IIIb is expressed in ectoderm and endothelial organ lining (Orr-Urtreger et al., 1993). FGFR3 is also important for long bone development as mutations lead to dwarfism conditions: thanatophoric dysplasia, achrondroplasia and hypochondroplasia (Meyers et al., 1995). The position of the mutation along the gene may be important as 99% of achondroplasia mutations are found in the transmembrane domain. Not all mutations in FGFR lead to craniosynostosis, indicating that specific mechanisms are involved in this disease process. For example, certain mutations of FGFR1 causes Kallmann's syndrome (Albuisson et al., 2005), where there is failure of gonadotrophin releasing hormone (GnRH) releasing neurons to migrate from the olfactory epithelium to the hypothalamus, resulting in hypogonadism and anosia. These FGFR1 mutations result in the KAL2 form of Kallmann's syndrome, which is autosomal dominant and thought to equate to a deficiency of FGFR1 signalling, leading to a failure of olfactory bulb development (Eswarakumar et al., 2005).

Two main mechanisms associated of FGFR associated craniosynostosis have been reported and are considered as gain-of-function (increased signaling), with an autosomal dominant inheritance (Carinci et al., 2005). One is a loss of ligand specificity, where the FGFR is activated by FGF ligands that do not normally bind that receptor. The other is the constitutive activation of the FGFR, which is independent of FGF induced FGFR activation. Many of the mutations occur in the third Ig domain of the receptor such as FGFR2-C278F (Figure 1.13). Interestingly the chance of inheritance is increased from a father with gain-of-function FGFR2 mutations such as Apert, as the FGFR signalling enhances sperm motility (Goriely et al., 2003; Wilkie, 2005).

The mechanisms underlying premature suture fusion are still poorly understood. Though FGFR2 regulates proliferation (Iseki et al., 1999; Yu et al., 2003), the key characteristic observed in craniosynostosis is premature bone differentiation. There are a number of

conflicting reports concerning the effects of FGFR gain of function mutations on proliferation (Marie et al., 2005), which are discussed in section 1.8.3.

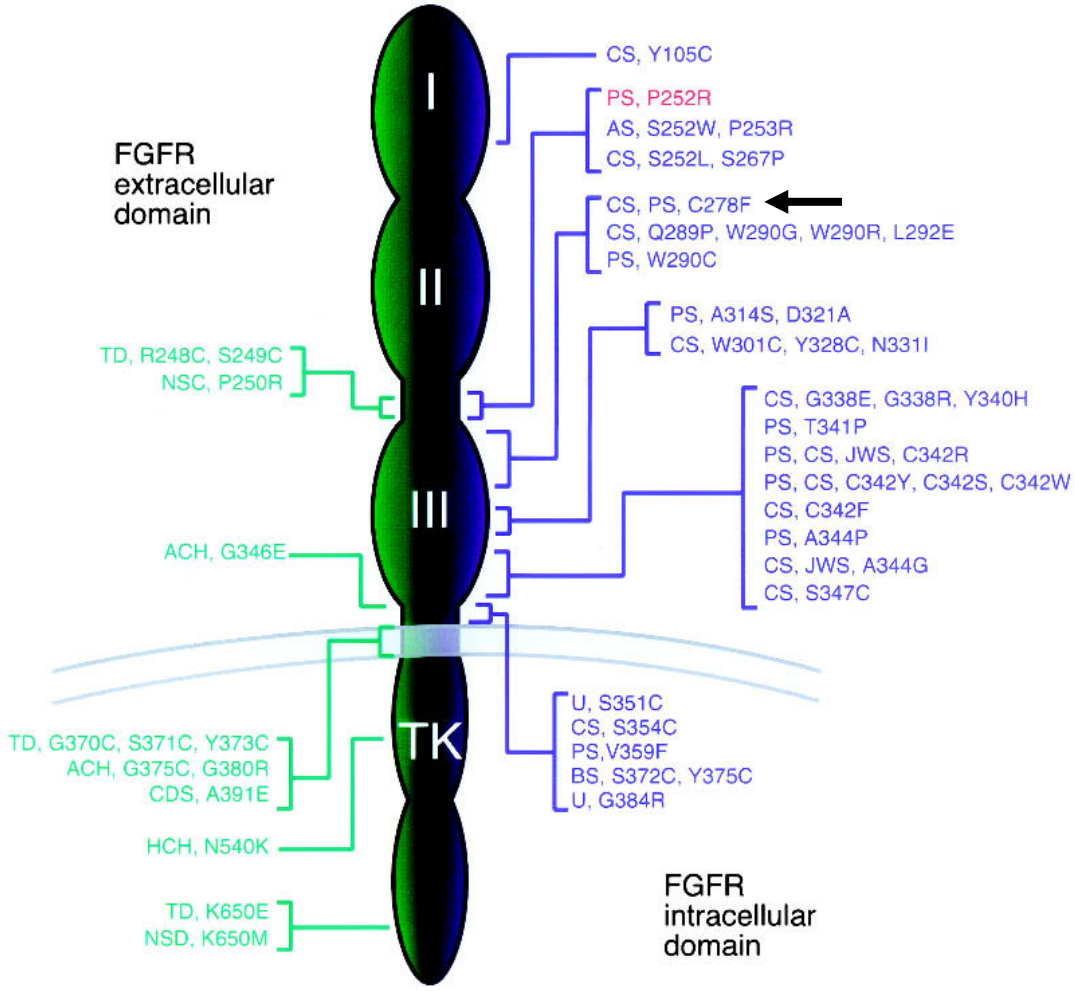

Figure 1.13 Point mutations reported in craniosynostosis (Ornitz and Marie, 2002)

AS: Apert syndrome. **CS:** Crouzon syndrome. **PS:** Pfeiffer syndrome. **JWS:** Jackson Weiss syndrome. C278F mutation (black arrow) is one of the most common mutations. For the latest comprehensive details see also the review by Passos-Bueno (Passos-Bueno et al., 2008).

1.7.1 Loss of ligand specificity of FGFR

These mutations increase receptor binding affinity for other FGF ligands to which they would not normally bind (Yu et al., 2000). Examples include the S252W and P253R mutations, which allow other FGF to bind as shown in Table 1.8 below:

Table 1.8 Change of ligand binding due to FGFR2 mutation (Yu et al., 2000)

Mutation	Receptor	Ligand binding	Abnormal Ligand binding
S252W (Apert)	FGFR2IIIc	FGF1, -2, -4, -5, -6	FGF7, FGF10
S252W (Apert)	FGFR2IIIb	FGF1, -3, -7, 10, -11	FGF2, FGF6 and FGF9

Fgf10, an activator of FGFR2IIIb was shown be involved in inducing craniosynostosis, because genetic abrogation of the ligand rescued craniosynostosis in an Apert syndrome mouse model (Hajihosseini et al., 2008).

1.7.2 Constitutive activation of FGFR

FGF ligands bind to their FGFR, then these complexes dimerise in association with Heparin Sulphate proteoglycan (HSPG) (Harmer, 2006). Constitutive activation is usually considered as a gain-of-function mutation, where FGF signalling is expected to be over stimulated. There are at least three mechanisms for constitutive activation of the FGFR receptor all described in Figure 1.14. These include covalent bonding between receptor monomers via cysteine, hydrogen bonding between receptors in the transmembrane region and autophosphorylation of a monomer via mutation of the tyrosine kinase domain (Webster and Donoghue, 1997).

A study of cysteine residues in FGFR2 has indicated that disruption of a disulphide bond at position 278 or 342 by mutations C278F, W290G, T341P and C342A in NIH3T3 leaves free cysteines in the IgIII domain that lead to receptor dimerisation and increased activation (Robertson et al., 1998). Increased activation was also found in C107A mutants, but not at positions 62, 179 and 231. Analysis of FGFR2-C278F in MC3T3 cells has shown that ligand independent dimerisation is intracellular and that the dimerisation may also occur if glycosylation of wild type FGFR is inhibited (Hatch et al., 2006). Thus it is likely that the presence of a free cysteine in the IgIII domain of an FGFR2 monomer may prevent complete glycosylation of FGFR2 and that complete glycosylation is necessary to prevent ligand independent FGFR2 dimerisation.

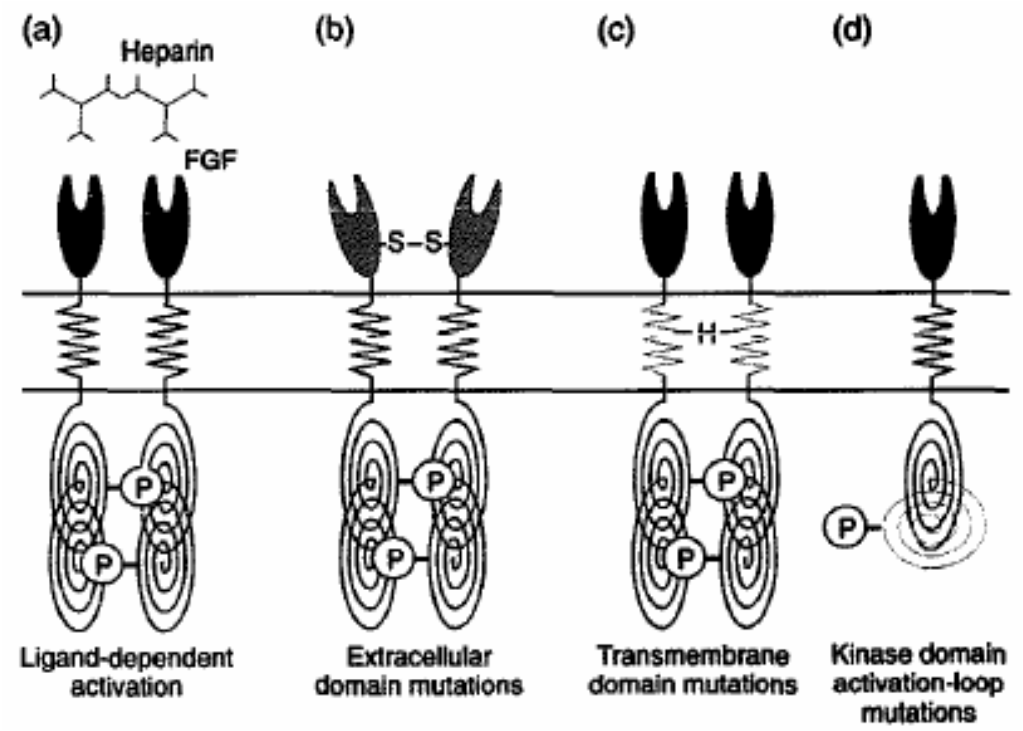

Figure 1.14 Changes in FGFR from FGFR mutations (Webster and Donoghue, 1997)

FGF signalling is normally initated by the formation of the FGF-FGFR complex (a) in association with Heparin or HSPG. Constitutive activation may occur where receptors are dimerised, for example at the extracellular domain (b) or in the transmembrane domain (c). Kinase activation loop mutations (d), where one ligand is constitutively active also exist.

1.8 The FGFR2-C278F mutation

The FGFR2-C278F mutation is one of the most common constitutively active FGFR mutation. It is thought to dimerise FGFR2 by disulphide bond formation between the extracellular domains. The FGFR2-C278F mutation is a nucleotide point mutation at position 883 from guanine to thymidine, resulting in an aminoacid change from cysteine to phenylalanine at position 278 in exon IIIa of the protein (Passos-Bueno et al., 1998). This breaks the normal disulphide bond between cysteine residues in the third Ig domain at position 278 and 342 (Figure 1.13 black arrow). The free cysteine at position 342 becomes involved in the disulphide bond dimerisation of FGFR2, leading to constitutive activation (Robertson et al., 1998).

A few studies have shown changes to osteoblast proliferation and signalling after transfection with FGFR2-C278F. In embryonic chick calvarial osteoblasts, proliferation is increased and differentiation decreased within 17 days of transfecting with FGFR2-C278F (Ratisoontorn et al., 2003). One report has shown that in MC3T3-E1(C4) cells, the FGFR2-C278F receptor was not expressed on the cell surface, but co-localised with the endoplasmic reticulum (ER) in a peri-nuclear pattern and was incompletely glycosylated (Hatch et al., 2006). This incomplete glycosylation was shown to increase dimerisation, subcellular trafficking, ubiquitination and degradation of FGFR2-C278F. Whereas FGFR2-C278F mRNA levels were significant; there were low protein levels, suggesting that significant protein degradation may have occured. In terms of signalling, there was increased receptor autophosphorylation shown by phosphorylation of FGFR2-C278F tyrosine. Furthermore, binding and activation of both phospholipase C γ (PLC-γ) and Frs2 to FGFR2-C278F was increased. This also implicated that Phospho-inositol-3 Kinase (PI3K) and MAPK pathways were also activated as they are downstream of Frs2. Metabolism may have increased as shown by the reduction of MTT (thiazolyl blue tetrazolium bromide), which was dependent on both PLC-γ and Frs2 signaling. There was also an increased basal level of anaerobic glycolysis, indicating an anaerobic metabolism occuring. The downstream signalling of PLC-γ, PI3-K and MAPK relative to the controls was not studied, therefore it is unknown whether the signalling is changed in these pathways.

In summary, FGFR2-C278F increases embryonic chick osteoblast proliferation and in MC3T3 cells is suggested to increase the level of downstream signalling via Frs and PL-C gamma, while increasing metabolism. Given Frs involvement, it is likely that MAPK and PI3-K signalling have been affected (section 1.4.3).

1.8.1 FGFR2-WT and FGFR2-C278F transfection of MC3T3

The Ferretti lab at the Institute of Child Health (London, UK) created a number of stably transfected cell lines, each with one specific FGFR gene. Two of these in MC3T3 contained either a human wild type FGFR2 (FGFR2-WT) or a human FGFR2 with a point mutation of cysteine to 278 phenylalanine (FGFR2-C278F), which is associated with a Crouzon's or Pfeiffer syndrome phenotype as shown in Figure 1.13 (Ornitz and Marie, 2002). Cell lines were initially labelled MC3T3, R2WT2 and R2M7, though subsequently were labelled MC3T3, R2-WT and R2-C278F for convenience.

1.8.2 Studies by the Ferretti lab on FGFR2-C278F

It has been shown that pre-migratory neural crest (NC) cells transfected with either FGFR1-K656F or FGFR2-C278F induced chondrogenesis (Petiot et al., 2002). As FGF2 treatment of pre-migratory NC cells also induced chondrogenesis, this indicated that FGFR2-C278F may elicit FGF signaling in a way similar to the effects of exogenous FGF2 signaling. Using the knowledge that Crouzon syndrome is inherited in an autosomal dominant manner (Shotelersuk et al., 2003), it was thought that stable transfection of FGFR2-C278F into MC3T3 cells may be able to simulate the effects of a naturally occurring mutation. Initial characterisation of differentiation (Santos-Ruiz et al., 2007), proliferation and apoptosis in MC3T3, FGFR2-WT and C278F cells were made by the Ferretti lab (unpublished).

Immunocytochemisty analysis revealed that Collagen1 (Col1) was present in most C278F cells at 2 days in culture (DIC) compared to MC3T3 and R2-WT cells, where it was confined to a few cells within very dense cell clusters. RT-PCR analysis of *Runx2* at preconfluence and confluence showed that *Runx2* expression was higher, when normalised to Glyceraldehyde-3-Phosphate Dehydrogenase *(Gapdh)* expression. Proliferation was compared using Immunocytochemistry with phosphorylated histone 3 (pH3), which showed that R2-C278F cells had the lowest percentage of pH3 staining. Apoptotic studies were performed with Terminal deoxynucleotidyl Transferase Biotin-dUTP Nick End Labeling (TUNEL) and revealed that at 1 and 2 DIC, R2-C278F cells had a higher percentage of apoptotic cells (2 to 3%) compared to MC3T3 (0.5 to 1%).

Together these data suggested that in C278F cells, proliferation had decreased, differentiation had increased and apoptosis had increased.

1.8.3 Comparison of cell behaviour in osteoblasts with FGFR2-C278F and other FGFR gain-of function mutants

A number of groups have tried to model FGFR2 mutations that lead to craniosynostosis. R2-C278F cell characteristics are similar to some of the human models, showing decreased proliferation, increased differentiation and apoptosis (Fragale et al., 1999; Marie et al., 2005). Among these was a study by Fragale et al on a human patient. In contrast, a number of mouse models studied displayed different characteristics: increased proliferation and decreased differentiation in osteoblasts. Details of the FGFR2 mutations concerning position 278 and 342 and the animal models are shown in the table below.

Table 1.9 Models FGFR2 gene mutations in osteoblasts known to cause craniosynostosis

	FGFR2 Mutation	Model	In-vitro / in-vivo
Eswarakumar et al, 2006	C342Y	Mouse	In-vivo
Fragale et al, 1999	C342R	Human patient	In-vitro
Mansukhani et al, 2000	C342Y	Mouse OB1 cells	In-vitro
Ratisoontorn et al, 2003	C278F	Chick	In-vitro

The diffferences in osteoblast phenotype between mouse, chick and human models demonstrate the complexity of FGF signalling even among similar FGFR2 mutations, however the results are also informative about any potential effects that mutant receptor may have on osteoblast behaviour (Marie et al., 2005; Ratisoontorn et al., 2003). These potential effects fro the receptor may have been influences by factors such as the animal used, whether the study was *in-vitro* or *in-vivo* and the exact experimental conditions (for example the serum for culturing).

1.9 Summary and aims

Craniofacial bone and suture development in humans and mice is finely regulated autonomously by the bone tissue and neighbouring structures such as the underlying dura. The key feature of all craniosynostoses is suture obliteration between two bone fronts, where there is a continuous layer of mineralised bone matrix secreted by differentiated osteoblasts.

As a number of genes have been implicated in human syndromic craniosynostosis, it is sensible to focus on one of the most commonly mutated genes, *FGFR2* (Passos-Bueno et al., 2008). Most of the point mutations occur at position 342 or 278 position (Passos-Bueno et al., 1998), but the one at the 278 position (FGFR2-C278F) has been less extensively studied. It is therefore of interest to gain further understanding of this mutation and to compare the similarities and differences between other "gain-of function" mutations at positions 278 and 342. FGFR2 and TGFbetas play a main role in osteoblast proliferation, which is altered by FGFR2-C278F. The *in-vitro* model using MC3T3, R2-WT and R2-C278F cells can be used to investigate the behaviour of FGFR2-C278F transfected osteoblasts, which may be difficult to study *in-vivo*. Currently there are several models for FGFR2 "gain of function" craniosynostoses, which differ in osteoblast phenotypes, particularly in proliferation for which FGFR2 has a major role.

My hypothesis is that there is a pattern to the relationship between constitutively activated FGFR and osteoblast proliferation, differentiation and apoptosis. Furthermore, disturbed FGF signalling in MC3T3 cells expressing FGFR2-C278F will affect TGFbeta signalling.

The aims of this thesis are as follows:

1. Characterise R2-C278F cell behaviour with respect to MC3T3 and the effects of FGFR2-WT expression in R2-WT cells and compare the level of proliferation, differentiation and apoptosis with reports of other FGFR2 "gain-of-function" craniosynostosis models to in order to explain the similarities and differences.
2. Determine what are the alterations to FGF signalling in R2-C278F cells and its downstream pathways that are involved in proliferation.
3. Investigate whether TGFbeta signalling is altered by the FGFR2-C278F mutation and also if and where TGFbeta interacts with FGF signalling in R2-C278F cells with respect to proliferation and differentiation.

Chapter 2 Materials

Materials were stored at room temperature unless specified otherwise. Most of the reagents were obtained from Sigma. Any pH adjustments were made with HCl or NaOH, unless specified. PBS mentioned in this chapter is at 1X unless stated otherwise.

2.1 General Materials and Reagents

Table 2.1 General Reagent Preparations	
Description	**Preparation and Storage**
Borate Buffer 0.1 M (pH9)	Boric Acid in 800 mL dH_2O, adjusted to pH 9.0, filled to 1L and autoclaved.
HCl 2 M	600 ml: Dilute 100 ml of concentrated HCl (37.25%) into 500 ml of dH_2O
Paraformaldehyde (PFA) / Sigma	4%: 40g PFA dissolved in 1 L PBS at 70 °C and aliquoted. Diluted in PBS as required. Stored at -20 °C
Phosphate Buffered Saline (PBS) / Oxoid, Basingstoke, UK	10x Stock: 100 tablets dissolved in 1 L dH_2O, autoclaved. Diluted in dH_2O to 1x and autoclaved as required.
Diethylpyrocarbonate (DepC) water	1x: 10 tablets dissolved in 1 L dH_2O, incubated at 37 °C overnight with the lid loose to allow for effervescene, then autoclaved.

The following reagents used for treating cells were all stored at -20 ºC:

Table 2.2 Reagents for treating cells		
Description	**Stock Preparation**	**Supplier / Product Code**
Phorbol 12-myristate 13-acetate (PMA/TPA)	1 mg/ml in DMSO	Sigma / P8139
SU5402	5 mM in DMSO	Calbiochem / 572630
rhTGFbeta1	1 µg/ml with 1 mg/ml BSA in 4mM HCl	R&D systems / 240-B-010
SB431542	10 mM in DMSO	Sigma / S4317
U0126	10-20 mM in DMSO	Cell Signaling Technology Inc. / 9903

2.2 Antibodies

Primary and secondary antibodies were ready to use on purchase. The dilutions for experiments were method specific and provided either in this chapter or methods. Although not stated in the Phospho-Histone 3 (pH3) datasheet, I have confirmed that this antibody cross reacts with mouse pH3 (Appendix Figure 8.1). Primary antibody details are provided in Table 2.3. Secondary antibody details are in Table 2.4.

The α-Tubulin, Opn and Runx2 were stored at 4 ºC, while the rest of the primary antibodies were kept at -20 ºC, according to the manufacturers' instructions.

Table 2.3 Primary Antibodies

Description	Supplier / Distributer	Source / binding	Product code
α-Tubulin (B-7)	Santa Cruz Biotechnology, inc	Mouse mAb / Human α-Tubulin, Aa 149-448	sc-5286
BrdU	AbD serotec	Rat mAb Clone BU1/75	OBT0030
ERK p44/42 MAPK	Cell signaling / New England biolabs	Rabbit pAb	9102
Phospho-ERK Phospho-p44/42 MAPK(E10)	Cell signaling / New England biolabs	Mouse mAb / Human ERK, Thr202/Tyr204	9106
Gapdh (14C10)	Cell signaling / New England biolabs	Rabbit mAb	2118
Phospho-Histone H3 (Ser10)	Upstate cell signaling solutions	Rabbit pAb / Human H3, aa 7-20	06-570
Opn	DSHB	Mouse mAb	MPIIIB10
Runx2	Santa Cruz Biotechnology, inc	Rabbit polyclonal / Mouse Runx2, aa 294-363	sc-10758

HRP and Biotin conjugated secondary antibodies were stored at 4 ºC (Table 2.4). The Alexa fluorochrome conjugated antibodies were kept at 4 ºC and single use aliquots were kept at -20 °C for longer term storage.

Table 2.4 Secondary Antibodies

Description	Supplier	Dilution	Product code
Goat Anti-Mouse Alexa 488	Invitrogen	FACS 1:350	A11001
Goat Anti-Mouse HRP	Dakocytomation	ICC 1:100 WB 1:1000	P0447
Rabbit Anti-Mouse HRP	Dakocytomation	ICC 1:100 WB 1:1000	P0260
Chicken Anti-Rabbit Alexa 647	Invitrogen	FACS 1:350	A21443
Goat Anti-Rabbit Alexa 488	Invitrogen	ICC 1:350	A11034
Goat Anti-Rabbit Biotin	Dakocytomation	ICC 1:100	P0432
Rabbit Anti-Rat HRP	Dakocytomation	BrdU ELISA 1:100	P0162

2.3 Cell Culturing

Cell culture medium for maintaining cultures had 10 % v/v of FBS and 1% v/v of 10,000 U/ml Streptomycin as described in Table 2.5. Most experiments used 10% of FBS, except a few where the percentage was stated (1% or 0%). All culturing materials were prepared under the sterile conditions of an Aura B4 (Bio Air Instruments s.r.l.) tissue culture hood.

Table 2.5 Culture reagents

Description / Supplier & code	Preparation & Storage
MEM-α Medium 1X / Invitrogen, 32571	None. Stored at 4 °C
Fetal Bovine Serum (FBS) / Invitrogen	Aliquotted to 2, 20 and 50 mls. Stored at -20 °C
Streptomycin Penecillin (10,000 U/ml) / Invitrogen, 15140122	Aliquotted into 5 mls. Stored at -20 ºC
Trypsin EDTA 1x / Gibco Invitrogen, 25300054	Transferred to 5 ml aliquots. Stored at -20 ºC
Trypan Blue 1x (0.4 %) / Sigma, T8154	Aliquotted into 5 mls.
PBS	Autoclaved (see section 2.1)

2.4 FACS

Table 2.6 Reagents for FACs

Description	Preparation & Storage
7AAD	Stock 0.1mg/ml: 1 mg powder dissolved in 100 µl DMSO, then diluted in 9.1 ml PBS. Stored at -20 ºC
Permeabilisation solution	0.1 % v/v Triton X-100, 0.1 % v/v Sodium citrate in dH_2O. Stored at 4 °C
1% PFA	4% PFA diluted to 1% with PBS at 37 °C. Stored at -20 ºC
Methanol Fixative	90% Methanol in PBS. Stored at -20 ºC
Incubation buffer	0.5g BSA in 100ml PBS. Stored at 4 ºC
Flow-check™ Fluorospheres / Beckman Coulter	None
PBS	See section 2.1.1

2.5 Immunocytochemistry

Table 2.7 Immunocytochemistry reagents	
Description	**Preparation & Storage**
PFA 2%	4% PFA diluted to 2% with PBS at 37 °C
Hydrogen Peroxide solution (H_2O_2, 30%)	H_2O_2 diluted to 3 % in dH_2O shortly before use
Sigma FAST™ 3,3- Diaminobenzidine (DAB)	One gold, one silver tablet dissolved in 2 ml dH_2O
Antibody buffer	0.1% BSA, 0.5% Triton X-100 in PBS. Stored at -20 °C
Hoescht 33258 / Molecular Probes, Invitrogen	Diluted to 1.2 mg/ml in dH_2O. Stored at -20 °C
Butanol / Fisher	None
Histoclear / National Diagnosis	None
Citifluor™ / Citifluor Ltd.	None

2.6 Methylene Blue

Table 2.8 Methylene Blue reagents	
Description	**Preparation / Storage**
1% PFA Saline (0.15M)	8.77 g Sodium Chloride and 10g paraformaldehyde dissolved in 1 L dH_2O.
Borate Buffer 0.01 M (pH8.5)	Dilute 100 ml of 0.1M Borate buffer (see section 2.1.1) with 900 ml dH_2O 1:10 readjust pH to 8.5.
Methylene Blue solution	10g of Methylene blue powder (Gurr®) diluted in 0.01 M Borate Buffer (pH8.5) to 1% w/v.
Ethanol 0.1 M HCl	1.25 ml of 2 M HCl dissolved in 25 ml dH_2O, then mixed with 25 ml of 100% Ethanol

2.7 Protein extraction, gel electrophoresis and western blotting

Table 2.9 Reagents for protein extraction, gel electrophoresis and western blotting	
Description	**Preparation / Storage**
Lysis (RIPA) Buffer	5 % of 3 M NaCl, 1 % Nonidet P-40, 1 % of 10 % SDS, 5 % of 1 M Tris pH 8.0 in dH_2O. Stored at 4 °C
Proteinase inhibitor / Complete, Roche	25x Stock: 1 tablet dissolved in 1 ml dH_2O. Stored at -20 °C
Sodium Orthovanadate (Na_3VO_4) / Sigma	100 ml of 200 mM Stock: 18.39 g of Na_3VO_4 in 80 ml dH_2O. The pH was adjusted to 10.0 with NaOH, boiled until colourless and cooled to room temperature. The pH adjustment, boiling and cooling were repeated until the solution remained colourless at room temperature. Stored at -20 °C
Loading Buffer	10 % 1 M Tris pH 6.8, 20 % Glycerol, 1 % 2-mercaptoethanol, 10 % SDS and a few crystals of Bromophenol blue in dH_2O. Stored at 4 °C
Running Buffer	10x Stock: 30 g/L Tris base, 144 g/L glycine and 10 g/L SDS in 1L dH_2O. Diluted 1:10 before use.
Transfer Buffer	0.5x Running buffer and 20 % methanol
Tris Buffered Saline (TBS)	10x Stock: 80 g NaCl, 2 g KCl and 30 g Trizma base dissolved in 800 mls dH_2O. The pH adjusted to 8.0 with concentrated HCl and filled to 1 L.
0.1% TBST	TBS with 0.1% Tween 20
Blocking Buffer	5 % milk protein in PBS with 0.1% Tween

2.8 RNA extraction, Reverse Transcription and PCR

RNA extraction and reverse transcription were carried out in two steps, allowing analysis of multiple genes from a single source of RNA.

Table 2.10 RNA extraction reagents	
Description	**Preparation & Storage**
TRI®-Reagent (Sigma)	None. Stored at 4 °C
Chloroform (Sigma)	None. Stored at 4 °C
2-propanol (Sigma)	None.
75% Ethanol + 25% DepC water	As described.

Table 2.11 Reverse Transcription	
Description / Supplier	**Preparation & Storage**
pN6 (Hexamer) 10pM / Roche	Diluted to 10pM in DepC water. Stored at -20 °C
10 mM dNTPs / Promega	2.5 µl of 100mM of each dNTP (ATP, GTP,TTP and UTP) in 90 µl of DepC water. Stored at -20 °C
RNAsin / Promega, N211B	None. Stored at -20 °C
MMLV / Promega , M170B	None. Stored at -20 °C
5x RT Buffer / Promega, M531A	None. Stored at -20 °C

2.8.1 PCR and Real time PCR reagents

Two types of taq polymerases were used in the course of this thesis, due to introduction of the GoTaq® range from Promega and the company's termination of sale of the old polymerase (Table 2.12).

Table 2.12 PCR reagents	
Description / Supplier	**Preparation & Storage**
10x Mg free Buffer / Promega	None. Stored at -20 °C
25 mM $MgCl_2$ / Promega	None. Stored at -20 °C
Taq Polymerase / Promega	None. Stored at -20 °C
5x GoTaq®Flexi Buffer / Promega, M891A	None. Stored at -20 °C
5x GoTaq®DNA Polymerase / Promega, M830B	None. Stored at -20 °C

Two methods were used for real time PCR, either with Taqman Gene Expession Assays and a TaqMan Master Mix or PCR primers with a SYBR green master mix (Table 2.13).

Table 2.13 Real time PCR reagents	
Reagent / Supplier	**Storage**
TaqMan® Fast Universal Master Mix (2X) with No AmpErase® UNG / Applied Biosystems	-20 °C
QuantiTect SYBR Green PCR Kit / Qiagen, 204143	-20 °C

2.8.2 PCR and Real time PCR Primers

Table 2.14 PCR Primers

Primer pair & length	Accesssion Number	Sequences (*forward*, reverse) (5'-3')	Product (bp) / Cycle no.	Tm (°C)
18S F=20, R=20	X00686	*GTC TGT GAT GCC CTT AGA TG* AGC TTA TGA CCC GCA CTT AC	177	60
GAPDH F=22, R=20	M32599	*TTC CAG TAT GAC TCC ACT CAC G* GGA TGC AGG GAT GAT GTT CT	492 / 24	55,57 ,60
FGF1 F=20, R=21	NM_010197	*ACC GAG AGG TTC AAC CTG CC* GCC ATA GTG AGT CCG AGG ACC	387 / 35	55
FGF2 F=20, R=24	NM_008006	*GCC AGC GGC ATC ACC TCG CT* TAT GGC CTT CTG TCC AGG TCC CGT	429 / 35	55
FGF18 F=19, R=20	NM_008005 .1	*AAG ACA TTC AAG TCC TGG G* AGC CCA CAT ACC AAC CAG AG	244 / 35	60
FGFR2IIIc F=24, R=24	M86441	*CCC ATC CTC CAA GCT GGA CTG CCT* CAG AAC TGT CAA CCA TGC AGA GTG	315 / 33	57
Human FGFR2 F=20, R=20	Z71929	*ATG GTG CGG AAG ATT TTG TC* TAG AAT TAC CCG CCA AGC AC	630 / 35	62
Osteocalcin F=20, R=20	NM_031368	*TGA GGA CCC TCT CTC TGC TC* GCG TCT GTA GGC GGT CTT TA	266	60

2.8.3 Taqman Real time PCR gene Expression Assays

Gene expression assays were purchased from Applied Biosystems (Table 2.15).

Table 2.15 Gene Expression Assays

Gene Expression Assay	**Part no / ID**
Eukaryotic 18S rRNA	Part no: 4352930E
Fgf1	Mm00438906_m1
Fgf2	Mm00433287_m1
Fgf18	Mm00433286_m1
GAPDH	Part no: 4352932E
TGFbeta1	Mm00441724_m1
TGFbeta2	Mm004366952_m1
TGFbeta3	Mm00436960_m1
Runx2	Mm01269515_mH
Spp (Osteopontin)	Mm01611440_mH
Twist1	Mm00442036_m1
Akt1	Mm00437443_m1
Smad1	Mm00484721_m1
Smad2	Mm00487530_m1
Dlx5	Mm00438430_m1

2.9 Agarose Gel Electrophoresis

Table 2.16 Agarose Gel Electrophoresis	
Description	**Preparation & Storage**
Gensieve LE agarose / Flowgen	None
0.0025 % Ethidium Bromide (EB)	None
0.5 M EDTA (pH8)	Stir 58.44g of EDTA powder into 300ml dH_2O. Raise the pH with NaOH until pH 8. Add dH_2O to 400ml.
TAE buffer	Mix 242g of Tris base powder into 100ml of 0.5M EDTA (pH8) and 57.1ml glacial acetic acid under a fume hood. Add water to 800ml level and stir until all the powder is dissolved. Fill to 1 L with dH_2O.
5x Orange G	Mix DepC water, 0.5 g/ml sucrose, 2.5 mg/ml Orange G and 0.25 mg/ ml Sodium azide. Stored at -20 °C
1kb DNA ladder Hyperladder IV / Bioline	None. Stored at 4 °C or -20 °C for long term storage
Formamide (BDH)	None. Store in a cabinet

Chapter 3 Methods

Details such as blocking and washing solutions are tabulised in the Materials chapter.

3.1 Cell Culture and harvesting

The cell lines MC3T3, R2WT2 and R2-C278F were grown and maintained in T75 culture flasks (TPP) with 10 to 12 ml of culture medium containing Minimum Essential Medium Alpha (MEM-α) medium with Glutamax (Gibco™, Invitrogen), 10% fetal bovine serum (FBS) and 1% of penicillin and streptomycin (100 U/ml). Cultures were seeded at a density of 20,000 cells per cm^2 and were maintained by replating every three days. Cells were observed for cuboidal morphology at confluence and were not used for analysis beyond 65 passages, because at this stage MC3T3-E1 has been reported to behave like aged osteoblasts, which have an altered response to TGFbeta1 (Chung et al., 1999).

Replating was performed as follows: Cultures in T75 flasks were washed prior to trypsinisation by replacing the culture medium with 8 ml PBS and then removing the PBS. Cells were trypsinized with 1 ml trypsin-EDTA (Invitrogen) for 5 minutes, then neutralised by resuspending with 5 ml of culture medium. This was transferred into falcon tubes and centrifuged at 1000 rpm for 5 minutes. The supernatant was removed, leaving the cell pellet which could be used for experiments. The cell pellet was resuspended in 5 ml culture medium before counting or directly seeding new cultures. When counting, 1.5 million cells from each of the cell lines were transferred into new T75 flasks containing 10 ml of culture medium. Otherwise, this was approximated to 1/12, 1/10 and 1/5 of MC3T3, FGFR2-WT and C278F cell suspensions respectively. For experimental cultures, the volumes of PBS, Trypsin-EDTA and culture medium were adjusted according to the size of culture plate or flask.

Counting was performed at three days in culture, using a dilution factor of 10 (50 µl of cell suspension into 200 µl Trypan Blue and 250 µl PBS) and counting on a haemocytometer (Bright Line®, Reichert) and averaging the totals counted from the 8 large corner squares. Where numbers were too high (above 50 per large square), the dilution factor was increased to 20. The cell number calculation was as follows:

$$Cells\ per\ ml = \frac{Cells\ counted}{8} \times Dilution\ Factor \times 1 \times 10^4\ cells/ml$$

Unless stated otherwise, cells for all experiments in this thesis were seeded at 20,000 per cm^2 for which the approximate numbers are given in Table 3.1.

Table 3.1 Number of cells to seed at 20,000 cells per cm^2

Plate	Diameter (cm)	Surface Area (cm^2)	Number of cells
T75	N/A	75	1.5 million
T25	N/A	25	0.5 million
6 well	3.4	9	182,000
12 well	2.1	3.5	70,000
24 well	1.5	1.8	35,000
96 well	0.8	0.5	10,000

3.1.1 Experimental cultures and medium compositions

Cells were seeded in the cell culture medium defined at the beginning of Section 3.1 for three hours before replacing with the experimental culture medium. Unless otherwise stated, the experimental culture mediums contained Minimum Essential Medium Alpha (MEM-α) medium with Glutamax (Gibco™, Invitrogen), 10% fetal bovine serum (FBS) and 1% of penicillin and streptomycin (100 U/ml). In experiments where 0% or 1% serum used, the remaining volume of FBS was replaced with MEM-α medium with Glutamax.

In TGFbeta1 treatment experiments, the control mediums contained 1 mg/ml BSA in 4mM HCl. The control mediums for PMA, SU5402, and U0126 treatment contained DMSO. The DMSO concentration in both control and experimental mediums never exceeded 0.2% v/v, as this was reported to induce differentiation and PKC signalling in MC3T3-E1 cells (Cheung et al., 2006).

3.1.2 RT-PCR and Real time PCR

Cells were seeded into T25 flasks. For harvesting, cells were washed in 4 ml PBS, trypsinized with 500 µl Trypsin-EDTA for 5 minutes at 37 ºC and neutralised in 4.5 ml of culture medium. Samples were centrifuged for 5 minutes at 1000 rpm and the supernatant aspirated before placing the pellet on ice and stored at -80 °C. Pellets were then used for RNA extraction.

3.1.3 FACS (Live cell analysis)

Cultures were seeded on a 12 well plate. For harvesting, the cultures were washed in 1 ml PBS, trypsinized in 100 µl of trypsin-EDTA for 5 minutes at 37 ºC and neutralised with 2 ml culture

medium. Samples were transferred to 5 ml FACS tubes and centrifuged (5 minutes at 1000rpm). The supernatant aspirated and the tubes placed on ice for analysis.

Samples intended for cell cycle analysis were resuspended in permeabilizing solution (300 µl) and kept on ice for up to 2 hours before analysis. Samples for cell counting and apoptotic studies were resuspended in PBS (300 µl) and kept on ice. Just before FACS analysis a 20 µl aliquot of 7 aminoactomycin D (7AAD) was added to all samples.

3.1.4 FACS (Fixed cells)

Cells were cultured on a 12 well plate in 2 mls of medium. Cells were trypsinised, neutralised, transferred to 5 ml falcon tubes and centrifuged at 1000 rpm for 5 minutes. The pellet was loosened by tapping before resuspending in 500 µl of 1% PFA in PBS to avoid clumping. Fixation was for 10 minutes at 37 ºC. The fixed samples were cooled on ice for 1 minute and centrifuged at 1000 rpm for 5 minutes. The supernatant was aspirated and the pellet resuspended and permeabilised in 90% methanol in PBS for 30 minutes on ice. Samples were stored for up to 7 days at -20 ºC before FACs immunostaining.

3.1.5 Immunocytochemistry

A 24 well plate was used to grow cells on sterilised 13 mm diameter coverslips. To prepare samples, the coverslips were washed with PBS and then fixed with 2% PFA in PBS at room temperature for 30 minutes or 4 °C overnight.

3.1.6 Methylene blue cultures

Cells were suspended in 200 µl of cell culture medium and seeded onto 96 well plates. Care was taken not to swirl the plates to avoid collecting cells at the centre of the wells. The medium replaced with 100 µl of the experimental medium. The experimental medium was replaced every 24 hours for 1, 2 or 3 days. In the experiments using TGFbeta1 or PMA with inhibitors such as SU5402 or U0126, the normal culture medium was replaced with 50 µl cell culture medium with inhibitor for 30 minutes, prior to adding 50 µl of cell culture medium with inhibitor and a 2x concentration of the TGFbeta or PMA.

3.1.7 Western blot cultures

Cells were seeded in a T25s and cultured for 2 or 4 days before harvesting. See section 3.10.1 for details for protein extraction.

3.1.8 Freezing

A medium for freezing cells composed of 8% DMSO, 20% FBS and MEM-Alpha medium was made and placed on ice, along with labelled cryotubes. After counting (see section 3.1 Cell Culture and harvesting), 6 million cells were transferred to falcon tubes tubes to be centrifuged (1000 rpm for 5 minutes). Supernatants were removed and each pellet resuspended with 3 ml of the medium for freezing and 1 ml aliquots were transferred to cryovials which were placed on dry ice. The cryovials (containing around 2 million cells) were frozen at -80 ºC overnight and placed in liquid nitrogen for long term storage.

3.1.9 Thawing

Cells were warmed rapidly in a 37 °C incubator and diluted in 10 ml of ice chilled fresh culture medium (MEM-Alpha medium, 10 % FBS and 1 % of penicillin and streptomycin) to slow the cell metabolism. The cells were then centrifuged at 1000 rpm for 5 minutes and the DMSO containing supernatant was removed by aspiration. The pellet was resuspended in 10 ml of fresh culture medium and plated to a T25 until 70% confluent, when they were transferred to a T75.

3.2 Cell imaging and categorisation

Cells were viewed in phase with an inverted light microscope (Axiovert 135M, Zeiss). A computerised system (Orbit, Improvision®) was used to focus on the cells. Photographs at 5, 10, 20 and 40x magnification were taken with either a Hamamatsu digital camera (C4742-95, Hamamatsu) controlled by the Openlab™ software (Improvision®) or a Hamamatsu ORCA-ER camera and with the Volocity™ software (Improvision®). These were exported as tiff files for publication and imported into Macromedia Fireworks MX® in a 1024 x 768 pixel canvas for resizing, cropping and adjusting for brightness and contrast. Images were selected (where possible) such that cell population densities were similar between the cell lines to compare morphologies.

For the cell categorisation experiment, a main grid of 250 x 250 pixel squares was overlayed onto the images with a smaller grid of 50 x 50 pixels. The same method for counting on a

Haemocytometer was used in order to count and categorise cells more accurately and to avoid double counting of cells.

3.3 FACS

7-Aminoactinomycin D (7AAD, Sigma) intercalates double stranded DNA between cysteine and guanine bases. Unlike Propidium Iodide (PI), the absorbance / emission range allows detection of other fluorochromes, giving the flexibility of adding other fluorescent markers for simultaneous measurements.

3.3.1 Cell counting and apoptosis

The cell pellet preparations in the 5 ml falcon tubes were knocked, in order to resuspend the cells and placed on ice. Prior to FACS analysis, 25 µl of fluorospheres (1000 beads per µl, Flow-check™, Beckman Coulter) were added to the samples. To assess cell viability, 20 µl 7AAD was added to each of the samples.

Samples were well mixed then analysed using a Beckman Coulter Epics XL Flow cytometer. A 488 nm laser was used to excite the 7AAD and the emission was detected at 675 nm with a band pass filter. Approximately 30,000 events were collected and 7AAD was used to label apoptotic cells. Beads enabled counting of cells by the formula:

$$Total\ cells\ in\ sample = \frac{Beads\ Added}{Beads\ Counted} \times Cells\ Counted$$

3.3.2 Cell cycle

The cell pellet was resuspended in permeabilizing solution (300 µl sodium citrate (0.1%) and Triton X-100 (0.1%) in dH_2O) and kept on ice for up to 2 hours before analysis. The DNA was intercalated with 20 µl of 7AAD and the tubes tapped lightly just prior to flow cytometry analysis (Epics XL, Beckman Coulter). Absorption of the 488 nm argon laser by 7AAD, resulted in emission in FL3 (peaked at 647 nm), which was detected at 675 nm with a band pass filter and the data recorded, using the EXPO32 software (Beckman Coulter).

The magnitude of a peak reading for individual cells and clumps of cells may be similar and could be hard to distinguish (Figure 3.1 A). Therefore a plot of peak vs area (FL3 fluorescence) was made in order to visualise regions of cell fragments, single cells and clumps of two or more cells (Figure 3.1 B). From G0 to M phase, the DNA becomes progressively more condensed as

shown by an increasing Peak value. The area also increases as more DNA is present, covering a larger area. A two cell clump would give relatively similar peak values, as the DNA is as condensed as other single cells, however a broad area would be detected. Doublet discrimination was performed by selecting the region of single cells (gating).

The selected region was plotted as a frequency vs area (Figure 3.1 C). The resulting curve was comprised of G0/G1, S and G2/M phase curves, which were mathematically analysed using MultiCycle for Windows (Phoenix flow systems, San Diego). The S phase was determined using the Dean and Jett method (Dean and Jett, 1974). This data was expressed as a graph that could be expressed as three smaller histograms (Figure 3.1 D).

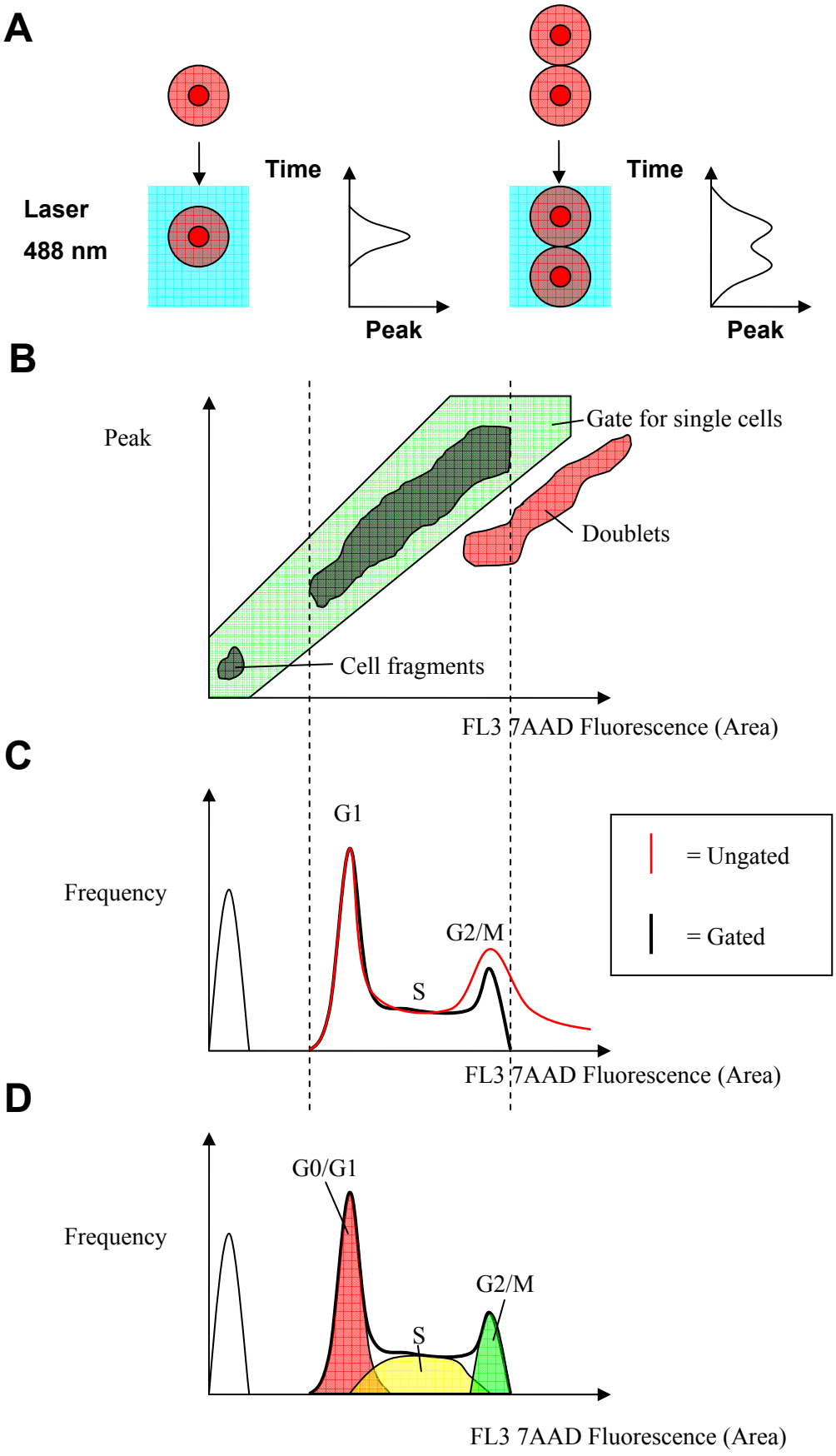

Figure 3.1 Doublet Discrimination and cell cycle analysis in flowcytometry

3.3.3 FACS immunocytochemistry

Methanol fixed samples were washed by adding 2 ml of incubation buffer (0.5% BSA in PBS) and centrifuging for 5 minutes at 1000 rpm before removing the supernatant by flicking out into a sink. The same wash step was repeated, except that on the second wash, vacuum pipetting was used in order to keep sample volumes similar for antibody incubations. The pellet was resuspended in 100 µl of incubation buffer for 10 minutes for blocking. 50 µl of primary antibody was added to the samples, then mixed and allowed to incubate for 1-2 hours. Samples were washed twice described previously. 50 µl of secondary antibody was added and incubated for 30 minutes. A final two washes were performed as described and then resuspended in 500 µl of PBS before analysis on the CyAn Flowcytometer (Dako).

3.3.4 Antibodies and conditions

Primary antibodies were added as 50 µl to the 100 µl of blocking solution; therefore the dilutions given below do not reflect the final antibody concentration in Table 3.2:

Table 3.2 Antibodies and conditions for FACS immunocytochemistry

1ry Ab	1ry Dilution	Origin	2ry Ab	2ry Dilution
Opn	1:10	Mouse	Goat Anti-Mouse Alexa 488	1:350
PCNA	1:100	Mouse	Goat Anti-Mouse Alexa 488	1:350
H_3	1:100	Rabbit	Chicken Anti-Rabbit Alexa 647	1:350
Runx2	1:10	Rabbit	Chicken Anti-Rabbit Alexa 647	1:350

Higher concentrations of primary and secondary antibodies were often higher than in standard immunocytochemistry, partly to compensate for the diluting effects of residual solution in FACS tubes after washing.

3.3.5 Analysis of pH3 immunostaining

To analyse cells for pH3 staining, viable cells were first gated, to exclude cell fragments and other debris (Figure 3.2 A). The pH3 was stained with anti-pH3 antibody and an alexa 647 conjugated secondary. Cells were plotted on FITC and alexa 647 wavelengths confirm a low level of the background stain in the negative control samples (Figure 3.2 B). The pH3 positive stains were also visualised on this plot to observe the quality of the stain, a good staining showing a space between the cells of high and low intensity staining (Figure 3.2 D). This was

then visualised along an Alexa 647 vs frequency axis and a gate (R29) was placed on this axis to exclude low background stains, to be used for the positive staining (Figure 3.2 E). This gate was adjusted to the negative control with the highest background. Any percentage of artefacts within the gate from the negative samples was subtracted from the positive samples for each cell line. A good pH3 stain would display two groups of cell populations (one above the other) along the alexa 647 axis with a space between them. Finally the percentage of pH3 positive cells were measured by taking the gated pH3 positive as a percentage of the total cells analysed.

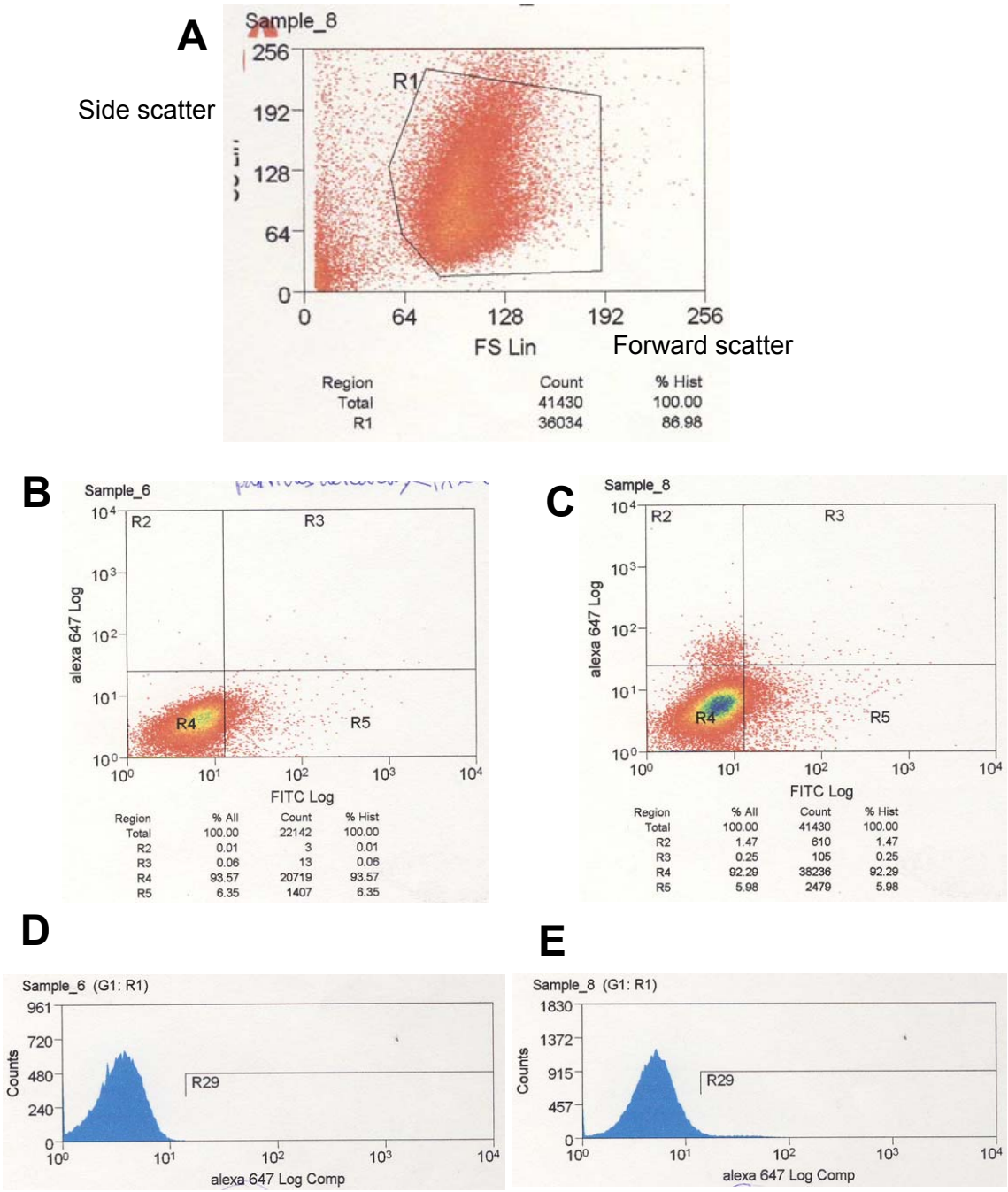

Figure 3.2 Gating cells for FACS analysis and for positive pH3 FACS stains

3.4 Immunocytochemistry

3.4.1 Enzymatic and Chromatographic stainings

Fixative was removed from the samples with three 10 minute PBS washes. Endogenous peroxidases were quenched with hydrogen peroxide (H_2O_2) solution (see section 3.5.2) for 20 minutes. After washing twice with PBS for 5 minutes, samples were blocked for 1 hour in 50 µl of either 5 or 10% Goat serum in PBS. The block was replaced with primary antibody in a humidified chamber overnight at 4 ºC. Following three 10 minute PBS washes, secondary HRP antibodies were incubated with the samples for 1 hour at room temperature, before another three 10 minute PBS washes. DAB was prepared and incubated with the samples, which were observed under light microscope until the brown product colour appeared whereby dH_2O was added to quench the reaction. Two 5 minute butanol washes and then two 5 minute histoclear washes were performed to dehydrate samples, before mounting on slides with a drop of DPX per coverslip to preserve the sample.

Where staining was weak, the secondary antibody used was biotin conjugated instead of an HRP conjugated antibody. ABC complex was made (A:B:PBS as 1:1:100 respectively). Samples were incubated with ABC in the dark for 30 minutes. ABC was removed with three 10 minute PBS washes before the DAB incubation.

3.4.2 Summary of Antibodies and conditions

Conditions for antibody use are given in Table 3.3:

Table 3.3 Antibodies and conditions for Immunocytochemistry (enzymatic)

1ry Ab	Block	Dilution	H_2O_2 solution
ERK	5 % Goat serum in PBS	1:100 in block	3% H_2O_2 in dH_2O
Gapdh	5 % Goat serum in PBS	1:800 in block	3% H_2O_2 in dH_2O
H_3	10 % Goat serum in antibody buffer	1:300 in antibody buffer	3% H_2O_2 in dH_2O
Opn	10 % Goat serum in antibody buffer	1:500 in antibody buffer	6% H_2O_2 & 10% Methanol in PBS
Runx2	10 % Goat serum in antibody buffer	1:300 in antibody buffer	6% H_2O_2 & 10% Methanol in PBS

Goat anti-rabbit HRP secondary antibodies were used (1:300) on primary antibodies with rabbit origin. For primaries sourced from mouse, rabbit anti-mouse HRP antibodies (1:300) were used.

3.4.3 Immunofluorescent stainings

Fixative was removed with three 10 minute PBS washes and samples were blocked for 1 hour in 50 µl of 10% Goat serum in PBS. The block was replaced with primary antibody in a humidified chamber overnight at 4 ºC, followed by three 10 minute PBS washes. Hoescht dye and flurochrome conjugated secondary antibodies were incubated with the samples for 1 hour in the dark at room temperature, before another three 10 minute PBS washes in the dark. The coverslips were mounted onto slides with a drop of Citifluor^{TM} per coverslip. The edges were dried off with a clean tissue, sealed with nail varnish and and kept in the dark at 4 °C.

3.4.4 Summary of Antibodies and conditions

Antibodies were diluted into antibody buffer (see section 2.6 Immunocytochemistry) and used as in Table 3.4:

Table 3.4 Antibodies and conditions for Immunofluorescent staining

1ry Ab	1ry Dilution	Origin	2ry Ab	2ry Dilution
Gapdh	1:800	Mouse	Goat Anti-Mouse Alexa 488	1:350
Opn	1:500	Mouse	Goat Anti-Mouse Alexa 488	1:350
PCNA	1:100	Mouse	Goat Anti-Mouse Alexa 488	1:350
ERK	1:100	Rabbit	Goat Anti Rabbit Alexa 488	1:350
H_3	1:300	Rabbit	Goat Anti Rabbit Alexa 488	1:100
Runx2	1:300	Rabbit	Goat Anti Rabbit Alexa 488	1:350

3.5 Methylene Blue Assay

The methylene blue assay protocol was adapted from that described in Oliver (1989). After culturing in 96 well plates, cell mediums were drained using a multichannel pipette and each well fixed with 100 µl of 4% PFA in 0.15 M saline for 30 minutes. Fixative was removed by a pronating flick of the wrist into a sink and the surface of the plate inverted and patted dry with at towel. 100 µl of methylene blue solution was added to each of the previously fixed wells for 30 minutes. The dye was removed by a pronating flick of the wrist as described before. The plate was placed upside down on a paper towel to remove the methylene blue. Excess methylene blue in each well was washed with 200 µl of 0.01 M borate buffer, by filling from left to right with a multichannel pipette, before flicking into the sink as described previously. The second wash was performed by filling from right to left, to ensure that the washing time per well was

the same on average. The first and second washes were repeated. The plate was then immersed in a tank of 0.01 M borate buffer and contents flicked out as before. The methylene blue that had stained the cells was extracted by adding a 100 µl mixture of 50% Ethanol and 50% 0.1 M HCl to each well.

Wells were shaken gently and absorbance at 650 nm (A_{650}) measured in each well with a microplate reader (Revelation v4.21, Dynex Technologies, inc) and the backround from empty wells subtracted. Samples were left for 1 to 2 hours at room temperature or overnight at 4 °C before measurement to allow most of the dye to exit the cells.

3.6 RNA extraction and Reverse transcription

The RNA extraction and reverse transcription protocols were the same for both RT-PCR and Real time PCR analysis. All reagents used were RNAse and DNase free.

3.6.1 RNA extraction

RNA extraction was based on the Sigma TRI-reagent protocol. Sample pellets from culturing were resuspended in 1 ml TRI®-Reagent, transferred to 1.5 ml tubes and pipetted until the pellet was no longer visible. The samples were left at room temperature for 5 minutes before adding 200 µl of chloroform and shaken for 15 seconds and left to stand for 15 minutes. A centrifuge was pre-cooled and the samples spun at 12000 rpm for 15 minutes at 4 °C. Three phases were formed from top to bottom; a clear phase, a white solid phase and a pink phase. The clear phase was transferred to new 1.5 ml tubes with complete avoidance of the visible solid phase (containing gDNA). 0.5 ml of isopropanol was added and the solution was mixed and left for 5 minutes at room temperature. The samples were then centrifuged at 12000 rpm for 10 minutes at 4 °C and the supernatant was removed. A solution of 75% ethanol in DepC water was added to the remaining pellet. This was centrifuged at 7500 rpm for 5 minutes at 4 °C. The supernatant was removed by pipetting, leaving the RNA pellet to partially dry within 2 minutes. The RNA pellet was resuspended in 40 – 50 µl of DepC water. A 1.5 µl aliquot of RNA was assessed for concentration and ratio (260/280), using the Nanodrop (ND-1000) and the ND-1000 software (v3.1.0). Ratios of 1.8-2.0 were used for qPCR. Agarose gel electrophoresis of the RNA was used to check the quality of the sample when suspect (ratios of 1.7 to 1.8).

3.6.2 Reverse Transcription (RT)

The RNA was diluted to 1 ng/µl in a 10 µl volume containing 2 µl of the random hexamer pN6 (10 pM) and DepC water. This was vortexed and heated to 70 °C for 10 minutes in a PTC-100 thermal cycler (MJ research inc.), before cooling for 5 minutes. The annealed RNA solution was mixed with 4 µl of RT buffer, 2 µl of 10 mM dNTPs, 1 µl RNAsin, 1 µl MMLV (reverse transcriptase) and DepC water. The final solution was heated in a thermal cycler (PTC-100) to 42 °C for 1 hour for reverse transcription and 95 °C for 10 minutes for denaturing the MMLV. Summaries of the components are given in Table 3.5 and Table 3.6.

Table 3.5 Components for annealing

Component	Volume
RNA	(1 ng / µl)
pN6 (Hexamer) 10pM	2
DEPC water	To fill to 10 µl
Total	10

Table 3.6 Components for reverse transcription

Component	Volume (µl)
Annealed solution	10
RT Buffer	4
10 mM dNTPs	2
DEPC water	2
RNAsin	1
M MLV	1
Total	20

3.7 PCR

PCR was performed in 25 µl volumes. PCR master mix was made in order to reduce variability of the PCR reactions and stored at -20 °C. The full PCR solution was made in Table 3.7 or Table 3.8. Gapdh PCRs were run as a control gene expression against which the target genes were normalised. Control samples of E13.5 mouse head were used for positive and negative controls for the primers.

Table 3.7 PCR Master mix		
	PCR Master mix	**Full solution**
Component	**Volume (µl)**	**Volume (µl)**
DepC water	14.9	14.9
10x mg free Buffer	2.5	2.5
10 mM dNTPs	2	2
25 mM $mgCl_2$	1.5	1.5
cDNA		2
10 µM Primer (Forward)		1
10 µM Primer (Reverse)		1
Taq Polymerase		0.1
Total Volume	20.9	25

Table 3.8 PCR Master mix with Gotaq® reagents		
	PCR Master mix	**Full solution**
Component	**Volume (µl)**	**Volume (µl)**
DepC water	12.4	12.4
5x GoTaq®Flexi Buffer	5	2.5
10 mM dNTPs	2	2
25 mM $mgCl_2$	1.5	1.5
cDNA		2
10 µM Primer (Forward)		1
10 µM Primer (Reverse)		1
GoTaq®DNA Polymerase		0.1
Total Volume	20.9	25

The PCR was performed on a PTC-100 (MJ Research Inc.) with the following command list:

1. 95 °C for 3 minutes
2. 95 °C for 30 seconds
3. (Annealing temperature) for 30 seconds
4. 72 °C for 1 minute
5. Goto step 2 for the maximum number of cycles required (see Table 2.14)
6. 4 °C for 10 minutes
7. END

The PCR products were then either kept at -20 °C or run on agarose gel.

3.8 Agarose Gel electrophoresis

RNA and PCR products were visualised using agarose gel electrophoresis. Gels were made on a basis of of 1.5 % agarose and 0.1 µl/ml of 0.0025 % ethidium bromide (EB) in TAE buffer depending on the volume requirements (see Table 3.9). The gel tray and combs were arranged and levelled with a circular spirit level. Agarose powder was weighed and transferred to a conical flask. TAE buffer was added to complete the gel volume. The solution was heated in a 900W microwave until all the powder had dissolved and then cooled to a hand hot temperature (~60 ºC). Ethidium bromide was added at a ratio of 1:10,000 and mixed into the solution before pouring into the gel tray for DNA intercalation. The gel was set for at least 30 minutes, then lowered into an electrophoresis tank (Horizon®, Life technology) and completely submerged with TAE buffer. 6 µl of 5x Orange G loading buffer was added and mixed into each 25 µl PCR product. 10 µl was loaded into each sample well and 5 µl of 1kb DNA ladder was loaded to reference the product size. The gel was run at 100 mV at 80-100 mA for at least 45 minutes to give separation of the bands of the ladder.

Table 3.9 Gel electrophoresis details

Gel Vol. (ml)	Agarose (g)	Microwave (minutes)	Ethidium bromide (µl)	Gel tank model	Gel run time
50	0.75	2	5	58	45 min +
100	1.5	3	10	11.14	1 hr +
250	3.75	5	25	20.25	1 hr 30 min +

3.8.1 Densitometry

Gels were then imaged using UV light with a camera capture system (Uvidoc system, Uvitec). Image files were saved and analysed by densitometry using Labimage (v2.7.1, Kapelan). Bands were cropped and measured for area. The data for the genes of interest were normalised with the endogenous control (*Gapdh*) for each sample. At least 3 PCR runs were performed for the same samples to account for variability in the technique.

3.8.2 RNA gel

The gels were prepared as describe previously. 8 µl formamide (BDH), 1 µl of RNA and 2 µl of 5x Orange G loading buffer were mixed in a fume hood (due to the toxicity of formamide). Hyperladder VI was used for relative size monitoring. The gel was run for 1 hour at 100 V, 80 mA. Two bands of 28S and 18S rRNA for an intact RNA would be present, or a smear below the 18S rRNA if there was significant degradation of the RNA (Figure 3.3). A complete loss of bands or a single smear would indicate degradation of most of the RNA.

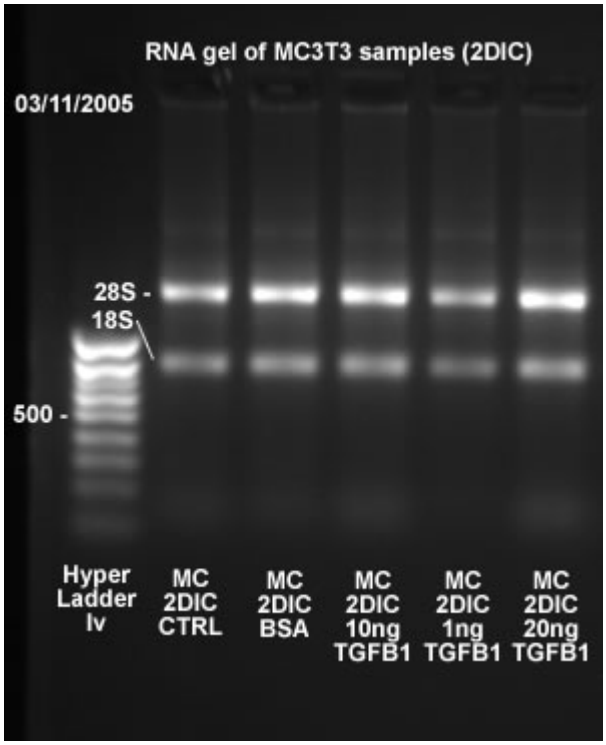

Figure 3.3 RNA gel run showing 28S and 18S bands

3.9 Real time PCR

Most of the real time PCR analysis in this thesis was carried out using Taqman® Gene Expression assays, unless stated that SYBR green was used. The Taqman® Gene Expression assays consist of forward and reverse primers with a FAM™ dye-labelled Taqman® MGB probe conjugated to a quencher molecule to bind both forward and reverse sequences. During transcription, the 5' nuclease activity of Taq DNA polymerase acts on the probe, releasing the FAM™-labeled MGB from its quencher molecule (Figure 3.4). This results in fluorescence proportional to the number of probes cleaved by the polymerase. The cDNA for PCR was prepared as described in section 3.7. Gene expression was relatively quantified using the CT method. Embryonic mouse head E13.5 was used as a calibrator sample.

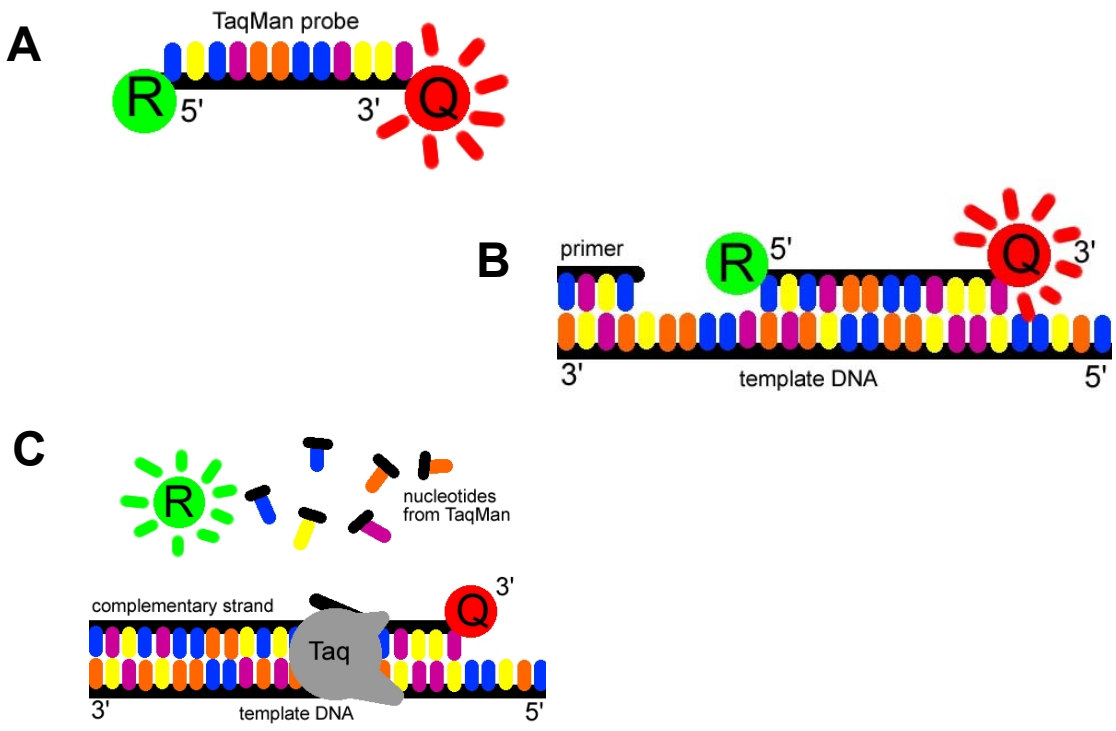

Figure 3.4 Taqman Real time PCR: the probe binding system

A: The Taqman probe is a primer with a fluorescent reporter dye (R), near a quencher fluorophore (Q), which reduces the fluorescence of the dye. **B:** The primer part of the probe binds to the cDNA. **C:** As the Taq polymerase synthesises the complemetary strand, the exonuclease activity on the probe releases the reporter dye from the proximity of the quencher, whereby it (R) becomes strongly fluorescent and is then detected by the real time PCR machine. Adapted from:
(http://www.bio.davidson.edu/Courses/Molbio/MolStudents/spring2003/Pierce/realtimepcr.htm)

A titration test was performed on the following genes (ordered from left to right); *18S* rRNA, *Tgfbeta1*, *Tgfbeta2*, *Tgfbeta3*, *Runt related transcription factor 2* (*Runx2*), *Osteopontin* (*Opn*), *Twist1*, *Akt1*, *Smad1*, *Smad2* as detailed in the Materials Chapter (see Section 2.8.3). The cDNA from mouse head was diluted 2 fold, 4 fold, 8 fold and 16 fold. The 4 fold dilution was found to be optimal for analysis. Mouse head cDNA was diluted with DepC water to 1/8 of the original concentration and used as a calibrator sample. TaqMan® Fast Universal Master Mix (2X) with No AmpErase® UNG was used. All necessary components were added to the wells (Table 3.10) and cycled for 40 or 50 repetitions of step 2 on the ABI 7500 FAST machine with a programme outlined in Table 3.11.

Table 3.10 Real time reation and PCR master mix composition

Component	µl/sample	Master mix for 10 samples
Master mix (2x)	12.5	125
Gene expression assay (20x)	1.25	12.5
cDNA	2.5	-
H_2O	8.75	87.5
Total	25	225

Table 3.11 Real time PCR cycling programme

Step	Temperature (°C)	Time (mm:ss)
1	50	2:00
	95	10:00
2	95	0:15
	60	1:00

Measurements were taken at the end of step 4.

3.9.1 Relative Quantification (RQ) of Real time PCR data

The amount of the gene target was normalised to endogenous reference and relative to the mouse head calibrator sample. The analysis was performed with the comparative CT method for relative quantification, using calculations completed by the ABI software. Sample data were entered into Microsoft Excel for graph plotting and into SPSS for statistical analysis.

3.9.2 Validation of Real Time PCR data

The 18S rRNA gene was used as a control gene for relative quantification. The gene expression assay (GEX) for 18S (Part no: 4352930E) is not intron spanning, unlike previous target gene expression assays. Therefore the 18S GEX would not distinguish between cDNA and gDNA. RNA extraction (section 3.7) was performed without visible contamination from gDNA. Contamination was further analysed by reverse transcription of DepC water, and mRNA (substituting the Reverse Transcriptase with DepC water). The sample material was diluted 4 fold as described earlier and compared to the positive controls. CTs of mRNA (31 cycles) and dH2O (34 cycles) were similarly low and 3 cycles apart. The CT difference between the cDNA (8 cycles) and mRNA was 23 cycles, an amount equivalent to less than 0.0001 % of the 18S rRNA reverse transcribed. This indicates that the error in the measurement of 18S by real time PCR analysis does not significantly affect the semi-quantification in this thesis.

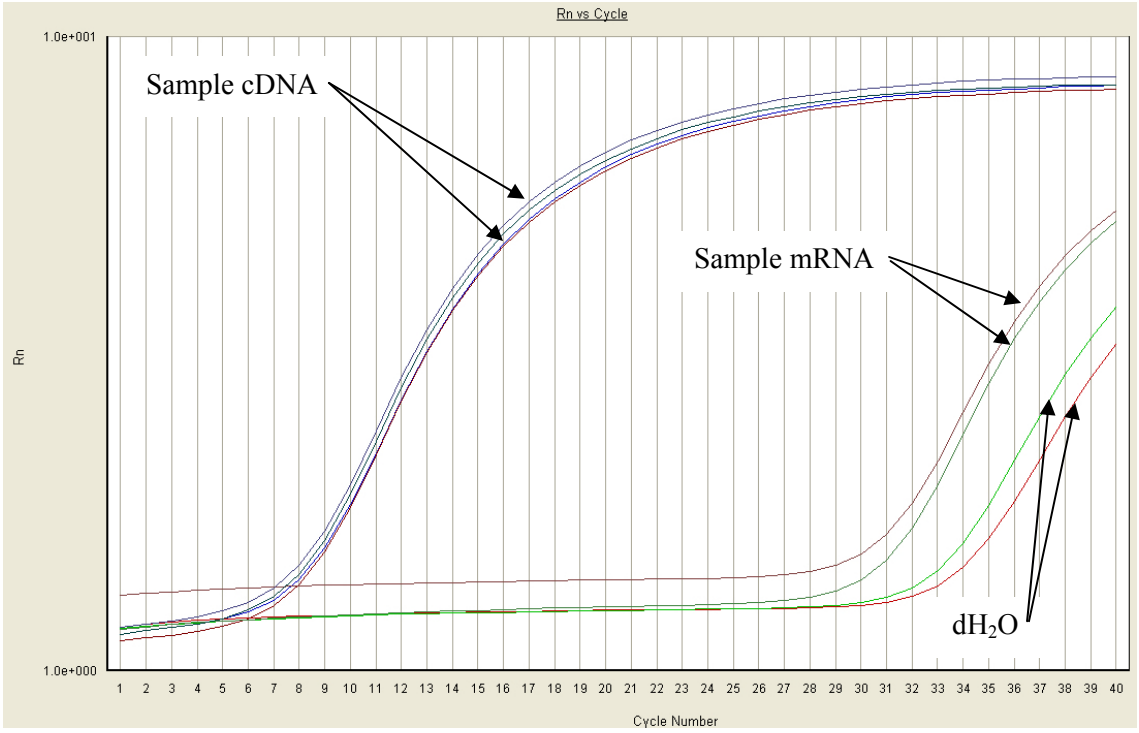

Figure 3.5 Real Time PCR amplification plots of 18S cDNA and 18S mRNA compared to water

3.9.3 SYBR Green Real Time PCR

The SYBR green PCR system uses a DNA intercalating fluorochome dye to bind to PCR product. Amplification of the PCR product results in many double stranded cDNA sequences for the target gene and hence a fluorescent level proportional to the amplification. Longer PCR products allow more of the SYBR green dye to intercalate, producing a greater fluorescence is greater per unit of PCR product, however a longer time is required for the transcription. The size of the PCR product was kept to less than 350 bp.

The SYBR green master mix (2X) was mixed with cDNA and loaded into the wells. The forward and reverse primers were mixed into distilled water and added to the wells. The resulting reaction mix (Table 3.12) was centrifuged for 3000 rpm a few seconds with a plate centrifuge, before analysing by real time PCR on an ABI 7500 FAST machine, using the program detailed in Table 3.13. Step 2 was repeated for 40 or 50 cycles as required.

Table 3.12 Real time SYBR Green master mix

Component	µl/sample
SYBR Green (2X)	6.25
Forward Primer	0.625
Reverse Primer	0.625
cDNA	1.2
dH_2O	3.8
Total	12.5

Table 3.13 Real time SYBR Green PCR Programme

Step	Temperature (°C)	Time (mm:ss)
1	95	15:00
2	95	0:15
	55	0:30
	72	0:30

3.10 Protein extraction and quantification

3.10.1 Protein extraction

The protein extraction was performed on ice to minimise enzyme and metabolic activity from the point of cell harvesting. A rapid dephosphorylation appeared to occur within seconds of removing the culture medium, thus the following washing and lysis step was completed within approximately 20 seconds for each sample. An ice cold lysis buffer containing 1:25 proteinase inhibitor and 1:200 of sodium orthovanadate (1 mM Na_3VO_4) was prepared in order to inhibit phosphatase activity during protein lysis. Culture medium was poured out of the T25 culture flasks and ice cold PBS poured in to reduce protease and phosphatase activity. The PBS was poured out and replaced with 50 - 200 µl of the prepared ice cold lysis buffer. Lysis occurred rapidly and the cell lysate was transferred to 1.5 ml tubes. Samples were sonicated for a few seconds where solids were visible until the lysate solutions were cloudy. The lysate was centrifuged at 13,000 rpm in 4 °C for 30 minutes. This pelleted the cell membranes and DNA, which were removed where possible by pipette and then the supernatant transferred to 0.5 ml tubes and stored at -20 °C.

3.10.2 BCA™ protein Assay

A small aliquot of the protein sample was diluted 1:10 and the protein concentration determined with the BCA™ Protein Assay Kit (Pierce Rockford, IL). Reagents A (sodium carbonate, BCA and sodium tartrate in 0.1M sodium hydroxide), and B (4 % cupric sulphate) were mixed at a ratio of 50:1 respectively and loaded at 200 µl per well on a 96 well plate. To this was added 25 µl of either standard protein (see Table 3.14) or sample protein. Standard protein concentrations were made by mixing BSA stock with distilled water as outlined in Table 3.14 for tubes A, B and C. Tube D was composed by mixing 175 µl distilled water (shown in the table) and 175 µl of tube B and mixed thoroughly. Similar compositions were made for tubes E to H using distilled water and the tubes as directed on Table 3.14 and mixed thoroughly. Duplicate wells for standard proteins (A-I) and triplicate wells for target proteins were used to reduce loading errors. The plate was placed onto a shaker for 30 seconds and then incubated at 37 °C for 30 minutes. The plate was cooled to room temperature before measuring absorbance at 560 nm with a microplate reader. The background absorbance (I) was subtracted from the samples. The protein standards were plotted against the optical density with a best fit curve. Sample protein concentrations were approximated from the standard curve.

Table 3.14 Composition of protein standards for protein concentration assay

Tube	**Distilled water (µl)**	**BSA Stock* (µl)**	**Final conc (µl/ml)**
A	0	300	2000
B	125	375	1500
C	325	325	1000
D	175	175B	750
E	325	325C	500
F	325	325E	250
G	325	325F	125
H	400	100G	25
I	400	0	0

*BSA Stock: 2mg/ml BSA in PBS

3.11 Sodium Dodecyl Sulphate Polyacrylamide Gel Electrophoresis (SDS-PAGE)

A clean gel apparatus (A large and small plate with two brackets, a comb and a backing, Biorad) were assembled and filled with water to test for leaks. The water was removed and combs were inserted and a level was marked about 2 mm below the comb teeth. Polyacrylamide gel solutions were composed as shown in Table 3.15 and mixed well. Ammonium Persulphate and TEMED were used to initiate and acceleratre polymerisation respectively. The gel was poured into the apparatus immediately to the marked level. To reduce evaporation and flatten the meniscus for even resolution, a layer of isopropanol was added. To confirm whether gels had set, the remaining gel solution was kept, while proteins were prepared. Protein samples (20-40 µg) were mixed with loading buffer in a 1:1 ratio and boiled at 100 °C for 10 minutes and cooled on ice. Meanwhile the isopropanol was washed out with distilled water and the stacking gel completed and poured into the gel apparatus. The comb was slowly lowered into the gel to avoid splash back and bubbles. Excess gel on the apparatus was removed with a paper towel. Remaining bubbles were removed by tapping the apparatus and the remaining gel kept to confirm that the stacking gel had set. The gel apparatus was transferred to a running tank filled with running buffer. Protein samples and 10 µl of protein standard (Precision Plus Protein™ Dual Color standards, Biorad) were centrifuged briefly, vortexed and loaded onto the gel. The protein load was made similar in each sample well by measuring protein concentration and using control protein α-Tubulin for relative quantification. The run was operated at 140 V and 140 mA for 1 - 2 hours and on ice to prevent the gel from overheating. Observations were made every 30 minutes to monitor the distance moved by the bands. Blotting was performed using either the wet or semi-dry method.

Table 3.15 Components for protein gels

Component	12 % resolving gel (ml)	5 % stacking gel (ml)
Distilled H_20	3.3	1.4
30 % Acrylamide	4.0	0.33
1.5M Tris pH 8.8	2.5	NONE
1.0M Tris pH 6.8	NONE	0.25
10 % SDS	0.1	0.02
10 % Ammonium persulphate (AP)*	0.1	0.02
TEMED*	0.004	0.004

*Mixed just before pouring gel solution. AP powder was freshly diluted in dH_2O.

3.12 Western blotting

Western blotting was performed with either wet or semi-dry transfer methods. The protein load was made similar in each sample well by measuring protein concentration and using control protein α-Tubulin for relative quantification.

3.12.1 Wet Transfer Method

Four sheets of 3MM chromatography paper (Whatman®) and one nitrocellulose sheet of Hybond™-C Extra (Amersham Life Science) were cut to a size slightly larger than the gel and soaked in transfer buffer. Two flat sponges were also soaked in transfer buffer. The gel was detached from the apparatus and placed in the transfer buffer to keep wet. The sponges were placed one on each electrode plate and two pieces of filter paper were placed on the side of the black electrode. The gel was gently separated from the plates and added on top of the filter paper. Nitrocellulose (Hybond) paper was added on top carefully to avoid bubbles between the gel and the paper. Two more filter papers were added on top and the red flat electrode put on top to sandwich the gel. This was placed in a transfer tank with transfer buffer to fill to the top. Electrodes were plugged in such that the gel was on the negative side and the H-bond membrane on the positive side. The transfer buffer was fun for 2 hours at 200 mV and 200 mA at 4 °C. Afterwards, the sandwich was opened up with the positive side (red) on the bottom. The papers were removed and the top right corner cut to mark that the membrane was face up. The gel was removed and the membrane kept in transfer buffer to stay moist.

3.12.2 Semi-dry Transfer Method

Six sheets of 3MM chromatography paper (Whatman®) and one nitrocellulose membrane of Hybond™-C Extra (Amersham Life Science) were cut to a size slightly larger than the gel and soaked in transfer buffer. Three pieces of the paper were placed on the surface of the bottom plate (anode), before placing the nitrocellulose membrane on top. The gel was placed on top and covered with three sheets of filter paper. Bubbles between the sheets were removed with a centrifuge tube at each stage of layering and the transfer performed at 400 mA and 20 V for one hour. Afterwards, the filter paper and gel were removed and the top right corner of the membrane was cut off in order to mark the top surface. Remaining gel was washed off the membrane with transfer buffer.

3.12.3 Ponceau S staining

It was necessary to confirm that the protein had transferred before proceding. The membrane was incubated in Ponceau S solution, rocking gently for 10 minutes. The Ponceau S solution was washed once in TBS and excess solution dried off with a paper towel. The membrane was placed in a plastic sheath and scanned on a Hewlett Packard Scanjet 5100C. A successful protein transfer was indicated when pink bands in the sample lanes with similar intensities between lanes were observed, as in Figure 3.6. Ponceau S solution was washed off with TBS.

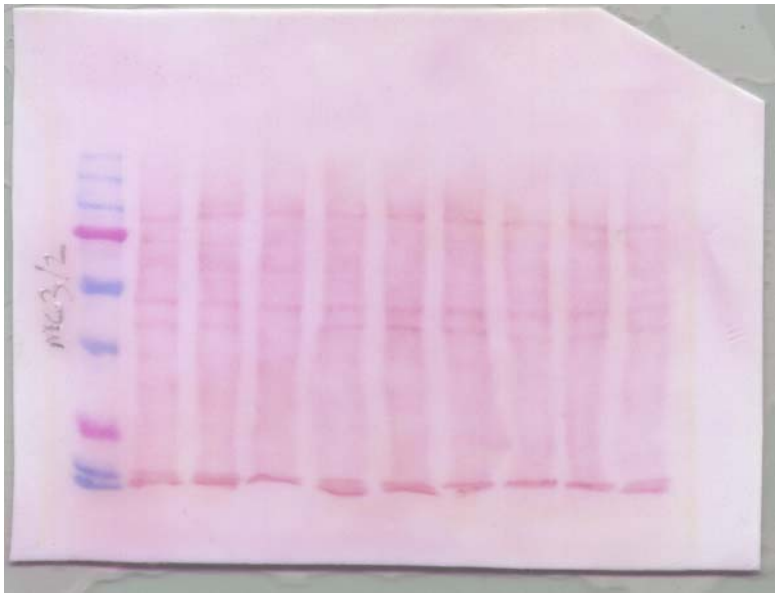

Figure 3.6 Ponceau S solution staining of proteins on a nitrocellulose membrane

3.12.4 Immunodetection

To prevent non-specific binding, the membrane was incubated with blocking buffer for 45 minutes at room temperature. Excess blocking buffer was drained with a paper towel before sealing the membrane in a plastic bag of primary antibody solution and incubating overnight at 4 ºC on a gentle shaker. The primary antibody was removed by washing in 0.1% TBST six times for 8-10 minutes. The membrane was placed in a plastic bag filled with secondary antibody solution, sealed and gently rocked for 1 hour at room temperature. Excess antibody was removed with six sets of 10 minute washes with 0.1% TBST.

Enhanced chemiluminescence reaction (ECL) was used to visualise the antibody bound to the target protein. 1ml of each ECL component was placed in a 50 ml tube. The membrane was placed inside and washed in ECL for 1-2 minutes. The membrane was lifted out and excess ECL drained on a paper towel to reduce back ground. The membranes were placed face up between two plastic sheets in a photographic plate and brought to a dark room. In the dark,

Chemiluminesence Film (Kodak Biomax Light Film, Sigma-Aldrich) was cut on the top right corner and moved to the top right part of the plate and closed. This was timed for 1 minute, before the film was taken out and placed in the film processor, and labelled with the time. This was repeated for 4 and 16 minutes and other times to find the appropriate time of exposure, such that the intensity of the bands was not completely saturated. The bands for the protein ladder were traced on top of the film. Bands on the films were orientated along a horizontal axis and scanned for densitometry (Hewlett Packard scanjet 5100C).

3.12.5 Densitometry

Labimage (v2.7.1, Kapelan) was used to analyse scanned blots. Brightness and contrast were optimised before proceeding with the analysis. Area information for each target band was obtained and analysed in Excel.

3.12.6 Summary of Antibodies and conditions

Antibodies were diluted in blocking buffer to the levels shown in Table 3.16:

Table 3.16 Antibodies and dilutions for western blot

Antibody	Dilution
Primary	
Alpha Tubulin	1:1000
ERK p44/42	1:1000
Phospho-ERK p44/42	1:2000
Gapdh	1:1000
Secondary	
Goat anti-rabbit HRP	1:1000
Rabbit anti-mouse HRP	1:1000
Goat anti-mouse HRP	1:1000

3.13 Sequencing

The sample cDNA and PCR product of Human FGFR2 was prepared using methods described in section 3.7 and 3.8. The human FGFR2-C278F was sequenced in R2-C278F cells to confirm the presence of the codon change from cysteine to phenylalanine (Figure 3.7).

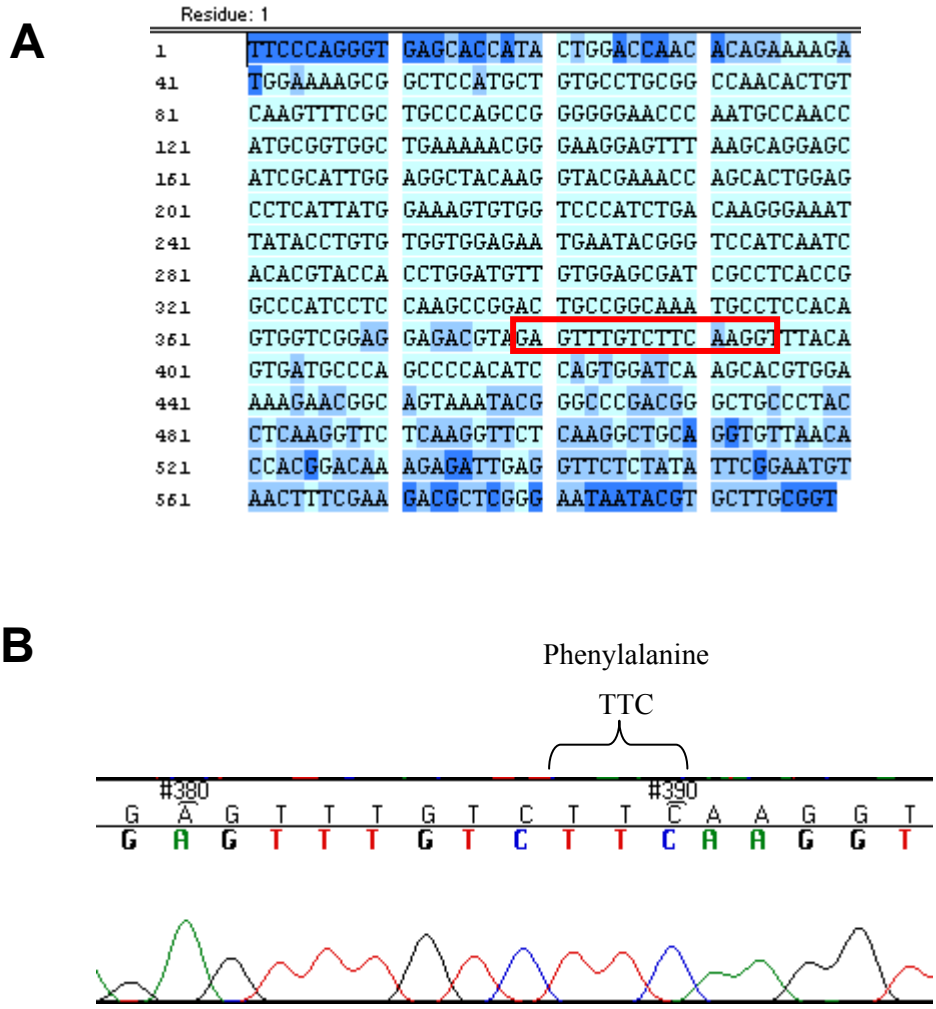

Figure 3.7 Sequence of FGFR2 in R2-C278F cells.

A: A short sequence of the region surrounding position 278 of the human FGFR2-C278F. The numbering of the nucleotides are arbitary. **B:** The chromatogram of the sequence of the highlighted in red in A. Position 278 is changed from TGC (cysteine) to TTC (phenylalanine).

3.14 Statistical analysis

SPSS (14, SPSS Inc. Chicago, IL, USA) was used for all statistical computations. The "n" provided in the results figures refer to the number of experiments for that study.

3.14.1 Tests of normality and distribution adjustments

The Shapiro-Wilks test was applied, using the "Explore function" in order to determine whether data was normally distributed before parametric tests were applied. Cases were excluded pairwise, as not all genes were analysed in all samples. Where data was not normally distributed (0.05 or below), data was logged and the test performed again.

Parametric data were compared with the two samples T-test, whereas non-parametric data were compared using Mann-Whitney U test. Statistical differences were stated for p-value < 0.05. Unless stated otherwise, the P values were given from a T-test. Levene's test was used to determine the equality of variances. Where the result was significant (0.05 or below), equal variances were not assumed in the T-Test.

For gene expression profiling, ANOVA was not applied for 3 groups as the number of replicates was less than the recommended numbers ($n < 20$) as suggested in the GOSH Statistics and Research Methodology course book (p142, 2005 edition). ANOVA was used for comparison between more than 3 groups to avoid further increase of type 1 errors. The bonferroni post hoc test was applied to conservatively assess any significant differences observed by ANOVA.

Chapter 4 Characterising MC3T3, R2-WT and R2-C278F cells

4.1 Introduction

Mutations of Fibroblast Growth Factor Receptor (FGFR) 1-3 that cause ligand independent receptor dimerisation, such as FGFR2-C278F or FGFR2-C342Y are associated with craniosynostosis (Mangasarian et al., 1997; Robertson et al., 1998). These types of mutation result in a ligand-independent constitutively activated (LICA) FGFR, which affects osteoblast cell behaviour.

It is implied that mutations that result in LICA FGFR2 have equivalent mechanisms of FGFR activation, although different results are observed in human and animal models. For example in cultured human osteoblasts carrying FGFR-C342R, proliferation is decreased and differentiation increased, whereas in both murine osteoblast cell lines (C342Y) and chick primary osteoblast cultures (C278F) proliferation is increased and differentiation decreased (Mansukhani et al., 2000; Marie et al., 2005; Ratisoontorn et al., 2003). Some hypotheses have been given for these discrepancies, such as different cell responses to FGF linked to osteoblast maturity and differences in human and murine genetic backgrounds, however they have neither been defined specifically or tested (Marie et al., 2005).

FGFR2-C278F is a common mutation resulting in Crouzon or Pfeiffer syndromes. The effect of this mutation on proliferation and differentiation has been studied in embryonic chick osteoblasts, but not at postnatal stages (Ratisoontorn et al., 2003). In the Ferretti lab, murine cell lines were established by transfecting osteoblastic MC3T3-E1 cells with either human wild type FGFR2 or FGFR2-C278F and the lines named R2-WT and R2-C278F respectively, to create a murine *in-vitro* model for craniosynostotic osteoblasts (Petiot, 2001). The initial work on this newborn postnatal cell line suggested that stable expression of FGFR2-C278F may reduce proliferation, increase differentiation and increase apoptosis in R2-C278F cells.

The first aim in this chapter is to confirm and extend published work by the Ferretti lab, focussing mainly on the stages of culture at pre-confluence and confluence (2 and 4 days in culture). The second aim is to extend the investigation into osteoblast behaviour by studying cell morphology, distribution and metabolism. The third aim is to define a working hypothesis to explain the similarities and discrepancies of craniosynostotic osteoblast phenotype reported in the literature.

4.2 Results

4.2.1 The effect of FGFR2-C278F on osteoblast morphology and distribution

Differences were found between the MC3T3, R2-WT and R2-C278F cell lines by two days in culture, using light microscopy (Figure 4.1A, C and E). MC3T3 cells were arranged in monolayered clusters of cuboidal cells surrounded by fibroblastic cells with processes that spanned the spaces between the clusters (Figure 4.1A). In contrast, R2-WT cells appeared to be more evenly distributed, arranged in smaller clusters of cuboidal cells and the cultures seemed to have more fibroblastic cells (Figure 4.1C). These monolayered clusters of cuboidal cells were also found in R2-C278F cultures, but with few fibroblastic cells spanning between clusters, compared to the MC3T3 cultures (Figure 4.1E). At 4 days in culture, almost all cells in the three cultures were cuboidal (Figure 4.1B, D and F). Both MC3T3 and R2-WT cell cultures had reached confluence and could not be distinguished from each other (Figure 4.1B and D). The R2-C278F cultures were not fully confluent; gaps between cells could be observed that made them easy to distinguish from both MC3T3 and R2-WT cultures (Figure 4.1F).

On closer observation of cell morphology, certain shapes could be clearly identified and were classified as follows: “fibroblastic”, “bright and round”, “small” (10 μm diameter approximately), “cuboidal” and finally “fried egg” (100 μm diameter approximately). The relative percentage of cuboidal cells was difficult to categorise, as the morphology of some of the small cells was also cuboidal or round, but not bright. To simplify, cells were therefore divided into four categories: bright round, small/cuboidal, fibroblastic and “fried egg” (Figure 4.2 A). The relative amount of these categories did not change between the MC3T3 and R2-WT, however in R2-C278F there was an increase in the percentage of the “bright round” and a decrease in the “fibroblastic” morphologies (Figure 4.2 B).

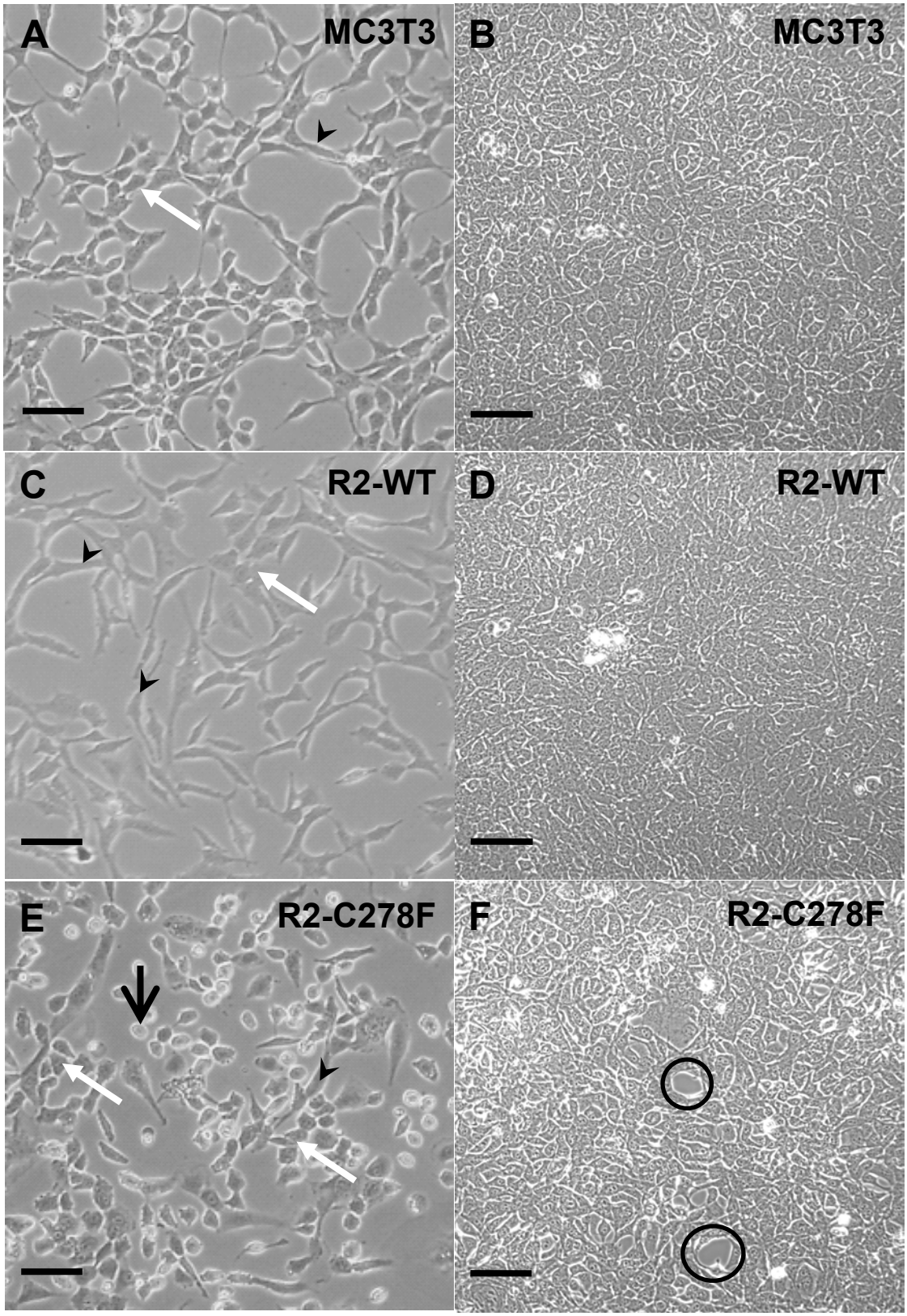

Figure 4.1 Phase contrast microscopy of MC3T3, R2-WT and R2-C278F at 2 and 4 days in culture
Fibroblastic cells (arrow heads) and cuboidal cells (white arrows) are present in MC3T3 cells at 2 days (A). In R2-WT cells (C) most appear fibroblastic and in R2-C278F cells (E) most appear cuboidal with more bright round cells (wide arrow). MC3T3 and R2-WT cultures are confluent at 4 days (B, D), but R2-C278F cultures (F) have spaces (black circles) between cells (Bar = 50 μm, n = 3, magnification 10x).

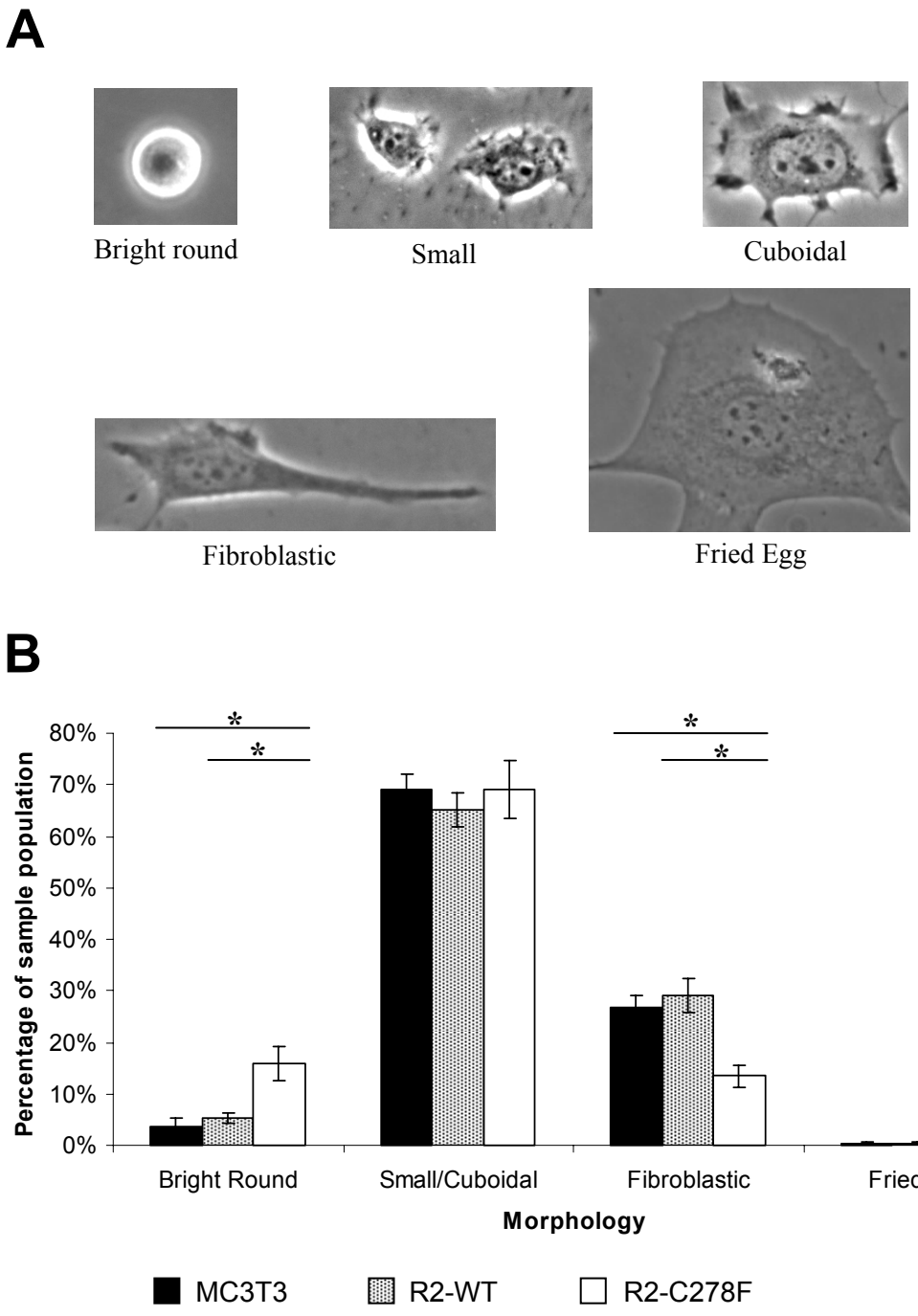

Figure 4.2 Classification of MC3T3, R2-WT and R2-C278F cell morphology at 2 days in culture

A: Examples of cell morphologies were used for quantification. **B:** The small and cuboidal cells constitute the largest percentage of the cells present in all three cell cultures. The percentage of bright round cells is significantly higher in R2-C278F cells, compared to MC3T3 and R2-WT controls. The percentage of fibroblastic cells is lower in R2-C278F cells. No significant differences are found between cell lines in the "fried egg" category ($n = 3$, $*p < 0.05$).

4.2.2 The effect of FGFR2-C278F expression on proliferation

To measure cell growth, cells were counted at 4 days in culture by FACS analysis. This was done by suspending the cultured cells in a known volume of PBS and adding a fixed number of beads. From this, the forward and sideways scatter plot was used to identify cells from beads and allow calculation of the percentage of beads to cells in MC3T3, R2-WT and R2-C278F cells (Figure 4.3 A, B and C). A higher percentage of beads to cells indicates a lower cell number. From this percentage, the original number of cells was assessed. MC3T3 cultures had the greatest number of cells, followed by R2-WT and then R2-C278F cells (Figure 4.3).

The DNA intercalating agent 7AAD was used to determine the proportion of cells at each stage of the cell cycle. A basic plot indicated that cells varied from haploid (low DNA content) to diploid (high DNA content). This plot was further analysed for the number of cells at each stage of the cell cycle, based on the Dean and Jett method (Dean and Jett, 1974). This produced three histograms underneath the original curve corresponding to G1, S and G2/M phase in MC3T3, R2-WT and R2-C278F cells (Figure 4.4 A, B and C). The curves were analysed, and the number of cells at each stage of the cell cycle were expressed as a percentage of the whole cell cycle (Figure 4.4 D). No significant differences were found between MC3T3 and R2-WT cells, however in R2-C278F cells there was a significant decrease in the proportion of cells in S and G2/M phase compared to that of both MC3T3 and R2-WT cells (Figure 4.4 D). The percentage of cells in G1 phase was also higher in R2-C278F cells than in the other cell lines.

To assess the amount of cells in M phase, the pH3 antibody stain was used and the cells analysed by FACS. The cell count was plotted against the log fluorescence intensity of the pH3 signal in each cell and a gate was placed to separate cells of low and high intensity, based on the negative control with the highest background (Figure 4.5 A, B and C). M phase was analysed by calculating the percentage of cells with high intensity stain. This showed that the percentage of M phase cells in R2-C278F (1.6%) were significantly lower than in MC3T3 (1.92%) and R2-WT (1.85%) cells (Figure 4.5 D).

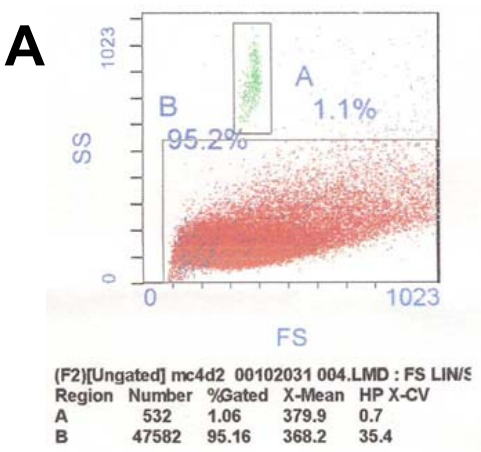

(F2)[Ungated] mc4d2 00102031 004.LMD : FS LIN/S

Region	Number	%Gated	X-Mean	HP X-CV
A	532	1.06	379.9	0.7
B	47582	95.16	368.2	35.4

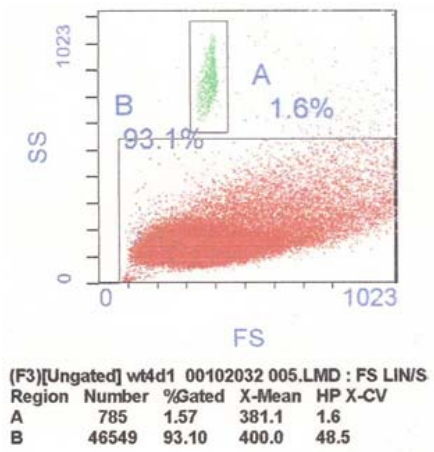

(F3)[Ungated] wt4d1 00102032 005.LMD : FS LIN/S

Region	Number	%Gated	X-Mean	HP X-CV
A	785	1.57	381.1	1.6
B	46549	93.10	400.0	48.5

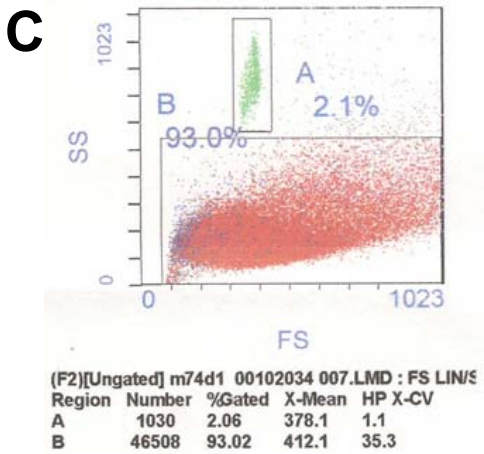

(F2)[Ungated] m74d1 00102034 007.LMD : FS LIN/S

Region	Number	%Gated	X-Mean	HP X-CV
A	1030	2.06	378.1	1.1
B	46508	93.02	412.1	35.3

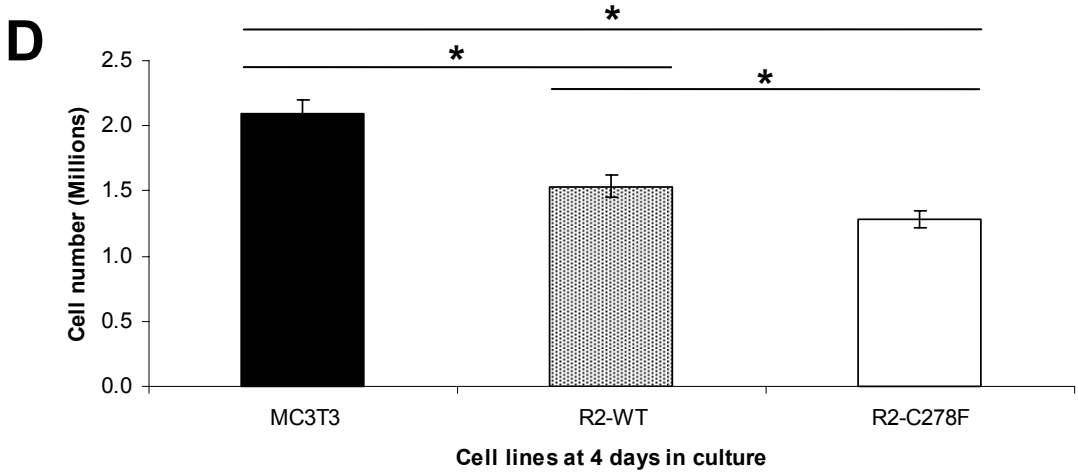

Figure 4.3 FACS analysis of cell number after 4 days in culture

Cell samples were mixed with a fixed number of fluorosphere beads and counting approximately 45,000 MC3T3 (A), R2-WT (B) and R2-C278F (C) cells. The percentage of beads (green) was used to calculate the total number of cells in the culture. **A-C:** The forward scatter (FS) was plotted against side scatter (SS) and the beads were gated and the percentage of beads to cells calculated for MC3T3, R2-WT and R2-C278F cells respectively given by percentage "A" on each plot. **D:** At 4 days in culture, the cell number is lower in R2-C278F cells than MC3T3 and R2-WT ($n = 3$, $*p < 0.05$).

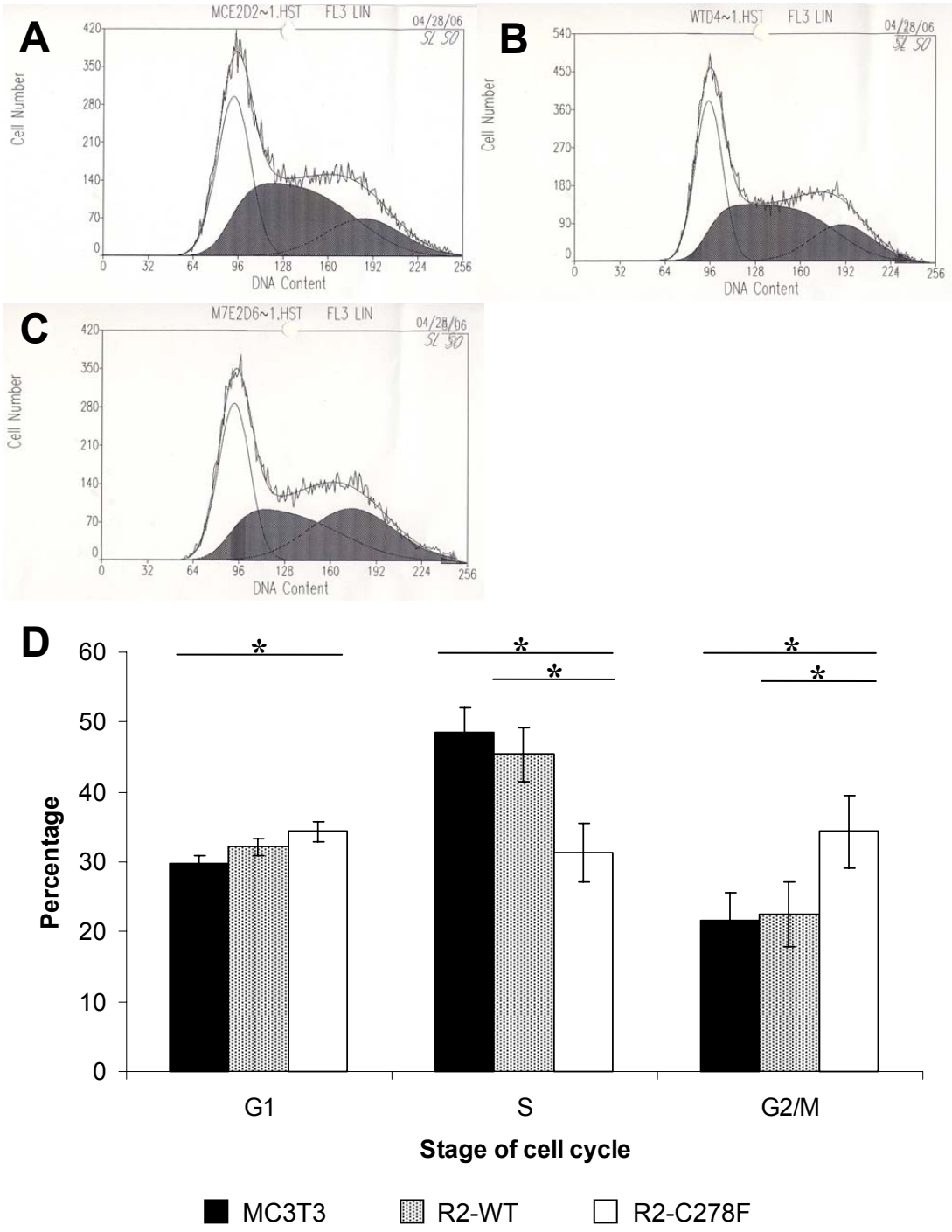

Figure 4.4 FACS cell cycle analysis of MC3T3, R2-WT and R2-C278F at 2 days in culture

7AAD was used to identify the phases of cell cycle as described in methods (3.3 FACS). Plots of cell number against DNA content for MC3T3 (A), R2-WT (B) and R2-C278F (C) cells. Three smaller plots corresponding to G1, S and G2/M phases of the cell cycle were made under the main curve, as explained in section 3.3.2 Methods. **D:** Data from the three plots analysed to assess the percentage of cells at different phases of the cell cycle. The percentage of cells in G1 phase is higher in R2-C278F cells than in MC3T3. The highest percentage of cells in MC3T3 and R2-WT are in S-phase. The percentage of cells in S-phase is significantly lower in R2-C278F. There is a significantly higher percentage of R2-C278F cells in G2 phase than in both MC3T3 and R2-WT cells ($n \geq 4$, $^*p < 0.05$ Mann-Whitney U test).

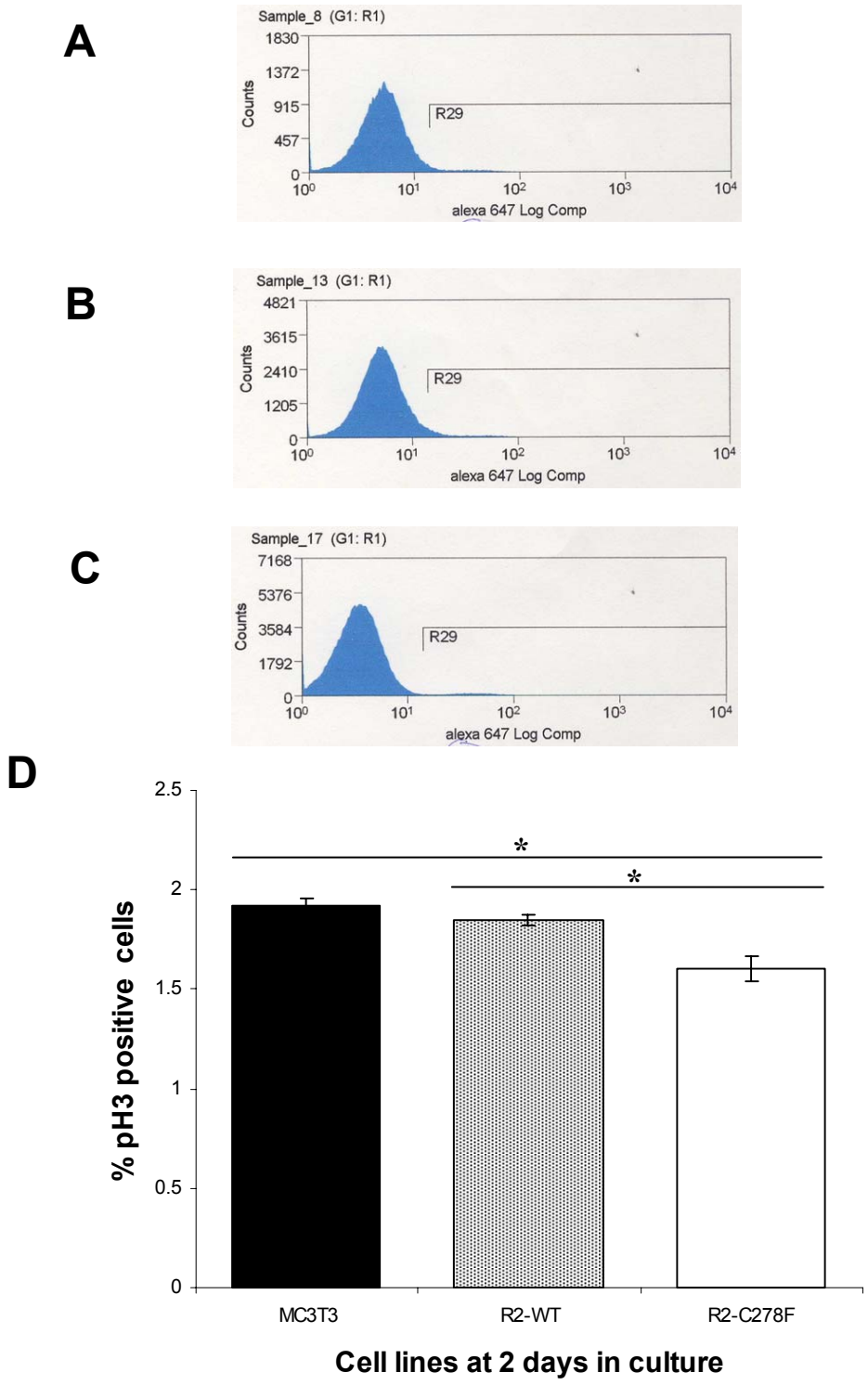

Figure 4.5 FACS M-phase analysis of MC3T3, R2-WT and R2-C278F at 2 days in culture

The cell count was plotted against the log intensity of phosphorylated histone antibody (pH3) in MC3T3 (A), R2-WT (B) and R2-C278F (C) cells. **A-C:** A gate (R29) was placed to only include cells with high intensity, corresponding to pH3 positive cells in M-Phase. **D:** The pH3 positive cells were expressed as a percentage of the total number of cells. This percentage is decreased significantly in R2-C278F cells (n = 3, *$p < 0.05$).

4.2.3 FGFR2-C278F increases apoptosis and cell death

Apoptosis as measured by 7AAD was performed at 2 and 4 days in culture. The level of apoptosis was low at 2 days, between 0.2 and 0.3 % in MC3T3 and R2-WT cells (Figure 4.6 A). In R2-C278F cells in the percentage of apoptotic cells was also small, but significantly higher (0.6 %), compared to both controls (Figure 4.6 A). Also at 4 days, the level of apoptosis was low in MC3T3 and R2-WT (between 0.5 to 0.9 %) with no significant difference between the two cell lines. The level of apoptosis in R2-C278F cells was 2 to 3 fold higher (1.7 %) than in MC3T3 and R2-WT cells respectively (Figure 4.6 B).

To further assess the extent of cell death in the different cell lines, cells were also cultured for 7 days without any change in medium, and both adherent and non-adherent cells were counted. Adherent cells were analysed for apoptosis and the non-adherent cells were considered as dead. The number of live and both dead and apoptotic cells were counted (Figure 4.7 A). Similar to the cell number at 4 days, the number of live cells was highest in the MC3T3, lower in R2-WT and lowest in R2-C278F cells. The number of dead / apoptotic cells was highest in the R2-C278F cells, followed by R2-WT and then MC3T3. The percentages of dead / apoptotic cells were 1.5, 6.6 and 25.7 % for MC3T3, R2-WT and R2-C278F cells respectively.

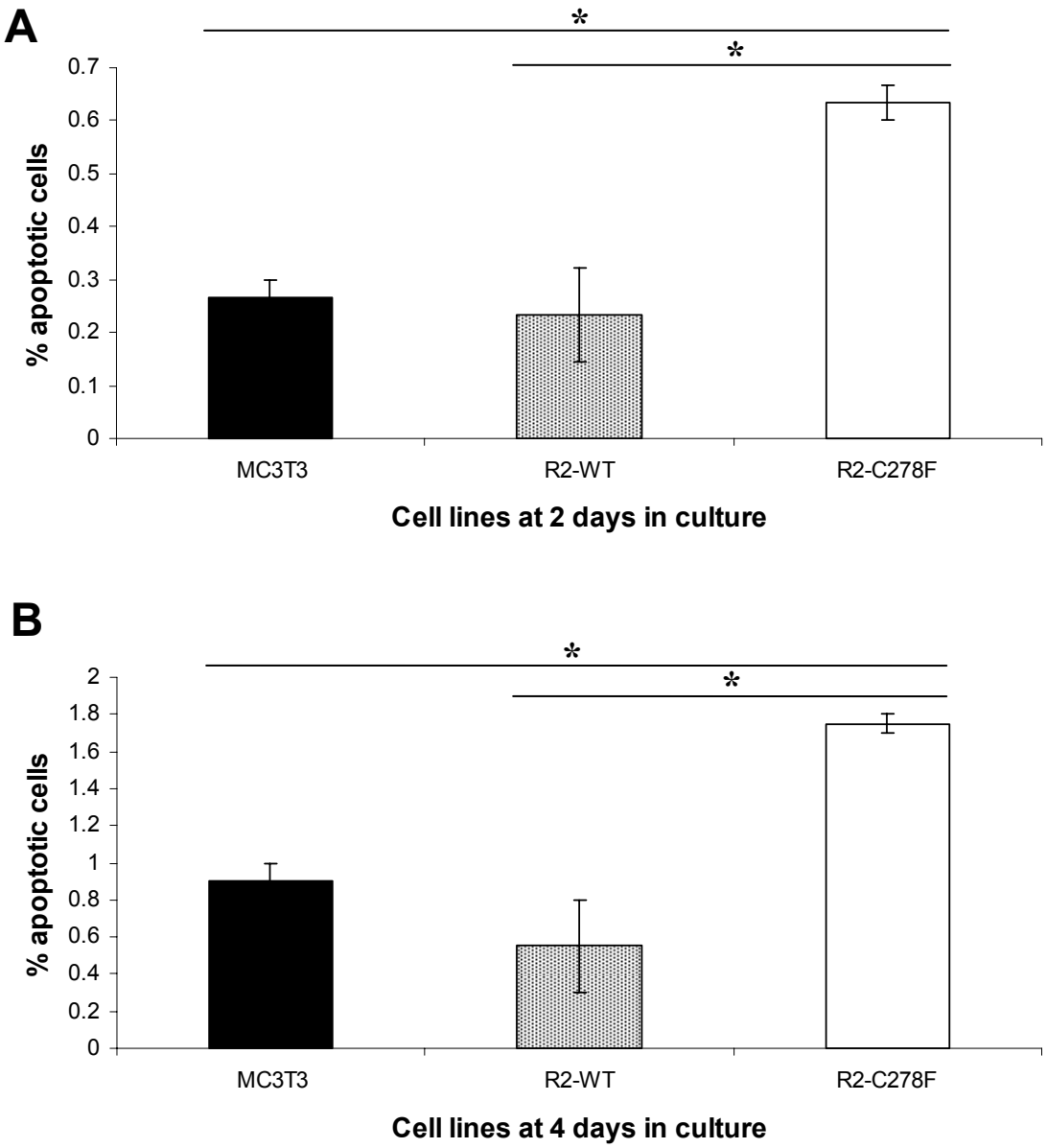

Figure 4.6 Analysis of apoptosis in MC3T3, R2-WT and R2-C278F cells by FACS using 7AAD

Apoptotic cells were detected by their increased uptake of the DNA intercalating agent, 7AAD. **A**: At 2 days in culture, there is no difference in apoptosis between MC3T3 and R2-WT cells, whereas in R2-C278F is increased significantly (n = 3). **B**: At 4 days in culture the level of apoptosis between MC3T3 and R2-WT cells is comparable, but is significantly lower than in R2-C278F cells (n = 4, *$p < 0.05$).

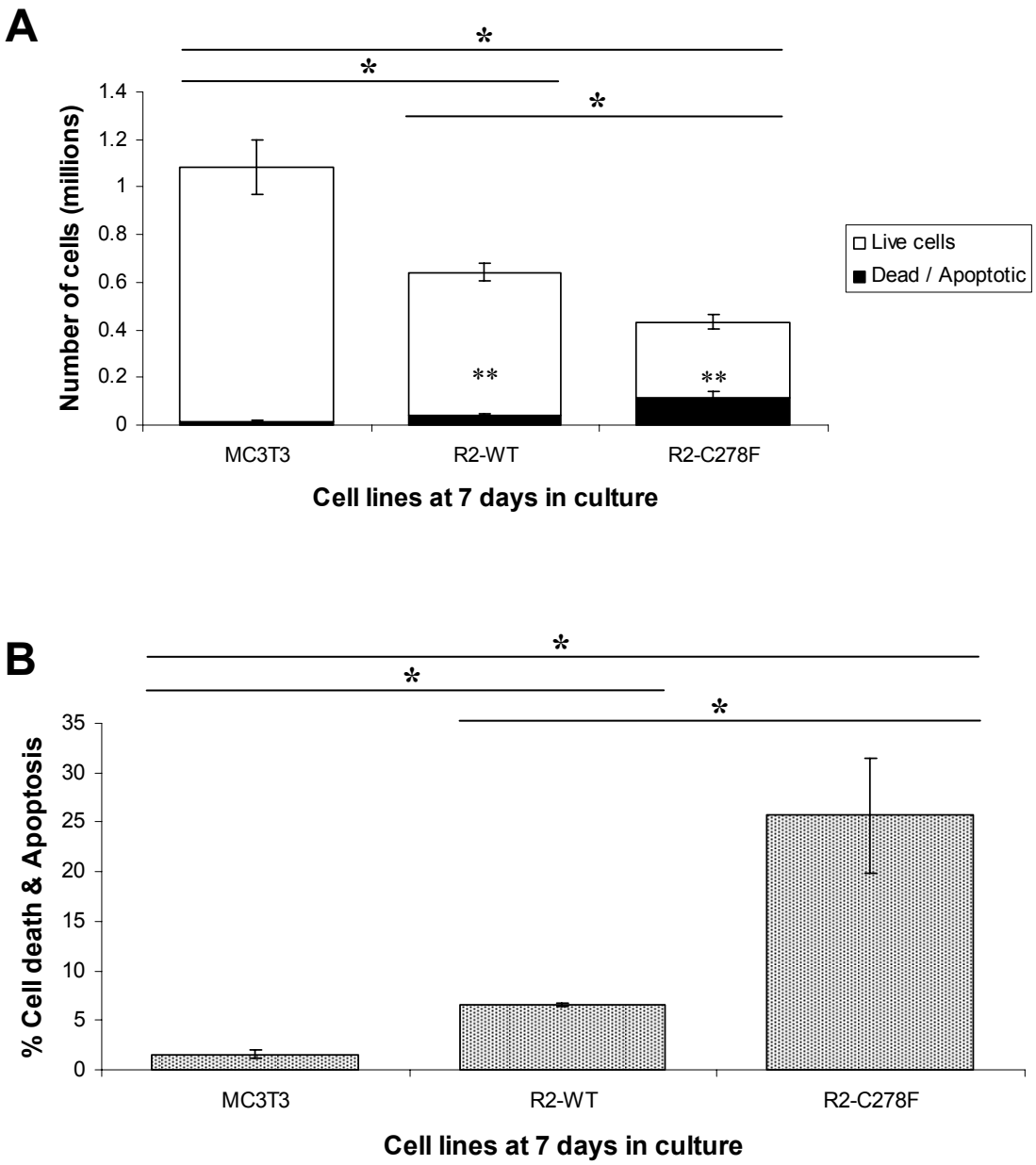

Figure 4.7 FACs cell count and cell death at 7 DIC without medium change

Adherent and non-adherent cells were counted after 7 DIC (A). The number of live cells was significantly smaller in R2-WT, compared to MC3T3, and even lower in R2-C278F cultures. The total number of dead cells (adherent and non-adherent) was significantly higher in R2-WT and R2-C278F cells compared to MC3T3 (** $p < 0.05$ *versus* MC3T3). No significant differences were found in the number of dead cells between R2-WT and R2-C278F cells. **B:** The number of dead / apopototic cells in (A) expressed as a percentage of the total cells counted. There is a significant increase in apoptosis in R2-C278F cells compared to both MC3T3 and R2-WT cells. R2-WT cells also show a higher level of apoptosis, compared to the MC3T3 cells ($n = 4$, *$p < 0.05$).

4.2.4 Metabolism is altered in R2-C278F cells

The behaviour of the three cell lines in the absence of serum was assessed by seeding cells for 24 hours in cell culture medium containing 10% FBS and then replacing this with a 0 % serum cell culture medium. Cell morphology and distribution were assessed. After 18 hours in 0 % serum, there were no obvious changes in cell distribution (Figure 4.8). There was an increased number of floating cells in the centre of the culture wells in all three cell lines, however the largest number of these cells was observed in R2-C278F cells. As osteoblasts are adherent cells unless sheared from their culture suface or trypsinized, this suggested that the amount of floating cells was associated the the amount of dead cells. Increased dependency on serum for survival in R2-C278F cells may have highlighted a potential metabolic abnormality.

To investigate potential metabolic defects in R2-C278F cells on a molecular basis, *Akt1* and *Gapdh* gene expression were analysed, because of their roles in cell survival and glucose metabolism respectively (Song et al., 2006). *Gapdh* expression in R2-C278F cells was significantly lower, compared to MC3T3 and R2-WT cells at both 2 and 4 days in culture (Figure 4.9A). Interestingly, at both timepoints the level of *Gapdh* expression in R2-WT cells was higher than in MC3T3 cells. *Akt1* expression was not significantly different between R2-WT cells and MC3T3, but in R2-C278F cells *Akt1* expression was significantly lower compared to MC3T3 (Figure 4.9B). No significant differences were observed in *Akt1* expression between the cell lines at 4 days in culture.

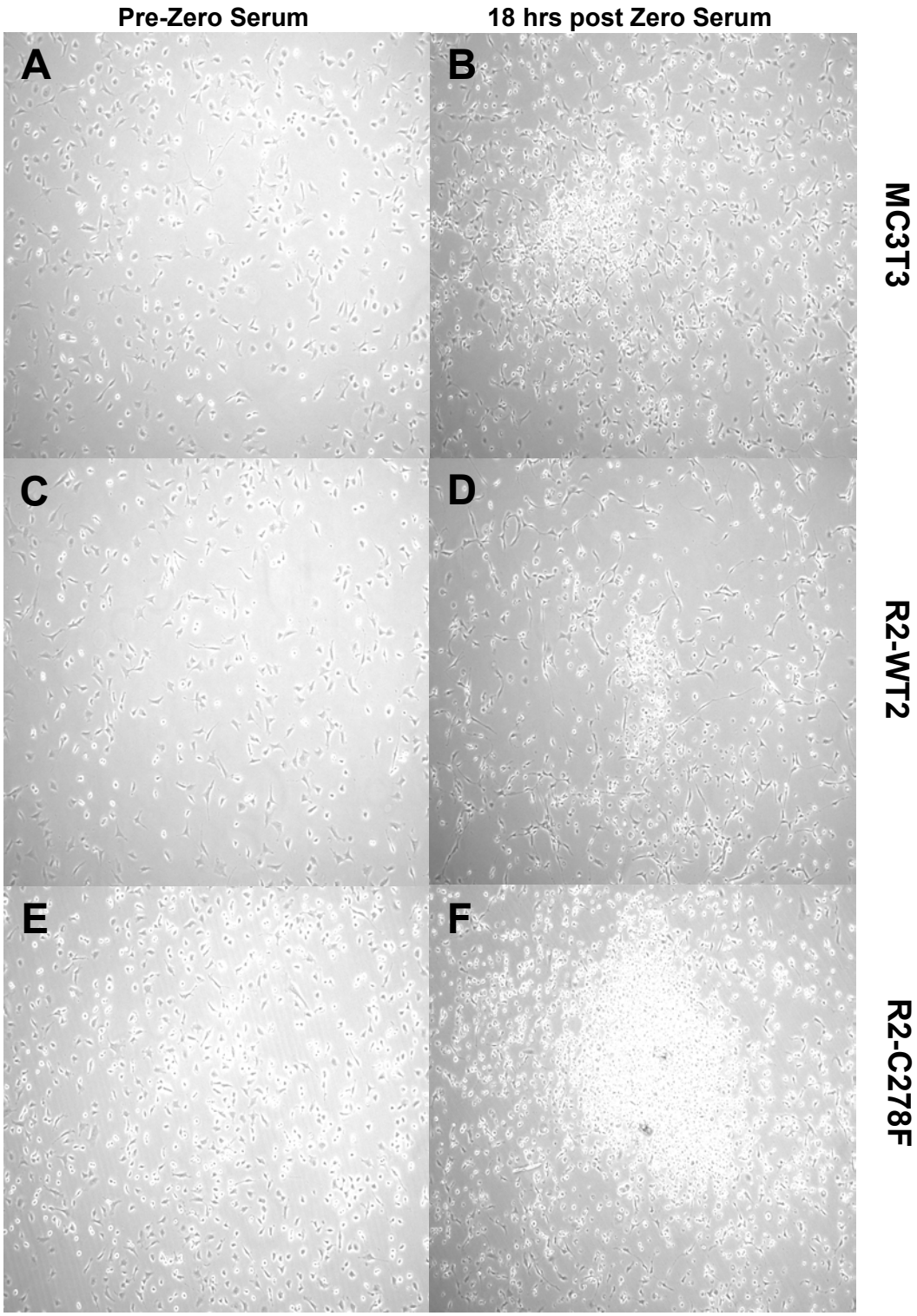

Figure 4.8 Phase contrast microscopy of serum starved cells after 18 hours

Cells were seeded at 20,000 cells per cm^2 on a 12 well plate for 24 hours in 10 % FBS containing cell medium (A, C and E), before culturing with 0 % FBS cell medium for 18 hours and swirling the wells gently to collect floating cells together for imaging (B, D and F). Bright floating cells found in MC3T3 and R2-WT cells (B and D). More of these floating cells were observed in the R2-C278F cell cultures (n = 4).

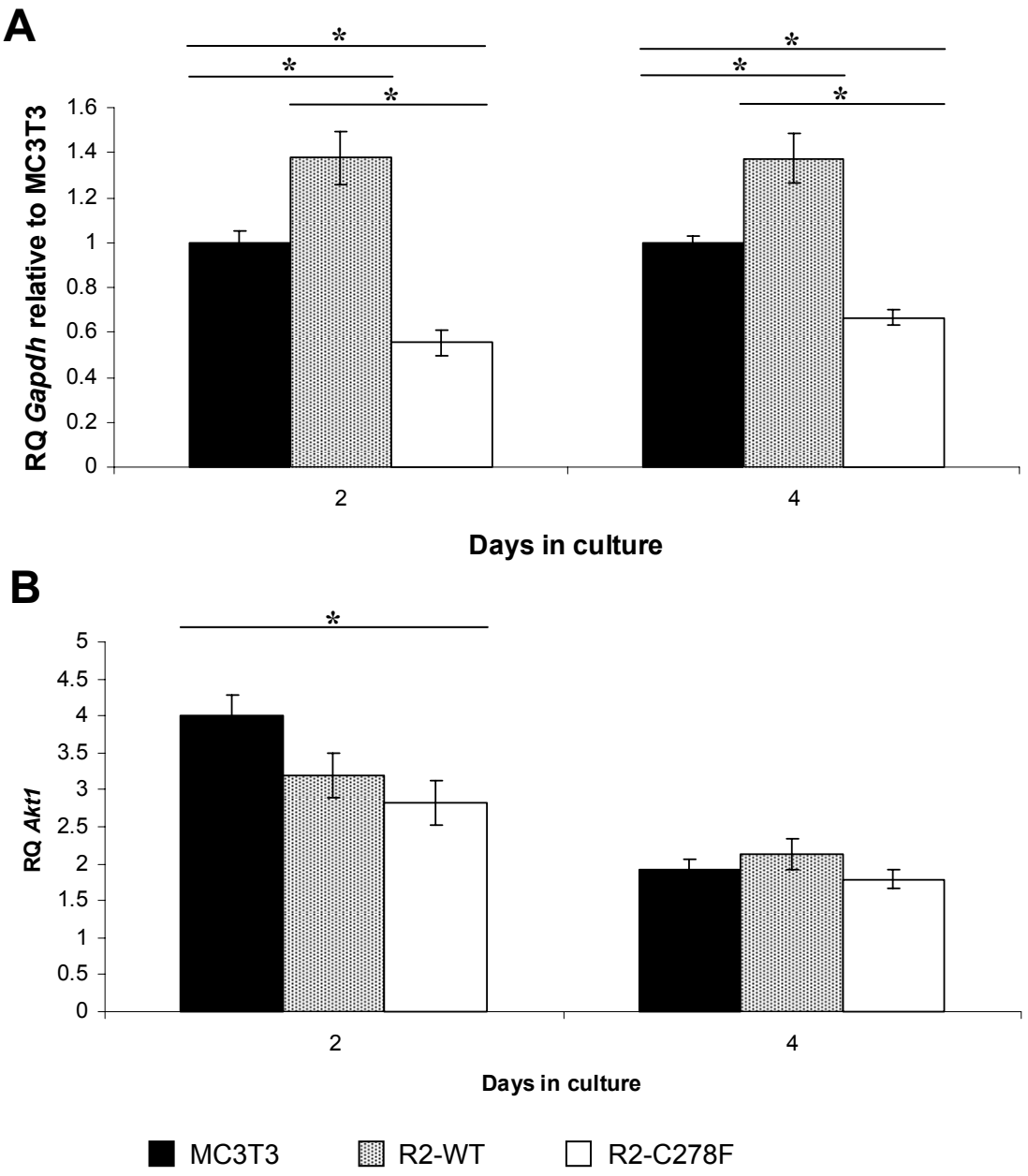

Figure 4.9 Real time PCR analysis of *Gapdh* and *Akt1* in MC3T3, R2-WT and R2-C278F cells

Relative Quantification (RQ) of gene expression against a calibrator (embryonic mouse head E13.5). **A:** For the analysis of *Gapdh* expression only, the RQ value was further normalised to the MC3T3 to compare several experiments, to determining whether *Gapdh* was higher in R2-WT cells than in MC3T3. Compared to MC3T3, at both 2 and 4 days in culture, *Gapdh* expression is significantly higher in R2-WT cells, and significantly lower in R2-C278F cells (n = 5). **B:** At 2 days in culture, the level of *Akt1* expression is not significantly different between MC3T3 and R2-WT cells, however it is significantly lower in R2-C278F cells compared to MC3T3 cells (n = 3, * $p < 0.05$).

4.2.5 The effects of FGFR2-C278F on differentiation

Differentiation had initially been shown to increase in R2-C278F cells compared to MC3T3 (Santos-Ruiz et al., 2007). To confirm this, MC3T3, R2-WT and R2-C278F were plated on a 24 well plate and grown for 2 days. The cells were then fixed and stained for the early differentiation marker, Runx2 using immunocytochemistry (Figure 4.10). The Runx2 protein was present in all three cell lines and generally nuclear in localisation. There were no obvious differences in the level of Runx2 between R2-C278F cells and the two control cell lines. To quantify Runx2 expression, cells were plated on a 12 well plate and cultured for 2 days before analysing Runx2 using FACs immunocytochemistry. This analysis of Runx2 protein expression showed that levels were very similar between all three cell lines at 2 days in culture (Figure 4.11).

Gene expression was analysed in all three cell lines at 2 or 4 days in culture. Culture medium was changed at 2 days for cells that were analysed at 4 days. Real time PCR was used to measure the expression of differentiation markers *Runx2*, *Twist1* and *Osteopontin (Opn)*. *Bsp* and *Osteocalcin (Oc)* were analysed by SYBR Green real time PCR. There were no significant differences in *Runx2* expression between the cell lines at 2 or 4 days in culture (Figure 4.12 A). All three cell lines expressed *Twist1* at 2 and 4 days without any significant differences between them (Figure 4.12 B). *Opn* expression was similar in all three cell lines at 2 days in culture, however at 4 days its expression level was significantly lower in R2-C278F cells, compared to MC3T3 or R2-WT (Figure 4.12 C). *Bsp* expression was not found in any of the three cell lines (Appendix Figure 8.5). *Osteocalcin* (*Oc*) expression was observed in all three cell lines at 4 days in culture. The level of *Oc* was higher in the R2-C278F cells than in the control MC3T3 cells and in R2-WT cells it was significantly higher than in both R2-C278F and MC3T3 (Figure 4.13).

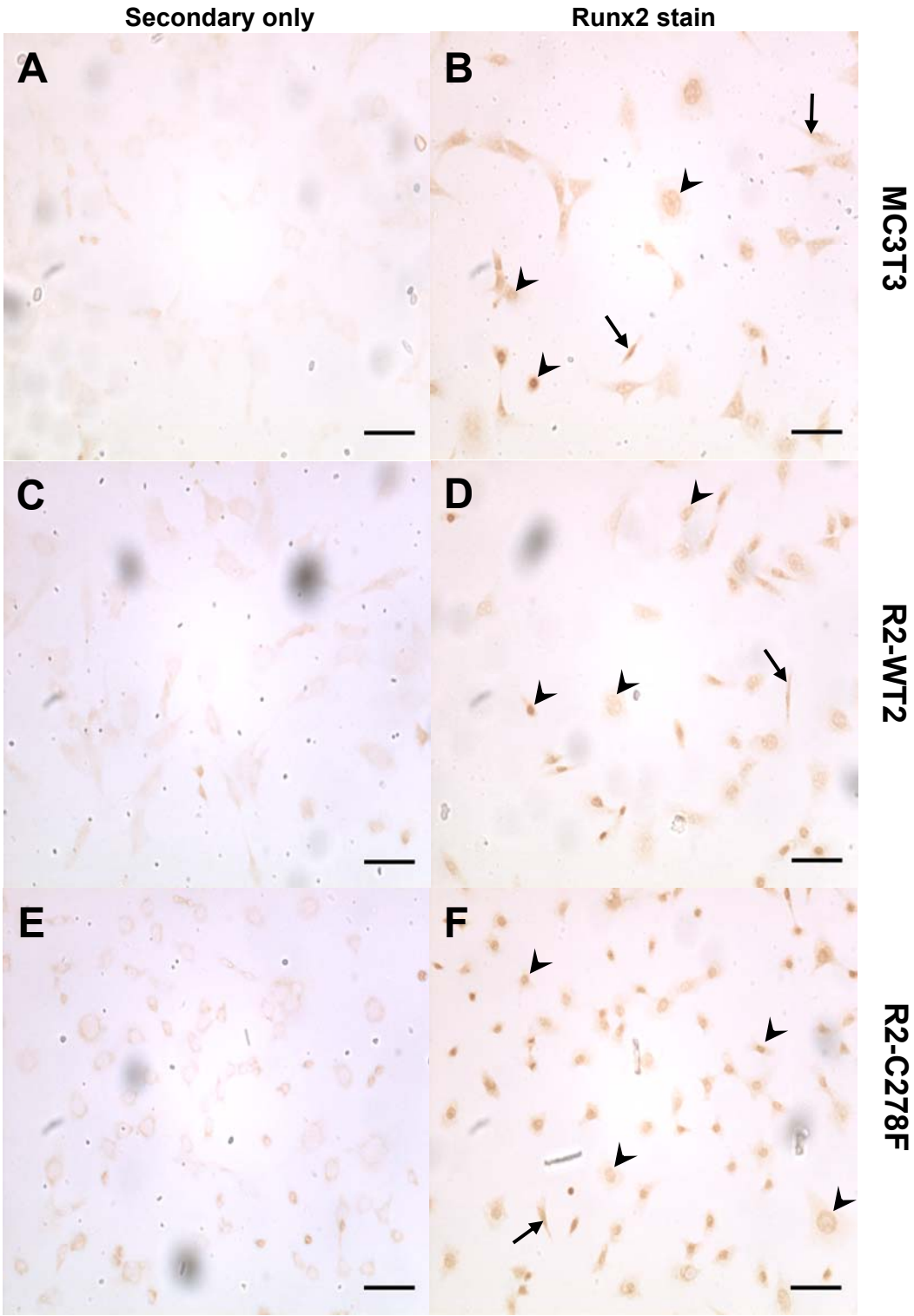

Figure 4.10 Runx2 expression in MC3T3, R2-WT and R2-C278F cells at 2 days in culture

Runx2 immunocytochemistry performed with DAB. **A, C** and **E:** Background control stainings where primary antibody was omitted. **B, D** and **F**: Runx2 staining is mainly nuclear (black arrow heads), and more intense in the nuclei of smaller cells (white arrow heads). The cell staining is more ubiquitous in some of the fibroblastic cells (black arrows) (n = 3, black bar = 50 μm).

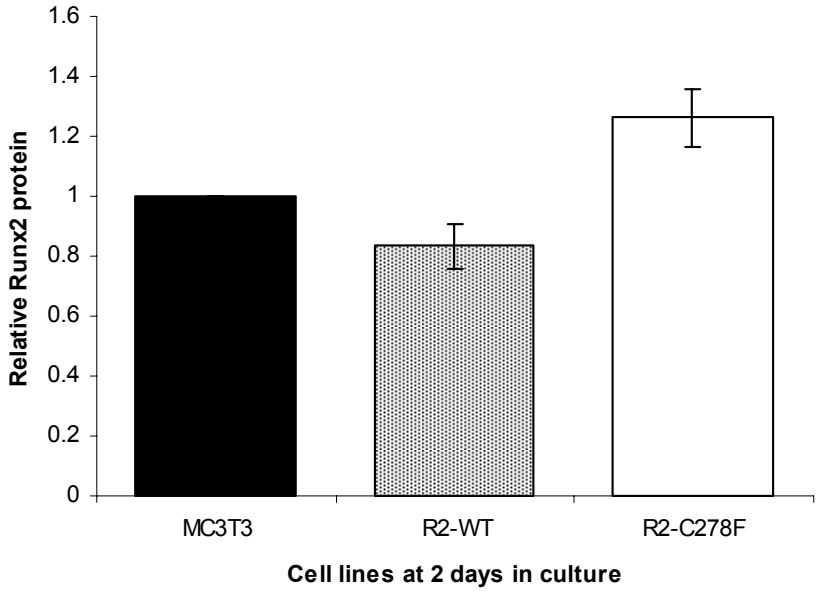

Figure 4.11 FACS analysis of Runx2 protein at 2 days in culture.

Cells were plated to a 12 well plate at 20,000 per cm^2, trypsinised after two days, stained with Runx2 antibody and a fluorescent secondary antibody (Alexa 647). Runx2 expression was normalised to the MC3T3 controls. No significant difference in Runx2 in protein expression level is observed. Note: The error bar is present in MC3T3, but the variability was too small to be visible (n = 3).

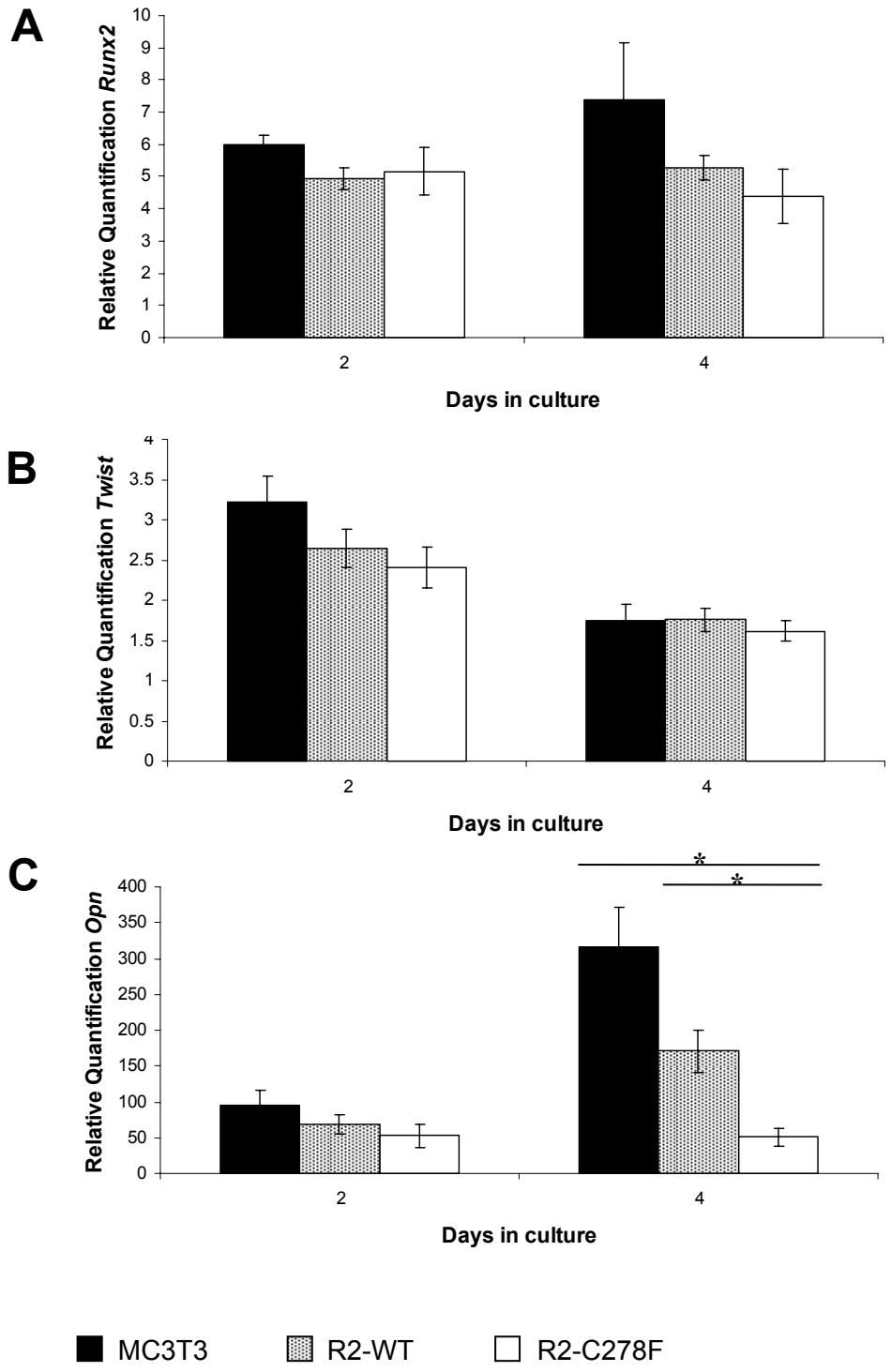

Figure 4.12 Real time PCR analysis of *Runx2*, *Twist* and *Opn* at 2 and 4 days in culture

The relative gene expression was quantified and normalised compared to that of mouse E13.5 at 2 and 4 days. **A**: No significant differences in *Runx2* between cell lines at 2 and 4 days in culture is observed (n = 4). **B:** *Twist1* expression is not significantly different between cell lines (n = 3). **C:** At 4 days *Opn* is signficantly lower in R2-C278F cells than in the other cell lines (n = 3, *p < 0.05).

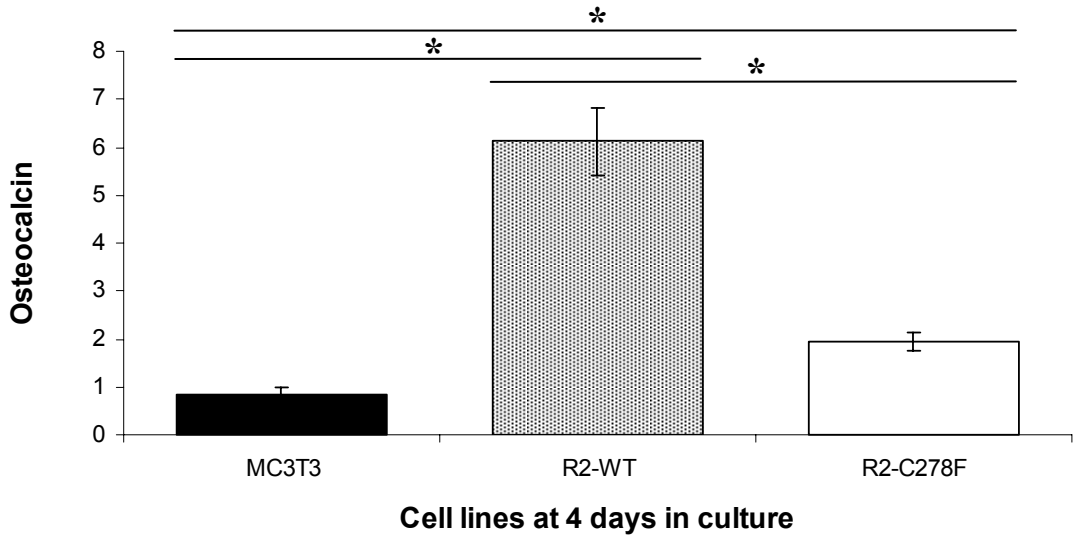

Figure 4.13 *Oc* Gene expression analysed by SYBR Green Real Time PCR analysis at 4 days
Osteocalcin expression was significantly higher in R2-C287F cells compared to MC3T3. In R2-WT cells the osteocalcin expression was significantly higher than in both MC3T3 and R2-C278F cells ($n = 3$, $p < 0.05$).

4.3 Discussion

4.3.1 R2-C278F cells are more differentiated in morphology than MC3T3

Reports have shown that fibroblastic pre-osteoblast cells found at preconfluence, whereas at confluence nearly all cells are cuboidal osetoblasts (Chung et al., 1999; Migliaccio et al., 1993; Sudo et al., 1983). This suggests that osteoblast maturation is associated with a change from fibroblastic to cuboidal morphology. These distinct differences in morphology have been used to classify maturity of cells at preconfluence: Isolation of clones from newborn mouse osteoblasts (OB) revealed that cultures with cells mostly of spindle shaped (fibroblastic) morphology (OB1) contained immature cells, whereas in cultures with a mainly cuboidal morphology (OB4), there are more mature osteoblasts (Mansukhani et al., 2000).

At preconfluence (2 days in culture), about 30% of the MC3T3 cell population are fibroblastic and at confluence (4 days in culture) all acquire cuboidal cell morphology, indicating that cells change morphology as they mature; consistent with the above reports. MC3T3 cells at preconfluence therefore appear to be more mature than OB1 cells according to morphological classifications. A similar shift from fibroblastic to cuboidal morphology is observed in R2-WT and R2-C278F between 2 to 4 days in culture. Therefore at confluence the stage of maturity cannot be distinguished amongst the three cell lines based on morphology as all cells are cuboidal.

The key morphological differences lie at preconfluence: R2-C278F cells have the lowest percentage of fibroblastic cells (15%), compared to both MC3T3 and R2-WT (30%), indicating that R2-C278F cultures contain fewer immature cells, suggesting that the mutant cells are more mature. Interestingly, in R2-C278F cultures there is a significant increase in the proportion of bright round cells, which could be apoptotic cells or dividing cells as rounding of the cells are observed during both of these events.

To summarise, R2-C278F cells are morphologically more differentiated than MC3T3 and R2-WT at preconfluence, but indistinguishable at confluence.

4.3.2 Osteoblast proliferation is significantly reduced in R2-C278F cells

Fgfr2 expression has been positively correlated to cell proliferation in bone (Iseki et al., 1997; Iseki et al., 1999; Ratisoontorn et al., 2003). However FGFR2-C278F, like other constitutively active FGFR2 mutations may either increase or decrease osteoblast proliferation (Marie et al., 2005). Therefore it is essential to characterise these cells properly for later comparison.

At preconfluence, there are no differences in proliferation between MC3T3 and R2-WT cells, as shown by cell cycle analysis (Figure 4.4 and Figure 4.5). At confluence however, there are fewer R2-WT cells than in MC3T3, which may suggest that FGFR2-WT expression may lead to a marginal decrease in proliferation as the cells approach confluence (Figure 4.3). The level of apoptosis at both preconfluence and confluence between R2-WT and MC3T3 are not significantly different, suggesting that this difference in cell growth is not cell survival related (Figure 4.6).

R2-C278F cells proliferate less than in MC3T3 and R2-WT cells, as shown by a lower percentage of cells in S-phase (Figure 4.4) and M-phase (Figure 4.5), which indicates a reduction in cells undergoing DNA synthesis and cell division. Moreover this is supported by the R2-C278F cell count at 4 days, which is lower than in both R2-WT and MC3T3 cells (Figure 4.3). An increased percentage of R2-C278F cells in G0/G1 phase compared to MC3T3, indicates a larger percentage of cells in growth arrest. There is also a significantly larger percentage of R2-C278F cells in G2/M phase than in both controls. As the percentage of cells in M-phase was very small (approximately 2% in all three cell lines), this suggested that most cells in G2/M phase were in G2 phase, inferring that the percentage of R2-C278F cells at G2 phase was higher than in controls.

These findings indicate that compared to MC3T3, normal FGFR2-WT does not significantly affect proliferation at preconfluence, but FGFR2-C278F significantly reduces cell proliferation, with more cells arrested at both the G0/G1 and at the G2 check point than in MC3T3 and R2-WT controls. It is possible that the increased percentage of G2 phase cells may relate to the increase in the percentage of bright round cells found in the previous section.

4.3.3 FGFR2-C782F increases apoptosis and metabolic requirements

Expression of constitutively active mutations of FGFR2 (FGFR2-C432Y) have been shown to significantly increase apoptosis in immature osteoblast clones (OB1) of newborn mice (Mansukhani et al., 2000). Increased apoptosis is also observed in a human model carrying the FGFR2-C342Y mutation (Marie et al., 2005). In this study, the level of apoptosis was significantly increased in R2-C278F cells compared to MC3T3 and R2-WT cells, indicating that FGFR2-C278F also leads to a small increase in apoptosis (Figure 4.6).

When the cell medium is not changed for 7 days, cell death is significantly greater in R2-C278F cells compared to both MC3T3 and R2-WT cells (Figure 4.7), suggesting that R2-C278F have a reduced ability to survive compared to the controls cell lines. As there were a higher number of MC3T3 cells in culture with a total number of apoptotic cells, this may suggest that the main limiting factor for R2-C278F survival may not be the medium nutrient content, but perhaps an increase in a metabolic waste. Increased metabolic waste has been indicated by a study showing that MC3T3 transfected with FGFR2-C278F acidify their medium to a greater extent than the controls after 5-7 days of culture (Hatch et al., 2006).

Apoptosis may be induced in MC3T3 by serum starvation (Wang et al., 2008). Floating cells were observed in MC3T3 18 hours after serum deprivation, supporting the Wang report, suggesting that serum components are essential for MC3T3 cell survival (Figure 4.8). R2-WT cells had a group of floating cells of a similar size suggesting that apoptosis was also induced in these cells. Many more floating cells were present in R2-C278F cells under the same conditions, compared to MC3T3 and R2-WT cultures, suggesting that R2-C278F have a higher dependency on serum for survival than both MC3T3 and R2-WT cells. FGF2 may rescue human osteoblasts from serum induced apoptosis for up to 50 hours before the percentage apoptosis becomes the same as untreated controls, but longer term FGF2 treatment results in increased apoptosis (Debiais et al., 2004). This 18 hour analysis indicates that FGFR2-WT signalling does not protect against apoptosis and actually may increase with aberrant FGFR2-C278F signalling. These findings indicate that FGF2 may not increase cell survival via FGFR2 signalling, but perhaps the other FGFRs, such as FGFR1IIIc, FGFR3IIIc and FGFR4.

Gapdh is an important molecule in metabolism with involvement in glycolysis, cell cycling, and apoptosis (Sirover, 1997). Although *Gapdh* is considered as a stable housekeeping gene and used as an internal control for analyses such as RT-PCR, its expression levels may vary with growth factor treatment and cellular transformation events such as epithelial-mesenchyme

transition (EMT) and neoplasia (Elberg et al., 2006; Gong et al., 1996). Gapdh is discussed in this section as there is reason to exclude the changes observed in Gapdh to cell proliferation.

Gapdh expression can be a function of proliferation (Meyer-Siegler et al., 1992). High *Gapdh* expression is found in cells that are at mid to late stage S-phase of cell cycling, whereas it is low in cells that are arrested in early S-phase and G2 phase (Mansur et al., 1993). R2-C278F cells have lower *Gapdh* expression, a decreased proportion in cells in S-phase and an increased proportion in G2 phase than MC3T3 and R2-WT controls. However, *Gapdh* expression is still lower in R2-C278F cells than in R2-WT cells and MC3T3 at confluence. An initial study (M-phase by FACS analysis) at confluence suggested that the level of proliferation may actually be higher in R2-C278F cells, compared to MC3T3, R2-WT and R2-C278F (Appendix Figure 8.2). This suggests low *Gapdh* expression is not linked to the low proliferation in R2-C278F cells.

Gapdh overexpression in fibroblasts increases apoptosis and sensistivity to apoptotic agents (Dastoor and Dreyer, 2001). The Nitric Oxide (NO) induced NO-GAPDH-Siah death casade is positively mediated by GAPDH (Hara and Snyder, 2006). However R2-C278F cells express lower levels of *Gapdh*, suggesting that their increased apoptosis and sensitivity to apoptosis is not via NO-GAPDH-Siah1 (Figure 4.9 A). Caspase independent cell death (CICD) is a type of Programmed Cell Death (PCD) that occurs alongside caspase dependent cell death in many cells including maturing osteoblasts (Broker et al., 2005). In HeLa cells undergoing CICD following Mitochondrial Outer Membrane Permeabilization (MOMP), *Gapdh* overexpression inhibits apoptosis by increasing glycolysis and autophagy (Colell et al., 2007). Low *Gapdh* expression in R2-C278F suggests that increased apoptosis in these cells could correlate with a CICD mechanism. An initial analysis of Gapdh protein expression indicates that it may be lower in R2-C278F cells compared to MC3T3 and R2-WT cells (Appendix Figure 8.4), supporting a basis to investigate CICD in R2-C278F cells.

Akt1 mediates osteogenesis, Runx2 dependent differentiation and inhibits apoptosis (Kawamura et al., 2007). There was a significant decrease in *Akt1* expression in R2-C278F cells compared to MC3T3 at 2 days in culture, indicating that increased apoptosis may be associated with lower *Akt1* expression (Figure 4.9 B). However the *Akt1* expression alone may not be the main driving factor behind the higher rate of apoptosis, as there was no significant difference in *Akt1* between all three cell lines at 4 days in culture, when the level of apoptosis was still higher in R2-C278F cells (Figure 4.6 B). Alternatively the decrease in *Akt1* expression could be a compensatory mechanism to reduce differentiation in R2-C278F cells, as overexpression of Akt1 positively induces differentiation in osteoblasts (Raucci et al., 2008). To confirm this suggestion, Akt1 protein expression and activation should be analysed.

4.3.4 FGFR2-C278F increases osteoblast differentiation

The Ferretti lab suggested that differentiation may be increased in R2-C278F, based on increased Col1 protein expression in these cells at preconfluence (unpublished), increased *Osteocalcin* expression at postconfluence and increased mineralisation (Santos-Ruiz et al., 2007). Runx2 is a master transcription factor for osteogenic cell differentiation by transcription of other markers of differentiation such as *Col1*, *Alp*, *Opn* and *Oc* (Ducy et al., 1997; Harada et al., 1999; Karsenty et al., 1999). Any change in the level of Runx2 would confirm an alteration in the progression of osteoblast differentiation. Neither the Runx2 gene expression or protein expression level or localisation were different in the R2-C278F cells compared to the MC3T3 cells, indicating that enhanced differentiation in R2-C278F cells suggested by morphology expression is not via Runx2 (Figure 4.10, Figure 4.11 and Figure 4.12A).

Twist is a negative regulator of osteoblast differentiation, which inhibits Runx2 transactivation, thereby inhibiting Runx2 induced differentiation (Bialek et al., 2004). *Twist* is expressed in osteoprogenitors and lost in mature osteoblasts (Rice et al., 2000). If R2-C278F cells were more differentiated, it would be expected that *Twist* expression would be lower than in MC3T3 and R2-WT cells. This was not the case, indicating that differentiation is not altered in R2-C278F cells with respect to *Twist* expresssion.

Osteopontin (Opn) is expressed in preosteoblasts and increases in expression as they differentiate into mature osteoblasts (Aubin, 2001). It also inhibits bone mineralisation (Boskey et al., 2002). Furthermore Opn is a negative regulator of differentiation and has been shown to negatively regulate *bone sialoprotein (Bsp)* and *osteocalcin (Oc)* expression (Huang et al., 2004). In MC3T3 and R2-WT2 cells, *Opn* expression appeared to increase from as cells reached confluence supporting the morphological observations that differentiation had occurred. However *Opn* in R2-C278F cultures did not appear to change upon reaching confluence, even though cells were morphologically cuboidal indicating an abnormality in differentiation (Figure 4.12 C). As Opn negatively regulates late stage differentiation, it can be interpreted that *Opn* expression that is lower in R2-C278F cells compared to the controls (Figure 4.12 C) may contribute to enhanced differentiation in the mutant cells. However it was necessary to analyse *Bsp* and *Oc* expression to confirm these effects, as an alternative explanation for this finding could be that R2-C278F cells are less differentiated therefore have lower *Opn* expression.

BSP is a late differentiation marker which has been found to be restricted to differentiated osteoblasts (Chen et al., 1994; Shapiro et al., 1993). Real time PCR analysis did not reveal any

Bsp expression at 4 days in culture compared to E13.5 mouse head, where *Bsp* expression was found (Appendix Figure 8.5). Bsp is expressed in differentiated rat osteoblasts that are actively forming mineralized bone (Chen et al., 1992). It is possible in this model; bone mineralisation is required before Bsp expression can be observed.

Oc is a late differentiation marker and restricted to differentiated osteoblasts (Mark et al., 1988; Yoon et al., 1987; Stein et al., 1990). *Oc* expression was higher in R2-C278F cells, based on *Gapdh* as an endogenous control (Santos-Ruiz et al., 2007). However in this chapter *Gapdh* expression was found to be reduced in R2-C278F cells, which would have altered the relative measurement of *Oc*. Therefore for this study the endogenous control, 18S was used instead. As suspected, R2-C278F cells have a higher *Oc* expression, confirming that the mutant cells have an enhanced level of differentiation (Figure 4.13). Interestingly the level of *Oc* expression was even higher in R2-WT cells than in R2-C278F, suggesting that these cells are also more differentiated than in MC3T3 at 4 days in culture. This also indicates that other factors related to FGFR2 signalling in addition to *Opn* are also regulating *Oc* expression.

4.3.5 Comparisons of the current findings to current literature

R2-C278F cell proliferation is decreased, apoptosis increased, differentiation increased and the metabolic requirements increased. There are similarities and differences in osteoblast behaviour between studies of craniosynostosis (Marie et al., 2005). The main similarities are that apoptosis has increased in all studies published, including this study. It is suggested that increased osteoblast apoptosis is due to compensation for either excessive proliferation or accelerated differentiation (Lemonnier et al., 2001; Mansukhani et al., 2000; Marie et al., 2005). There are two distinct osteoblast characteristics between models of LICA FGFR2: either proliferation increases and differentiation decreases, or proliferation decreases and differentiation increases.

These two patterns have been explained by differentiation occurring secondary to proliferation, therefore increased proliferation results in decreased differentiation and vice versa (Mansukhani et al., 2000; Marie et al., 2005). However, this does not explain why proliferation is different between studies. There are many possible factors. Firstly, the gene mutations may not be the same and cause different effects in the osteoblasts. There is also the issue with transient and stable transfections used to create the animal models; transient transfections may have higher levels of gene expression if the analysis is carried out before the sample cells can divide or the may have very low expression if they are allowed to divide several times before analysis. Stable transfections often have a low and stable level of expression; however the site of integration may affect assessibility to transcription factor binding or disrupt expression of other genes.

Genetic and environmental background may also contribute, such as the actual mutation and the animal used for modelling (Marie et al., 2005).

Point mutations in FGFR2 such as positions C278F, C342A and C342Y lead to receptor dimerisation and activation (Mangasarian et al., 1997; Robertson et al., 1998). As these mutations disrupt the same 278-342 disulphide bond, it is possible that the same or similar mechanism of constitutive ligand independent activation exists and therefore the same pathology would follow. This is supported by the observations that both Crouzon and Pfeiffer syndromes have been found not only with these mutations but also C342R, C342S and C342W (Ornitz and Marie, 2002).

In this review mouse, chicken and human models will be compared with the assumption LICA FGFR2 mutations have the same mechanism(s) of action. Fgfr2 positively regulates osteoblast proliferation (Eswarakumar et al., 2002; Iseki et al., 1999; Ratisoontorn et al., 2003). The FGFR2-C342Y mouse craniosynostotic phenotype is rescued by blocking or attenuating the FGFR2-C342Y signalling (Eswarakumar et al., 2006; Perlyn et al., 2006). Therefore aberrant FGFR2 signalling can be hypothesised to produces either a strong positive signal (increased proliferation and decreased differentiation) or a negative feedback (reduced proliferation and increased differentiation).

The pattern of osteoblast behaviour is dependent on the stage of development. In chick embryonic day 13 osteogenic cells, FGFR2-C278F increases proliferation and decreases differentiation, indicated by decreased *Col1* and *Alp* expression, increased *Opn* expression, and decreased mineralisation (Ratisoontorn et al., 2003). FGFR2-C342Y expression also increases proliferation in immature murine coronal osteoblasts at E14.5 but not in more mature osteoblast cultures at P1, where a decrease in proliferation is postulated (Eswarakumar et al., 2004). In that report, osteoblasts at E18.5 also showed an increase in cell growth with an increased *Opn* expression, which may be an indication of decreased differentiation. Immature osteoblasts isolated from newborn mice calvarial (OB1) showed a mild increase in proliferation and decrease in differentiation as shown by low Alp expression (Mansukhani et al., 2000). In a three month old craniosynostosis patient with the FGFR2-C342R mutation there was reduced osteoblast proliferation, an increased ALP expression and decreased Opn expression, which may suggest increased differentiation (Fragale et al., 1999). Together these reports suggest that LICA FGFR2 increases osteogenic cell proliferation at an embryonic stage and at some point postnatally may decrease proliferation and increase differentiation.

Therefore a working hypothesis is that LICA FGFR2 increases proliferation in embryonic osteoblasts and decreases proliferation in postnatal osteoblasts. As mentioned, FGFR2-C278F mutation in chick embryonic osteoblasts show increased proliferation and decreased differentiation, which is consistent with the hypothesis. R2-C278F cell proliferation is decreased and differentiation increased, which also fits the hypothesis, as the MC3T3 background is derived from postnatal newborn mouse calvaria (Sudo et al., 1983). However there is a discrepancy between these findings and that of the OB1 clones from Mansukhani (Mansukhani et al., 2000). It has been suggested that osteoblast response to Fgf signalling may depend on the stage of maturation. In less mature osteoblasts proliferation increases and differentiation decreases with Fgf2 treatment, whereas in mature osteoblasts proliferation is not affected and differentiation increases (Debiais et al., 1998). Similarly in the Mansukhani report, in immature OB1 cells there was a great increase in proliferation following Fgf treatment, whereas the more mature OB4 cells responded to Fgf treatment with a small increase in proliferation (Mansukhani et al., 2000). The Ferretti lab has studied cell growth in all three cell lines with respect to Fgf2 and Fgf18 treatment, which resulted in a small increase in cell growth in all three cell lines in low serum conditions. This indicates that MC3T3 in this model resembles mature OB4 cells more, which may suggest that the response to Fgf may contribute to the mutant cell phenotype as R2-C278F cells are already more differentiated than MC3T3.

Reduced proliferation in R2-C278F cells does not follow from earlier FGFR2-C278F expression during embryogenesis, as FGFR2-C278F was stably transfected at a postnatal stage. Therefore the main difference between the two in craniosynostotic phenotypes could be a result of differing responses to FGFR2 signalling, intrinsic to the age or maturation stage of the osteoblast. The mechanism(s) underlying this switch in cellular responses to LICA FGFR2 for now are unknown. It is speculated that increased positive FGFR2 signalling will be found in embryonic and immature early postnatal osteoblasts, whereas increased negative feedback on FGFR2 is found in postnatal and more mature cells, such as those in human patients (Fragale et al., 1999). Further investigation of FGF's downstream pathways may help uncover this/these mechanisms in both embryonic and postnatal cells. A review of the phenotypes are given in Table 4.1.

Table 4.1 Effect of FGFR2 mutations 278 and 342 in osteoblasts					
	Ratisoontorn et al[1]	Eswarakumar et al[2]	Mansukhani et al[3]	**Present study** & Santos-Ruiz et al[4]	Fragale et al[5]
Stage	Embryo	Embryo (E18.5)	Postnatal	Postnatal	3 month
Osteoblast source	Chick calvaria	Mouse	Mouse OB1 cell line	Mouse MC3T3 line	Human patient
Type	*In-vitro*	*In-vivo*	*In-vitro*	*In-vitro*	*In-vitro*
Mutation	C278F	C342Y	C342Y	C278F	C342R
FGFR	M	M	M	H	H
Proliferation	↑	↑	↑	**↓***	↓
Apoptosis				**↑***	
Differentiation	↓	↓	↓	**↑***	↑
RUNX2		↑		=	
ALP	↓		↓	↑	↑
COL	↓			↑	
TWIST				=	
OPN	↑	↑		**↓***	↓
OC	=	=		**↑***	
Mineralisation	↓ (Alizarin R)		↓ (von kossa)	↑ (Alizarin R)	↓

H = Human FGFR2, M = Mouse FGFR2, bold arrow* = investigated in this thesis.

References:

1: Ratisoontorn et al., 2003, 2: Eswarakumar et al., 2004, 3: Mansukhani et al., 2000, 4: Santos-Ruiz et al., 2007, 5: Fragale et al., 1999

4.4 Conclusion

R2-C278F cells have a reduced proliferation, increased differentiation and apoptosis and higher metabolic requirements for survival. Proliferation is reduced in R2-C278F cells compared to R2-WT and MC3T3 cells at preconfluence. Increased differentiation in R2-C278F cells is indicated by a lower proportion of cells with a fibroblastic morphology at pre-confluence and both a low *Opn* expression and a high *Oc* expression at confluence. *Twist1* and *Runx2* gene expression is not significantly affected in R2-C278F cells; however this does not exclude functional changes to the protein that might affect the cell phenotype. R2-C278F cells show increased apoptosis both at preconfluence and confluence. The FGFR2 mutant cells also have an increased dependency on serum for survival and low *Gapdh* expression, which is speculated to be a result of increased caspase independent cell death (CICD). Increased apoptosis is also speculated to be a result of compensation for enhanced osteoblast differentiation.

The stage of development appears to be crucial in determining the phenotype of ligand independent constitutively active (LICA) FGFR2 craniosynostotic osteoblasts. The FGFR2 mutant osteoblasts at the embryonic stage show increased proliferation and decreased differentiation, whereas most of the models at the postnatal stage including the current R2-C278F model are consistent with decreased proliferation and increased differentiation. It is hypothesised that during embryogenesis LICA FGFR2 mutations display a true “gain-of-function” demonstrated by the proliferative phenotype. In contrast postnatal LICA FGFR R2-C278F cell phenotype may result from a negative feedback on FGFR2 signalling on proliferation and that increased differentiation is a secondary effect leading to craniosynostosis.

Chapter 5 FGF signalling in R2-C278F cells

5.1 Introduction

The most fascinating property of the FGFR2-C278F mutation is its ability to dimerise and signal without FGF (Mangasarian et al., 1997), previously termed as ligand independent constitutively activated (LICA) FGFR2. This property in NIH3T3 fibroblasts is observed in a number of FGFR2 point mutations including W290G, T341P, C342A and C342Y (Robertson et al., 1998). All of these mutations dimerise FGFR2 by disulphide bridging at position 278 or 342, suggesting that these different point mutations may share the same mechanism of aberrant FGF signalling that leads to craniosynostosis. As suggested in chapter 4, there is a pattern to how osteoblast cell behaviour is altered by LICA FGFR2 depending on whether they are embryonic or postnatal, supporting the hypothesis that these mutations share a similar disease mechanism.

FGFR2-C278F initiates signalling in MC3T3 cells via FRS and PLC-γ, and due to incomplete glycosylation this receptor has increased degradation (Hatch et al., 2006). Craniosynostosis in mice expressing FGFR2-C342Y may be rescued by either attenuating the TK domain of this mutant receptor or simply inhibiting FGFR TK activation (Eswarakumar et al., 2006). This suggests that the aberrant FGFR2 signalling, rather than the effects of receptor degradation alone, is responsible for inducing a craniosynostotic phenotype. The FGF signalling pathway is complex, because of the large numbers of ligands, receptors and intracellular binding sites for FGF, FGFR and FGF-FGFR signal initiation involved. Moreover there is direct (protein level) and indirect (transcriptional) feedback signalling on FGF. The Fgf ligands essential for normal bone formation and Fgfr2 activation are more likely to be involved in craniosynostosis, as bone formation is affected. FGFR2 signalling is mediated by downstream pathways such as the Mitogen Activated Protein Kinase (MAPK) - Extracellular Related Kinase (ERK) 1/2 pathway and the Protein Kinase C (PKC) pathway. Both pathways affect proliferation and differentiation in osteoblasts and may be relevant to the aberrant signalling of FGFR2-C278F, given the R2-C278F cell phenotype. Normal FGFR2 may positively regulate osteoblast proliferation (Iseki et al., 1999), yet FGFR2-C278F expression in MC3T3 reduces proliferation and increases differentiation, suggestive of some effects of negative feedback (Chapter 4).

The aim of this chapter was to find alterations within the FGFR signalling pathway in R2-C278F cells and relate these to their cell phenotype.

5.2 Results

5.2.1 *Fgf1, -2, -18* and *Fgfr2IIIc* expression in osteoblasts

Fgf1, -2 and -18 are important in both bone formation and Fgfr2 activation as they affect osteoblast proliferation and differentiation. Their expression levels were analysed by PCR in case they were linked to the proliferation and differentiation defects of R2-C278F cells. The main Fgfr2 isoform expressed in osteoblasts and essential for normal bone development is Fgfr2IIIc (Eswarakumar et al., 2002; Orr-Urtreger et al., 1993). The endogenous *Fgfr2IIIc* gene expression was analysed. The samples for all three cell lines were cultured for 2 or 4 days, with a change of culture medium at 2 days for the 4 day samples. *Fgf1*, *-2* and *Fgfr2IIIc* were analysed by RT-PCR, using *Gapdh* as an endogenous control. SYBR green real time PCR was used to further analyse *Fgfr2IIIc* with *18S* as an endogenous control. *Fgf18* expression was analysed by real time PCR.

The conditions for measuring *Fgf1* and *-2* were optimized. *Fgf1* expression was present in mouse head E13.5 (Figure 5.1 A). However *Fgf1* expression was undetectable in MC3T3, R2-WT and R2-C278F cells at both 2 and 4 days in culture (Figure 5.1 B and C). Although *Fgf2* was expressed in E13.5 mouse head (Figure 5.2 A), it was undetectable in all three cell lines at 2 and 4 days in culture (Figure 5.2 A and B). The expression level of both genes was later analysed using real time PCR, which revealed a low expression level for each cell line at 2 and 4 days (Chapter 6). *Fgfr2IIIc* was present in all three cell lines (Figure 5.2 A and B). Densitometry of *Fgfr2IIIc* normalised to *Gapdh* showed no significant differences between all three cell lines at 2 days and at 4 days, but a trend towards increased expression was observed in R2-C278F cells (Figure 5.2 C). *Fgfr2IIIc* was further analysed at 2 days in culture using SYBR green real time PCR with *18S*. This revealed that the expression level of *Fgfr2IIIc* had increased in R2-C278F cells, relative to MC3T3 (Figure 5.3 A). Interestingly, the *Fgfr2IIIc* expression had also increased in R2-WT cells, compared to MC3T3. At 4 days in culture, the levels of *Fgfr2IIIc* were not significantly different among the three cell lines (Figure 5.3 B). *Fgf18* was expressed in all three cell lines at 2 and 4 days in culture (Figure 5.4). At 2 days in culture, there were no significant differences in the expression level of *Fgf18* amongst all three cell lines. At 4 days in culture, *Fgf18* expression in both R2-WT and R2-C278F cells was significantly higher compared to the MC3T3 cells. The *Fgf18* expression in R2-WT cells was also higher than in R2-C278F cells.

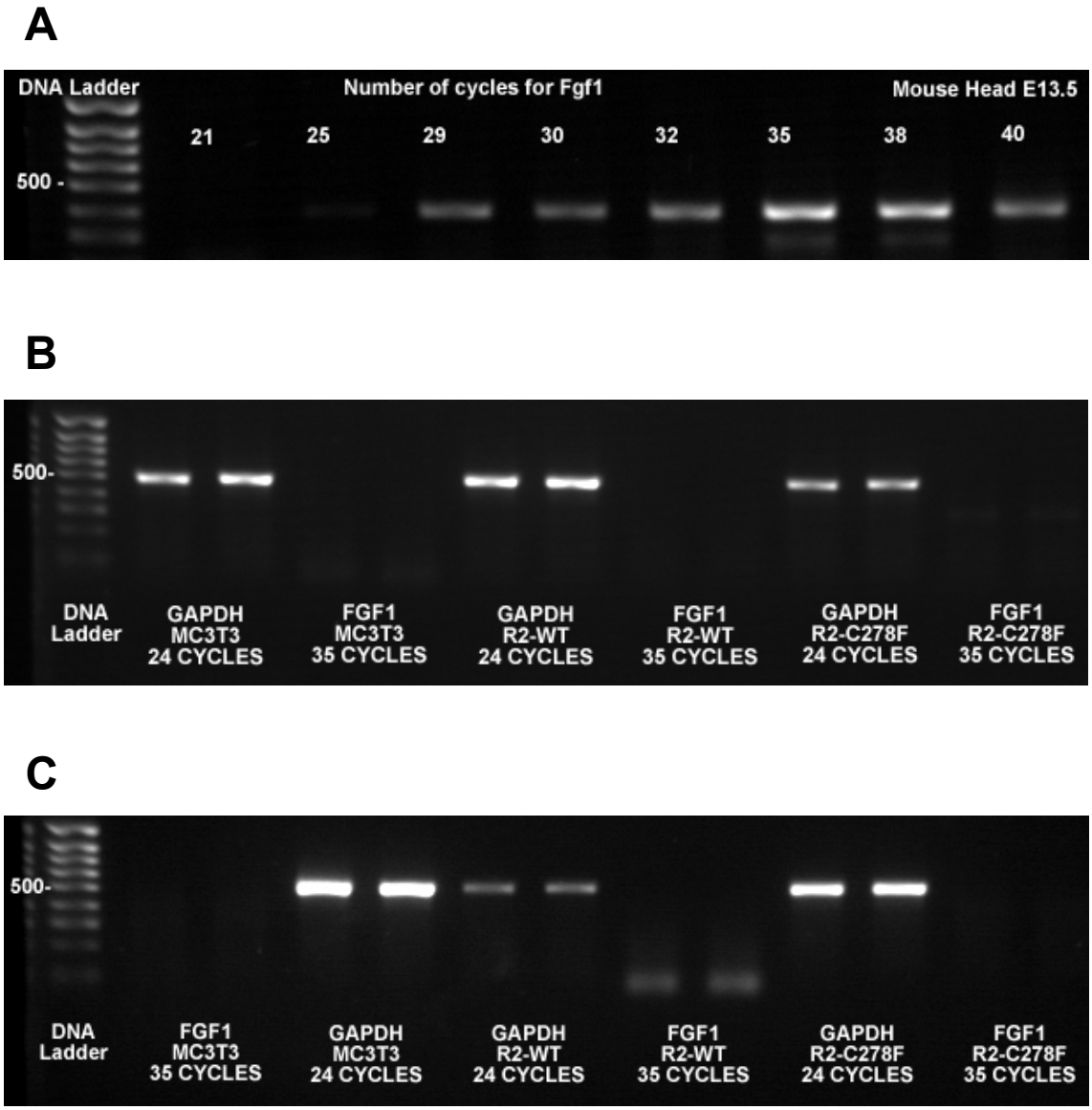

Figure 5.1 *Fgf1* gene expression analysis by RT-PCR in MC3T3, R2-WT and R2-C278F cells

MC3T3, R2-WT and R2-C278F cells were cultured for 2 or 4 days before gene expression analysis by RT-PCR. Fgf1 and Gapdh PCR products of RT-PCR were analysed at 2 and 4 days in culture using gel electrophoresis. **A:** The *Fgf1* transcript is detectable in E13.5 mouse head (387 bp). **B:** Although *Gapdh* (492 bp) is clearly visible in all three cell lines at 2 days in culture**,** *Fgf1* is undetectable in MC3T3 and R2-WT; it is barely detectable in R2-C278F cells. **C:** *Gapdh* is present at 4 days in culture, however *Fgf1* is undetectable in all three cell lines (n = 3).

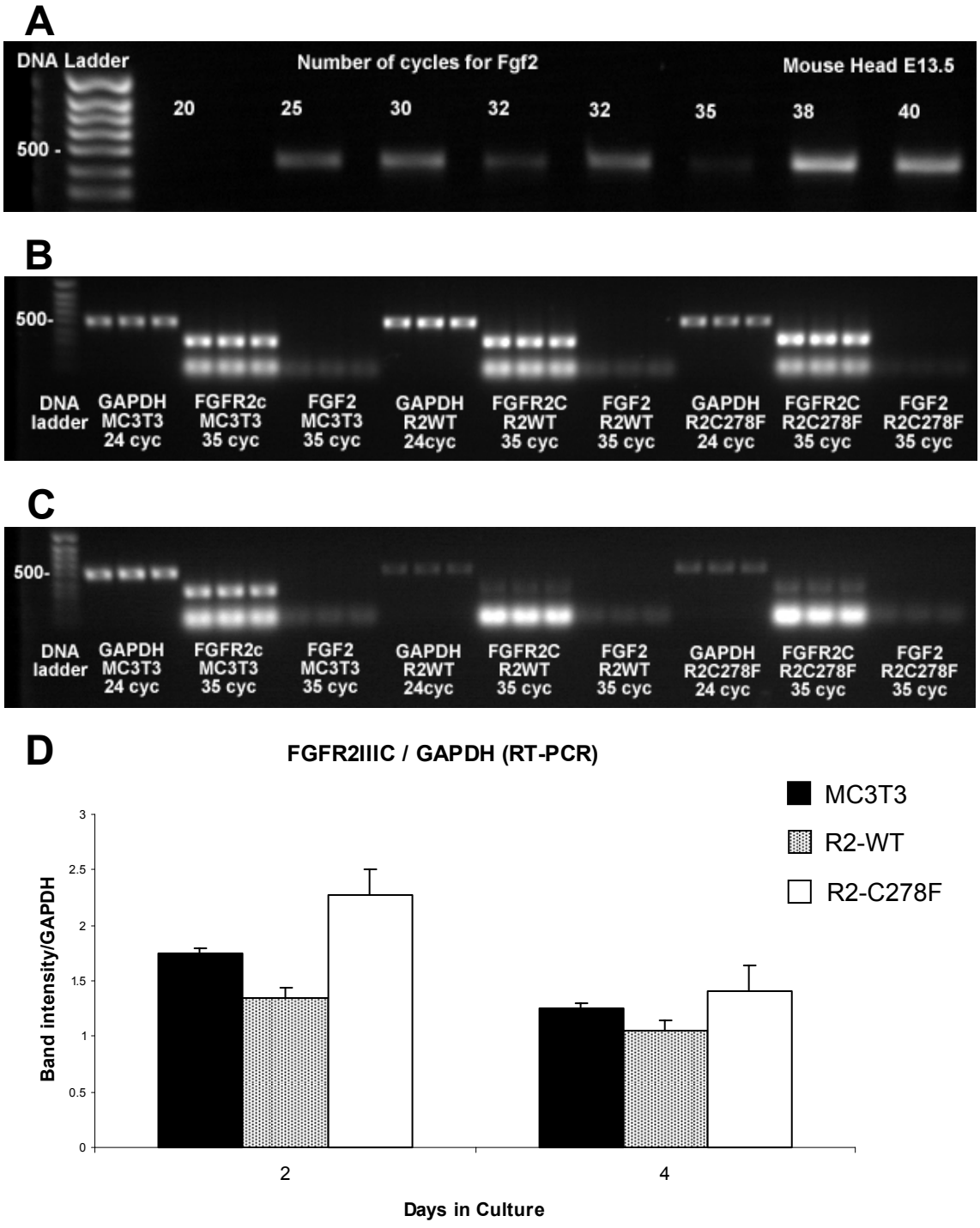

Figure 5.2 *Fgf2* and *Fgfr2* expression in MC3T3, R2-WT and R2-C278F cells by RT-PCR

Fgf2, *Fgfr2IIIc* and *Gapdh* expressions were analysed in MC3T3, R2-WT and R2-C278F cells at 2 and 4 days in culture. **A:** *Fgf2* amplification product of size 429 is detectable in E13.5 mouse head. **B:** *Fgf2* is not detectable in any of the three cell lines at 2 days in culture, however *Fgfr2IIIc* (315 bp) and *Gapdh* (492 bp) are present. **C:** At 4 days in culture, *Fgf2* is not detectable, but both *Fgfr2IIIc* and *Gapdh* are present. **D:** Densitometry of *Fgfr2IIIc* expression in MC3T3, R2-WT and R2-C278F cells, normalised the *Gapdh* expression (n = 3).

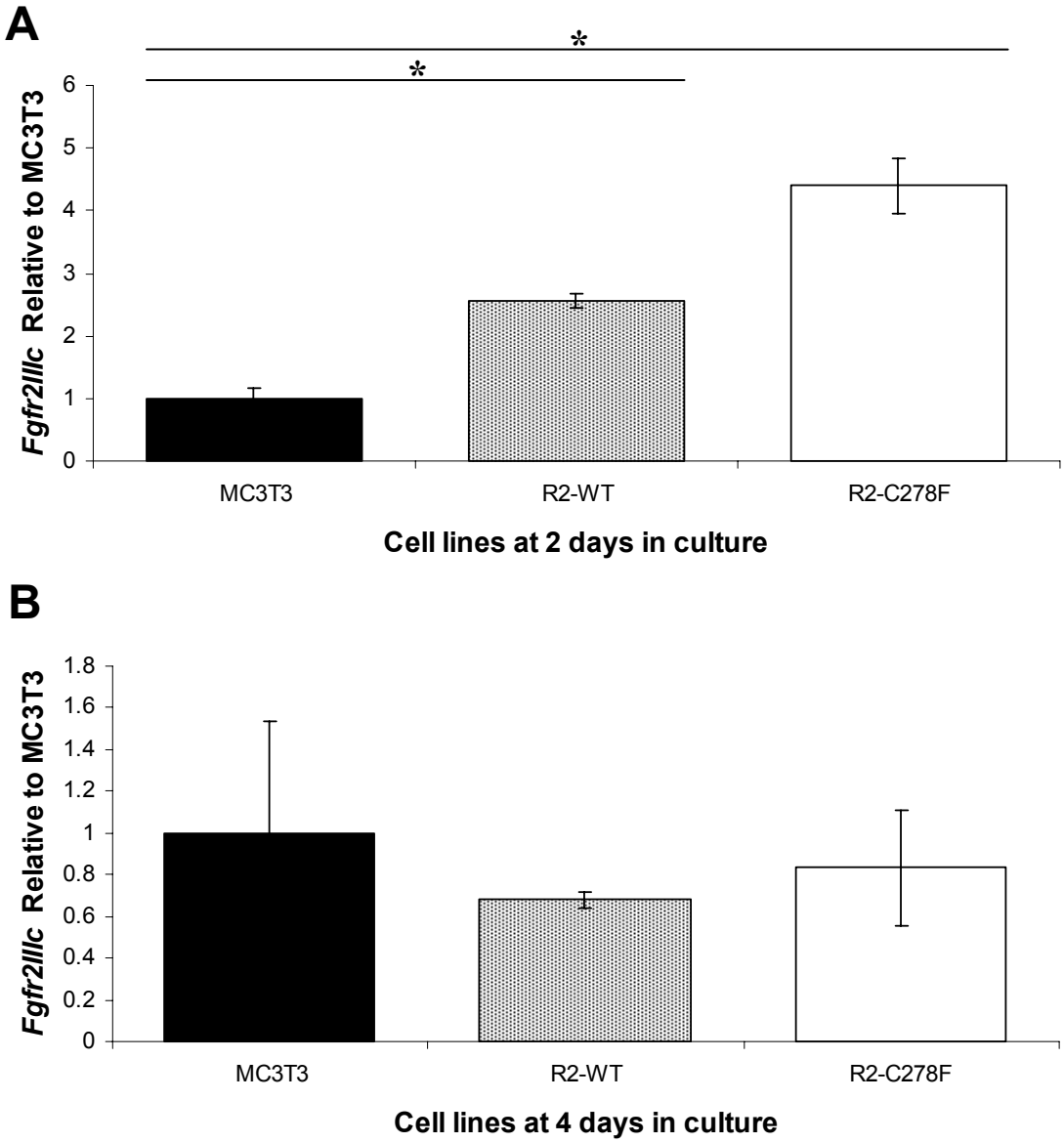

Figure 5.3 Analysis of *Fgfr2IIIc* expression by SYBR Green real time PCR at 2 and 4 days culture
Cells were grown for 2 and 4 days in culture for *Fgfr2IIIc* expression studies. For each cell line the expression levels were normalised to that of the MC3T3 controls. **A:** Compared to MC3T3, the level of *Fgfr2IIIc* is higher in R2-C278F and R2-WT cells at 2 days. *Fgfr2IIIc* expression is also higher in R2-WT cells, compared to MC3T3 at 2 days. **B:** At 4 days in culture, there are no differences in the Fgfr2IIIc expression between all three cell lines ($n = 3$, * $p < 0.05$).

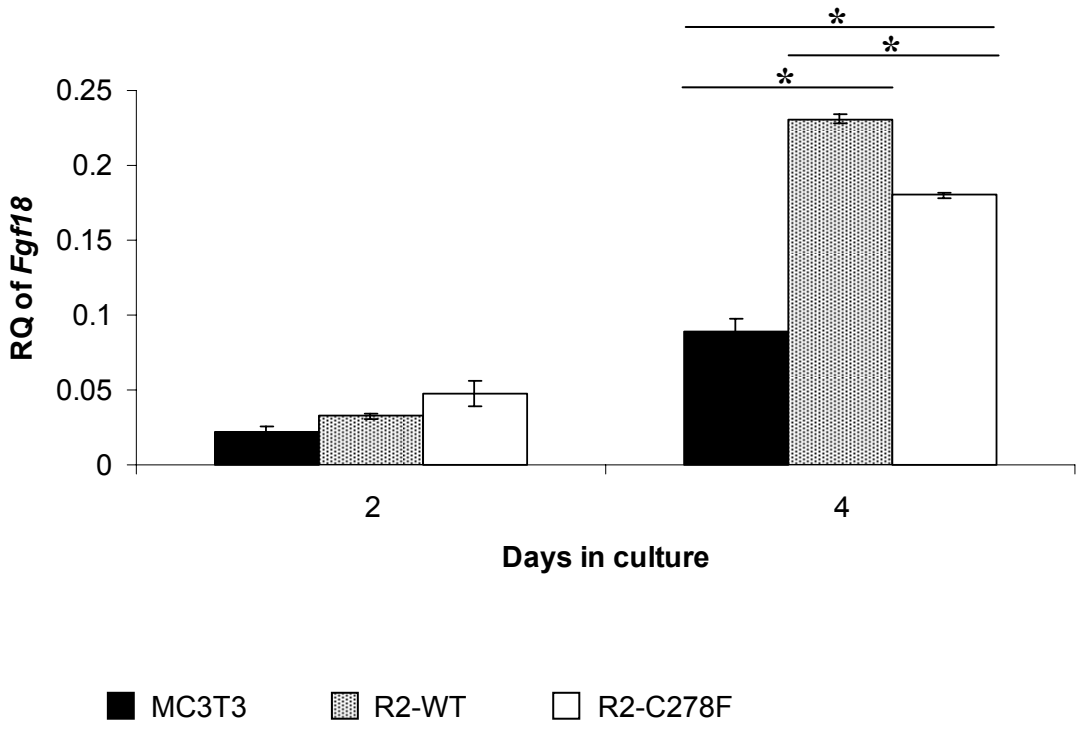

Figure 5.4 Real time PCR analysis of *Fgf18* expression in MC3T3, R2-WT and R2-C278F cells

MC3T3, R2-WT and R2-C278F cells were cultured for 2 or 4 days. The level of *Fgf18* expression was normalised to *18S*. This was then normalised to an E13.5 mouse head calibrator to give a Relative Quantification (RQ) value. *Fgf18* expression levels are not significantly different between cell lines at 2 days in culture. However at 4 days, the level of *Fgf18* expression in R2-C278F cells is significantly higher than in MC3T3 cells. In R2-WT cells, *Fgf18* is significantly higher than both MC3T3 and R2-C278F cells ($n = 3$, $*p < 0.05$).

5.2.2 Erk1 protein levels increase relative to Erk2 in R2-C278F cells

MAPK Erk1/2 is a downstream pathway essential for Fgf induced proliferation and differentiation in osteoblasts (Lai et al., 2001; Spector et al., 2005). To assess this pathway for changes during the proliferative phase in culture, Erk1/2 protein expression was measured at 2 days in culture using FACS analysis. This revealed that the total Erk1/2 protein expression was significantly higher in R2-C278F cells than in both MC3T3 and R2-WT cells (Figure 5.5 A). To make an assessment of Erk1/2 activation, cells were fixed and the level of phospho-Erk (pErk) analysed by FACS. No significant differences were found in pErk1/2 between the cell lines (Figure 5.5 B).

Erk1 and Erk2 protein expression was assessed in 2 and 4 day cultures by Western blotting and semi-quantified using Alpha tubulin. This showed no significant differences between the total level of Erk1/2 in each cell line, but a high variability between experiments was observed (Appendix Figure 8.9). The raw Alpha tubulin levels were carefully compared, using equal protein loading. This revealed that the level of Alpha tubulin was significantly higher in R2-C278F cells compared to MC3T3 and R2-WT cells (Appendix Figure 8.9). The level of Alpha tubulin was also higher in R2-WT cells compared to MC3T3. To reduce the variability and compare the relative expression of Erk1 and Erk2, Erk1 was normalised to Erk2 to give a ratio between Erk1 and Erk2 protein expression, hereafter defined as the Erk1/Erk2 ratio. In R2-C278F cells the Erk1/Erk2 ratio was higher than in MC3T3 at 2 days, at 0.61, 0.62 and 0.83, for MC3T3, R2-WT and R2-C278F respectively (Figure 5.6 A). At 4 days in culture the Erk1/Erk2 ratio was still higher in R2-C278F with values of 0.83, 0.86 and 1.21, for MC3T3, R2-WT and R2-C278F respectively (Figure 5.6 B). There were no significant differences in the Erk1/Erk2 ratio between MC3T3 and R2-WT cells at either 2 or 4 days in culture.

Phosphorylation of Erk1/2 was analysed using Western blotting. The pErk1 band intensity was normalised to that of pErk2 to give the ratio of activation hereafter termed the pErk1/pErk2 ratio. Cells were incubated for 10 minutes with the Protein Kinase C (PKC) activator phorbol 12-myristate 13-acetate (PMA) before protein analysis in order to activate pErk1 and pErk2. PMA appeared to induce a small increase in pErk1/pErk2 activation in MC3T3 and R2-WT at 2 days in culture, as shown by an increase in the pErk1 band intensity, but not in R2-C278F cells (Figure 5.7 A). Without activation, the pErk1/pErk2 ratios in untreated MC3T3, R2-WT and R2-C278F cells were approximately 0.4, 0.4 and 0.75, respectively (Figure 5.7 B). However there were not enough control samples for a proper statistical analysis to confirm that these ratios were different. Amongst the PMA treated groups, no significant differences were found in the pErk1/pErk2 ratio (Figure 5.7 B). At 4 days in culture the ratio of untreated R2-C278F was

significantly higher than in untreated MC3T3 and R2-WT (Figure 5.8 B). The PMA treatment did not significantly change the Erk1/Erk2 ratio between untreated and treated cells of the same cell line. No significant differences in ratios were found when the treated R2-C278F samples were compared to the treated MC3T3 and R2-WT samples. Interestingly, the ratio of treated R2-WT remained significantly lower than the untreated R2-C278F.

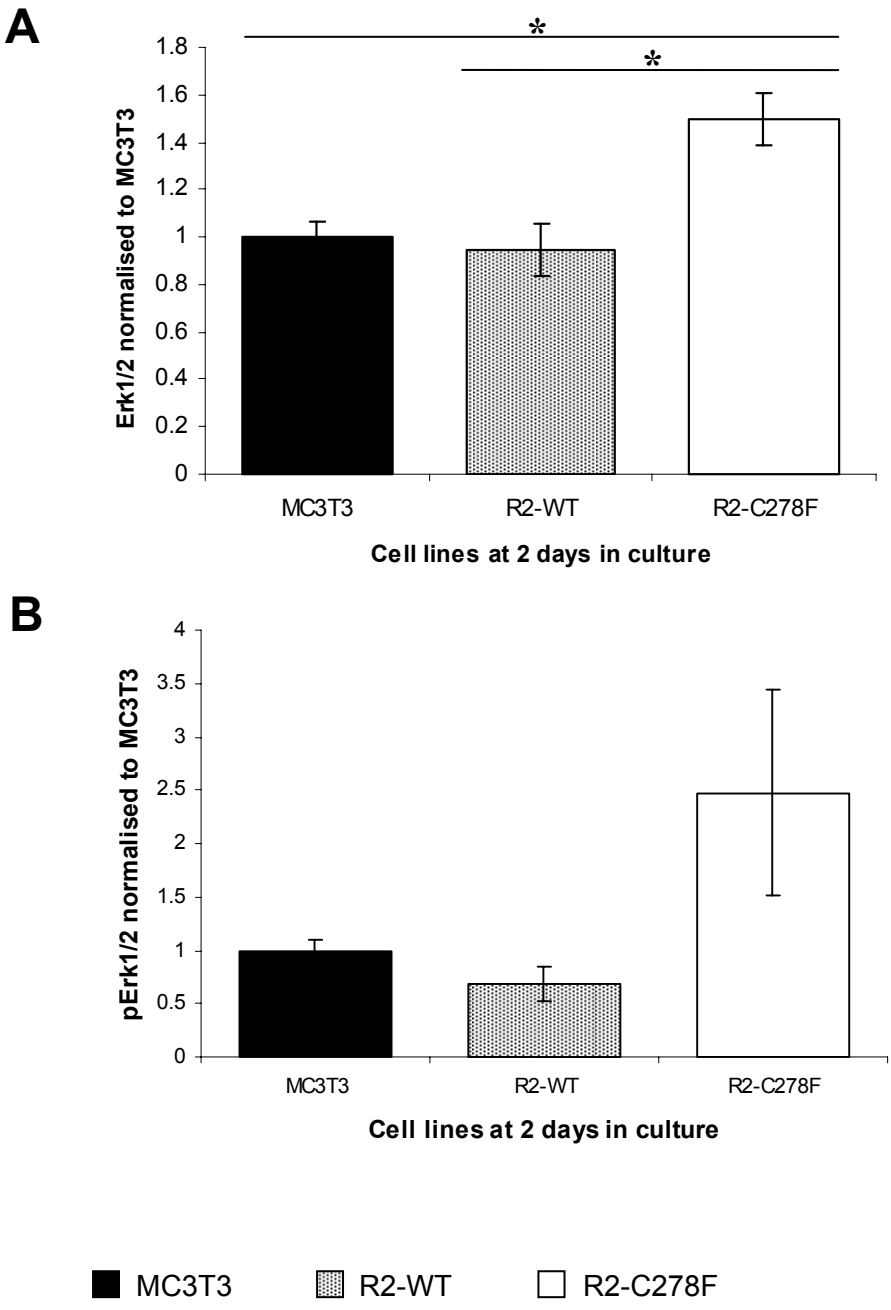

Figure 5.5 Erk1/2 and pErk1/2 in MC3T3, R2-WT and R2-C278F cells analysed by FACS

MC3T3, R2-WT and R2-C278F cells were growth for 2 days in culture prior to FACS analysis. The average Erk1/2 and pErk1/2 fluorescence for each experiment was normalised to the value of the MC3T3 control in order to analyse all the data together. **A:** The level of Erk1/2 in R2-C278F cells is significantly higher than in R2-WT and MC3T3 cells by approximately 1.5 fold. **B:** No significant differences are found in the level of pErk1/2 between the three cell lines ($n = 3$, $*p < 0.05$).

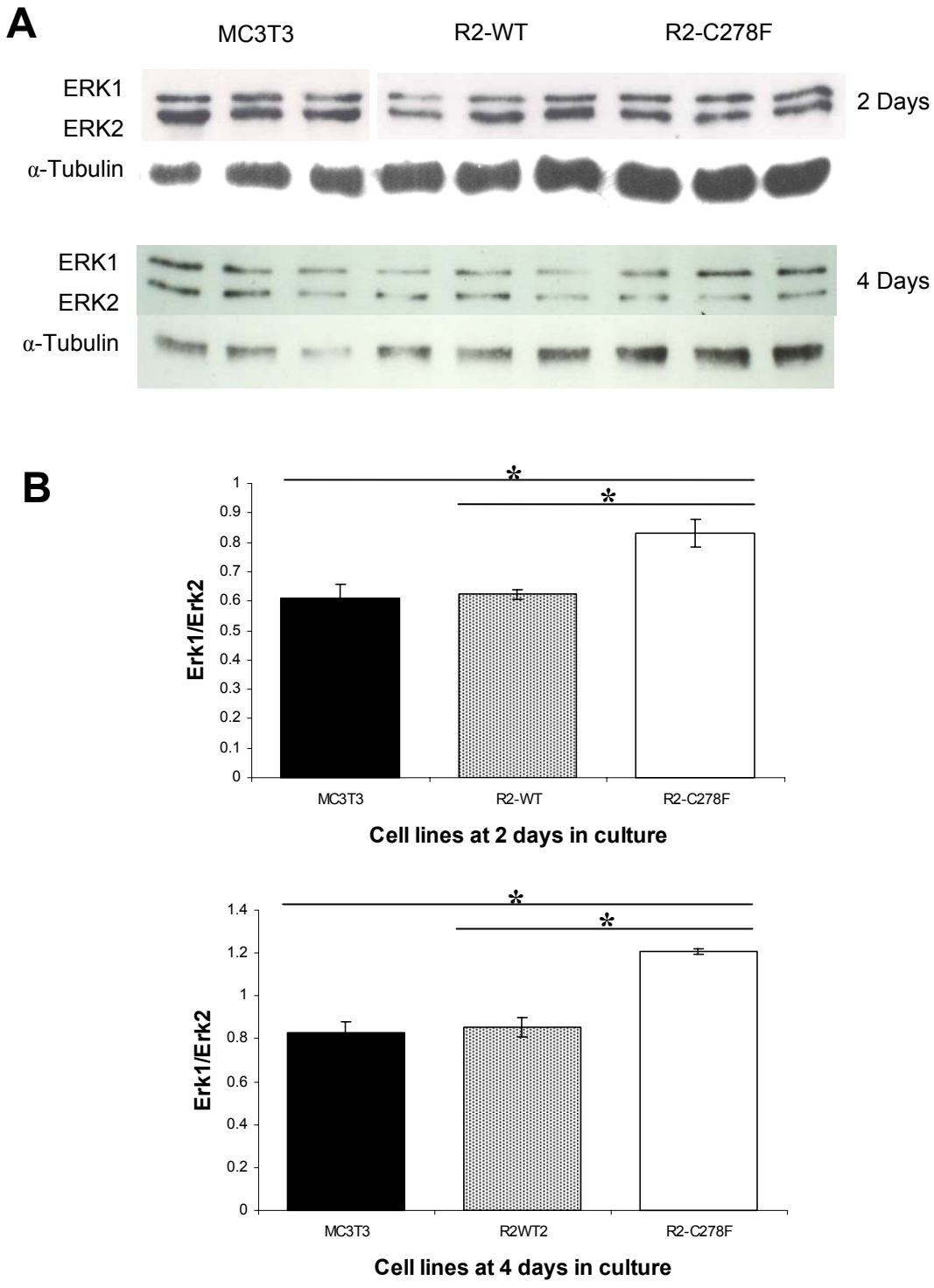

Figure 5.6 Western blot analysis of Erk1/2 expression in MC3T3, R2-WT and R2-C278F cells

A: Erk1/2 was detected in cells cultured for 2 or 4 days. α-Tubulin was used as a loading control **B:** Erk1/Erk2 ratio at 2 and 4 days in culture. The areas of Erk1 and Erk2 bands were measured by densitometry and the area of Erk1 divided by Erk2 to obtain the ratio shown in the graphs. Erk1/Erk2 ratios are similar between MC3T3 and R2-WT cells, but significantly higher in R2-C278F than in the other cell lines both at 2 and 4 days in culture ($n = 5$, $*p < 0.05$).

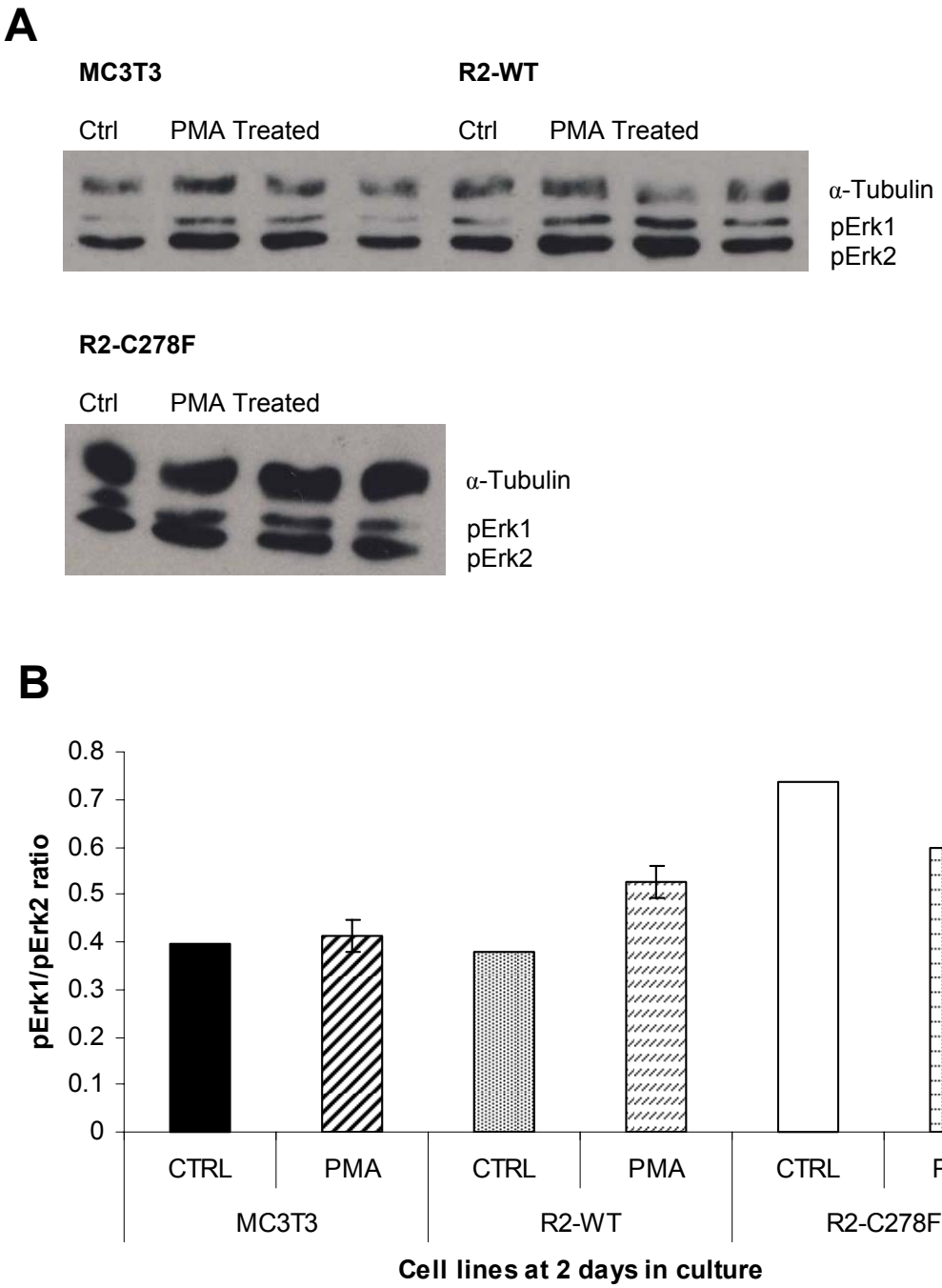

Figure 5.7 Phospho-Erk expression ratios with PMA treatment in cells at 2 days in culture

A: Western blotting of MC3T3, R2-WT and R2-C278F cells cultured for 2 days and treated with 50 ng/ml of PMA 10 minutes prior to protein extraction. **B:** Densitometry analysis of pErk expression detected by western blot of pErk1/pErk2 in cells treated in (A). No significant differences were found between the pErk1/pErk2 ratios of the PMA treated cells (n = 3).

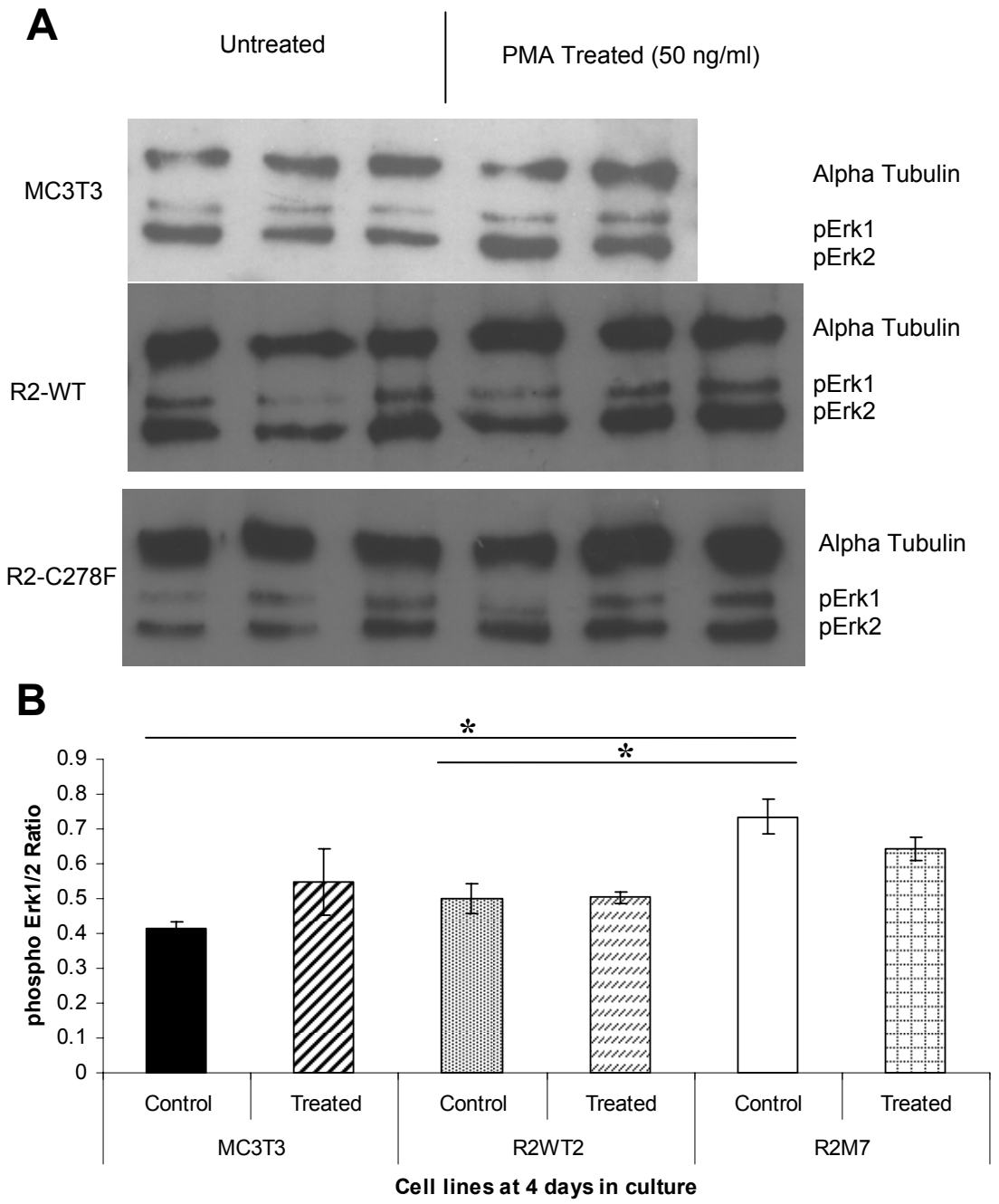

Figure 5.8 pErk expression ratios of PMA treated cells at 4 days in culture

A: Western blotting of MC3T3, R2-WT and R2-C278F cells cultured for 4 days and treated with 50 ng/ml of PMA 10 minutes prior to protein extraction. **B:** Densitometry of pErk1/pErk2 in cells treated in **(A).** Between the untreated groups, there is no significant difference in the pErk1/pErk2 ratio between MC3T3 and R2-WT cells, however in R2-C278F cells the Erk1/Erk2 ratio is significantly higher than in both controls. The ratio of pErk1/pErk2 between the untreated and PMA treatment groups of each respective cell line are not significantly different. The pErk1/pErk2 ratio is significantly higher in control R2-C278F cells compared to the treated R2-WT cells ($n = 3$, $*p < 0.05$ ANOVA).

5.2.3 The effect of FGF signalling manipulation on cell growth

Blocking of FGFR2-C342Y signalling in mice has been shown to rescue suture obliteration normally found in craniosynostosis (Eswarakumar et al., 2006). As FGFR2-C278F is thought to constitutively signal (Hatch et al., 2006), it was hypothesised that there may be oversignalling of FGF. FGFR signalling was assessed with respect to proliferation with FGFR TK inhibitor SU5402 and measuring cell growth. FGF signals are transduced by downstream pathways such as Pkc and Erk1/2, which are both involved in osteoblast proliferation (Ghayor et al., 2005; Lai et al., 2001), therefore these pathways were assessed in a similar manner. MC3T3, R2-WT and R2-C278F cells were seeded in 96 well plates before treating the cells with reagents as described below. Cell proliferation (in terms of the number of cells) was inferred by the scale of optical density values, analysed from the methylene blue assay (Details in methods section 3.1.6).

Initial FGFR inhibition with SU5402 from 5 to 10 μM revealed that cell growth inhibition in all three cell lines was greater with a higher dose (Appendix Figure 8.12). SU5402 (5μM) was used in 10 and 1% FBS containing medium every 24 hours for 3 days. This resulted in decrease in cell proliferation in all three cell lines in both 10 and 1% serum (Figure 5.9 A and B). In 10% FBS cell culture medium, the percentage cell proliferation in SU5402 treated MC3T3, R2-WT and R2-C278F compared to their controls was 81, 69 and 52%, respectively.

For inhibition of Erk1/2, the MEK1/2 inhibitor U0126 was added to the cells in 10% FBS containing medium every 24 hours and cell growth analysed at 1, 2 or 3 days. No significant changes in cell growth were observed after 1 day in culture (Figure 5.10 A). By 2 days in culture MC3T3, R2-WT and R2-C278F cells displayed a decrease in cell proliferation of 34, 29 and 46% respectively (Figure 5.10 B). Decreased cell proliferation was also observed in MC3T3 (35%), R2-WT (40%) and R2-C278F (58%) cells (Figure 5.10 C).

Effective inhibition of Pkc activation was not easily attainable, as most inhibitors of Pkc can only bind to one or a few of the many Pkc isoforms. Thus, to further study the role of Pkc with respect to cell growth, the approach taken was to activate Pkc every 24 hours using PMA for 3 days in 1% FBS containing culture medium. PMA cotreated with U0126 was carried out to investigate any possible relationship between Pkc and Erk1/2 pathways. These experiments revealed that both PMA and U0126 treatments can reduce cell growth in MC3T3 cells (Figure 5.11 A). The cell growth was lower with a combination of PMA-U1026 than both untreated and PMA treated groups but this was not significantly different to U0126 alone. In R2-WT cells, treatment with PMA did not have any significant effect on cell growth (Figure 5.11 B). R2-WT

cell growth decreased with U0126 treatment and with the PMA-U0126 combination treatment, however no significant differences were found between these treatment groups. Following PMA treatment, cell growth increased in R2-C278F cells. U0126 treatment and the PMA U0126 combination treatment significantly reduced cell growth compared to controls, however between these two treatment groups no significant differences were found (Figure 5.11 C).

The effect of PMA was also tested in the presence of 10% FBS. At 3 days in culture with 10% serum, PMA did not significantly alter cell growth in MC3T3 and R2-WT cells, whereas it decreased cell growth in R2-C278F cells (Figure 5.12).

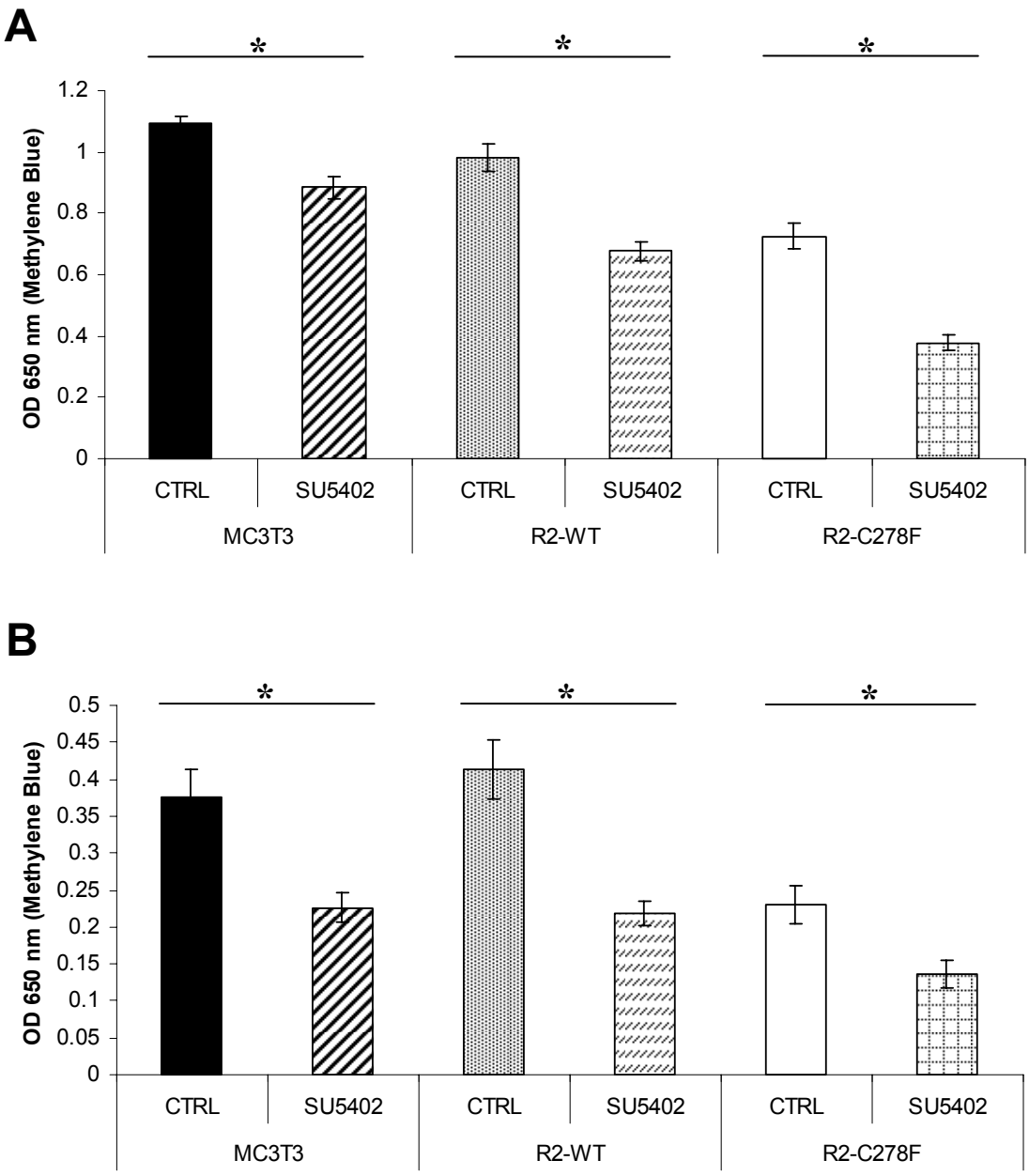

Figure 5.9 Cell growth analysis by Methylene blue assay of SU5402 treated cells after 3 days

MC3T3, R2-WT and R2-C278F cells treated with fresh medium containing 5 μM of SU5402 every 24 hours for 3 days. Cell growth was indicated by the magnitude of the optical density in the Methylene blue assay. **A:** In 10% serum, SU5402 treatment causes a significant decrease in cell growth compared to the untreated controls in all three cell lines ($n = 16$, $^*p < 0.05$). **B:** In 1% serum there is also a significant decrease in cell growth with SU5402 treatment in all three cell lines compared to the controls ($n = 5$, $^*p < 0.05$).

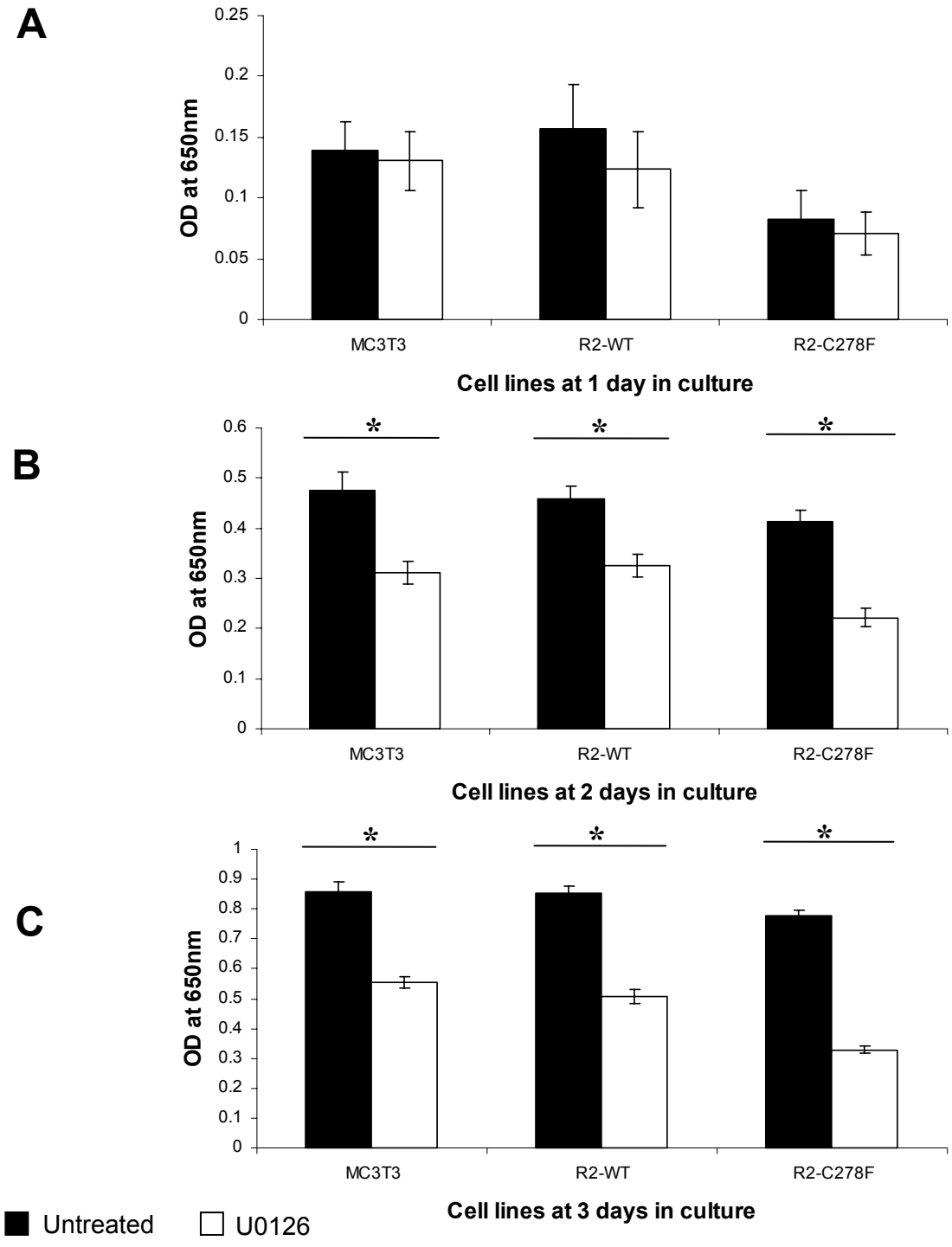

Figure 5.10 Cell growth assessed by Methylene Blue assay in U0126 treated cells

MC3T3, R2-WT and R2-C278F Cells were cultured and treated with 20μM of U0126 for 1, 2 and 3 days in 10% FBS containing culture medium prior to analysis. **A:** At 1 day, no significant differences in cell growth were found with U0126 treatment. **B:** By 2 days, U0126 treatment decreases cell growth in MC3T3, R2-WT and R2-C278F compared to the untreated controls. **C:** At 3 days, cell growth is also significantly decreased in U0126 treated MC3T3, R2-WT and R2-C278F cells compared to the controls ($n = 3$, $*p < 0.05$).

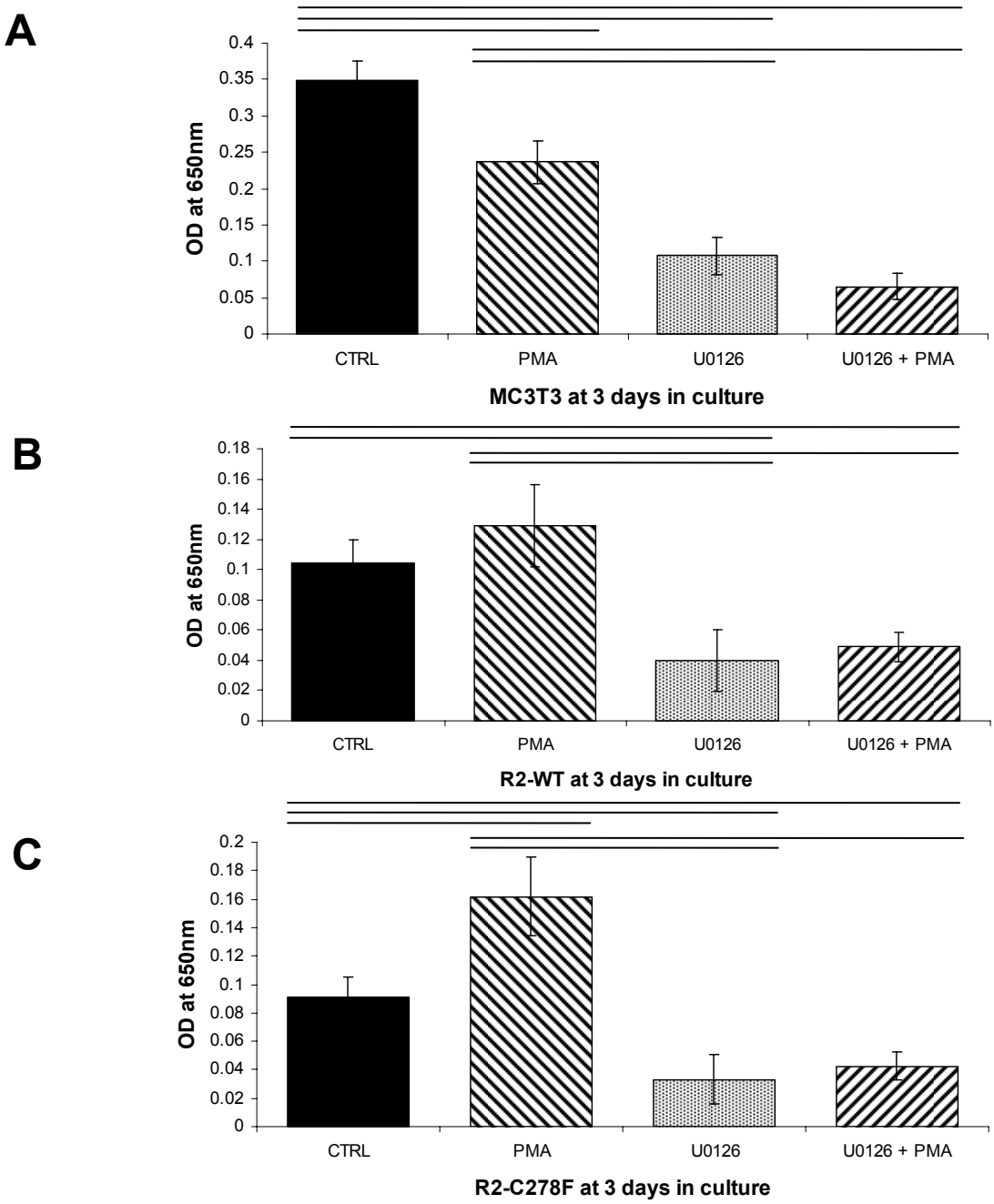

Figure 5.11 Effects of PMA and U0126 on cell growth in MC3T2, R2-WT and R2-C278F cells

Cells were cultured with 1% FBS containing culture medium and treated with 50 ng/ml of PMA and 20 μM U0126 every 24 hours for 3 days. **A:** PMA treatment reduces cell growth in MC3T3. With U0126 treatment cell growth is reduced to a greater extent. U0126 treated cells do not show any significant differences compared with cells treated with both PMA and U0126. **B:** PMA treatment does not alter cell growth in R2-WT cells. U0126 and a combination of U0126 and PMA treatment induce a comparable decrease in cell growth. **C:** In R2-C278F cells, PMA increases cell growth. U0126 or U0126 and PMA treatments result in a similar decrease in cell growth compared to controls. (n = 3, lines denote $p < 0.05$ ANOVA).

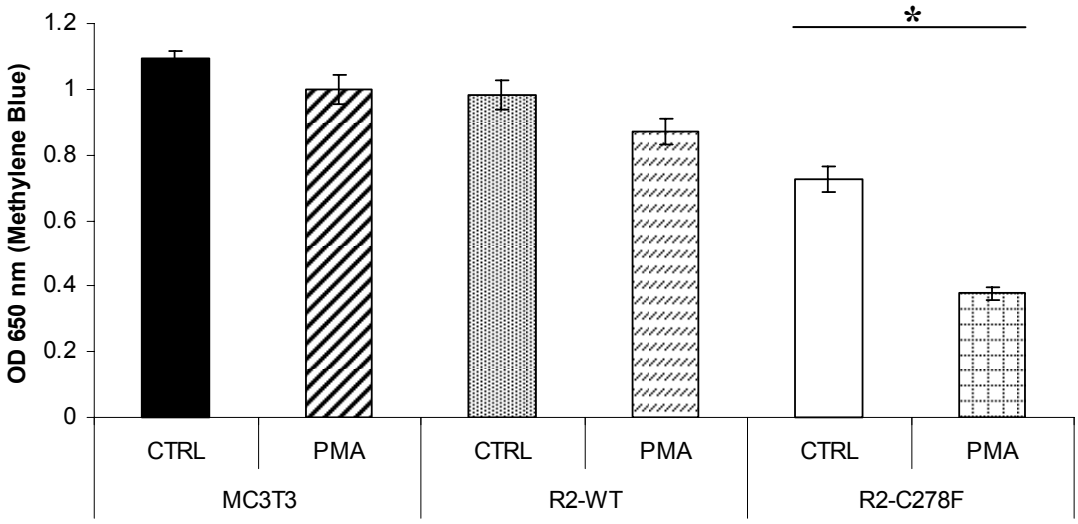

Figure 5.12 Cell growth in MC3T3, R2-WT and R2-C278F cells with PMA in 10% FBS medium
Cells were seeded for 3 hours and treated every 24 hours with PMA in 10% FBS containing culture medium and grown for 3 days. Cell growth was analysed with the methylene blue assay. Treatment with PMA does not significantly affect cell growth in MC3T3 and R2-WT cells, but in R2-C278F cells there is a significant decrease in cell growth ($n = 3$, * $p < 0.05$).

5.2.4 Morphology of MC3T3, R2-WT and R2-C278F cells treated with SU5402 and PMA

The effect of SU5402 and PMA on cell morphology was examined in order to gain some information on the differentiation state of the cells. The cells were seeded and cultured in cell culture medium containing 1% FBS for three days, with a change of culture medium every 24 hours.

SU5402-treated MC3T3 cells appeared to have an increased number of processes per cell, compared to their untreated controls (Figure 5.13 A and B). Most control cells had one large process extending to a neighbouring cell, whereas with SU5402 treatment, many cells had a extended several thinner processes towards neighbouring cells. The PMA-treated MC3T3 cells were nearly all cuboidal in appearance as compared to the untreated group (Figure 5.13 A and C).

There was some difference in the morphology of SU5402-treated R2-WT cells in that there were more cells with a larger number of processes, but not as obviously as in MC3T3 cultures (Figure 5.14 A and B). There appeared to be a slight increase in the proportion of cuboidal cells in the PMA treated R2-WT cells and their distribution and arrangement appeared to be similar to the untreated controls (Figure 5.14 A and C).

SU5402 treatment visibly reduced the number of cells in R2-C278F cultures. The morphology appeared unchanged; however there were visibly fewer cells. Cells treated with PMA appeared to contain a higher proportion of cuboidal cells than controls (Figure 5.15 A and B).

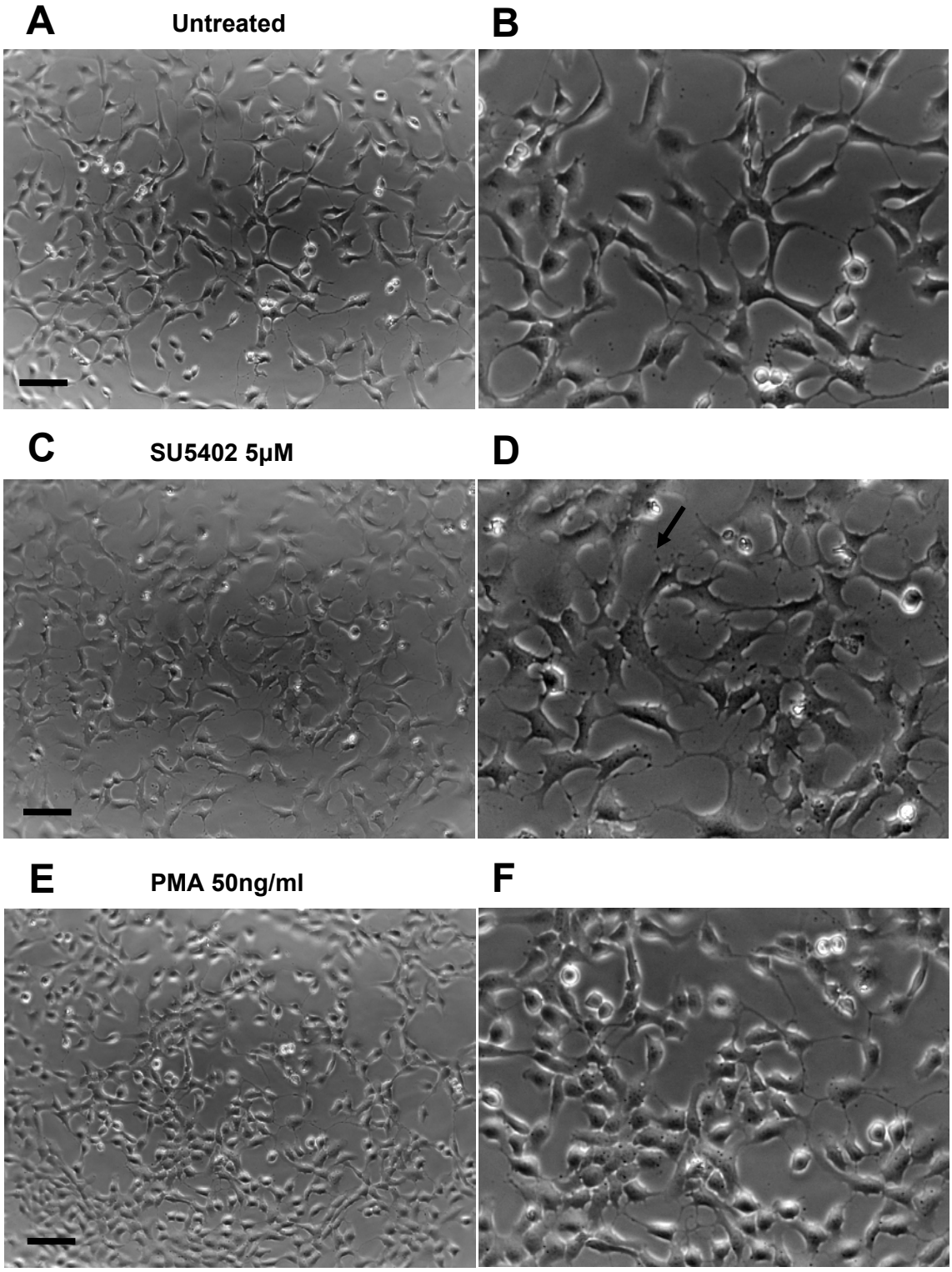

Figure 5.13 Phase contrast images of MC3T3 cells treated with SU5402 or PMA for 3 days

Cells were treated with PMA (10 ng/ml) or SU5402 (5 μM) in cell medium with 1% FBS every 24 hours for 3 days in culture before imaging at 5x magnification. **A**, **C** and **E**: Untreated, SU5402-treated and PMA-treated cells respectively. **B**, **D** and **F**: The 4x enlargement of A, C and E respectively. SU5402-treated cells (D) have shorter and finer processes than the controls (arrows) (B). PMA treated cells (F) have a round morphology compared to the fibroblastic morphology of the controls (B) (n = 4, Bar = 50 μm).

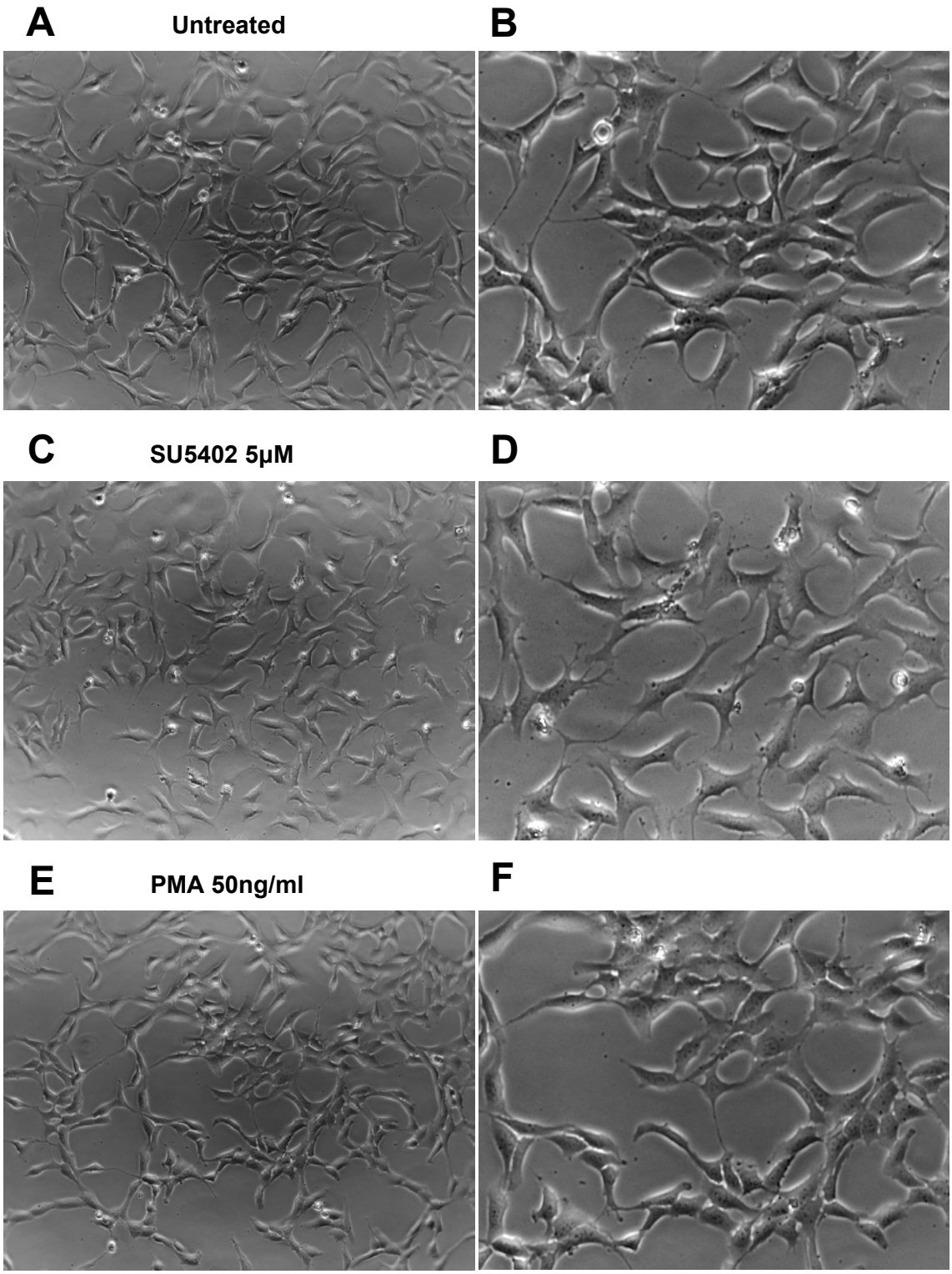

Figure 5.14 Phase contrast images of R2-WT cells treated with SU5402 or PMA for 3 days

Cells were treated with PMA (10 ng/ml) or SU5402 (5 μM) in cell medium with 1% FBS every 24 hours for 3 days in culture before imaging at 5x magnification. **A**, **C** and **E**: Untreated, SU5402-treated and PMA-treated cells respectively. **B**, **D** and **F**: 4x enlargement of A, C and E respectively. Compared to the controls (B), SU5402-treated cells appear to have more processes. Cell morphology in PMA-treated cells (F) are slightly more cuboidal than the untreated controls (B), but they still maintain a similar distribution (n = 4, Bar = 50 μm).

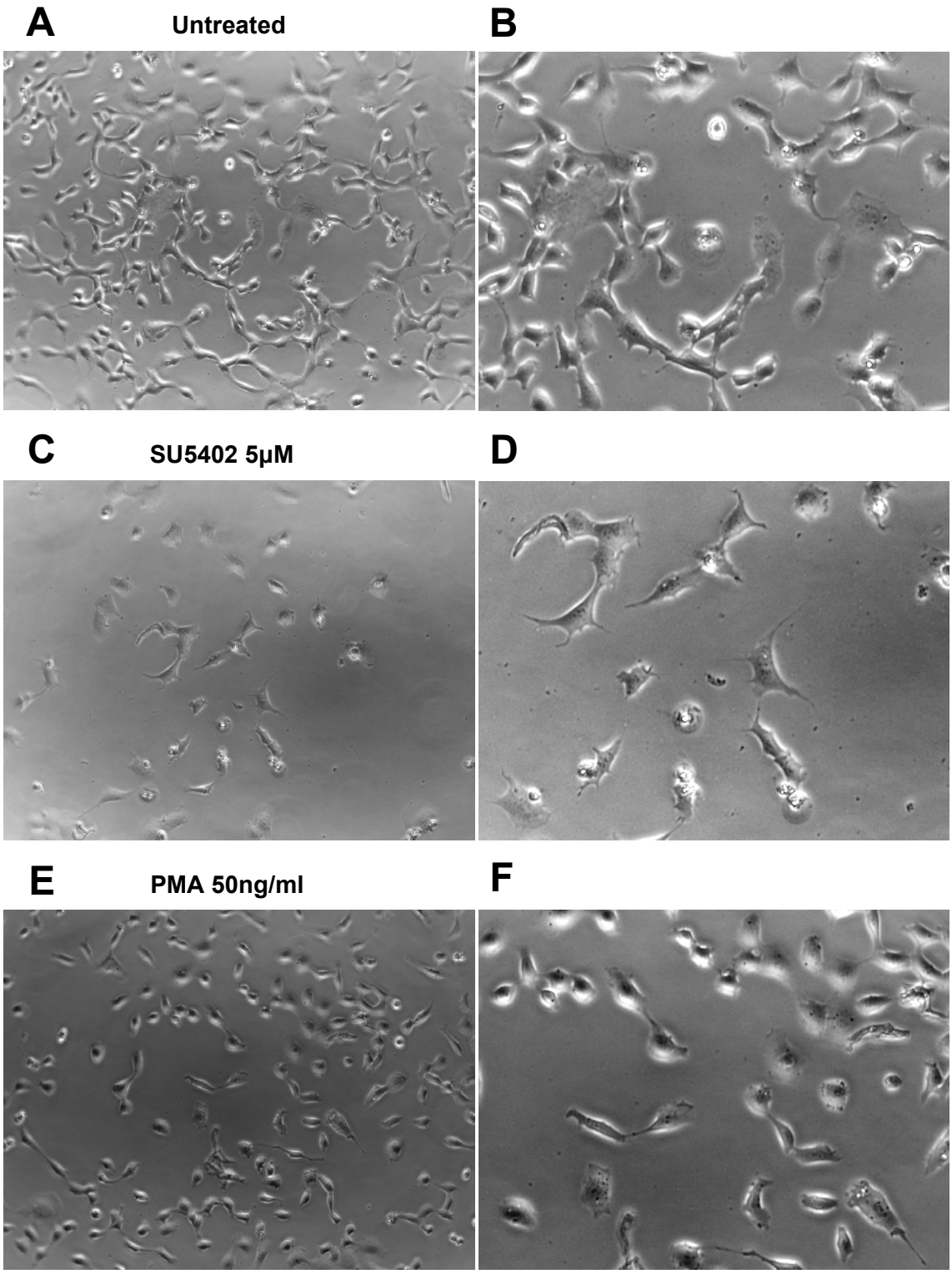

Figure 5.15 Phase contrast images of R2-C278F cells treated with SU5402 or PMA for 3 days

Cells were treated with PMA (10 ng/ml) or SU5402 (5 μM) in cell medium with 1% FBS every 24 hours for 3 days in culture before imaging at 5x magnification. **A**, **C** and **E**: Untreated, SU5402 treated and PMA treated cells respectively. **B**, **D** and **F**: 4x enlargement of A, C and E respectively. SU5402 treatment (D) results in a visible decrease in the cell density than in controls (B). More rounded cells are found with PMA treatment (F) than in the untreated controls (B) (n = 4, Bar = 50 μm).

5.3 Discussion

5.3.1 FGFR2-C278F alters *Fgf18* and *FGFR2IIIc* expression

Fgf1, -2 and -18 are the main Fgfs involved in bone formation that also bind to endogenous Fgfr2IIIc, therefore the expression of these ligands and the receptor would be useful indications of endogenous changes in response to aberrant signalling from FGFR2-C278F.

Fgf1 and *-2* expressions were undetectable in all three cell lines by RT-PCR (Figure 5.1 and Figure 5.2). A real time PCR analysis performed later in Chapter 6 revealed a low level of gene expression, which suggests that although *Fgf1* and *-2* are involved in bone development, they do not play a main role producing the R2-C278F phenotype shown in Chapter 4.

Fgf18 is expressed in all three cell lines, suggesting that it has a significant role in FGF signalling in osteoblasts in culture. Fgf18 is important for osteoblast proliferation and differentiation (Ohbayashi et al., 2002). Neither FGFR2-WT nor FGFR2-C278F expression in MC3T3 significantly affects *Fgf18* expression at preconfluence, suggesting *Fgf18* expression *per se* is not related to the low proliferation in R2-C278F cells (Figure 5.4). *Fgf18* expression is upregulated by FGFR2-WT and FGFR2-C278F at confluence, indicating that Fgf18 may play a role in the late stage of differentiation of R2-WT and R2-C278F cells. It has been shown that Fgf18 can drive differentiation by *Osteopontin* (*Opn*) and *Osteocalcin* (*Oc*) expression (Liu et al., 2002). As *Fgf18* expression is higher in R2-WT cells than R2-C278F cells, this suggests the ligand's expression is finely controlled by FGFR2 signalling.

Fgfr2IIIc expression decreases in differentiating osteoblasts (Iseki et al., 1999). From these reports it was expected that in R2-C278F cells *Fgfr2IIIc* expression would be lower due to expression of FGFR2-C278F and increased differentiation as shown in Chapter 4. In this study, the level of *Fgfr2IIIc* expression increases in both R2-WT and R2-C278F cells at 2 days in culture (Figure 5.3 A), suggesting that FGFR2 signalling may positively regulate itself. At confluence, there is no difference in *Fgfr2IIIc* expression amongst all three cell lines (Figure 5.3 B), indicates that FGFR2 signalling is not the main factor controlling Fgfr2IIIc expression at the stage in culture. Fgfr2IIIc may be downregulated in differentiating osteoblasts following exogenous Fgf2, which is also known to activate other FGFRs (Iseki et al., 1999; Mathy et al., 2003).

Together, these data suggest that Fgf signalling in R2-C278F cells is altered via increased *Fgfr2IIIc* expression at preconfluence and increased *Fgf18* at confluence. As temporally the expressions do not coincide, both ligand and receptor may have different roles.

5.3.2 FGFR and Erk1/2 signalling with regard to proliferation is reduced in R2-C278F cells

SU5402 was initially considered as an FGFR1 specific TK blocker, however other studies have provided evidence that it actually blocks the TK domains of FGFR1-3 (Mohammadi et al., 1997; Paterson et al., 2004; Bernard-Pierrot et al., 2004; Zhang et al., 2007). As discussed in Chapter 1, FGFR2 is the main isoform associated with osteoblast proliferation (Iseki et al., 1999; Ratisoontorn et al., 2003). Treatment with SU5402 reduced proliferation in MC3T3 and R2-WT cells, indicating that FGFR signalling is mitogenic (Figure 5.9). Furthermore, the level of cell growth decreases to a greater degree by SU5402 treatment in R2-C278F cells, than in both MC3T3 and R2-WT cells (Figure 5.9). This suggests that R2-C278F cells have a lower level of FGFR2 signalling than MC3T3 and R2-WT, given that FGFR2 signalling is normally proliferative.

The reduced FGFR2 signalling suggested above may be mediated by Erk1/2, as it is downstream of FGF and plays a positive role with respect to osteoblast proliferation (Lai et al., 2001; Kapur et al., 2003) Erk1/2 inhbition with U0126 resulted in a greater percentage reduction in R2-C278F cell growth compared to controls (Figure 5.10), suggesting that Erk1/2 signalling is also lower in the mutant cells.

5.3.3 The effect of SU5402 on osteoblast morphology

SU5402 reduced the number of large processes in MC3T3 and R2-WT cells and increased the number of small processes (Figure 5.13 B and D, Figure 5.14 B and D). R2-C278F do not have the cell morphology described in SU5402 treated MC3T3 and R2-WT cells, indicating that the effect of FGFR2-C278F on morphology is not directly equivalent to a lower level of FGFR signalling. In fact SU5402 had a similar effect in R2-C278F cells, although less apparent (Figure 5.15 B and D). It is possible that signalling from other FGFR isoforms may contribute to process formation and size in osteoblasts. FGFR signalling affects the number of processes in other cell types, for exmple in dorsal marginal zone (DMZ) cells during gastrulation where there was a reduction in filipodia following SU5402 treatment (Chung et al., 2005).

5.3.4 Pkc induced cell growth in R2-C278F cells is Erk1/2 dependent

The PKC pathway can mediate cell proliferation and differentiation. PKC activation by Phorbol 12-myristate 13-acetate (PMA) has been suggested to increase proliferation in MC3T3 cells (Kozawa et al., 1989). DMSO induced PKC activation may induce differentiation in MC3T3 cells (Cheung et al., 2006).

Interestingly cell growth after PMA treatment in 1% FBS culture medium decreases in MC3T3, has no significant effect in R2-WT cells and increases in R2-C278F cells. This indicates that Pkc signalling is different in each of the three cell lines. A possible reason for the differences in proliferative effect between the literature and this study could be the duration of PKC stimulation and the type of analysis. Cell growth was measured after 2 days in this study, whereas DNA synthesis analysis was performed at 22 and 24 hours, respectively (Kozawa et al., 1989; Villa et al., 2003). PMA induced cell growth in R2-C278F cells is blocked by Erk1/2 inhibition, indicating the effect is dependent on Erk1/2 signalling (Figure 5.11), which is consistent with another report showing that PKC induced cell proliferation is Erk1/2 dependent in MC3T3 (Ghayor et al., 2005). In 10% serum conditions, PMA had no effect on cell growth in MC3T3 and R2-WT cells, whereas in R2-C278F cells it decreased. This suggests that the effects of Pkc on proliferation are modulated by serum components.

5.3.5 The effect of PMA on cell morphology

The PMA treatment induced an almost ubiquitous change to cuboidal morphology in MC3T3 cultures, which may also indicate a strong induction to differentiation (Figure 5.13 B and F). In R2-WT cells there was also a change to cuboidal morphology, although in to a lesser degree, which may indicate that the FGFR2 signalling may block or interfere with the differentiation signals by PKC. Interestingly R2-C278F cells have an appearance similar to those in PMA treated MC3T3 and Pkc treatment of R2-C278F cells slightly increases the amount of cuboidal cells. It is possible that R2-C278F cells have increased stimulation via Pkc, which could be investigated. This data supports the suggestion in the last section, that there is a difference in the PKC signalling between MC3T3, R2-WT and R2-C278F. PMA induces differentiation by activation of *Osteocalcin* in human osteoblast-like cells (Opperman et al., 1997), which might provide a clue to why osteoblasts appear to be more differentiated in morphology. Further investigation of PKC induction of differentiation markers such as osteocalcin may yield more information regarding the way in which PKC may have changed osteoblast behaviour.

5.3.6 Erk1/2 expression and activation is affected in R2-C278F cells

Erk1/2 activation is essential for osteoblast cell growth and differentiation (Lai et al., 2001), both of which are altered in R2-C278F cells, but how Erk1/2 performs both functions is less clear. Erk1/2 signalling with respect to proliferation depends on the relative amount of the Erk1 compared to the Erk2 isoforms (Pouyssegur and Lenormand, 2003; Vantaggiato et al., 2006). In addition, the timing of Erk1/2 signalling such as short term, sustained and oscillating, may all lead to different phenotypical outcome (Nakayama et al., 2008). The effects may also be cell type specific, for example late and sustained Erk1/2 activation induces fibroblast proliferation, whereas sustained Erk1/2 activation causes growth arrest and differentiation in PC12 pheochromocytomas cells (Chambard et al., 2007). Other factors such as cross talk of Erk1/2 with Akt may also contribute, but investigation of this idea is beyond the scope of this thesis (Raucci et al., 2008).

The level of Erk1/2 protein is higher in R2-C278F cells than in MCT3 and R2-WT cells (Figure 5.5 A), however FACS analysis of pErk1/2 in fixed osteoblasts did not show any significant differences in Erk1/2 activation. This suggests that the basal level of Erk1/2 activation is not limited by the Erk1/2 protein expression in all three cell lines (Figure 5.5 B). One research group has suggested that MAPK activation levels do not differ between the constitutively active FGFR mutants and controls, because of a rapid turnover of the pErk1/2, making protein activation assessments more difficult (Mansukhani et al., 2000).

The total increase in Erk1/2 and in Erk1 expression relative to Erk2 in R2-C278F cells is very interesting and consistent with the change in cell behaviour. In different cellular structures of the brain, different ratios of Erk1 to Erk2 naturally occur, implicating different and specific types of Erk1/2 signalling, that are as yet undefined (Ortiz et al., 1995). Although Erk1 and Erk2 are part of the same signalling pathway, they have distinct roles with respect to proliferation (Fremin et al., 2007; Pouyssegur and Lenormand, 2003; Vantaggiato et al., 2006). Erk2 is vital for proliferation in MC3T3 osteoblasts, NIH3T3 fibroblasts, and hepatocytes (Fremin et al., 2007; Lai et al., 2001; Vantaggiato et al., 2006). Erk1 is not responsible for proliferation in hepatocytes and only weakly induces proliferation in NIH3T3 fibroblasts with a lack of Erk2 (Fremin et al., 2007; Lefloch et al., 2008). In NIH3T3 fibroblasts, Erk1 overexpression experiments have indicated that either normal or kinase inactive Erk1 competitively inhibits Erk2 activation by Ras (Lai et al., 2001). Moreover shRNA silencing of Erk1 increased NIH3T3 cell proliferation, highlighting an inhibitory role of Erk1 upon Erk2 proliferation (Vantaggiato et al., 2006). Collectively these data suggest that Erk2 is essential for proliferation, whereas Erk1 does not play a major role in proliferation, but inhibits Erk2 by

competing with Erk2 for activation. The increase in Erk1 relative to Erk2 appears to correlate with the observed effects on fibroblasts and hepatocytes in the literature, and it is possible that Erk1 competes with Erk2 for activation, resulting in a defect in R2-C278F cells proliferation, due to lowering the level of Erk2 activation for a given upstream stimulus. Interestingly, the Erk1/Erk2 ratio is still higher in R2-C278F cells at confluence compared to MC3T3 and R2-WT cells, suggesting that this Erk1/Erk2 ratio may also have an involvement in cell differentiation. To date, Erk1/2 inhibition with a dominant negative Erk1 has blocked osteoblast differentiation, indicating that Erk1 and/or Erk2 is required for osteoblast differentiation (Lai et al., 2001).

Stoichiometric analysis of Erk1/2 has shown that the ratio of Erk1/Erk2 correlates with the ratio pErk1/pErk2 (Lefloch et al., 2008). In this study, the analysis of ratios by Western blotting was not stoichiometric, as the value of the ratios could be affected by the differences in binding affinity of the anti-Erk1/2 and anti-pErk1/2 antibodies to Erk1 and Erk2. If in this model a stoichiometric relationship exists, a raised Erk1/Erk2 ratio in R2-C278F cells would also result in a raised pErk1/pErk2 ratio in R2-C278F compared to both controls. Although a statistical test could not be applied, the pErk1/pErk2 ratios in untreated cells at 2 days in culture appeared to be higher in R2-C278F cells than in MC3T3 and R2-WT cells (Figure 5.7). In untreated cells at 4 days in culture, the pErk1/pErk2 ratio was significantly higher compared to MC3T3 and R2-WT (and Figure 5.8).

In summary, an important effect of the FGFR2-C278F mutation in MC3T3 is that Erk1/2 signalling is altered. The increase in Erk1/Erk2 ratio leads to an increased pErk1/pErk2 ratio, which correlates with a shift toward growth arrest as less Erk2 will be activated for a given level of stimulation. As Erk1/2 positively regulates osteoblast differentiation, it is possible that Erk1 is the isoform that induces differentiation.

5.4 Conclusions

It has been confirmed that FGF signalling is altered in R2-C278F cells. There is a raised *Fgfr2IIIc* gene expression in R2-C278F cells at preconfluence, which may compensate for impaired Fgfr2 signalling, as indicated by FGFR inhibition with SU5402. Furthermore there is a reduction Erk1/2 signalling (as suggested by Erk1/2 inhibition with U0126) and an increased Erk1/Erk2 ratio. These effects are indicated to contribute to decreased cell proliferation.

At confluence, FGF signalling is altered in R2-C278F cells by an increase in *Fgf18* expression. Fgf18 may be associated with increased differentiation, because it can induce *Osteocalcin* (Oc) expression, which is raised in R2-C278F cells. At this stage in culture the Erk1/Erk2 ratio is increased and Pkc signalling is also altered. Pkc signalling in R2-C278F cells is speculated to be increased, because in human SG12 osteoblasts Pkc activation with PMA induces *Osteocalcin* expression (Boguslawski et al., 2000), which was raised in R2-C278F cells (as shown in Chapter 4) and that Pkc activation by PMA induces a shift from fibroblastic morphology observed in MC3T3 cells to the more cuboidal morphology of R2-C278F cells.

Chapter 6 TGFbeta signalling in R2-C278F cells

6.1 Introduction

The TGFbetas are important in both bone and suture formation and maturation (Lee et al., 2006; Opperman et al., 1997; Opperman et al., 2000; Opperman et al., 2002a; Opperman et al., 2002b). Addition of TGFbeta *in-vivo* induces rapid closure of skull defects (Beck et al., 1991), however TGFbeta mutations have not been reported to result in craniosynostosis except for one case of a patient with TβRI-D400G (Loeys et al., 2005). Studies of calvarial cultures indicate that the addition of TGFbeta3 into sutures may inhibit or delay suture fusion, whereas addition of TGFbeta2 into the same region may accelerate suture fusion (Opperman et al., 2000). It has been suggested that TGFbeta plays a secondary role in sutural morphogenesis and is part of a complex multiple regulated mechanism (Cabiling et al., 2007). Together, these reports suggest that TGFbetas may contribute, but are not essential to suture maintenance and fusion. TGFbeta signalling via TβRII is essential for frontal bone and the caudal region of the skull (Hosokawa et al., 2007; Sasaki et al., 2006). Interestingly CNC cell proliferation induced by TGFbeta signalling is mediated by FGF signalling.

In bone development, the TGFbetas regulate bone formation and resorption by influencing osteoblast and osteoclast development respectively (Filvaroff et al., 1999). In osteoblasts, the TGFbetas are involved in proliferation, differentiation. For example TGFbeta1 increases early proliferation and inhibits late stage differentiation and mineralisation (Alliston et al., 2001; Centrella et al., 1994). TGFbeta2 and -3 may also increase pre-osteoblast proliferation (Bosetti et al., 2007; Centrella et al., 1994; Opperman et al., 2000). Though TGFbetas are well known to signal via the SMAD downstream pathways (Miyazawa et al., 2002), they also activate MAPK and PKC pathways (Ghayor et al., 2005; Lee et al., 2002; Sowa et al., 2002). One of the complex mechanisms in osteoblasts are the interactions between TGFbeta and FGF, such as FGF induced TGFbeta1 expression (Noda and Vogel, 1989). FGFR2-C278F signalling, suggested in Chapter 5, alters FGF signalling, therefore FGF-TGFbeta interactions may also be altered in R2-C278F cells. As FGF and TGFbeta signalling can converge along MAPK and PKC downstream pathways, investigation of their interactions may be performed using TGFbeta treatment and inhibition with respect to cell proliferation and differentiation.

The first aim of this chapter is to find whether FGF-TGFbeta interactions are altered by the FGFR2-C278F mutation. The second aim is to identify where these interactions occur using TGFbeta treatment and inhibition on R2-C278F cells.

6.2 Results

6.2.1 TGFbeta expression in MC3T3, R2-WT and R2-C278F cells

To make an assessment of the level of TGFbeta signalling, expression of the *Tgfbeta1, -2* and *-3* transcript was analysed at 2 and 4 days in culture using real time PCR. TGFbetas, like BMPs signal via the SMAD pathway (Miyazawa et al., 2002). In general, TGFbeta is known to signal via SMAD2 and -3, whereas BMPs activate SMAD1, -5 and -8; however TGFbeta has also been known to signal via SMAD1 and -5. Therefore, *Smad1* and *-2* expressions were measured by real time PCR in order to investigate the downstream pathways of Tgfbeta and Bmp.

Tgfbeta1 expression was significantly lower in R2-C278F cells than in MC3T3 and R2-WT cells at both 2 and 4 days in culture (Figure 6.1 A). There were no significant differences in *Tgfbeta1* expression between MC3T3 and R2-WT cells. *Tgfbeta2* levels appeared to be low compared to the E13.5 mouse head, but was present in all three cell lines and no significant differences in expression were found amongst the three cell lines at 2 or 4 days in culture (Figure 6.1 B). *Tgfbeta3* expression was significantly lower in R2-C278F cells compared to MC3T3 and R2-WT cells at 2 and 4 days in culture (Figure 6.1 C). In R2-WT cells the *TGFbeta3* expression was also significantly lower than in MC3T3 cells.

No significant differences in *Smad1* expression were found between the three cell lines at 2 days. (Figure 6.2 A). At 4 days, the pattern of *Smad1* expression in all three cell lines was similar to that at 2 days, with no significant differences to report.

Smad2 expression at 2 days was not significantly different between MC3T3 and R2-C278F cells, but in R2-WT cells *Smad2* expression was higher than in R2-C278F cells (Figure 6.2 B). At 4 days, no significant difference in *Smad2* expression was found between the three cell lines.

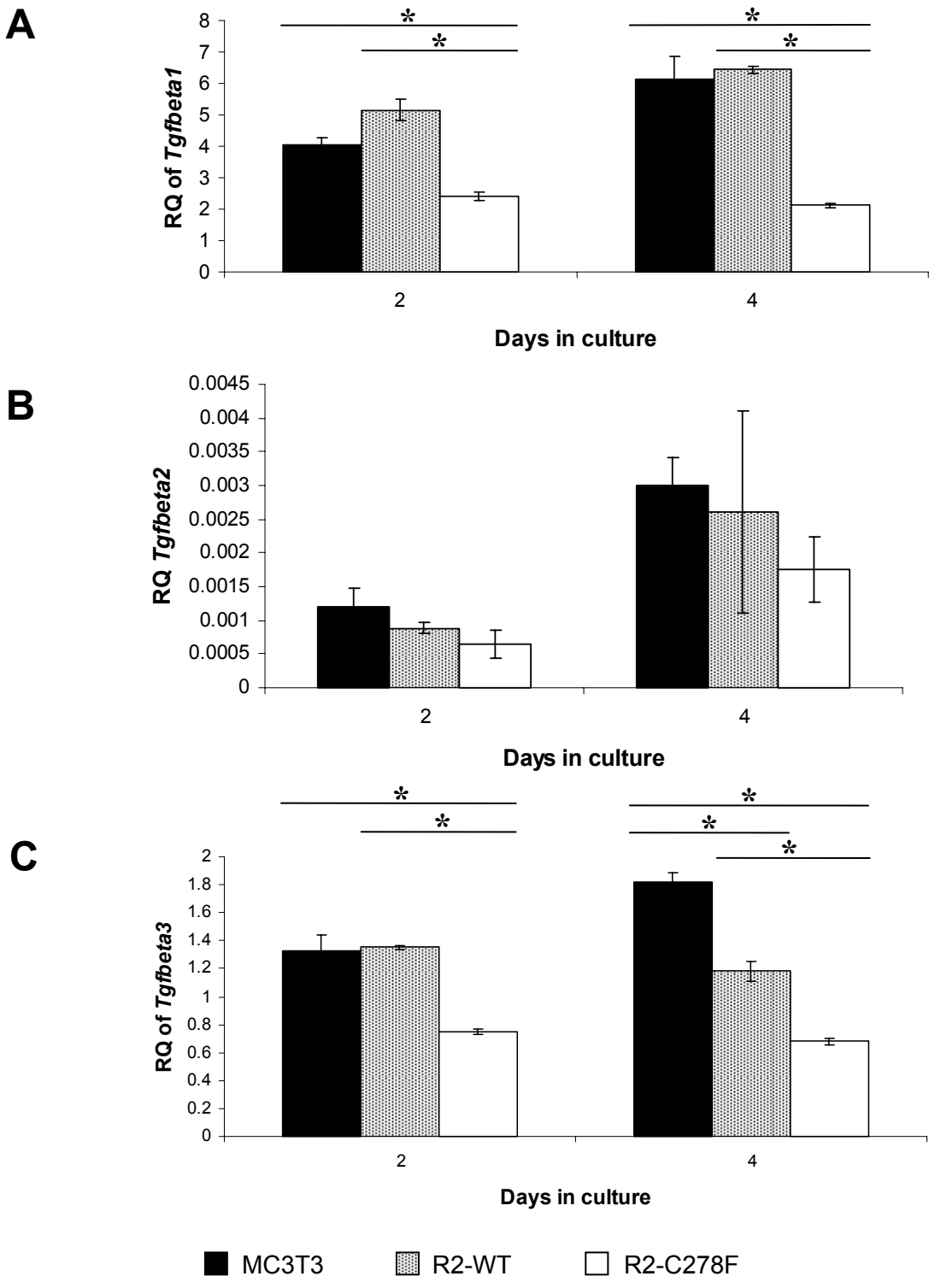

Figure 6.1 Real time PCR analysis of *Tgfbeta1*, *-2* & *-3* in MC3T3, R2-WT and R2-C278F cells

Cells were cultured for 2 and 4 days before relative quantification (RQ) of Tgfbeta expressions. **A:** Compared to MC3T3 and R2-WT cells, *Tgfbeta1* expression is significantly lower in R2-C278F cells at 2 and 4 days in culture. **B:** *Tgfbeta2* expression is not significant different between the three cell lines at 2 or 4 days. **C:** *Tgfbeta3* expression is lower in R2-C278F cells at 2 and 4 days than in both controls. At 4 days, *Tgfbeta3* is higher in MC3T3 cells than in R2-WT cells (n = 3, *p < 0.05).

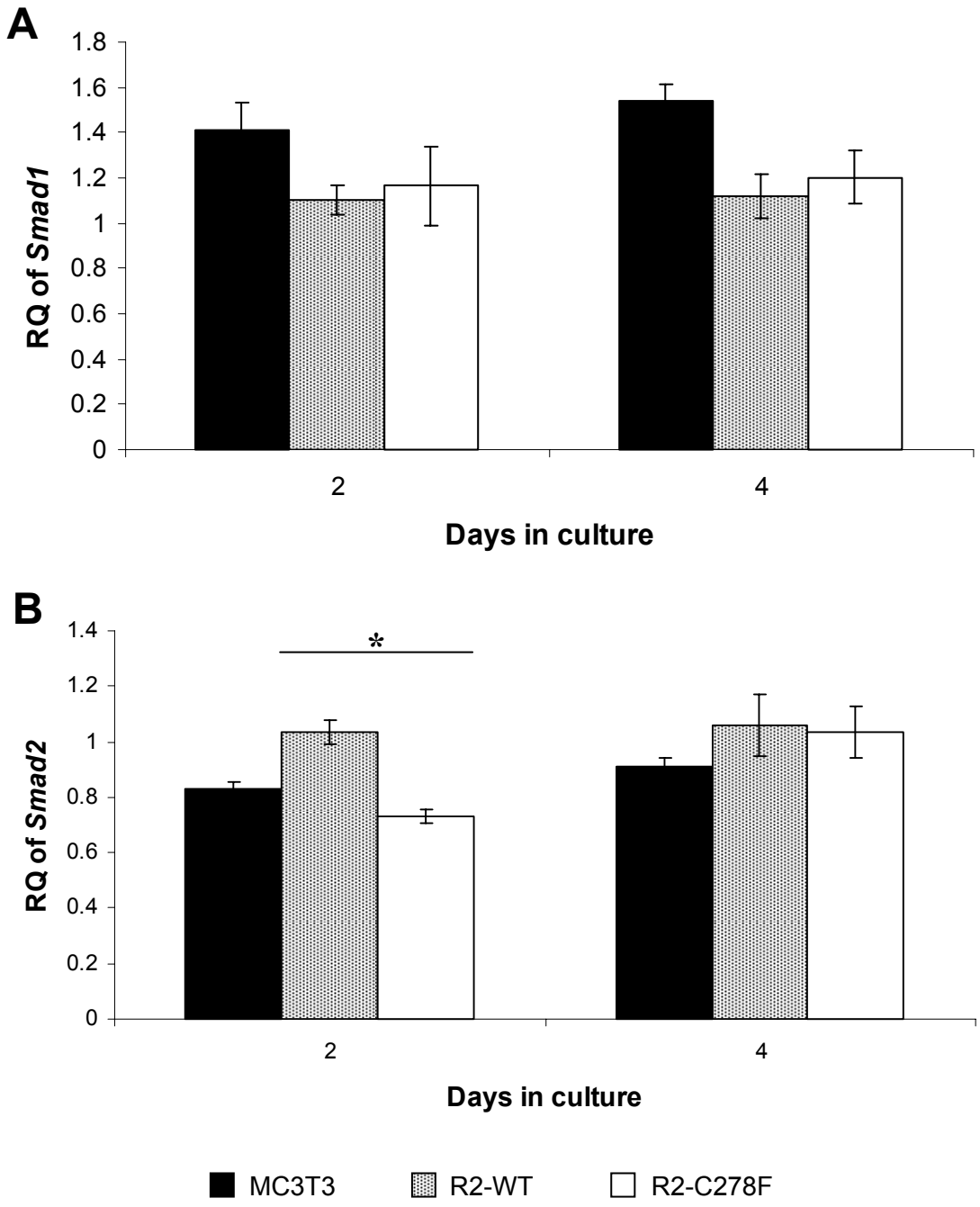

Figure 6.2 Real time PCR analysis of *Smad1* & *-2* in MC3T3, R2-WT and R2-C278F cells

Cells were grown for 2 and 4 days in culture before relative quantification (RQ) of gene expression by real time PCR. **A:** No significant differences in *Smad1* expression were found between MC3T3, R2-WT and R2-C278F cells at 2 and 4 days in culture (n = 3). **B:** At 2 days, MC3T3 and R2-C278F cells do not show any significant differences in *Smad2* expression, however in R2-WT cells the level of *Smad2* expression is significantly higher compared to R2-C278F cells. At 4 days there are no significant differences in *Smad2* expression between all three cell lines (n = 4, *$p < 0.05$).

6.2.2 Effects of exogenous TGFbeta1 on cell morphology

Of the TGFbetas in osteoblasts, TGFbeta1 was used as a candiate treatment in this chapter, due to its reported mitogenic effects and also its inhibition of late differentiation. MC3T3, R2-WT and R2-C278F cells were grown in T25 flasks were treated with 1, 10 and 20 ng/ml of recombinant human TGFbeta1 every 24 hours for 2 or 4 days in culture, before capturing phase contrast images. As TGFbeta1 was suspended in 1 mg/ml BSA in 4mM HCl, this was used as a BSA control for the effects of the solvent.

In MC3T3 cells at 2 days there were no morphological differences between untreated and BSA control cultures in MC3T3 cells (Figure 6.3 A and B). All levels of TGFbeta1 treatment led to an increased number of bright round cells, which did not appear to be dose dependent (Figure 6.3 C, D and E). No other morphological differences were found between the treated and untreated MC3T3 cells. Untreated and BSA controls in R2-WT cultures were similar in morphology at 2 days (Figure 6.4 A and B). No morphological changes were observed with any of the TGFbeta1 treatments compared to the controls (Figure 6.4 A, B, C, D and E). In R2-C278F cultures at 2 days, untreated and BSA controls were morphologically similar (Figure 6.5 B). No noticeable differences were found between TGFbeta1 treated R2-C278F cells and their controls (Figure 6.5 A, B, C, D and E).

At 4 days in MC3T3 cells, both the untreated and BSA control cultures reached confluence and did not appear to be different to each other (Figure 6.6 A and B). Similarly, all TGFbeta1 treated cultures reached confluence and interestingly there was an increase in the number of bright apoptotic figures, which appear like bright round cells, but without a dark centre (Figure 6.6 C, D and E). Under the microscope, the number of apoptotic figures did not appear to be correlated with the dose. In R2-WT cells no differences were observed between the untreated and the BSA control cultures, which were both confluent at 4 days (Figure 6.7 A and B). TGFbeta1 treated R2-WT cells also reached confluence and interestingly the morphology was markedly different, as demonstrated by the presence of many cells of thin elongated cells arranged in striae (Figure 6.7 A, B, C , D, and E). All three concentrations of TGFbeta1 treatment affected cell morphology in the same fashion. In R2-C278F cells, the untreated and BSA controls were almost 100% confluent at 4 days and there were no differences in morphology between the two groups (Figure 6.8 A and B). The TGFbeta1 treated R2-C278F cells were also near confluence, but there was a great increase in the number of bright round cells figures and an increase in the number of spaces between the cells (C, D and E). Both cell density and number of bright round cells did not appear to depend on the dose of TGFbeta1 used.

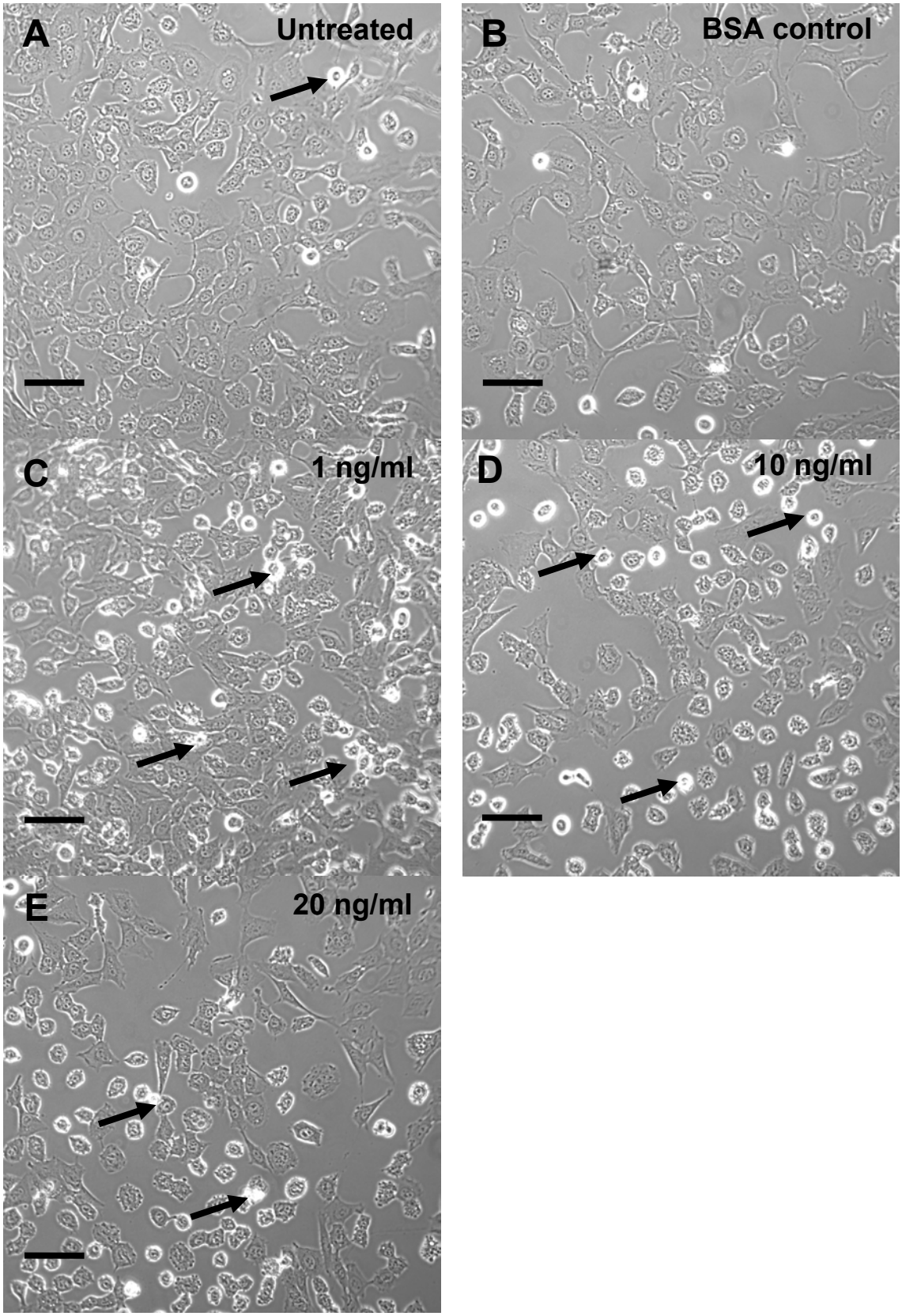

Figure 6.3 Phase contrast microscopy of TGFbeta1 treated MC3T3 cells at 2 days in culture

Cells were treated TGFbeta1 every 24 hours for 2 days. **A** and **B**: Untreated and BSA control. **C**, **D**, and **E**: Treated with TGFbeta1 at 1, 10 and 20 ng/ml respectively. Treatment with TGFbeta1 may increase the number of round bright cells (black arrows), (n = 3, bar = 50 μm).

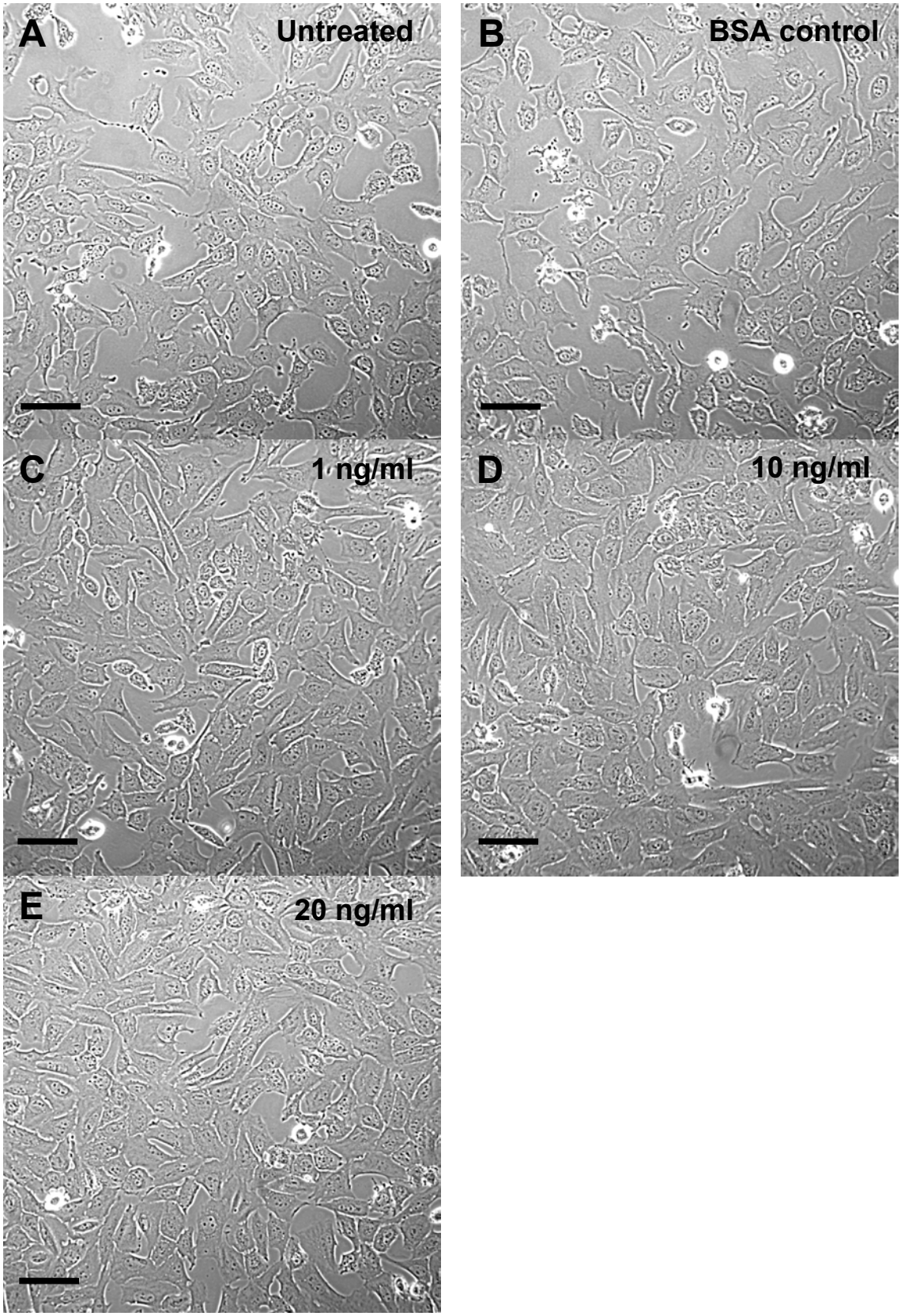

Figure 6.4 Phase contrast microscopy of TGFbeta1 treated R2-WT cells at 2 days in culture

Cells were treated TGFbeta1 every 24 hours for 2 days. **A** and **B**: Untreated and BSA control. **C**, **D**, and **E**: Treated with TGFbeta1 at 1, 10 and 20 ng/ml respectively. Cell morphology is the same in the controls (A and B) as compared to TGFbeta1 treated samples (C-E), (n = 3, bar = 50 μm).

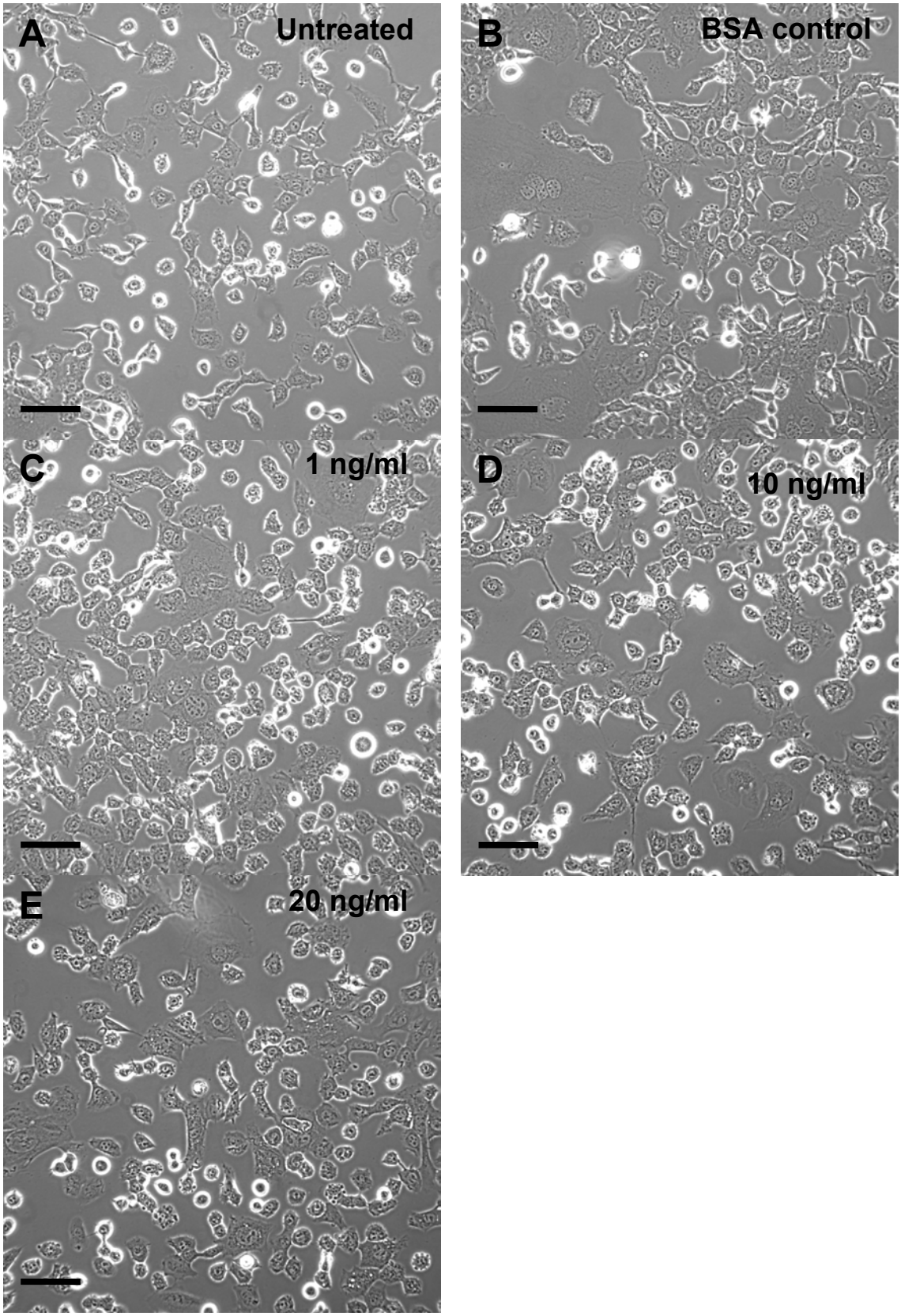

Figure 6.5 Phase contrast microscopy of TGFbeta1 treated R2-C278F cells at 2 days in culture

Cells were treated TGFbeta1 every 24 hours for 2 days. **A** and **B**: Untreated and BSA control. **C**, **D**, and **E**: Treated with TGFbeta1 at 1, 10 and 20 ng/ml respectively. Control cell morphology (A and B) are the same as with TGFbeta1 treatment (C-E), (n = 3, bar = 50 μm).

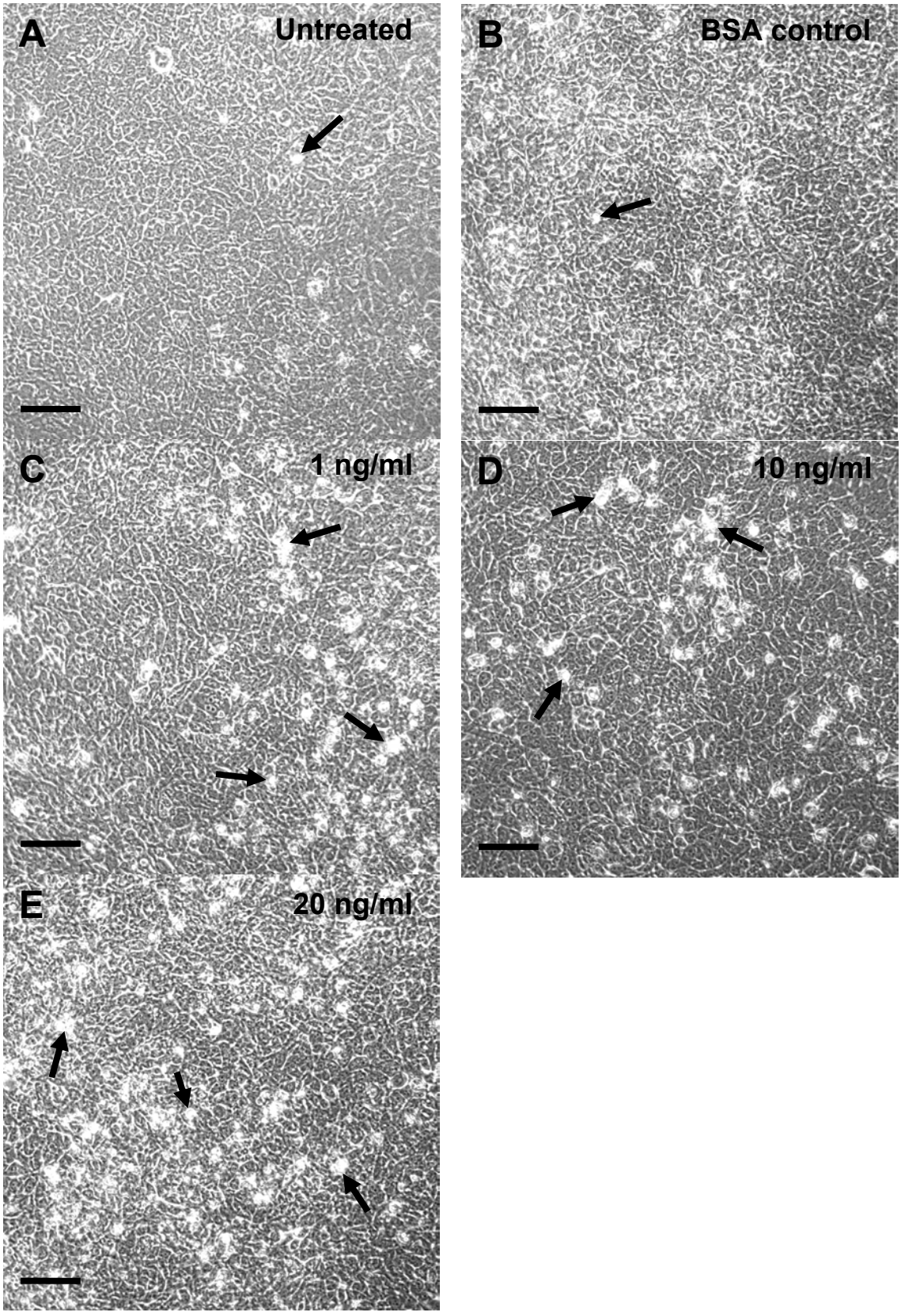

Figure 6.6 Phase contrast microscopy of TGFbeta1 treated MC3T3 cells at 4 days in culture

Cells were treated TGFbeta1 every 24 hours for 4 days. **A** and **B**: Untreated and BSA control. **C**, **D**, and **E**: Treated with TGFbeta1 at 1, 10 and 20 ng/ml respectively. More bright apoptotic figures (black arrows) are found in TGFbeta1 treated cells (C-E) than in controls (A and B). (n = 3, bar = 50 μm).

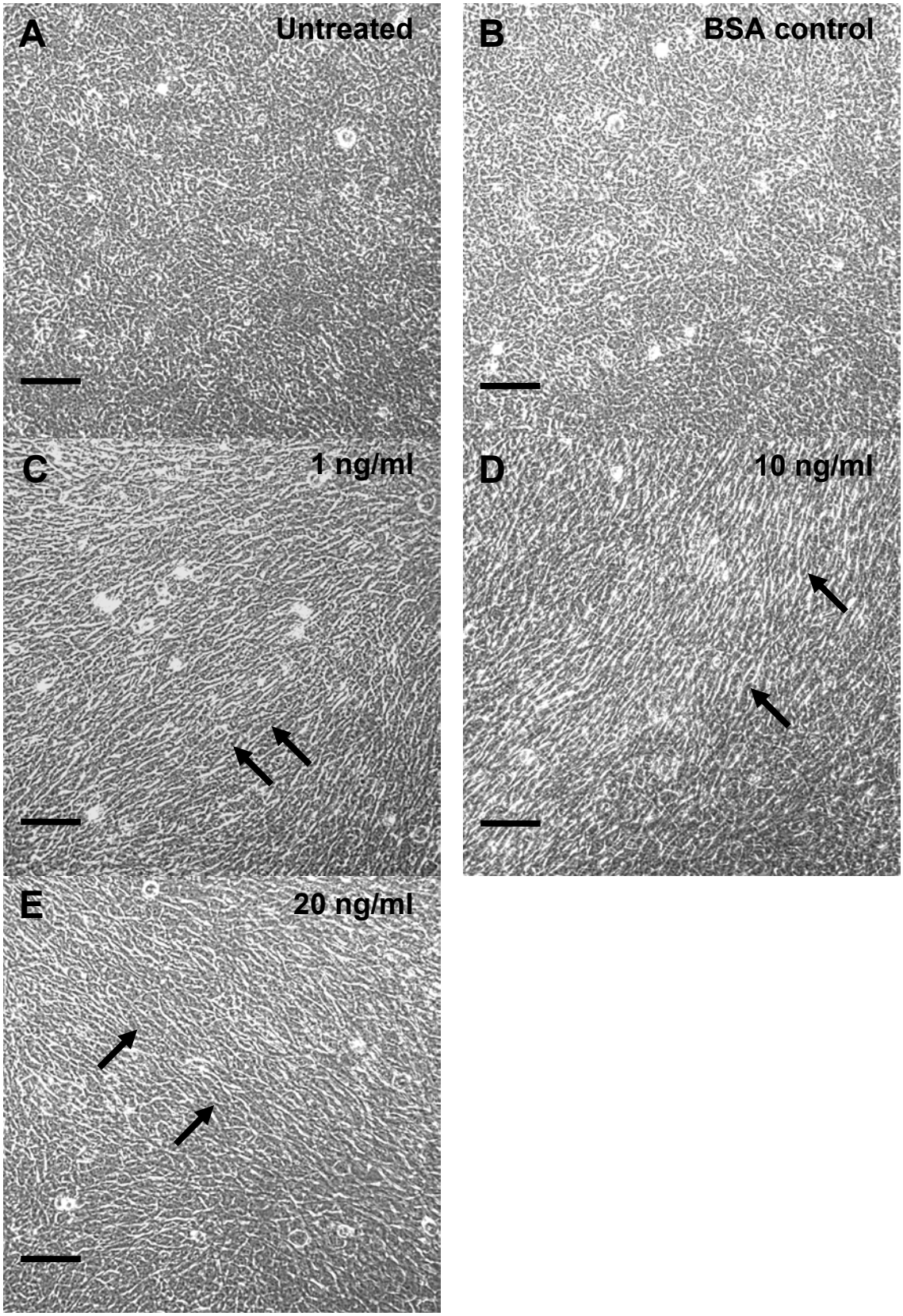

Figure 6.7 Phase contrast microscopy of TGFbeta1 treated R2-WT cells at 4 days in culture

Cells were treated TGFbeta1 every 24 hours for 4 days. **A** and **B**: Untreated and BSA control. **C**, **D**, and **E**: Treated with TGFbeta1 at 1, 10 and 20 ng/ml respectively. Treated cells (C, D and E) are more aligned (black arrows) compared to untreated controls (A and B), (n = 3, bar = 50 μm).

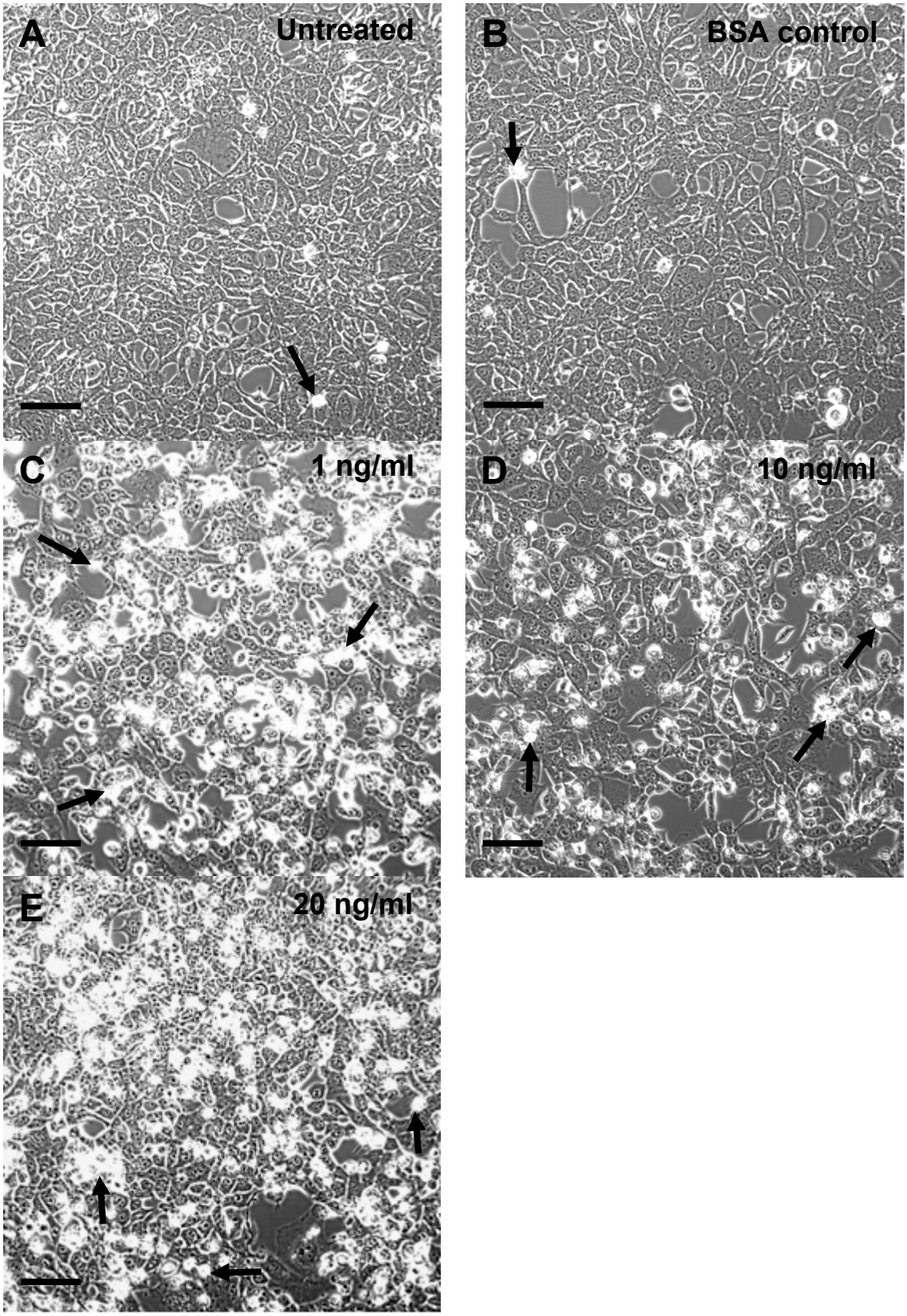

Figure 6.8 Phase contrast microscopy of TGFbeta1 treated R2-C278F cells at 4 days in culture

Cells were treated TGFbeta1 every 24 hours for 4 days. **A** and **B**: Untreated and BSA control. **C**, **D**, and **E**: Treated with TGFbeta1 at 1, 10 and 20 ng/ml respectively. TGFbeta1 treated cells (C-E) have many apoptotic figures (black arrows), than in the controls (A and B), (n = 3, bar = 50 μm).

6.2.3 The effect of TGFbeta1 and U0126 on cell morphology

To assess whether the morphological changes previously observed with TGFbeta1 were dependent on the Erk1/2 pathway, U0126 was used to inhibit Erk1/2 when cells were treated with TGFbeta1. MC3T3, R2-WT and R2-C278F cells were cultured in 96 well plates and treated with 10 ng/ml of TGFbeta1 and 10 μM of U0126 in 1 % serum. The treatment was given every 24 hours for 3 days. Images were then taken in phase contrast.

MC3T3 cell morphology did not change with TGFbeta1 at 3 days (Figure 6.9 A and B). Erk1/2 inhibition with U0126 treatment led to visibly fewer cells and a decrease in cells with fibroblastic morphology (Figure 6.9 C). The cell morphology in the TGFbeta1 and U0126 combined treatment group was indistinguishable from the U0126 treated group (Figure 6.9 D).

In R2-WT cells, there was no obvious change in morphology with TGFbeta1 treatment at 3 days (Figure 6.10 A and B). With U0126 treatment there were visibly fewer cells and the cell morphology was less fibroblastic and more cuboidal (Figure 6.10 C). The same effects were observed with the TGFbeta1-U0126 combined treatment (Figure 6.10 D).

The morphology of R2-C278F cells at 3 days did not appear to change with TGFbeta1 treatment (Figure 6.11 A and B). With U0126 treatment, the cell morphology was less fibroblastic than in the untreated control (Figure 6.11 C). Interestingly with both TGFbeta1 and U0126 treatments there were more cells with a rounded morphology than in the U0126 treated group (Figure 6.11 D).

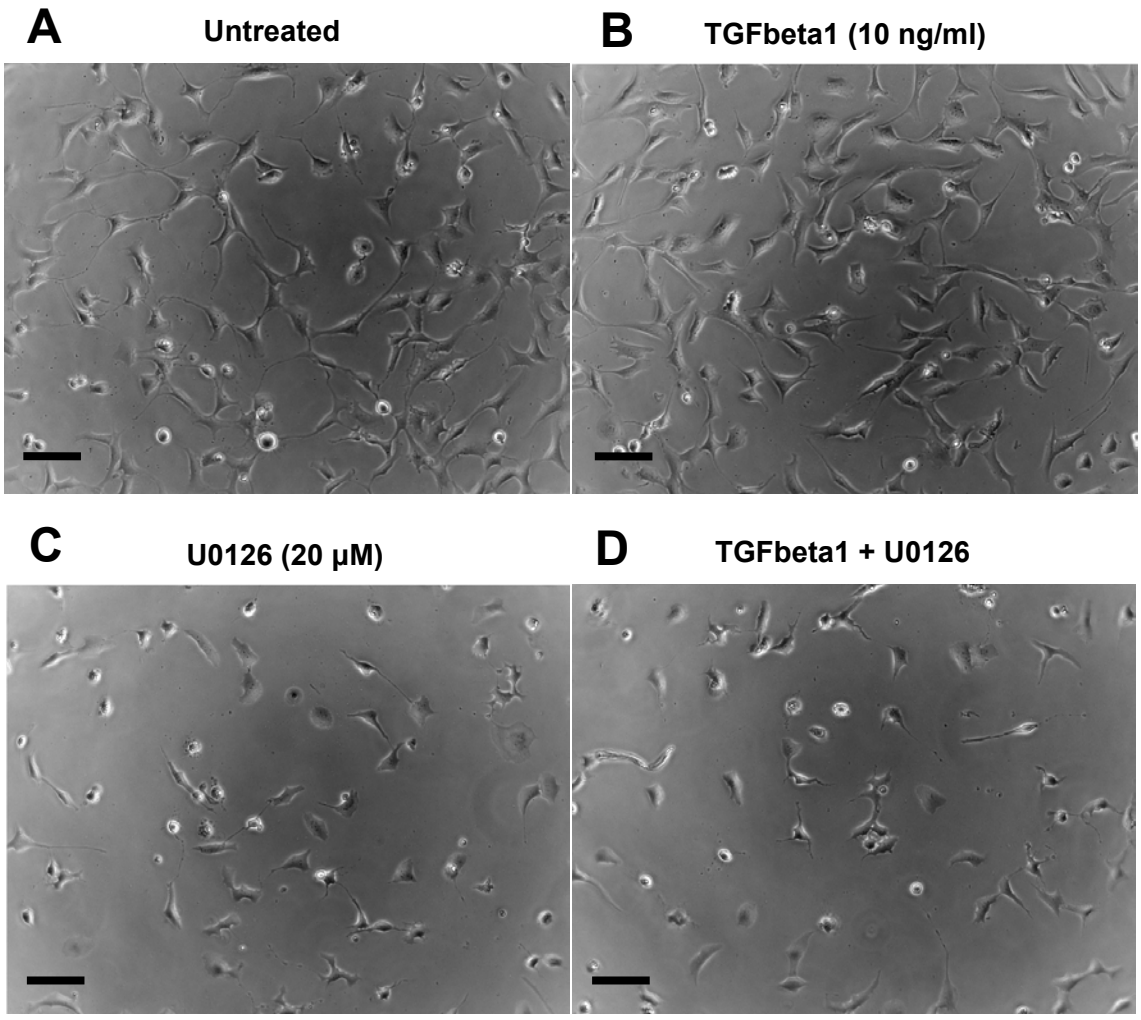

Figure 6.9 Phase contrast images of MC3T3 cells treated with TGFbeta1 and U0126 in 1% serum
Untreated cells (A) and TGFbeta1 treated cells (B) have a similar morphology. U0126 treatment (C) markedly reduces the number of cells, particularly fibroblastic cells. The number of cells and their morphology in the TGFbeta1 + U0126 treatment group (D) is similar to (C) the U0126 treatment group (n = 3, bar = 50 μm).

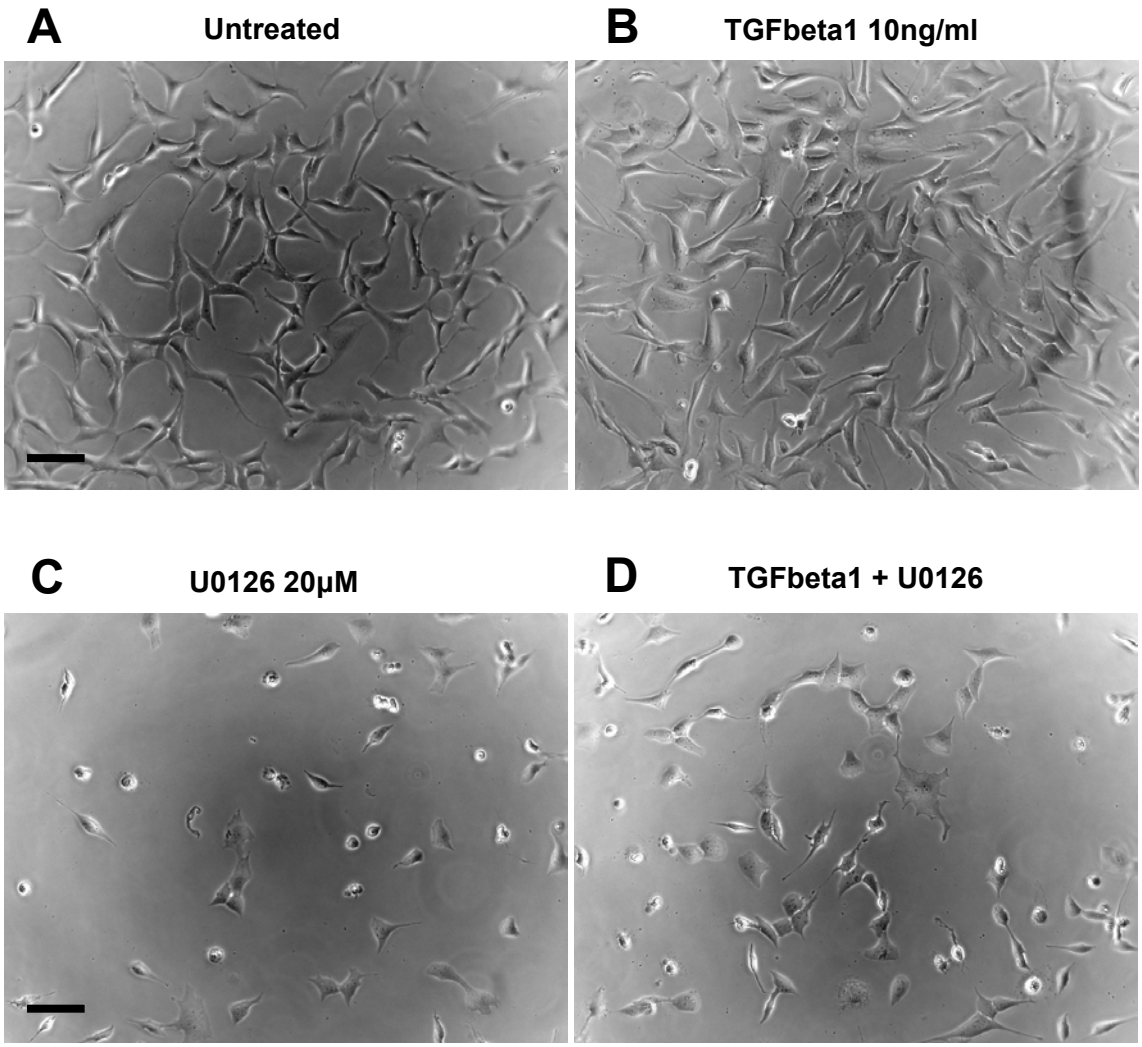

Figure 6.10 Phase contrast images of R2-WT cells treated with TGFbeta1 and U0126

Untreated (A) and TGFbeta1 treated cells (B) were similar in morphology. U0126 treatment (C) led to a visible loss of cells, especially cells with fibroblastic morphology. The combination of TGFbeta1 and U0126 treatment (D) also led to a reduction in the number of cells, particularly fibroblastic-like cells (n = 3, bar = 50 μm).

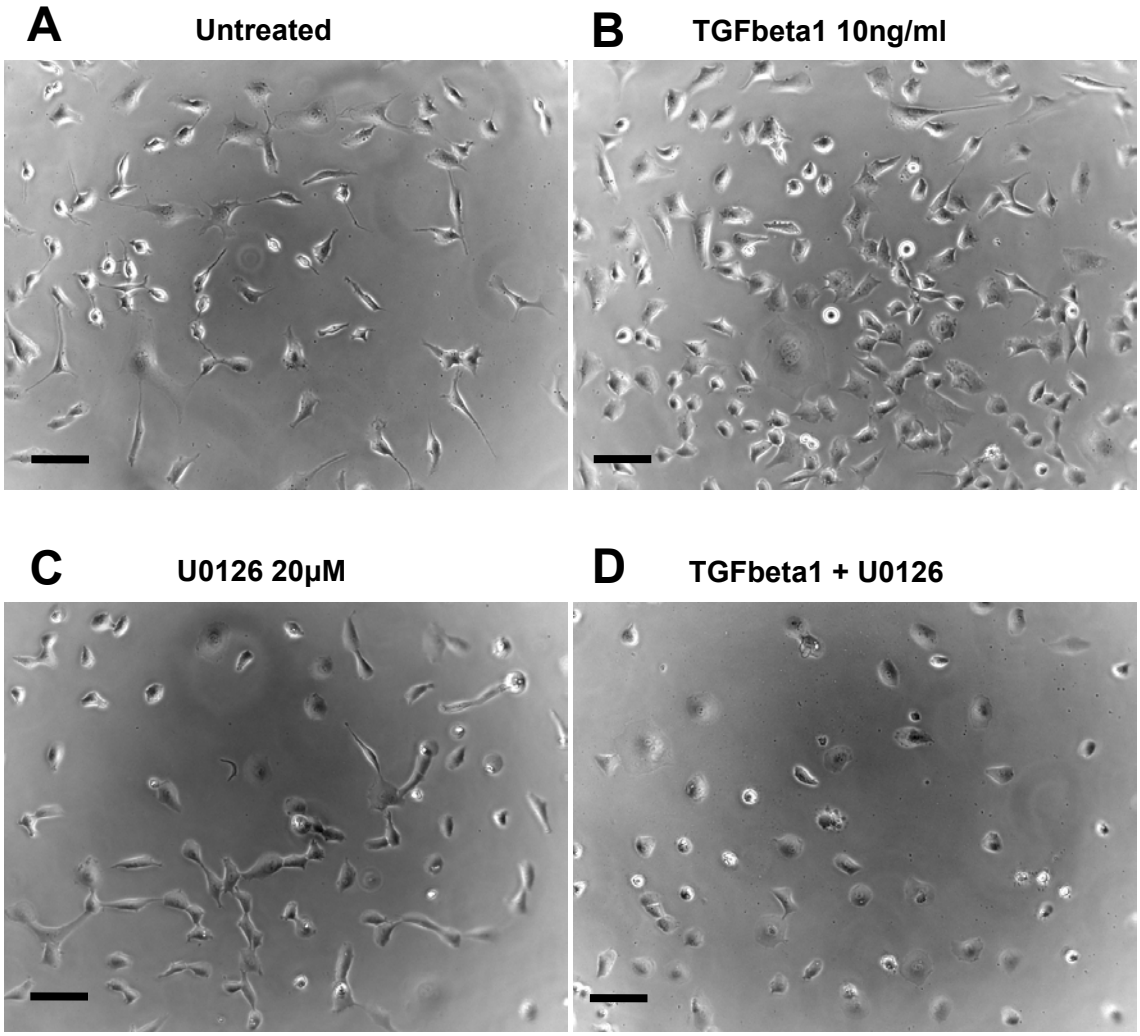

Figure 6.11 Phase contrast microscopy of R2-C278F cells treated with TGFbeta1 and U0126
Morphology of TGFbeta1 treated cells are less fibroblastic (B) compared to the untreated controls (A). U0126 treatment (C) reduces the number of fibroblastic cells and the number of cellular processes. The effect of TGFbeta1 and U0126 treatment (D) induces a greater loss of fibroblastic cells (n = 3, bar = 50 µm).

6.2.4 Effects of exogenous TGFbeta1 on *Fgf* expression

Fgf1, *-2* and *-18* expressions were analysed in MC3T3, R2-WT and R2-C278F cells to investigate whether TGFbeta1 interacts with FGF signalling by altering expression of these ligands. Three hours after seeding, cells were treated with 10 ng/ml of TGFbeta1 every 24 hours for either 2 days or 4 days in culture.

Analysis by Real Time RT-PCR at 2 days revealed that *Fgf1* was barely detectable particularly in the R2-WT and R2-C278F cells, with a high cycle threshold (CT) value (35 cycles) and in some cases it was undetectable (Figure 6.12 A). When untreated groups were compared, the level of *Fgf1* was significantly higher in R2-WT cells than in MC3T3 and R2-C278F cells. Treatment with TGFbeta1 did not statistically change the expression of *Fgf1*.

At 2 days, *Fgf2* expression was also very low in all three cell lines and there was no significant change in *Fgf2* expression with TGFbeta treatment (Figure 6.12 B). The levels of *Fgf2* were not significantly different between cell lines.

A significant increase in *Fgf18* expression was found at 2 days in MC3T3 and R2-C278F cells after TGFbeta1 treatment, but not in R2-WT cells (Figure 6.13 A). At 4 days, after TGFbeta1 treatment, *Fgf18* expression also increased in MC3T3, but not in R2-WT or R2-C278F cells (Figure 6.13 B).

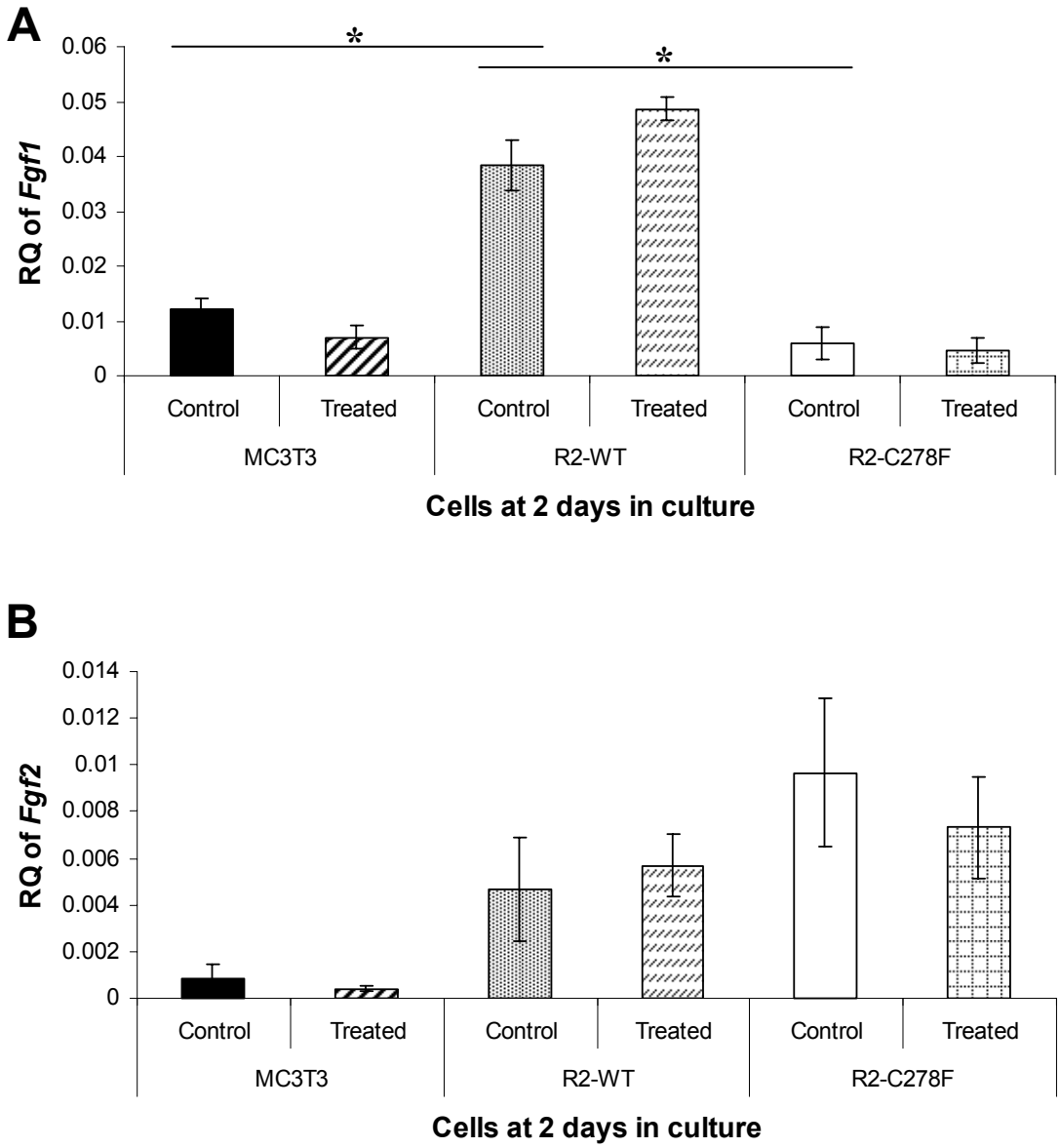

Figure 6.12 Real time PCR analysis of *Fgf1* and *-2* expressions in TGFbeta1 treated cells

Cells were grown for 2 days in culture with 10 ng/ml of TGFbeta1 before relative quantification (RQ) of gene expression by real time PCR. **A:** *Fgf1* is expressed at very low levels in all three cell lines and Tgfbeta1 treatment in each cell line does not induce any significant changes compared to their respective untreated controls. The level of *Fgf1* in untreated R2-WT cells is significantly higher than in both untreated MC3T3 and R2-C278F cells. **B:** *Fgf2* is barely detectable in all three cell lines. No significant differences in *Fgf2* expression were found between cell lines. TGFbeta1 treatment did not alter *Fgf2* expression levels (n = 3, *p<0.05 ANOVA).

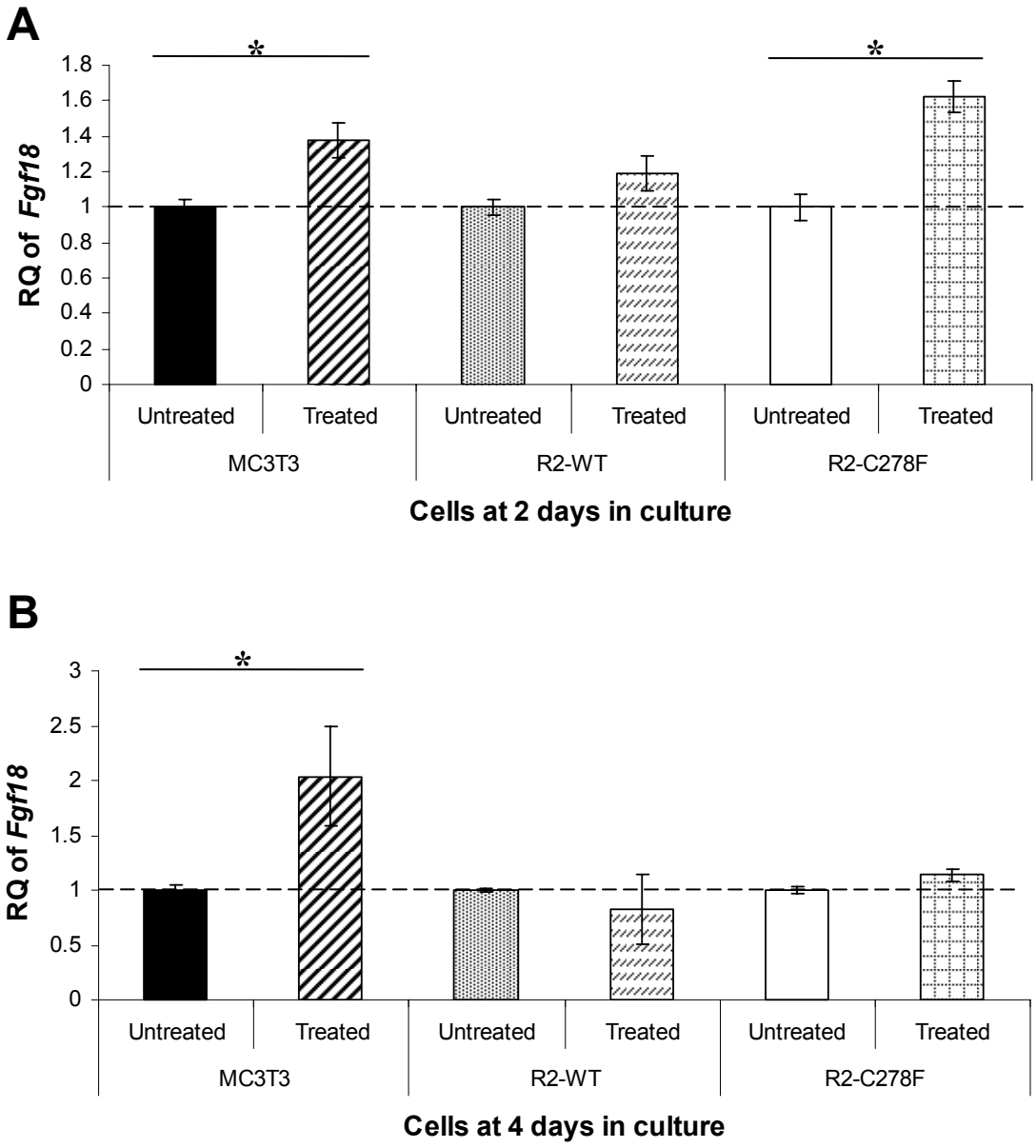

Figure 6.13 Real time PCR analysis *Fgf18* with TGFbeta1 treatment

MC3T3, R2-WT and R2-C278F cells were treated with 10 ng/ml of TGFbeta1 every 24 hours for 2 or 4 days. For each cell line the expression levels were normalised to the untreated controls. **A:** At 2 days in culture, TGFbeta treatment significantly increases *Fgf18* in MC3T3 and R2-C278F, but not in R2-WT cells. **B:** *Fgf18* is also increased in MC3T3 with treatment at 4 days in culture. No significant changes are observed in both R2-WT and R2-C278F after treatment ($n = 3$, $*p < 0.05$).

6.2.5 Effects of Exogenous TGFbeta1 on cell growth

Tgfbeta1 may induce proliferation in osteoblast cells (Reyes-Botella et al., 2002). As low *TGFbeta1* expression was found in R2-C278F, exogenous TGFbeta1 was used to determine whether the R2-C278F cell proliferation could be increased. Cells were seeded onto a 96 well plate and treated with 10 ng/ml of TGFbeta1 in 10% FBS every 24 hours for 1, 2 and 3 days before cell growth analysis using the methylene blue assay. Untreated controls were cultured in normal cell culture medium with 1 mg/ml BSA in 4 mM HCl, the solution for TGFbeta1 suspension. This experiment was repeated with 10 ng/ml of TGFbeta1 treatment in cell culture medium containing 1 % FBS, after seeding in 10 % FBS for 3 hours.

After 1 day, TGFbeta treatment induced significantly more cell growth in MC3T3, whereas in R2-WT and R2-C278F cells there was no significant increase in cell growth (Figure 6.14 A). By 2 days, cell growth significantly increased in both MC3T3 and R2-WT with TGFbeta treatment, but there was no change in R2-C278F cells (Figure 6.14 B). In MC3T3 and R2-WT at 3 days there was still a significant increase in cell growth, however no change was found in R2-C278F cells.

In 1% serum after 1 day of TGFbeta treatment, no significant increase in cell growth was observed in any of the three cell lines (Figure 6.15 A). By 2 days, TGFbeta1 treatment resulted in significantly increased cell growth in MC3T3, R2-WT and R2-C278F cells (Figure 6.15 B). At 3 days in culture, all three cell lines showed a significant increase in cell growth when treated with TGFbeta1 (Figure 6.15 C).

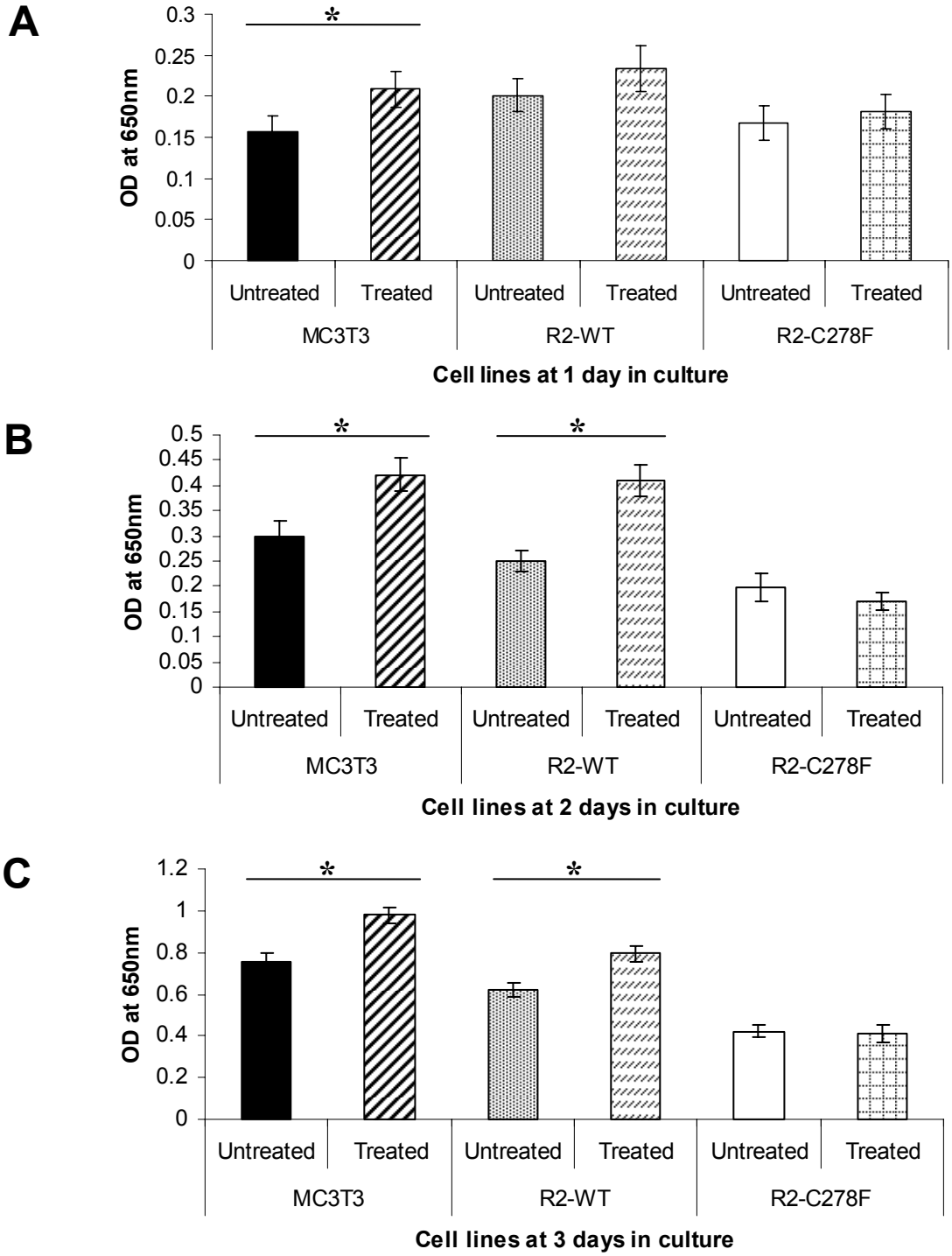

Figure 6.14 Methylene blue analysis of TGFbeta1 treated MC3T3, R2-WT and R2-C278F cells

Cells were cultured in 10% FBS containing serum and treated with 10 ng/ml TGFbeta1 every 24 hours for 1, 2 or 3 days. By 1 day (A) there is a significant increase in cell growth in MC3T3 after TGFbeta treatment, but not in R2-WT and R2-C278F cells. By 2 and 3 days (B and C), the treated groups in both MC3T3 and R2-WT cells showed increased cell growth, whereas there was no difference between treated and untreated groups in R2-C278F cells ($n = 3$, $*p < 0.05$).

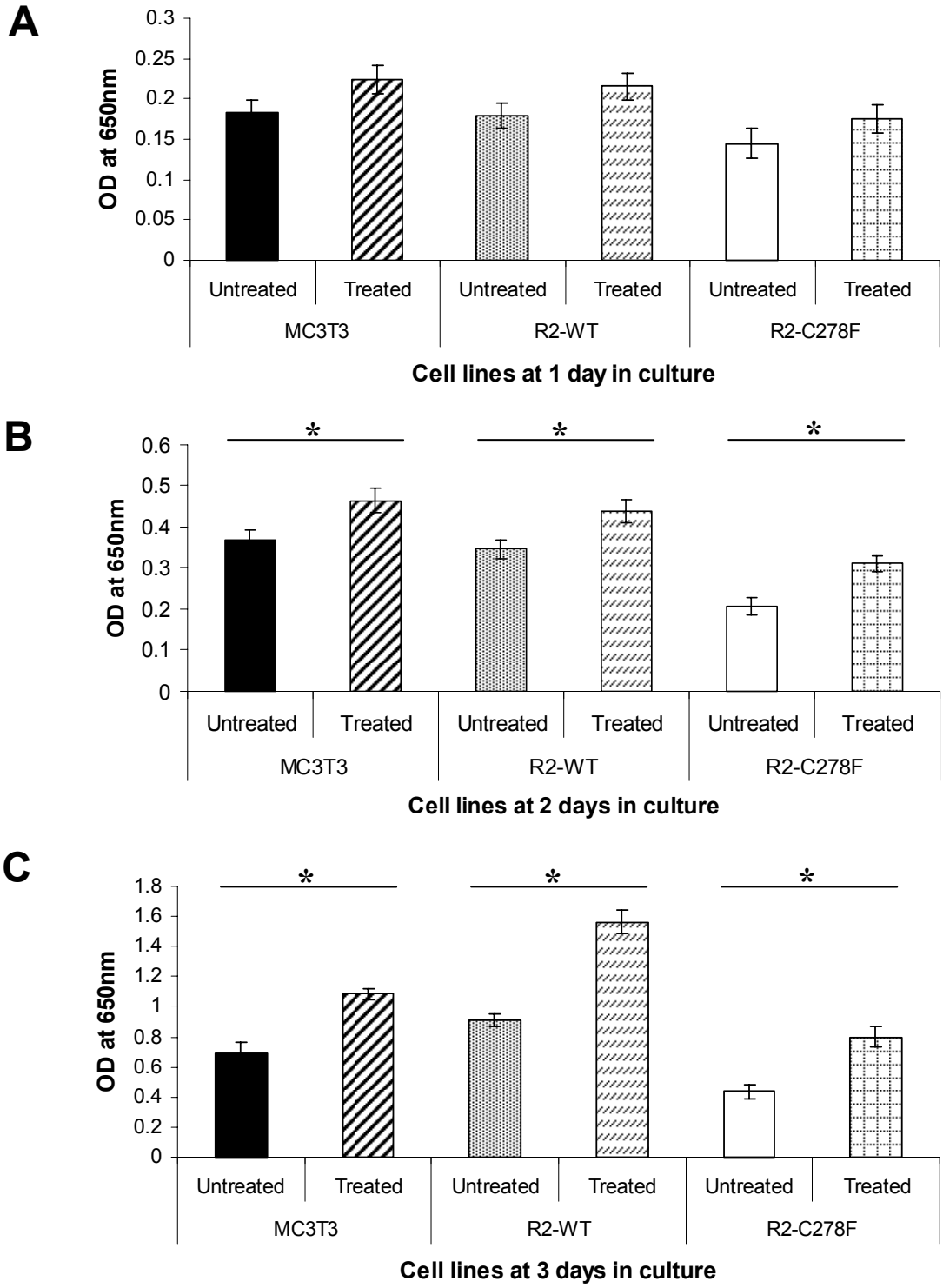

Figure 6.15 Methylene blue analysis of TGFbeta1 treated cells in 1% FBS

MC3T3, R2-WT and R2-C278F cells were treated with 10 ng/ml TGFbeta1 in 1% FBS containing culture medium every 24 hours for 1, 2 or 3 days. By 1 day (A), TGFbeta does not significantly affect cell growth in any of the three cell lines. At 2 and 3 days (B and C), cell growth is significantly increased with TGFbeta treatment in MC3T3, R2-WT and R2-C278F cells (n = 3, *$p < 0.05$).

6.2.6 The effect of TGFbeta1, U0126 and SB431542 on cell growth

TGFbeta1 was used in conjunction with Erk1/2 inhibitor U0126 on MC3T3, R2-WT and R2-C278F cells to determine whether cell growth induced by TGFbeta1 is dependent on Erk1/2. To investigate the the level of TGFbeta signalling resulting in cell growth, TβRI activation was inhibited with SB431542. The cells were treated after seeding every 24 hours for 3 days as described in Section 3.1.6. Treatment with TGFbeta and U0126 were performed in 1 % serum for 3 days.

In all cells TGFbeta1 treatment significantly increased cell growth, whereas with U0126 treatment cell growth decreased (Figure 6.16). The cell growth after TGFbeta1 and U0126 combined was not significantly different to U0126 alone, in MC3T3 and R2-WT cells. In R2-C278F cells, TGFbeta1 and U0126 treated cells had a significantly higher level of cell growth than the group treated with U0126 alone.

Treatment of MC3T3 with SB431542 in 10 % FBS had no effect on cell growth at 1 μM in MC3T3 and R2-WT cells, but decreased cell growth maximally in R2-C278F cells, as higher doses did not further inhibit R2-C278F cell growth (Figure 6.17). In contrast, increasing the dose to 10 μM led to a further decrease in cell growth in MC3T3 and R2-WT cells and further still in MC3T3 treated with 20 μM.

At 1% serum conditions, there was a dose dependent decrease in cell growth from 1, 10 to 20 μM in MC3T3 (Figure 6.18 A). 1 μM in R2-WT cells also reduced cell growth and this was further reduced with 20 μM (Figure 6.18 B). In R2-C278F cells there was a significant decrease in cell growth with 1 μM, but 10 and 20 μM did not lead to a further decrease in cell growth beyond that of the 1 μM dose (Figure 6.18 C).

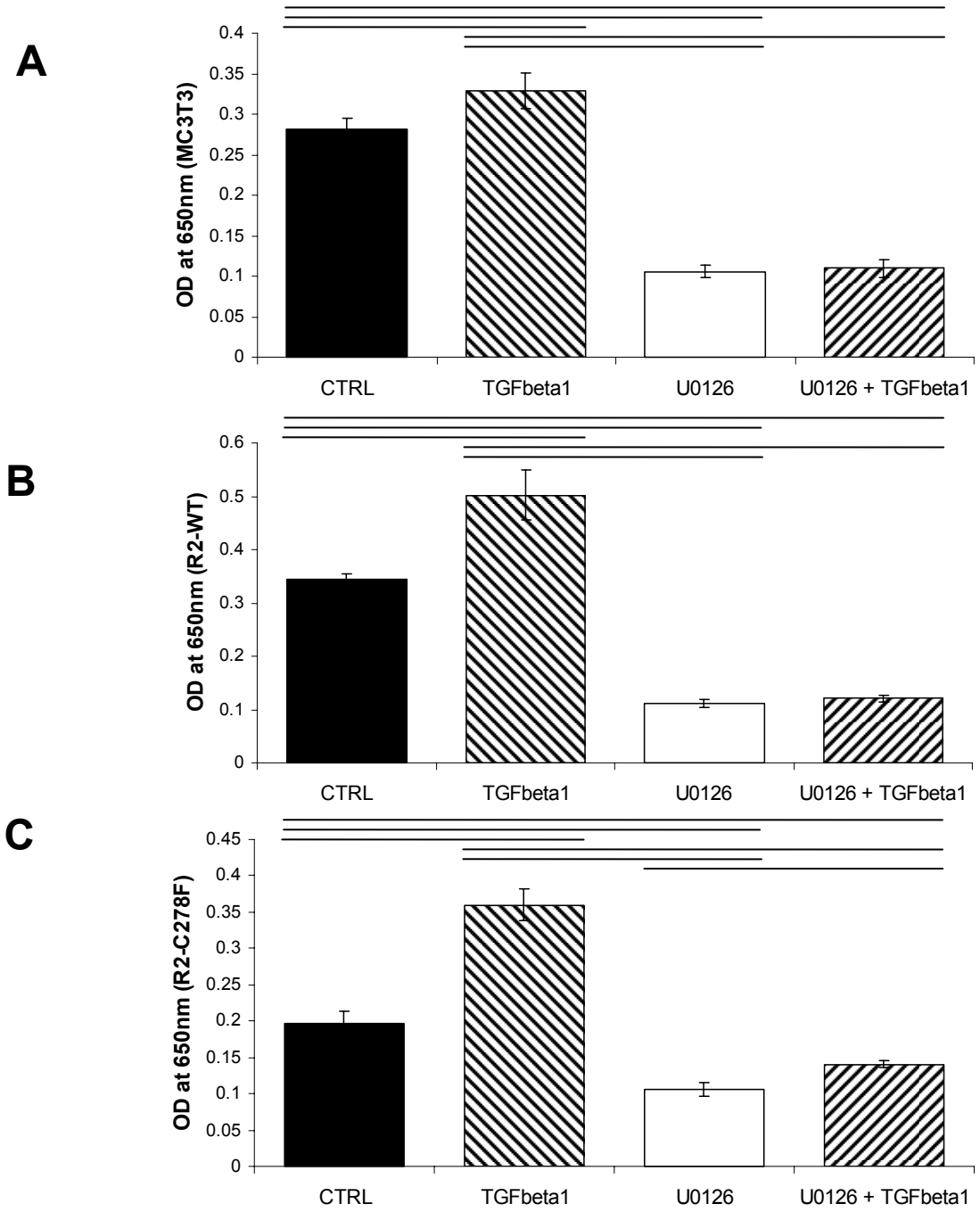

Figure 6.16 Methylene Blue analysis of cell growth in TGFbeta1 and U0126 treated cells in 1% FBS
Cells were cultured with TGFbeta1 (10 ng/ml) and U0126 (20 uM) for three days before analysis. **A, B** and **C**: Treatment TGFbeta1 increases cell growth in all three cell lines. For each cell line, the cell growth in the U0126 treated groups are significantly lower, compared to both untreated and TGFbeta1-treated groups. Cell growth in the combined treatments of TGFbeta1 and U0126 are not significantly different compared to U0126 treatment alone, except in (C) R2-C278F cells ($n = 4$, line $p < 0.05$ ANOVA).

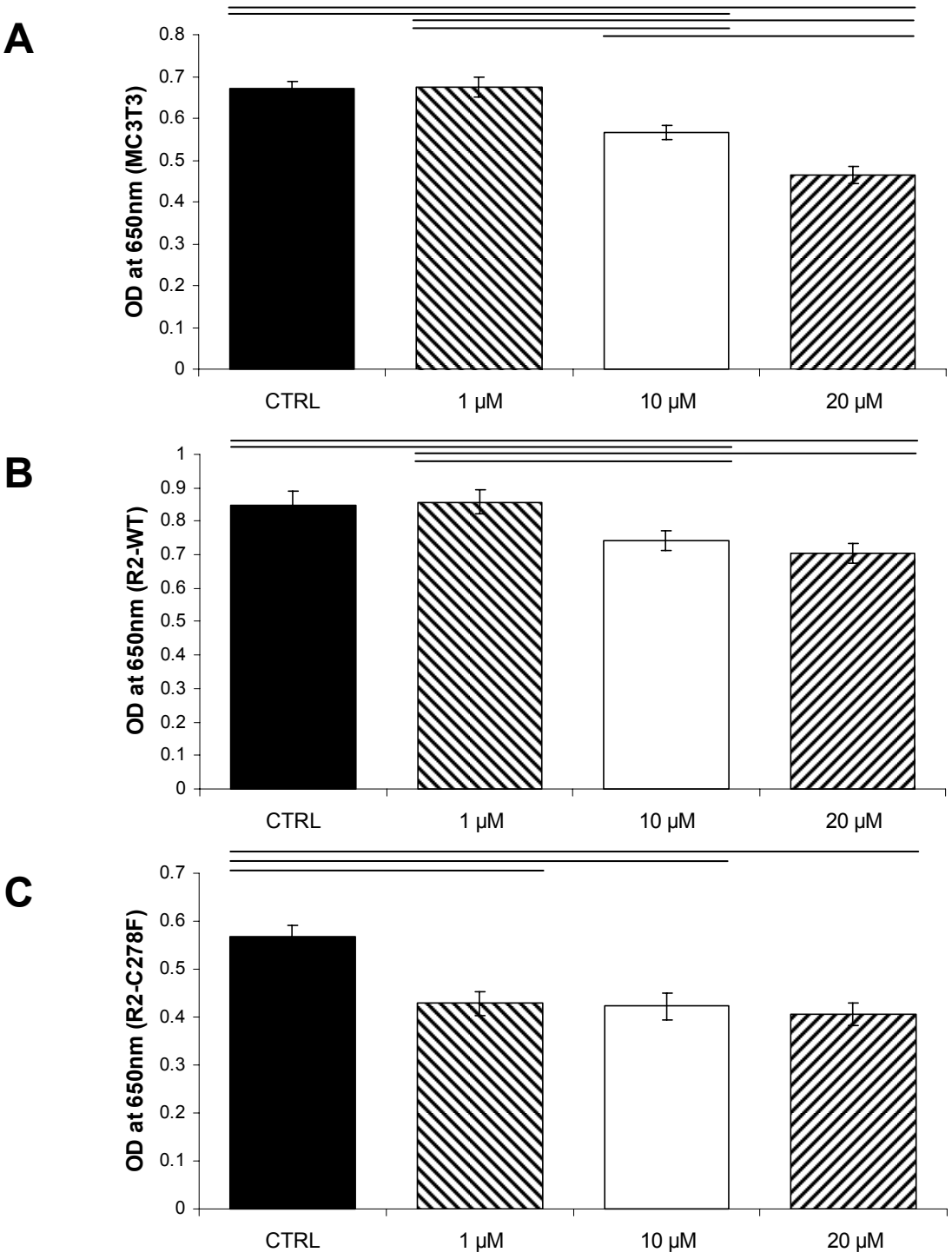

Figure 6.17 Methylene blue analysis of cell growth in SB431542 treated cells in 10% FBS

Cells were treated with SB431542 at 1, 10 and 20 µM for three days before analysis. **A:** The decrease in MC3T3 cell growth is dose dependent. **B:** In R2-WT cells, 10 µM is sufficient to reduce cell growth, but 20 µM has no further effect. **C:** 1 µM is sufficient to reduce cell growth significantly in R2-C278F cells and this effect is not enhanced by increasing dose (n = 3, line denotes $p < 0.05$ ANOVA).

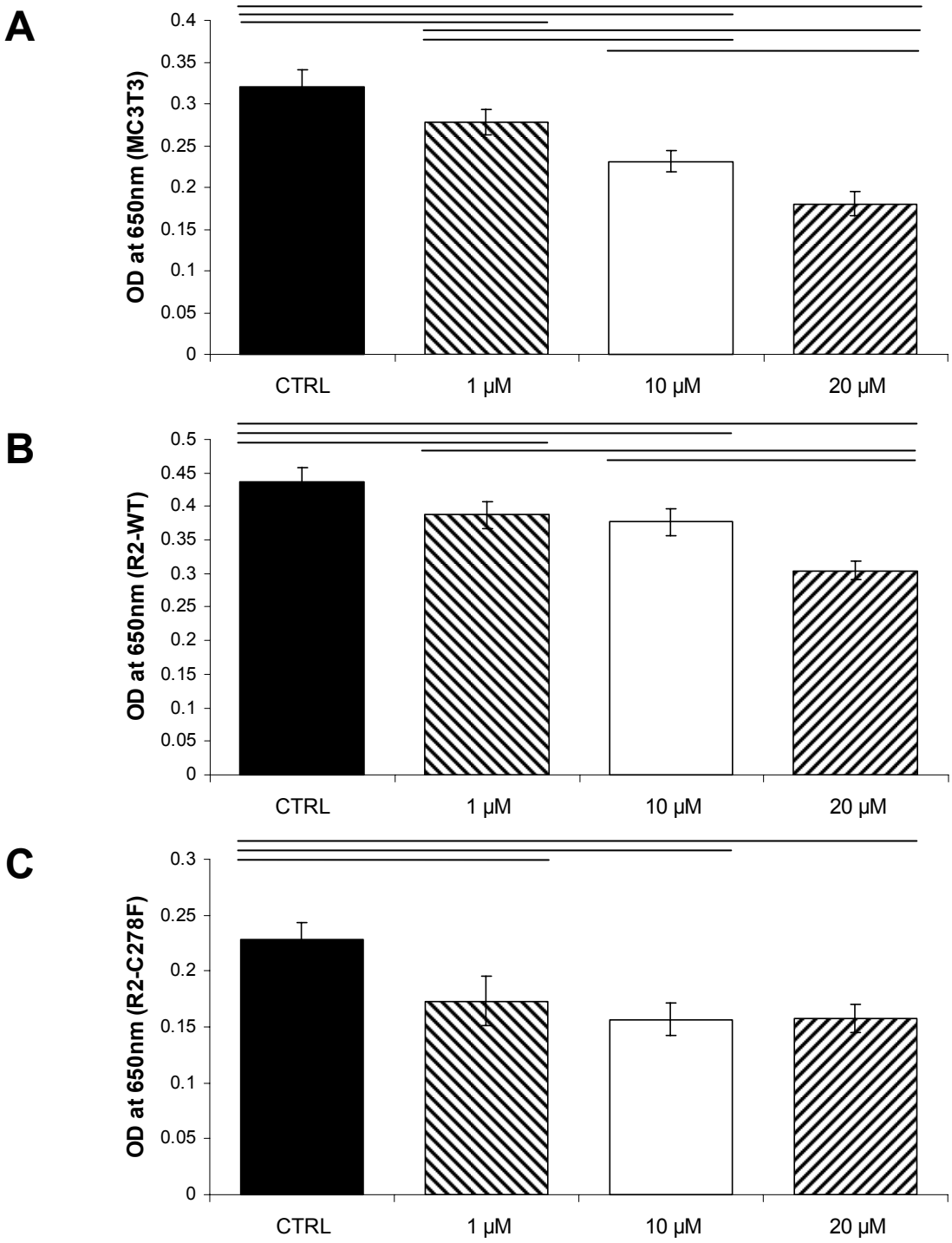

Figure 6.18 Cell growth with TGFbeta receptor inhibitor SB431542 in 1% FBS

Cells were treated with SB431542 at 1, 10 and 20 µM for three days before analysis. **A:** Cell growth decreases in MC3T3 at all concentrations used. **B:** In R2-WT cells, 1 µM decreases cell growth and a further decrease is observed with 20 µM. **C:** 1 µM already induces maximal cell growth inhibition in R2-C278F cells (n = 3, line denotes $p < 0.05$ ANOVA).

6.2.7 Effects of exogenous TGFbeta1 on differentiation

TGFbeta may inhibit late stage differentiation in osteoblasts by control of *Runx2* and *Opn* expression (Noda et al., 1988; Viereck et al., 2002). Therefore the expression of *Runx2* and *Opn* was analysed in MC3T3, R2-WT, R2-C278F cells following TGFbeta1 treatment. Cells were treated with 10 ng/ml of TGFbeta1 treatment every 24 hours for 2 and 4 days.

After 2 days of TGFbeta1 treatment, all three cell lines showed a significant increase in *Runx2* expression (Figure 6.19 A). At 4 days, TGFbeta1 treated MC3T3 and R2-WT cells showed significantly increased *Runx2* expression compared to their untreated controls, whereas in R2-C278F, *Runx2* decreased with TGFbeta1 treatment (Figure 6.19 B).

Opn expression significantly decreased in TGFbeta1-treated MC3T3 cells at 2 days, while in R2-WT cells *Opn* significantly increased with treatment; in R2-C278F cells TGFbeta did not significantly change the level of *Opn* (Figure 6.20 A). At 4 days both MC3T3 and R2-WT cells responded to TGFbeta1 treatment by significantly increasing *Opn* expression; however in R2-C278F cells there was no significant difference in *Opn* expression (Figure 6.20 B).

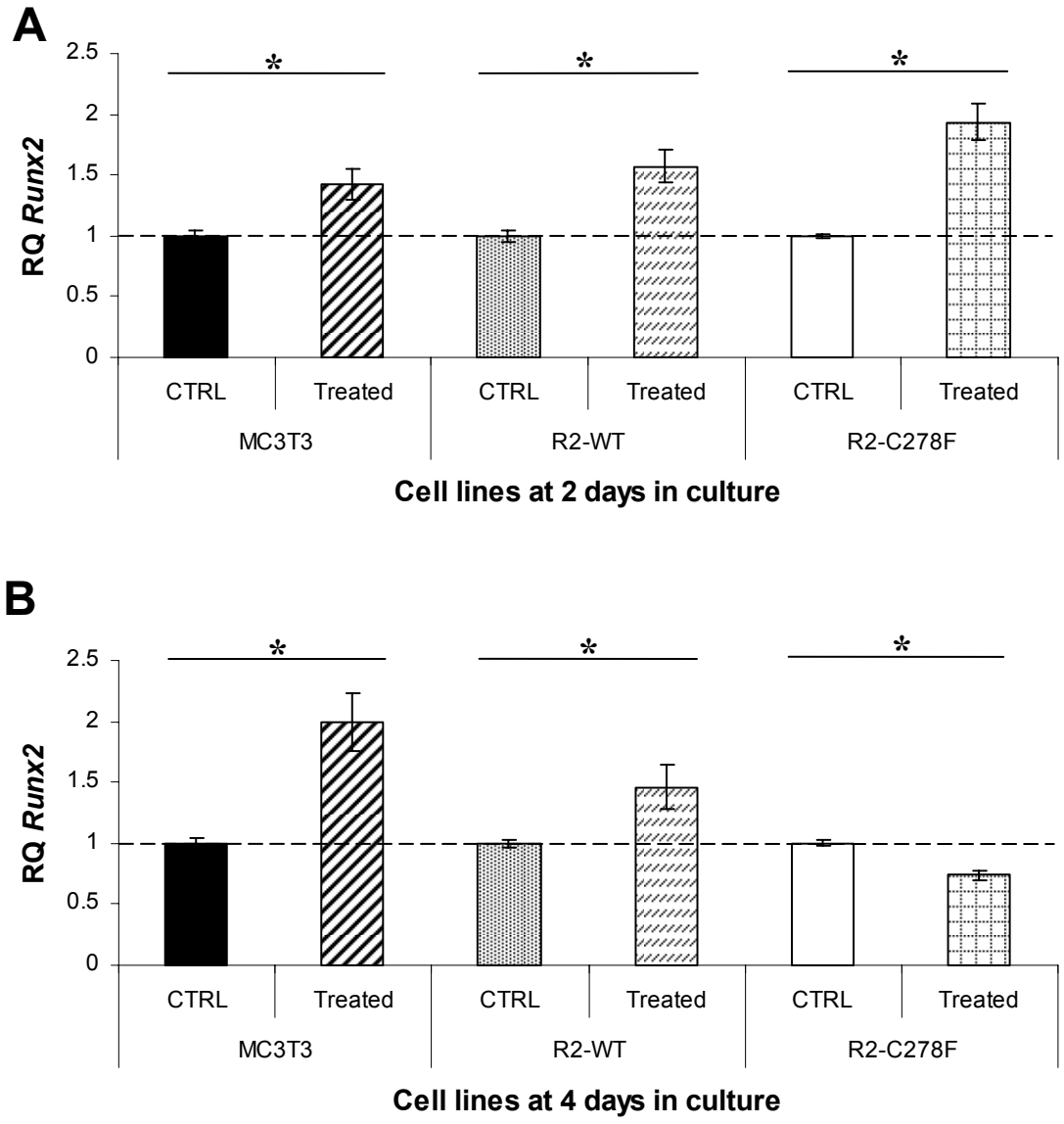

Figure 6.19 Real time PCR analysis of *Runx2* expression in MC3T3, R2-WT and R2-C278F cells
Cells were treated with 10 ng/ml of TGFbeta1 for 2 and 4 days in culture before relative quantification (RQ) of gene expression by real time PCR. For each cell line the expression levels were normalised to the untreated controls. **A**: TGFbeta1 treatment significantly increases *Runx2* levels in MC3T3, R2-WT and R2-C278F cells at 2 days compared to their respective controls. **B**: *Runx2* expression increases in TGFbeta1 MC3T3 and R2-WT cells at 4 days, but decreases in R2-C278F cells ($n = 3$, $*p < 0.05$).

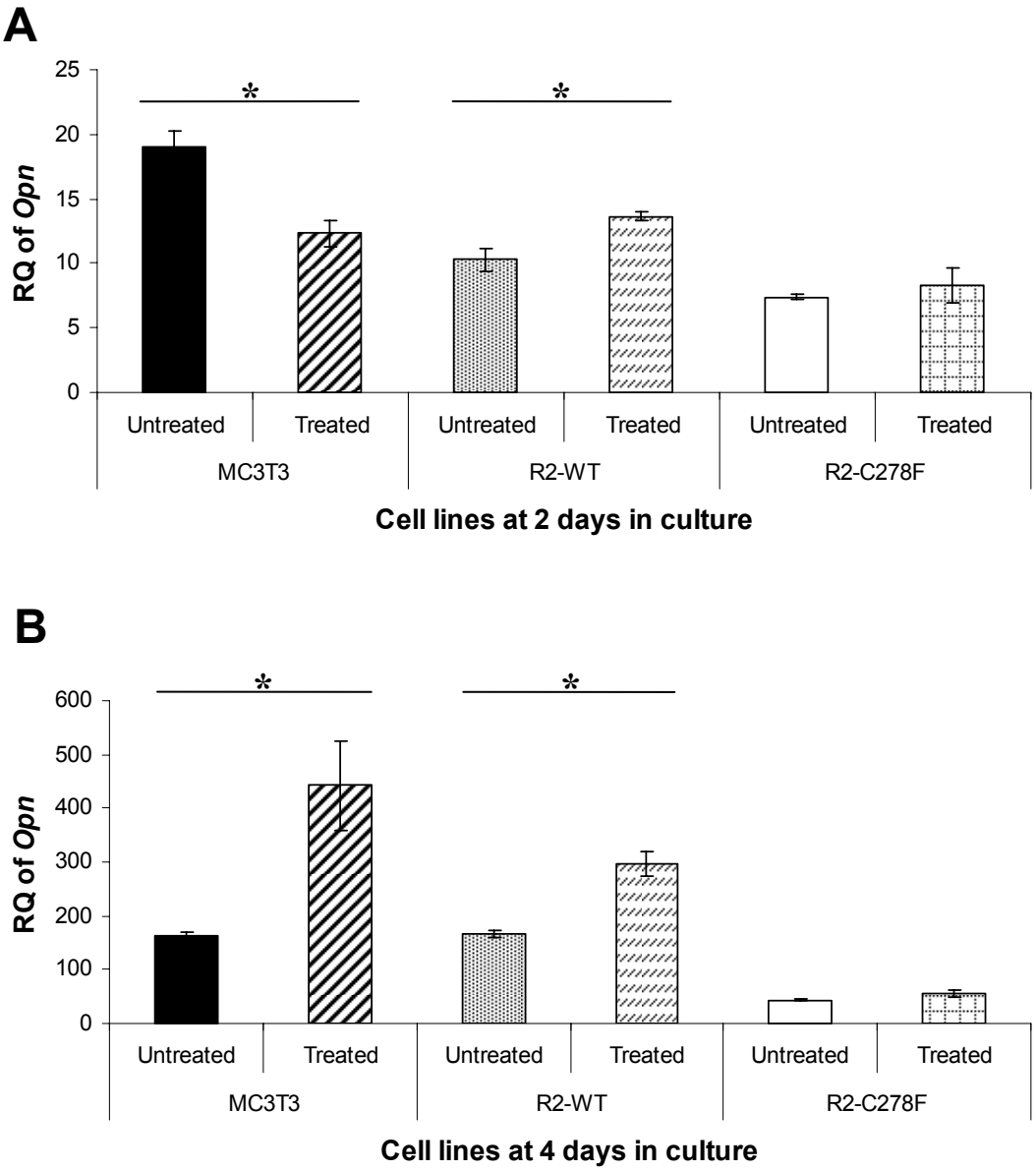

Figure 6.20 Real time PCR analysis of *Opn* expression in MC3T3, R2-WT and R2-C278F cells

Cells were treated with 10 ng/ml of TGFbeta1 for 2 and 4 days in culture before relative quantification (RQ) of gene expression by real time PCR. **A**: *Opn* decreases in MC3T3, increases in R2-WT and does not significantly change in R2-C278F cells at 2 days in culture. **B**: At 4 days, TGFbeta1 treatment increases *Opn* expression in MC3T3 and R2-WT, but not in R2-C278F cells ($n = 3$, $*p < 0.05$).

6.2.8 The effect of TGFbeta1 on *Smad2* expression

Given that FGFR signalling may have had some effect on *Smad2* expression, its expression was analysed following TGFbeta1 treatment. Cells were treated with 10 ng/ml of TGFbeta1 treatment every 24 hours for 2 or 4 days.

TGFbeta treatment did not significantly affect *Smad2* expression in any of the three cell lines at 2 days (Figure 6.21 A). At 4 days, *Smad2* expression increased in both MC3T3 and R2-WT cells with TGFbeta1 treatment, whereas in R2-C278F cells TGFbeta1 treatment decreased *Smad2* expression (Figure 6.21 B).

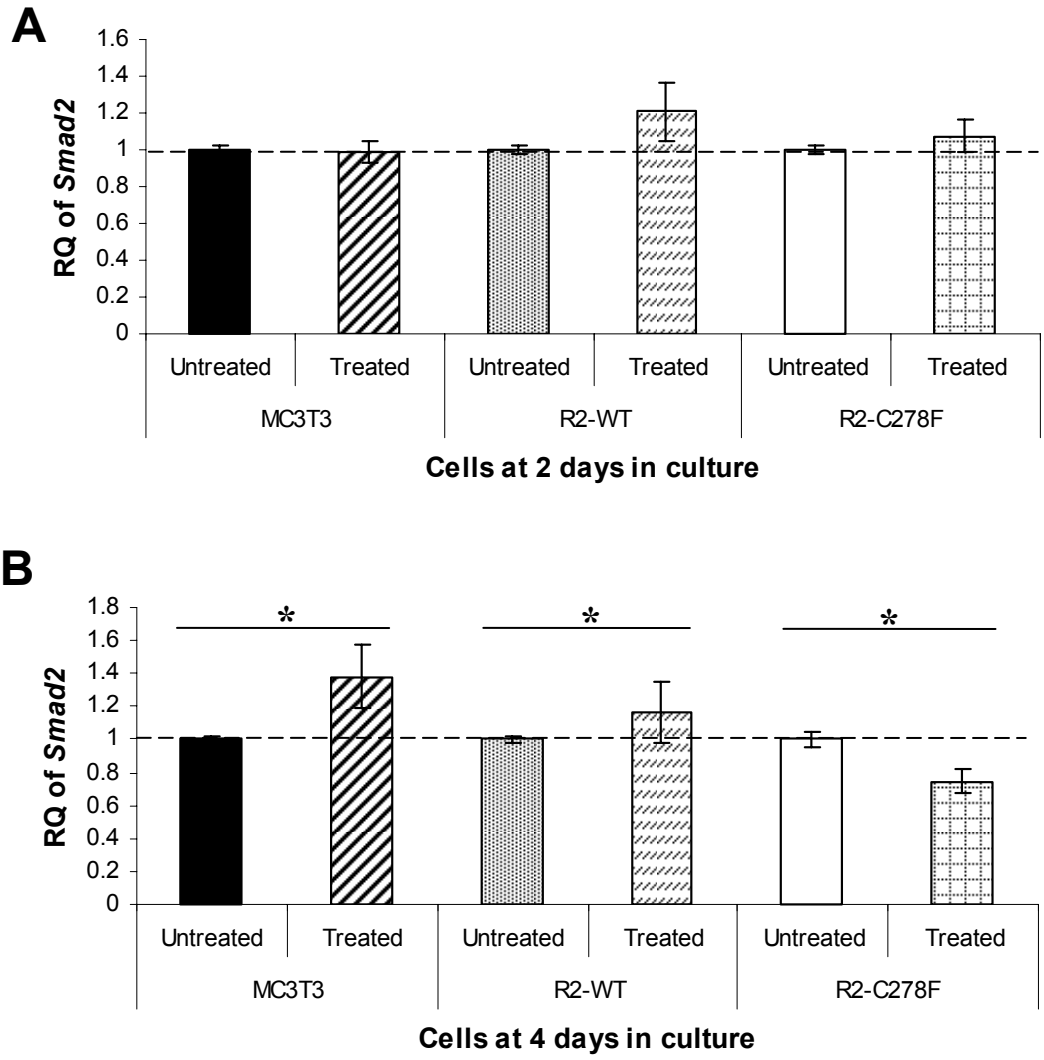

Figure 6.21 Real time PCR analysis of *Smad2* levels in MC3T3, FGFR2-WT and R2-C278F cells. Cells were seeded for 3 hours then treated with 10 ng/ml of TGFbeta1 for 2 and 4 days in culture before relative quantification (RQ) of gene expression by real time PCR. The gene expression for each cell line was normalised to the untreated control. **A**: *Smad2* expression does not change significantly after TGFbeta treatment in all three cell lines at 2 days. **B**: TGFbeta1 treatment after 4 days significantly increases *Smad2* expression in MC3T3 and R2-WT cells, but it significantly decreases it in R2-C278F cells ($n = 3$, $*p < 0.05$).

6.2.9 The affect of TGFbeta1 treatment on *Gapdh* expression

As reported in Chapter 4, *Gapdh* gene expression was reduced in R2-C278F cells (Figure 4.9 A) and it was suggested that this change could be related to an altered metabolism with an increased dependency on serum for cell survival. To investigate whether the low expression of *Gapdh* could be corrected by exogenous TGFbeta1 MC3T3, R2-WT and R2-C278F cells were treated with 10 ng/ml of TGFbeta1 for 2 to 4 days in culture.

At 2 days, treatment with TGFbeta1 did not significantly change *Gapdh* expression in MC3T3, R2-WT and R2-C278F cells (Figure 6.22 A). By 4 days in culture, treatment with TGFbeta1 did not significantly affect *Gapdh* expression MC3T3 or R2-WT cells; however *Gapdh* significant decreased in R2-C278F cells (Figure 6.22).

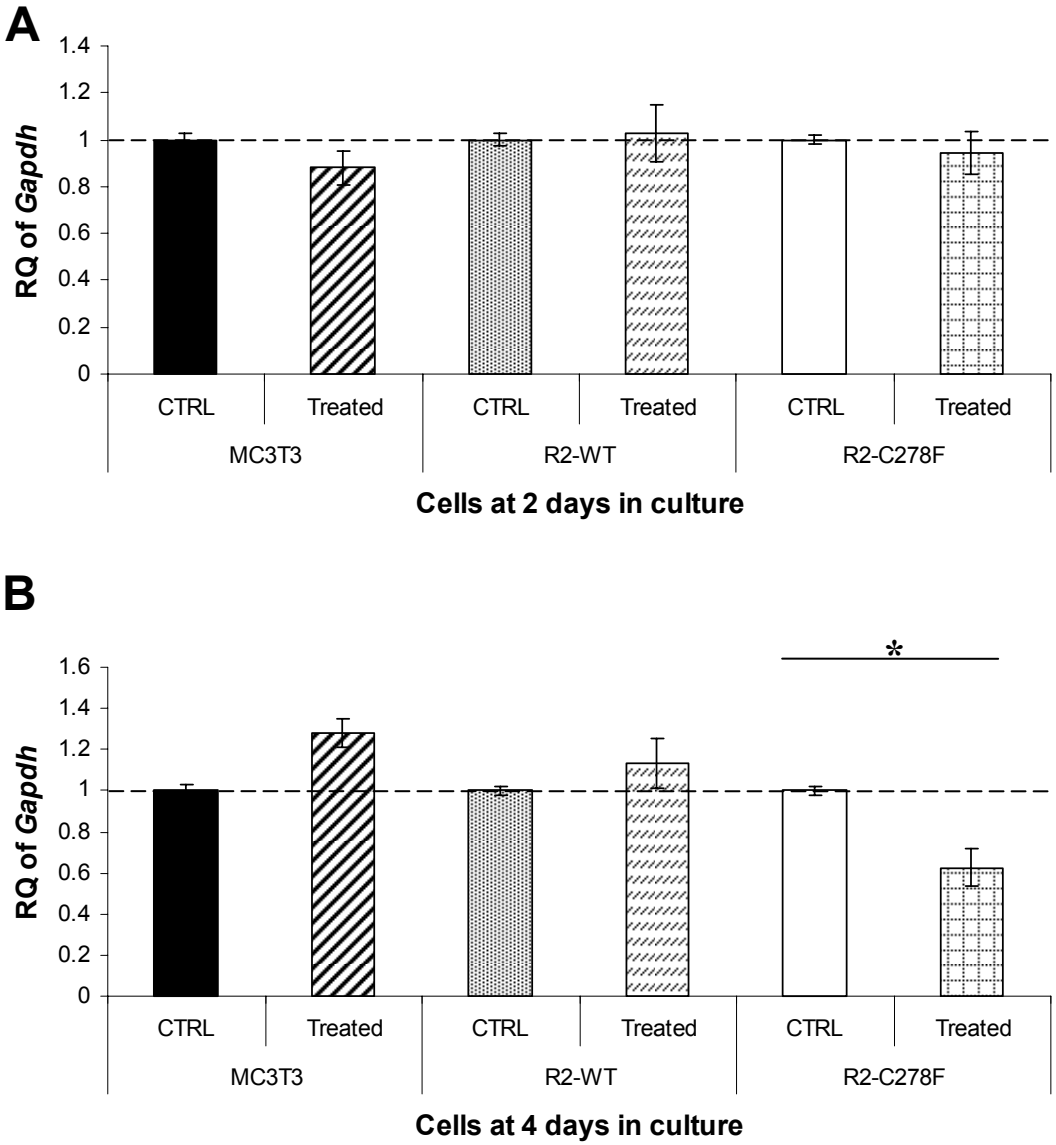

Figure 6.22 Real time PCR analysis of *Gapdh* expression in MC3T3, FGFR2-WT and C278F cells. Cells were treated with 10ng/ml of TGFbeta1 for 2 and 4 days in culture before relative quantification (RQ) of gene expression by real time PCR. The gene expression for each cell line was normalised to the untreated control. **A**: TGFBeta1 increases expression in R2-WT at 2 day. **B**: At 4 days, *Gapdh* expression does not significantly change with TGFBeta1 treatment in MC3T3 and R2-WT cells, however in R2-C278F cells TGFbeta1 significantly decreases *Gapdh* expression ($n = 3$, $*p < 0.05$).

6.3 Discussion

6.3.1 FGFR2-C278F downregulates *TGFbeta1* and *-3* expression

The main objective in this chapter is to identify whether FGFR2-C278F changes TGFbeta signalling. FGF2 treatment for 48 hours increases the steady state expression levels of *Tgfbeta1* in MC3T3-E1, rat and human osteosarcoma cells, (Noda and Vogel, 1989). In this study at preconfluence, *Tgfbeta1* and *-3* expressions are reduced in R2-C278F cells, compared to MC3T3 and R2-WT controls (Figure 6.1 A), confirming that Tgfbeta signalling is altered by FGFR2-C278F. Interestingly FGF2 and FGFR2-C278F have different transcriptional control of Tgfbeta signalling.

At 4 days in culture, in R2-WT cells, the level of *Tgfbeta3* was also lower than MC3T3, but higher than R2-C278F. This suggests that the FGF-TGFbeta3 interaction is abnormally altered in R2-C278F cells, but in a more profound manner than in R2-WT cells. TGFbeta3 expression is also reduced in osteoblasts following 24 hours of FGF2 treatment (Mathy et al., 2003). As the FGF2 and FGFR2-WT upregulate Tgfbeta3, it is possible that FGF2 signalling acts via FGFR2. *Tgfbeta2* expression is not altered by FGFR-C278F (Figure 6.1 B), indicating that Tgfbeta2 signalling may not be altered by FGFR2-C278F signalling at the gene expression level.

Smad2 was significantly higher in R2-WT cells compared to R2-C278F, but not significantly different to MC3T3 (Figure 6.2 B), indicating that it is unlikely that FGFR2-WT or FGFR2-C278F has a significant effect on *Smad2* expression levels.

Underexpression of TGFbeta1 and -3 proteins and the overexpression of TGFbeta2 protein found in the perisutural regions of fused sutures is associated with craniosynostosis in rabbits (Poisson et al., 2004). It is possible that the low *Tgfbeta1* and *-3* may precede the suture obliteration event and that *Tgfbeta2* expression, although not significant in R2-C278F cells, could be involved later during suture obliteration. In summary, FGFR2-C278F expression reduces *TGFbeta1* and *-3*, which may contribute to low R2-C278F proliferation as these ligands induce osteoblast proliferation (Opperman et al., 2000; Reyes-Botella et al., 2002).

6.3.2 TGFbeta signalling is lower in R2-C278F cells

TGFbetas are mitogens, particularly in less mature osteoblasts (Centrella et al., 1994). In 10 % serum conditions, inhibition of TβRI with 10 μM of SB431542 decreased cell growth in all three cell lines (Figure 6.17), confirming that TGFbeta positively regulates proliferation in this model. Interestingly a smaller dose of SB431542 (1 μM) reduced cell growth only in R2-C278F cells (Figure 6.17), indicating that TGFbeta signalling is reduced in these mutant cells compared to MC3T3 and R2-WT controls. In contrast to MC3T3 and R2-WT cells, increasing the dose of SB431542 did not further reduce R2-C278F cell growth, providing more evidence that TGFbeta1 signalling is lower in the mutant cells. In 1 % serum conditions, cell growth decreased in all cell lines with 1 μM SB431542 (Figure 6.18), suggesting that serum concentration positively affects the level of TGFbeta signalling, at least in MC3T3 and R2-WT cells. Increasing the dose to 20 μM produced a further decrease in cell growth in MC3T3 and R2-WT cells, but this was already maximal in R2-C278F cells as no further decrease was observed, indicating that in 1 % serum, the level of TGFbeta signalling is still the lowest in R2-C278F cells. It is possible that serum also positively affects the level of TGFbeta signalling in R2-C278F cells, but the current study does not provide enough evidence for this effect.

In summary, FGFR2-C278F reduces the level of TGFbeta signalling in R2-278F cells, regardless of serum conditions.

6.3.3 TGFbeta1 induced cell growth impaired in R2-C278F cells and dependent on Erk1/2

Increased proliferation in MC3T3 with TGFbeta1 treatment has been observed in subconfluent rat osteoblast cell cultures when treated with 0.15 to 15 ng/ml of TGFbeta1 (Centrella et al., 1987). Likewise, TGFbeta1 induces cell growth in MC3T3 and R2-WT cells in 10% serum conditions in this model. However there is no significant effect on R2-C278F cells, suggesting that the effect of TGFbeta1 is impaired by FGFR2-C278F.

In 1% serum conditions, TGFbeta1 treatment increases cell growth in all three cell lines (Figure 6.15), indicating that the effect of TGFbeta1 is modulated by serum conditions. Under these conditions, TGFbeta1 induced cell growth is dependent on Erk1/2 signalling in all three cell lines as TGFbeta1 could not rescue the inhibition of proliferation induced by Erk1/2 inhibitor U0126 (Figure 6.16).

6.3.4 TGFbeta1 does not alter MC3T3 cell morphology

In R2-C278F cell cultures, the proportion of fibroblastic cells is lower than in both MC3T3 and R2-WT cells, as shown in Chapter 4. In osteoblasts, TGFbeta1 may inhibit late stage differentiation (Alliston et al., 2001). If differentiation is inhibited by TGFbeta1, it is conceivable that the proportion of fibroblastic cells could be increased.

At preconfluence (2 days in culture), TGFbeta1 treatment does not change MC3T3, R2-WT nor R2-C278F cell morphology, indicating that it does not alter morphology in proliferating osteoblasts nor rescue R2-C278F cells from their differentiated phenotype.

Compared to MC3T3, TGFbeta1 treated R2-C278F cultures at confluence (4 days in culture) displayed a greater number of bright apoptotic figures, clearly indicating that the reduced *TGFbeta1* expression is not related to the R2-C278F cell phenotype normally found at this stage of culture. Interestingly it indicates that FGFR2-C278F signalling in R2-C278F cells increases sensitivity to TGFbeta1 induced apoptosis, as a small increase in the number of bright apoptotic figures, suggesting increased apoptosis in MC3T3 (Figure 6.6). It is possible that this may be an effect of TGFbeta1 to inhibit differentiation by inducing apoptosis at confluence. However in osteoblasts grown in DMEM with differentiation medium (L-ascorbic acid 2-phosphate), TGFbeta1 does not have any effect on osteoblast apoptosis (Cabiling et al., 2007), indicating that the above effects may also be depend on culture medium conditions. In R2-WT cells, TGFbeta1 induces an elongated morphology where cells are arranged in striae along the confluent monolayer (Figure 6.7), which may suggest that TGFbeta alters R2-WT differentiation with regard to morphology. This osteoblast elongation effect by TGFbeta1 has been observed in MC3T3 seeded onto bone slices, where it was suggested to be mediated by a MAPK p38 dependent mechanism (Karsdal et al., 2001). It is possible that the culture conditions in this study do not permit MC3T3 to change morphology in response to TGFbeta1, whereas in bone slices there is a permissive environment, perhaps mediated by FGFR2 in the surrounding tissue.

Overall, the reduced Tgfbeta1 does not affect preconfluent cell morphology, but greatly increases the number apoptotic figures in R2-C278F cells and alters R2-WT morphology, indicating a role in apoptosis and differentiation in these two cell lines.

6.3.5 Erk1/2 inhibition alters osteoblast morphology

In 1% FBS, TGFbeta1 did not alter the morphology of MC3T3 and R2-WT cells except for R2-C278F where it appeared to increase the number of cells with cuboidal morphology. This further indicates that in R2-C278F cells TGFbeta1 cannot restore osteoblast morphology to that of MC3T3. Erk1/2 inhibition using U0126 treatment resulted in a loss of fibroblastic cells in MC3T3, R2-WT and R2-C278F cultures, which may suggest that differentiation is increased. However Erk1/2 inhibition with Erk1DN suppresses differentiation in MC3T3 (Lai et al., 2001), and the morphology of MC3T3 cells expressing Erk1DN also appears similar to the U0126 treated cells of this study. Another report has shown that Erk1/2 has been reported positively affect differentiation (Raucci et al., 2008). This may indicate that the cuboidal morphology resulting from Erk1/2 inhibition with U0126 treatment causes a decrease in differentiation. To confirm this interpretation, differentiation markers should be analysed in cells with U0126 treatment.

Following U0126 treatment MC3T3 (Figure 6.9) morphology was similar to U0126 treated R2-WT (Figure 6.10). The morphology of U0126 treated cells was similar to the TGFbeta1 and U0126 combined treatment in all three cell lines, suggesting that TGFbeta1 does not compensate for the morphological changes by U0126.

6.3.6 FGFR2-C278F impairs upregulation of *Fgf18* by TGFbeta1 at confluence

This study shows that Fgf18 expression is affected by exogenous TGFbeta1, but not Fgf1 and -2 at preconfluence (Figure 6.12). It is likely that the effect of exogenous TGFbeta1 at preconfluence on *Fgf18* expression is mediated by FGFR2-WT as TGFbeta1 induced *Fgf18* was only observed in MC3T3 and R2-C278F cells at 2 days (Figure 6.13). In metatarsal bone, *Fgf18* expression also increases with TGFbeta1 treatment (Mukherjee et al., 2005).

Interestingly in R2-WT cells *Fgf1* expression is significantly higher than in MC3T3 and R2-C278F cells, suggesting that FGFR2-WT mediates Fgf1 expression levels, but this effect is not associated with the R2-C278F cell phenotype.

At confluence, TGFbeta1 still induces *Fgf18* expression in MC3T3, but not in R2-WT and R2-C278F cells, suggesting that at confluence both FGFR2-WT and FGFR2-C278F expressions block the effects of TGFbeta1 on *Fgf18* expression.

6.3.7 FGFR2-C278F impairs differentiation marker responses to TGFbeta1

TGFbeta1 treatment significantly increases *Runx2* expression all 3 cell lines at preconfluence (Figure 6.19 A), which suggests that it may enhance early differentiation. *Runx2* expression has also been reported to increase as immature osteoblasts differentiate and mature (Aubin, 2001). TGFBeta1 induces *Runx2* at confluence in MC3T3 and R2-WT cells; an effect also observed in mature osteoblasts (Viereck et al., 2002). However *Runx2* is decreased in R2-C278F cells at confluence (Figure 6.19 B). TGFbeta1 can decrease *Runx2* expression in rat osteosarcoma cells and also downregulate *Oc* (Alliston et al., 2001). R2-C278F cells may respond like osteosarcoma cells, however to confirm this *Oc* expression should be measured in R2-C278F cells following TGFbeta1 treatment. The results would indicate whether TGFbeta1 can affect late stage differentiation in R2-C278F cells.

At preconfluence TGFbeta1 treatment in MC3T3 cells decreases *Opn* expression, which may suggest that differentiation is induced. *Opn* expression also decreases after 48 hours of TGFbeta1 treatment in MC3T3 in differentiation medium (beta-glycerophosphate and ascorbic acid) (Pungchanchaikul, 2008). This was not expected as TGFbeta1 has been reported to increase *Opn* expression in osteoblasts (Cabiling et al., 2007; Noda, 1989). FGFR2-WT may interact with TGFbeta as TGFbeta1 is induced *Opn* expression in R2-WT cells (Figure 6.20 A). FGFR2-C278F appears to block any change in *Opn* expression following TGFbeta1 treatment, suggesting that FGF and TGFbeta signalling interact to control *Opn* expression.

At confluence *Opn* expression increases in MC3T3 and R2-WT cells after TGFbeta1 treatment, which is consistent with reports of increased *Opn* expression following TGFbeta1 treatment in mature osteoblasts (Noda et al., 1988; Sodek et al., 1995). FGFR2-C278F impairs TGFbeta1 induced *Opn* expression (Figure 6.20 B). The changes in *Opn* expression do not correlate with the changes in *Runx2* expression, which may reflect the findings that TGFbeta may affect *Opn* expression independently of *Runx2* (Bae et al., 2007).

Together at preconfluence, the increased *Runx2* and decreased *Opn* expression in MC3T3 induced by TGFbeta1 suggests that differentiation is increased following TGFbeta1 treatment. The increase in both *Runx2* and *Opn* in R2-WT suggests that early differentiation is increased and late differentiation is inhibited. In R2-C278F cells, the increase in *Runx2* and no change to *Opn* expression suggests that early differentiation is increased. At confluence in both MC3T3 and R2-WT, when both *Runx2* and *Opn* are increased, this suggests that late stage differentiation is inhibited. The decrease in *Runx2* and no change in *Opn* in R2-C278F cells

suggest that differentiation is affected, but requires an analysis of *Oc* expression to clarify whether differentiation is enhanced or inhibited.

6.3.8 FGFR2-C278F impairs TGFbeta1 induced *Smad2* expression at confluence

TGFbeta1 did not significantly change *Smad2* expression in any of the three cell lines at preconfluence, which suggests that TGFbeta1 induced proliferation is not associated with alteration of *Smad2* expression. At confluence, TGFbeta1 treatment induced *Smad2* expression in both MC3T3 and R2-WT cells, whereas in R2-C278F cells its expression decreased (Figure 6.21 B). This suggests that TGFbeta1 plays a role in controlling *Smad2* expression in mature osteoblasts, which may feed back into the level of TGFbeta signalling. It is possible that at confluence, Smad2 may be associated with osteoblast differentiation occurring at this stage in culture and that FGFR2-C278F may act downstream of TGFbeta1 induced Smad2 expression. In mature osteoblasts, overexpression of *Smad2* decreases *Runx2* expression and *Oc* expression (Li et al., 1998). This pattern does not correlate to the increased *Smad2* and *Runx2* found in MC3T3 and R2-WT cells in this model, which suggests that TGFbeta1 does not control *Runx2* expression via *Smad2* expression *per se*.

6.3.9 TGFbeta1 downregulates *Gapdh* expression in R2-C278F cells at confluence

TGFbeta1 treatment does not significantly alter *Gapdh* expression in all three cell lines at preconfluence, suggesting that *Gapdh* expression is not involved in TGFbeta1-induced proliferation and effects on differentiation R2-C278F cells (Figure 6.22 A). FGFR2-C278F interacts with TGFbeta by causing R2-C278F cells to reduce *Gapdh* expression in response to TGFbeta1 at confluence (Figure 6.22), which may be associated to an increase of bright apoptotic figures at confluence observed from the previous morphological studies under the same experimental conditionss. As suggested in Chapter 4, a caspase independent cell death (CICD) mechanism may be responsible for these observations, which should be further investigated.

6.4 Conclusions

This study confirms that Tgfbeta signalling is altered in R2-C278F cells and has revealed a number of interactions with FGFR2-C278F and TGFbeta1 signalling. Firstly, FGFR2-C278F reduces the level of TGFbeta1 signalling as shown by inhibition of TGFbeta with SB431542. It also decreases *TGFbeta1* and *-3* gene expression. FGFR2-C278F blocks TGFbeta1 induced osteoblast proliferation in R2-C278F cells 10% serum conditions. At confluence, FGFR2-C278F expression may alter the downstream signalling of TGFbeta1 by downregulation *Smad2* expression, instead the normal upregulation of *Smad2* observed in MC3T3 and R2-WT cells. Rescue of R2-C278F cell growth with TGFbeta1 treatment is limited to 1% serum conditions and this is dependent on Erk1/2 signalling.

The FGFR2-C278F abnormally interacts with exogenous TGFbeta1 to alter Fgf18 signalling, as it inhibits TGFbeta1 induced *Fgf18* expression at confluence. FGFR2-C278F impairs the effect of TGFbeta1 on osteoblast differentiation, particularly at confluence by reversing the normal upregulation of *Runx2* expression observed in MC3T3 and R2-WT cells and blocking TGFbeta1 induced *Opn* expression. FGFR2-C278F interacts with exogenous TGFbeta1 to lower *Gapdh* expression, which may be associated with increased apoptosis as suggested by morphological observations of TGFbeta1 treated R2-C278F cells at confluence.

In summary, FGFR2-C278F alters FGF-TGFbeta interactions in MC3T3 by both lowering the level of TGFbeta signalling and impairing its downstream cellular responses. It also interferes with the effect of TGFbeta1 on cell differentiation.

Chapter 7 Final Discussion

The aim of this thesis was to determine how FGF signalling was impaired in craniosynostotic osteoblasts and investigate whether TGFbeta signalling was also affected, using an *in-vitro* model of MC3T3-E1 cells, which expressed human FGFR2-C278F. In this model, a number of alterations were found in both FGF signalling, and interactions with TGFbeta were successfully identified. Here I discuss in detail the relationships between these alterations and the craniosynostotic R2-C278F cell phenotype. I will also propose mechanisms to link FGF and TGFbeta signalling to proliferation phenotype of R2-C278F cells to be tested in further studies into Ligand Independent Constitutively Active (LICA) FGFR2.

7.1 R2-C278F cells show lower proliferation and increased differentiation and apoptosis

R2-C278F cells have a reduced proliferation rate, a higher level of differentiation and an increased level of apoptosis (Chapter 4). This phenotype is similar to that reported in a number of human models (Marie et al., 2005), suggesting that results from this model may reflect the defects and mechanisms that exist in human osteoblasts of patients with FGFR2-related craniosynostosis. It is likely that the changes to proliferation and differentiation are the main factors influencing the craniosynostotic phenotype, as the changes observed in apoptosis in this thesis are relatively small. It may be hypothesised from this data and the literature concerning LICA FGFR2 craniosynostosis, that embryonic osteoblast proliferation is increased and differentiation decreased until birth. Afterwards, osteoblast proliferation decreases and differentiation increases (Table 7.1).

Table 7.1 Hypothesised effects of LICA FGFR2 mutations on osteoblast behaviour

Stage	Proliferation	Differentiation	Apoptosis
Embryonic	Increase[1]	Decrease[2]	Increase[3]
Postnatal	Decrease[4]	Increase[5]	Increase[6]

References:

1: Ratisoontorn et al., 2003 and Eswarakumar et al., 2004

2: Ratisoontorn et al., 2003

3: Lemonnier et al., 2001, Mansukhani et al., 2000 and Marie et al., 2005

4: This study and Fragale et al., 1999

5,6: This study and Marie et al., 2005

7.2 This model *in-vitro* can be compared to bone fronts *in-vivo*

Fgf2 is normally present in bone and adjacent to the site of suture fusion, but not in bone fronts of presumptive and patent sutures (Opperman, 2000). Other tissues, such as dura express *Fgf2* (Li et al., 2007) and *Fgf1* embryonically (Ogle et al., 2004), suggesting that bone fronts receive Fgf1 and -2 from their neighbouring tissues. The low level of *Fgf2* expression in MC3T3, R2-C278F and R2-WT cultures indicates that they may mimic osteogenic cells of the bone front before suture fusion. As the expression levels of *Fgf1* and *-2* were normal in R2-C278F cells compared to controls; these ligands did not appear to contribute to the mutated phenotype, although it did not exclude a signalling role for the two ligands *in-vivo*.

Proliferation of osteoprogenitors is essential for bone growth (Lana-Elola et al., 2007), which occurs adjacent to the bone front. The decreased proliferation in R2-C278F cells and in other craniosynostotic osteoblasts reviewed postnatally (Table 7.1) may explain why bone repair and regrowth is limited in LICA FGFR2 mutated osteoblasts, following the craniofacial surgery for craniosynostosis.

7.3 FGFR signalling is decreased in R2-C278F cells

Work in this thesis has provided evidence that Fgf signalling was downregulated in R2-C278F cells, as shown by the data regarding cell proliferation before and after inhibition of Fgfr signalling. The key point to note is that Fgfr2 positively regulates osteoblast proliferation (Eswarakumar et al., 2002; Iseki et al., 1999; Ratisoontorn et al., 2003). Fgfr inhibition in R2-C278F produced the greatest reduction in cell growth among the three cell lines (MC3T3, R2-WT and R2-C278F), suggesting that Fgfr signalling was reduced in the mutant cells.

It is clear that although FGFR2-C278F is a LICA-FGFR2, constitutive activation does not result in an increased osteoblast growth. Of the four FGFR isoforms, only FGFR2IIIc is reported as essential for inducing osteoblast proliferation (Chapter 1, Section 1.3.3). Together this data suggests that there is a decrease in Fgfr2 signalling in R2-C278F cells, resulting in reduced cell proliferation (Figure 7.1).

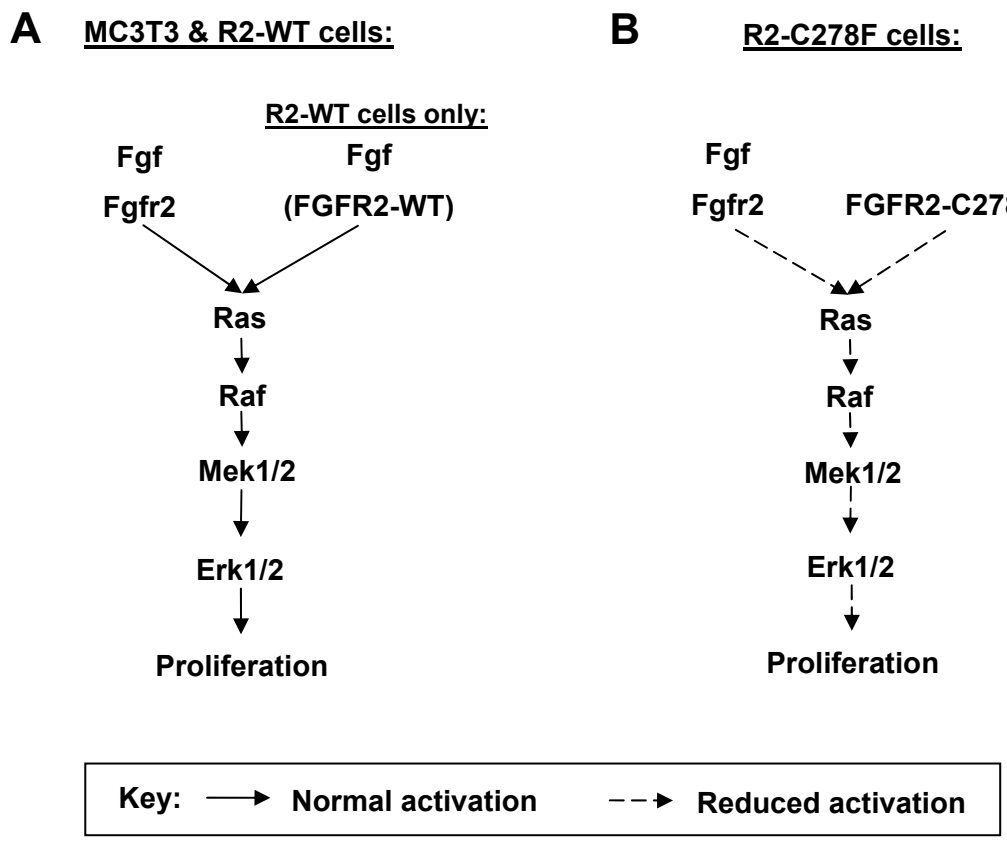

Figure 7.1 FGFR2 signalling and proliferation defects in R2-C278F cells

A: Fgfr2-Erk1/2 signalling pathway resulting in proliferation. **B:** FGFR2-C278F reduces the level of Fgfr2-Erk1/2 signalling, which results in a reduction of proliferation in R2-C278F cells.

7.4 Fgf18 may be involved in R2-C278F cell differentiation

Although Fgf18 may induce proliferation in osteoblasts (Ohbayashi et al., 2002), in R2-C278F cells appears to correlate to enhanced differentiation rather than proliferation, because the expression in R2-C278F cells is similar to MC3T3 at preconfluence, but higher than MC3T3 at confluence (Chapter 5). Furthermore, studies in our laboratory have shown that the addition of exogenous Fgf18 does not significantly increase cell growth in MC3T3, R2-WT or R2-C278F cells in 10% serum conditions (unpublished data). Functionally, Fgf18 treatment may influence osteoblast differentiation by increasing the gene expression of differentiation markers *Osteopontin* (*Opn*) and *Osteocalcin* (*Oc*) (Liu et al., 2002). A similar relationship between Fgf18 and Oc is found in R2-WT and R2-C278F cells, as *Fgf18* and *Oc* expression was raised compared to MC3T3 at confluence (Chapters 4 and 5). These findings indicate a positive association between *Fgf18* and *Oc* expression in R2-WT and R2-C278F cells. This relationship is suggested in Figure 7.2, where Fgf18 is speculated to increase osteoblast differentiation in

both R2-WT and R2-C278F cells. Interestingly the expression of *Oc* is greater in R2-WT cells than in both MC3T3 and R2-C278F cells at confluence. It is possible that *Oc* expression may also be linked to an increased *Fgf1* expression found in R2-WT cells compared to MC3T3 and R2-C278F cells (Chapter 6), as Fgf1 also enhances *Oc* expression in osteoblasts (Ignelzi, Jr. et al., 2003).

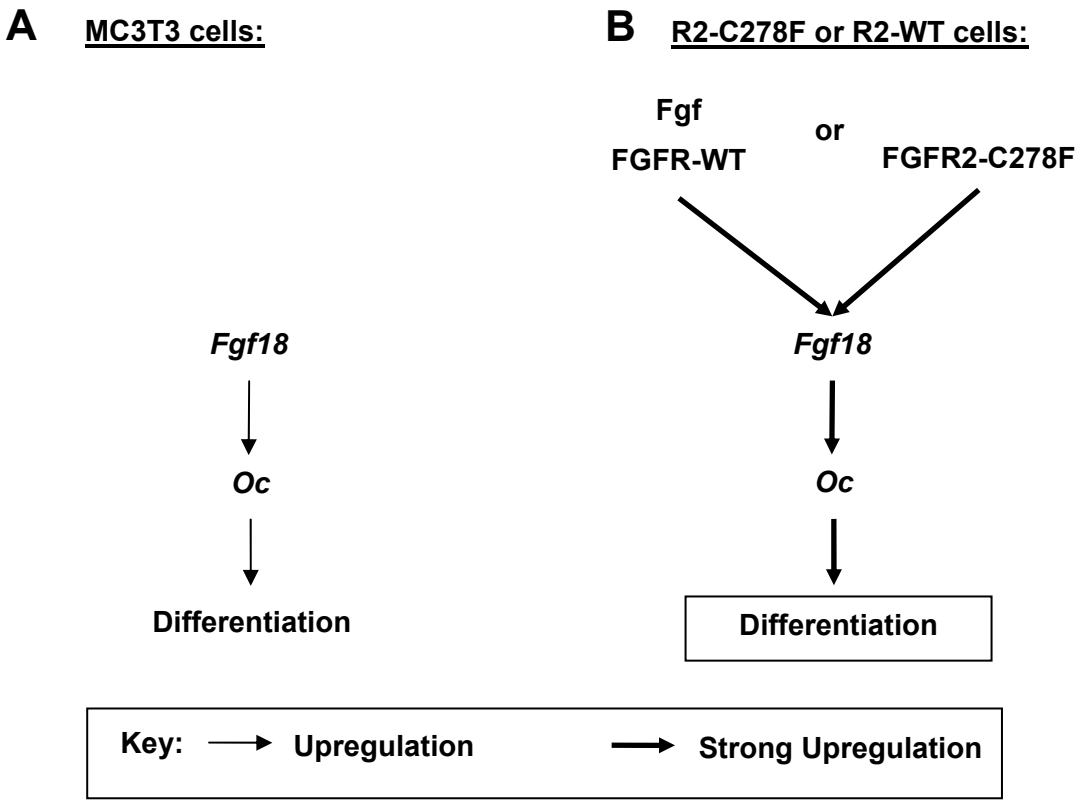

Figure 7.2 Hypothesised effects of FGFR2-C278F on *Fgf18* and differentiation

A: Fgf18 induces *Oc* expression by increasing osteoblast differentiation (Ohbayashi et al., 2002). **B:** FGFR2-C278F expression results in increased expression of *Fgf18*, which is known to upregulate Oc expression and hence enhance differentiation in R2-C278F cells.

In contrast to *Oc* at confluence, there is no clear relationship between *Fgf18* and *Opn* expression in R2-WT and R2-C278F cells. *Opn* expression was not higher in R2-WT compared to MC3T3 cells, whereas in R2-C278F cells *Opn* was actually lower than in MC3T3 and R2-WT cells. Fgf18 therefore is not the main factor modulating *Opn* expression in this model. Although *Oc* expression is increased in R2-WT and R2-C278F cells, the differences in *Opn* expression indicate that the two cell lines are not at the same stage of differentiation.

7.5 Changes in Erk1/2 may underlie defective FGFR signalling in R2-C278F cells

Two important changes in Erk1/2 signalling have been identified: an increased Erk1/Erk2 ratio and a decreased level of Erk1/2 signalling as shown in Chapter 5, which were suggested to cause impaired R2-C278F cell proliferation (Figure 7.3).

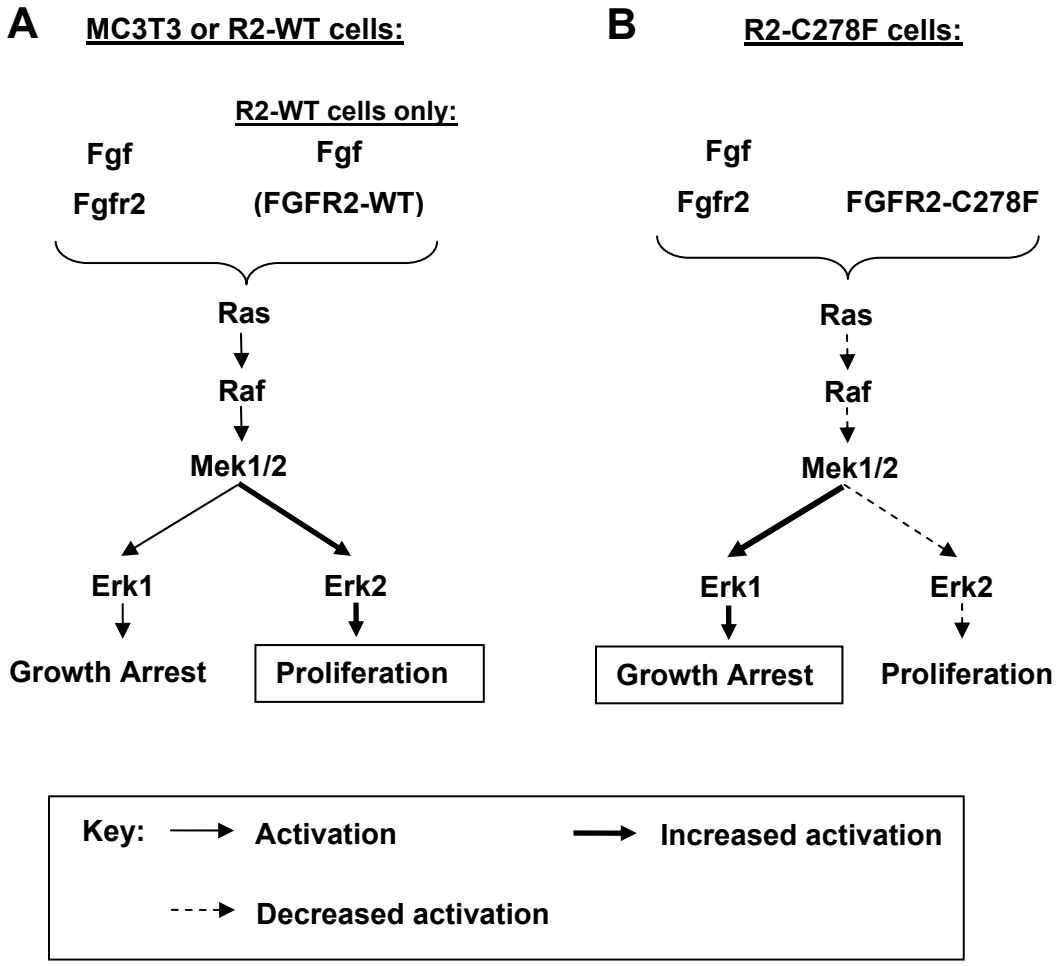

Figure 7.3 Proposed mechanism leading to reduced proliferation signalling in R2-C278F cells
A: FGFR2 increases osteoblast proliferation via activation of Erk2. **B:** FGFR2 signalling is reduced and Erk1/2 signalling is directed towards the Erk1 part of the pathway by increasing the Erk1/Erk2 ratio, reducing the level of proliferation in R2-C278F cells.

As Erk1 and Erk2 compete for activation by MEK1/2, the increased Erk1/Erk2 ratio may reduce the activation of Erk2, the key Erk isoform mediating growth factor induced proliferation (Fremin et al., 2007; Vantaggiato et al., 2006). The level of Erk1/2 signalling is essential for osteoblast proliferation and when reduced, it leads to a decrease in proliferation (Lai et al., 2001).

7.6 Changes in Erk1/Erk2 ratio correlate with cell cycle changes in R2-C278F cells

In the cell cycle, Erk1/2 facilitates G1 transition to S phase (Wu et al., 2006), and from G2/M to G0/G1 phase (Roberts et al., 2006). In NIH3T3 fibroblasts, Erk1 and Erk2 are strongly phosphorylated in G1 phase, but only Erk2 is strongly phosphorylated in G2 and M Phase (Suzuki et al., 2002b). These reports suggest that both Erk1 and Erk2 facilitate G1 to S phase transition, but Erk2 predominantly facilitates transition from G2/M to G0/G1 phase. The relative expression of Erk2 has been shown to decrease compared to Erk1 in R2-C278F cells, which correlates with a higher proportion of cells in G2 phase. It is possible that the relatively low Erk2 activation results in slower progression of cells from the G2 phase into G1.

7.7 Pkc signalling is altered in R2-C278F cells

Pkc signalling is altered in R2-C278F cells compared to MC3T3 and R2-WT cells, but the level of signalling and the relationship to the R2-C278F cell phenotype is unclear as the effects of Pkc stimulation differ depending on the serum concentration. For example, I have shown that Pkc activation with PMA in 10% serum decreases cell growth in R2-C278F cells, but not in control cells. In 1% serum, cell growth increases in R2-C278F, does not change in R2-WT and decreases in MC3T3 cells. Pkc is known to affect proliferation and differentiation (Sabatini et al., 1996; Boguslawski et al., 2000), therefore the altered Pkc signalling may play a role in both proliferation and differentiation in R2-C278F cells. Aperts FGFR mutations constitutively activate PKC-α, which in turn increases apoptosis (Lemonnier et al., 2001). It is possible that Pkc also induces apoptosis in R2-C278F cells, however the same changes in Pkc activation should be confirmed, as FGFR signalling by loss of ligand specificity in Aperts is not equivalent to constitutively active FGFR2.

7.8 FGF-TGFbeta interactions and their relevance to R2-C278F cell phenotype

As concluded in Chapter 6, FGFR2-C278F altered FGF-TGFbeta interactions in MC3T3 by lowering the level of TGFbeta signalling and impairing its downstream cellular responses. It also suggested that overstimulation by FGF2 could not be directly compared to LICA FGFR signalling due to the differences in *Tgfbeta1* expression, which was upregulated by FGF2 (Noda and Vogel, 1989) and down regulated by FGFR2-C278F (Chapter 6). Although similarities exist in that FGF2 may induce craniosynostosis (Crane et al., 2005), the mechanisms underlying the craniosynostoses are likely to differ.

7.8.1 Proliferation is regulated by FGF-TGFbeta signalling interactions through a convergent pathway

TGFbeta1 may induce proliferation in immature osteoblasts in serum, without differentiation medium (Bosetti et al., 2007; Centrella et al., 1994; Chung et al., 1999; Janssens et al., 2005; Reyes-Botella et al., 2002). As similar conditions have been used in this thesis, the low *TGFbeta1* expression found in R2-C278F cells may reflect a reduction in TGFbeta-induced proliferation.

The combination of reduced FGF and TGFbeta signalling found in R2-C278F cells may explain the low proliferation observed in Chapter 4. Osteoblasts *in-vivo* are able to receive TGFbeta1 released from surrounding bone tissue (Janssens et al., 2005), whereas osteoblasts *in-vitro* rely on endogenous TGFbeta production alone. However exogenous TGFbeta1 could not stimulate cell growth in R2-C278F cells; cell growth was only inducible in MC3T3 and R2-WT cells. This suggests that R2-C278F osteoblasts *in-vivo* would not be able to respond correctly to signals from bone and other tissues such as the dura in which TGFbeta is strongly expressed (Mehrara et al., 1999). Our laboratory has also experimented on the three cell lines using exogenous Fgf2 and -18, which in 10% serum conditions did not have any significant effects on cell growth, but in 1% led to a small increase in cell growth (data unpublished). This suggests that at 10 % serum conditions, that Fgf signalling may be maximally stimulated with respect to the proliferative effects.

As TGFbeta induced signalling with regard to proliferation is mediated by Erk1/2 (Ghayor et al., 2005), the abrogation of TGFbeta1 induced proliferation in R2-C278F cells in 10% serum

may be related to the increased Erk1/Erk2 ratio, which may potentially limit proliferative responses to growth factors. Interestingly, at 1% serum conditions TGFbeta1 increased cell growth in R2-C278F cells (Chapter 6). FCS-induced proliferation is dependent on Erk1/2 signalling (Suzuki et al., 2002a), suggesting that serum induces proliferation by activating the Erk1/2 pathway. In 1% serum conditions, the small amount of serum may reduce the level of Erk1/2 activation, resulting in a lower proliferation. When Erk2 activation was severely limited, Erk1 has been shown to increase proliferation in osteoblasts (Lefloch et al., 2008). It is likely that in 1 % serum Erk2 is also limited; therefore Erk1 may stimulate proliferation, which would be consistent with increased cell growth in R2-C278F cells, following Erk1/2 stimulation by TGFbeta. An alternative explanation could be that under these conditions, even a small amount of Erk2 activation could result in R2-C278F reaching their maximal proliferation rate.

7.8.2 Decreased FGF and TGFbeta signalling may increase differentiation

FGFR2 is required for proliferation, but it is not necessary for osteoblast differentiation (Yu et al., 2003), suggesting that increased differentiation in R2-C278F cells may not be a direct effect of the FGFR2-C278F signalling. R2-C278F cells were suggested to be more differentiated, based on cuboidal cell morphology at preconfluence, which was supported by observations that Col1 was increased compared to both controls (Santos-Ruiz et al., 2007). Low *Opn* expression and high *Oc* expression at confluence further suggested that R2-C278F cells were more differentiated than MC3T3 cells. It appears that the expression of FGFR2-C278F blocks TGFbeta1-induced *Opn* expression that is normally observed in MC3T3 (Chapter 6), indicating that FGF signalling mediates the effect of TGFbeta on osteoblast differentiation.

Downstream of FGF and TGFbeta, Erk1/2 activation increases Opn protein expression in MC3T3 (Kono et al., 2006). *Opn* expression is also increased by inorganic phosphate via Erk1/2, Pkc and proteosome activity (Beck, Jr. and Knecht, 2003). Assuming that TGFbeta1 utilises the same downstream pathways it is possible that the changes to Erk1/2 or Pkc signalling may facilitate the inhibition of TGFbeta1-induced *Opn* by FGFR2-C278F (Section 7.2.1). The relationship was hypothesised with TGFbeta and Erk1/2 (Figure 7.4), but not for Pkc as it has not yet been determined whether Pkc signalling is increased or decreased.

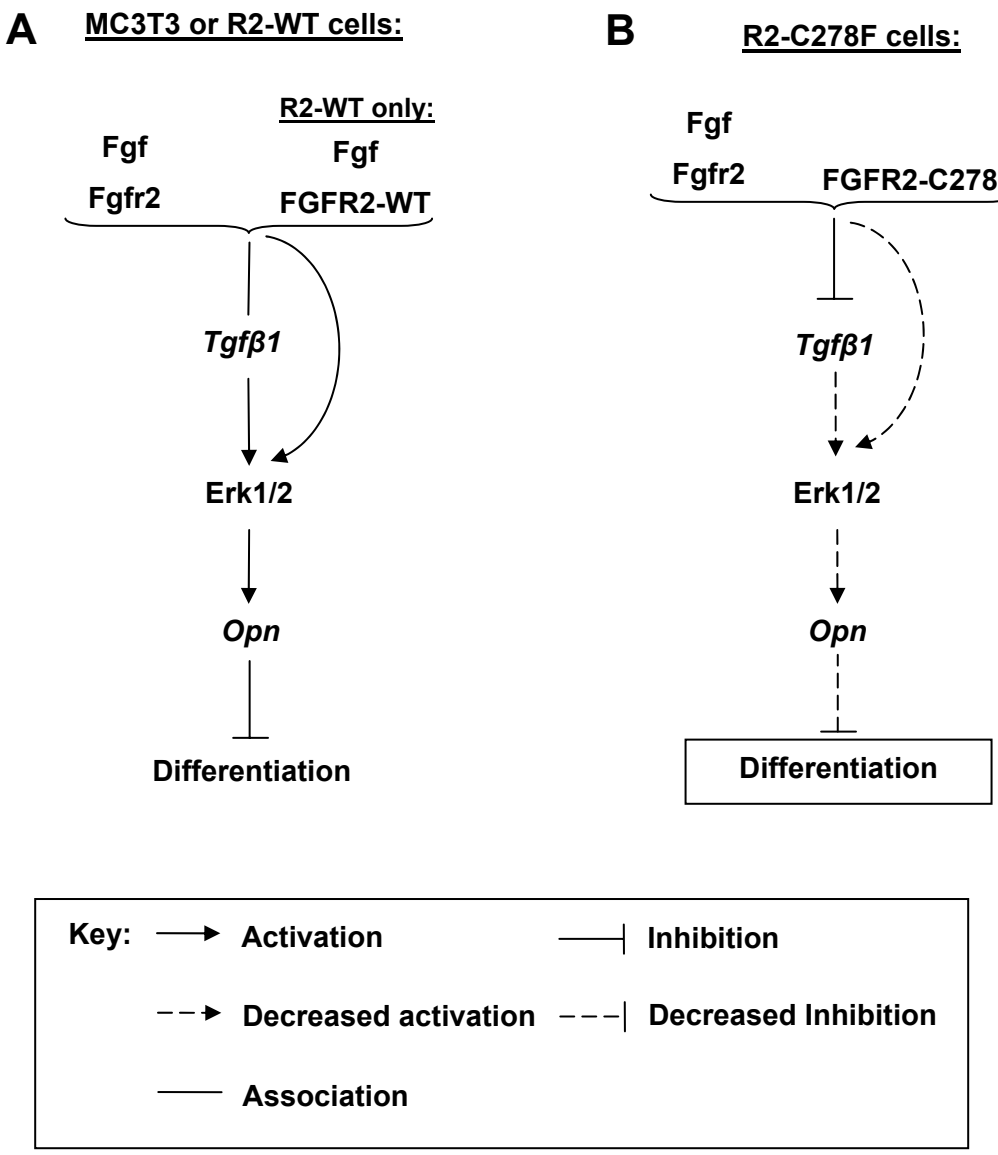

Figure 7.4 Hypothesised connection between FGF-TGFbeta-Erk1/2 signalling and differentiation
A: *TGFbeta1* is present in cells with normal FGFR2 and FGFR2-WT signalling, which via Erk1/2 activation induces *Opn* expression and inhibits differentiation. **B:** Downregulation of TGFbeta1 by FGFR2-C278F and decreased FGFR signalling may decrease Erk1/2 activation, resulting in lower *Opn* expression and increased differentiation.

7.8.3 FGF-TGFbeta-Smad and differentiation

As mentioned above, the mutation in FGFR may alter the downstream pathways of Erk1/2 and Pkc, which are shared with TGFbeta signalling. Furthermore, the mutation also affects TGFbeta signalling via Smad. In Chapter 6, TGFbeta1 treatment in R2-C278F cells decreased *Smad2* expression in R2-C278F cells, but increased *Smad2* in both MC3T3 and R2-WT cells. As Smad2 interacts with Runx2 (Selvamurugan et al., 2004), R2-C278F cell differentiation may have been affected. It was indicated In Chapter 6 that FGFR2-C278F did not affect *Smad1* expression. An intial analysis of *Smad1* expression after TGFbeta1 treatment at confluence showed that *Smad1* expression was induced in MC3T3 and R2-WT cells, but had no effect on R2-C278F cells (Figure 8.6). As Smad1 may increase *Opn* expression (Yang et al., 2000), the defect in TGFbeta-induced *Smad1* may have prevented TGFbeta1-induced Opn expression in R2-C278F cells (Chapter 6). However this does not explain the reduced *Opn* expression in R2-C278F cells at confluence (Chapter 4), as there was no difference in *Smad1* expression between all three cell lines (Chapter 6). It is possible that the reduced level of TGFbeta signalling (indicated in Chapter 6) may lower Smad1 activation by TGFbeta, which would limit Smad1 induced *Opn* expression. FGFR2-C278F may therefore have a role in preventing TGFbeta from inhibiting late stage differentiation in R2-C278F cells by lowering Smad1 activation via reducing TGFbeta signalling. Assessment of the Smad1 activation level at confluence by TGFbeta stimulation is required to confirm this interpretation.

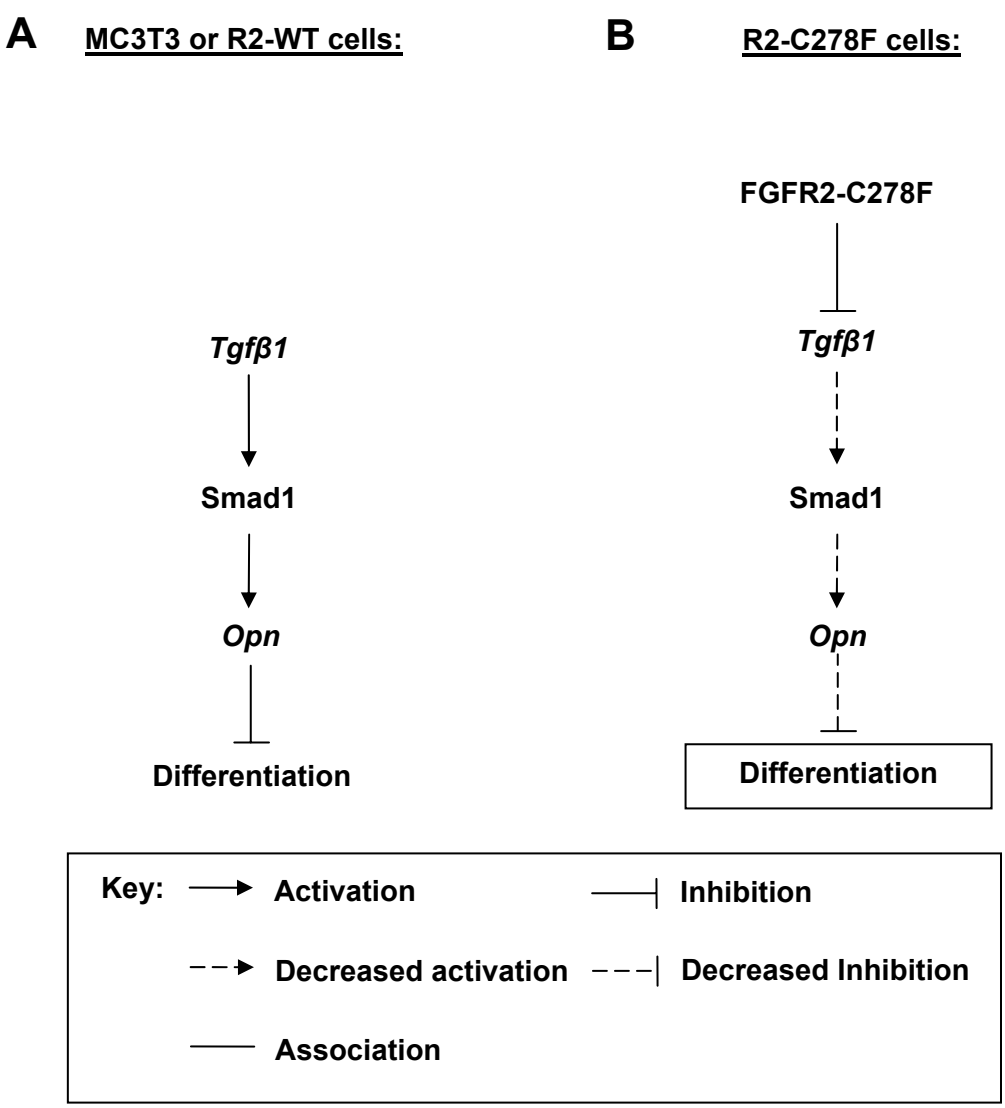

Figure 7.5 Hypothesised pathway of FGFR2-C278F-TGFbeta-Smad1 and differentiation
A: *TGFbeta1* activates Smad1 (Miyazawa et al., 2002). Smad1 induces *Opn* expression and inhibits differentiation (Yang et al., 2000). **B:** Reduced expression of TGFbeta1 in R2-C278F cells may result in decreased Smad1 activation, and consequently lower *Opn* expression.

7.8.4 Metabolism and apoptosis

The work in this thesis has suggested that increased apoptosis in R2-C278F cells may be functionally related to a low *Gapdh* expression (Chapter 4) by a caspase independent cell death (CICD) mechanism. Low *Gapdh* levels may also affect metabolism in R2-C278F cells, as Gapdh activity is required to complete the glycolysis pathway and generate ATP. The putative

relationship between FGF, *Gapdh* and cell survival is shown in Figure 7.6. The addition of TGFbeta1 to R2-C278F cells (Chapter 6) greatly increased the number of bright apoptotic figures and decreased *Gapdh* at confluence compared to both MC3T3 and R2-WT cells, suggesting that FGFR2-C278F may play a positive role with TGFbeta in mature osteoblast apoptosis. However the lack of TGFbeta signalling in R2-C278F cells (Chapter 6) did not result in less apoptosis (Chapter 4), which indicated that apoptosis was secondary to the change in *Gapdh* expression.

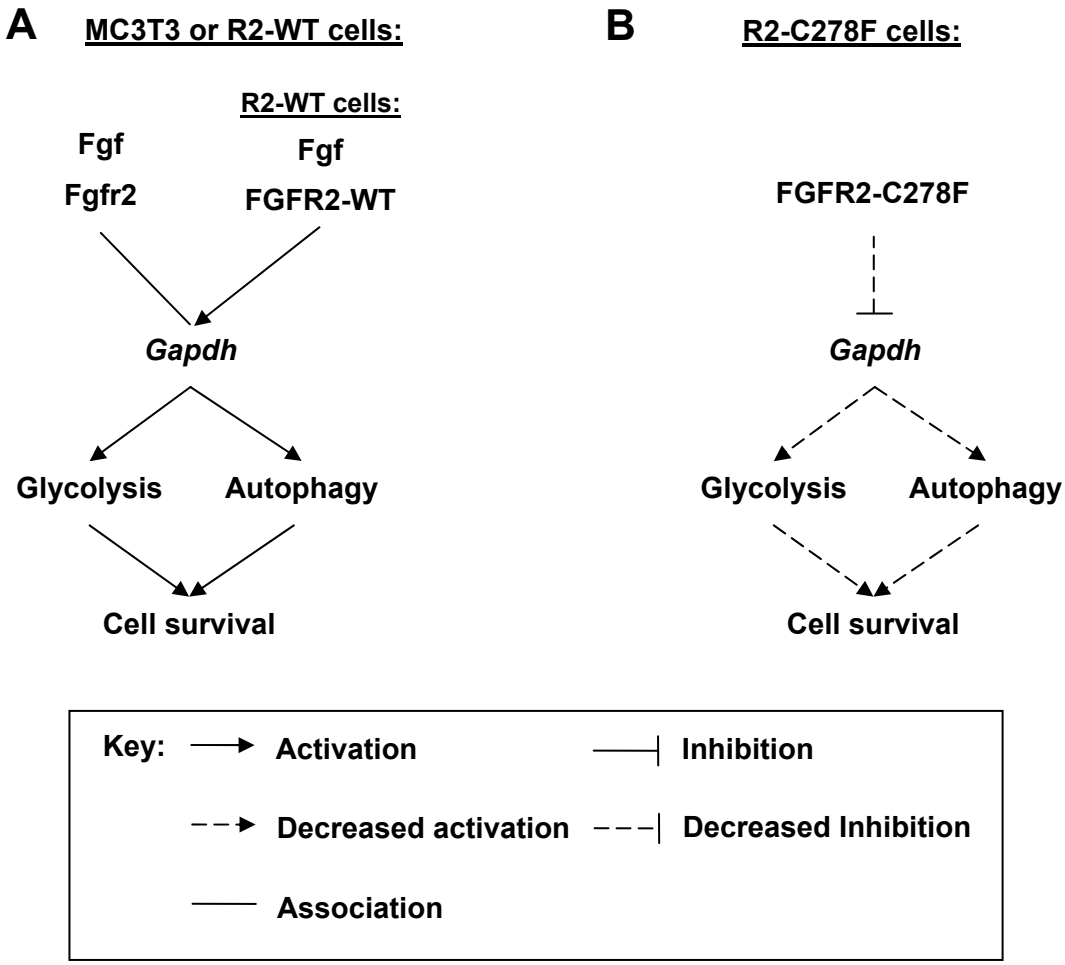

Figure 7.6 Hypothesised changes leading to increased apoptosis in R2-C278F cells

A: Gapdh protects cells from CICD dependent apotosis by increasing glycolysis and autophagy (Collell 2007). **B:** Loss of Gapdh caused by FGFR2-C278F cells may reduce the level of glycolysis and autophagy, leading to decreased cell survival.

7.9 Conclusions

The results in this thesis support a working hypothesis that FGFR-C278F increases osteoblast proliferation and decreases differentiation during embryonic development, whereas postnatally osteoblast proliferation is decreased and differentiation increased, which concurs with the current literature findings. Regarding apoptosis, the expression of FGFR2-C278F lowers the level of *Gapdh*, which may limit glycolysis and contribute metabolic requirements of R2-C278F cells. The lack of *Gapdh* may be associated with increased apoptosis via caspase independent cell death (CICD).

In the postnatal stage model used in this thesis, ligand independent constitutively active receptor mutations such as FGFR2-C278F are thought to result in a gain-of-function in signalling; however the phenotype of osteoblasts does not reflect the direct consequence of increased FGFR2 signalling. Instead, R2-C278F cells show decreased proliferation, a result that implies a negative feedback on FGFR2 signalling in craniosynostotic osteoblasts.

FGFR2-C278F alters FGF and TGFbeta signalling in R2-C278F cells. Three mechanisms have been suggested to impair cell proliferation. The first is a decrease in the overall level of Fgfr / FGFR2 signalling. The second is a decrease in the level of TGFbeta signalling. The third is an increased Erk1/Erk2 ratio, diverting the downstream signalling away from Erk2. The combined changes are shown in the pathway, presented in Figure 7.7. In addition to lowering the level of TGFbeta signalling, FGFR2-C278F expression also appears to block the proliferative response of osteoblasts following TGFbeta1 treatment.

Differentiation is increased in R2-C278F cells and changes in Fgf and Tgfbeta signalling may be involved, however the exact role is not as clear as with proliferation. It is possible that the increased differentiation in R2-C278F cells is associated with decreased Erk1/2 signalling and increased Fgf18 signalling. Mechanisms of enhanced differentiation may include Fgf18 induction of *Oc* expression, and impairment *Opn* expression following low Erk1/2 activation. It is also possible that low TGFbeta signalling may contribute to low *Opn* expression via low levels of Smad1 activation. Control of differentiation by FGF and TGFbeta may converge on *Opn* expression (Figure 7.8).

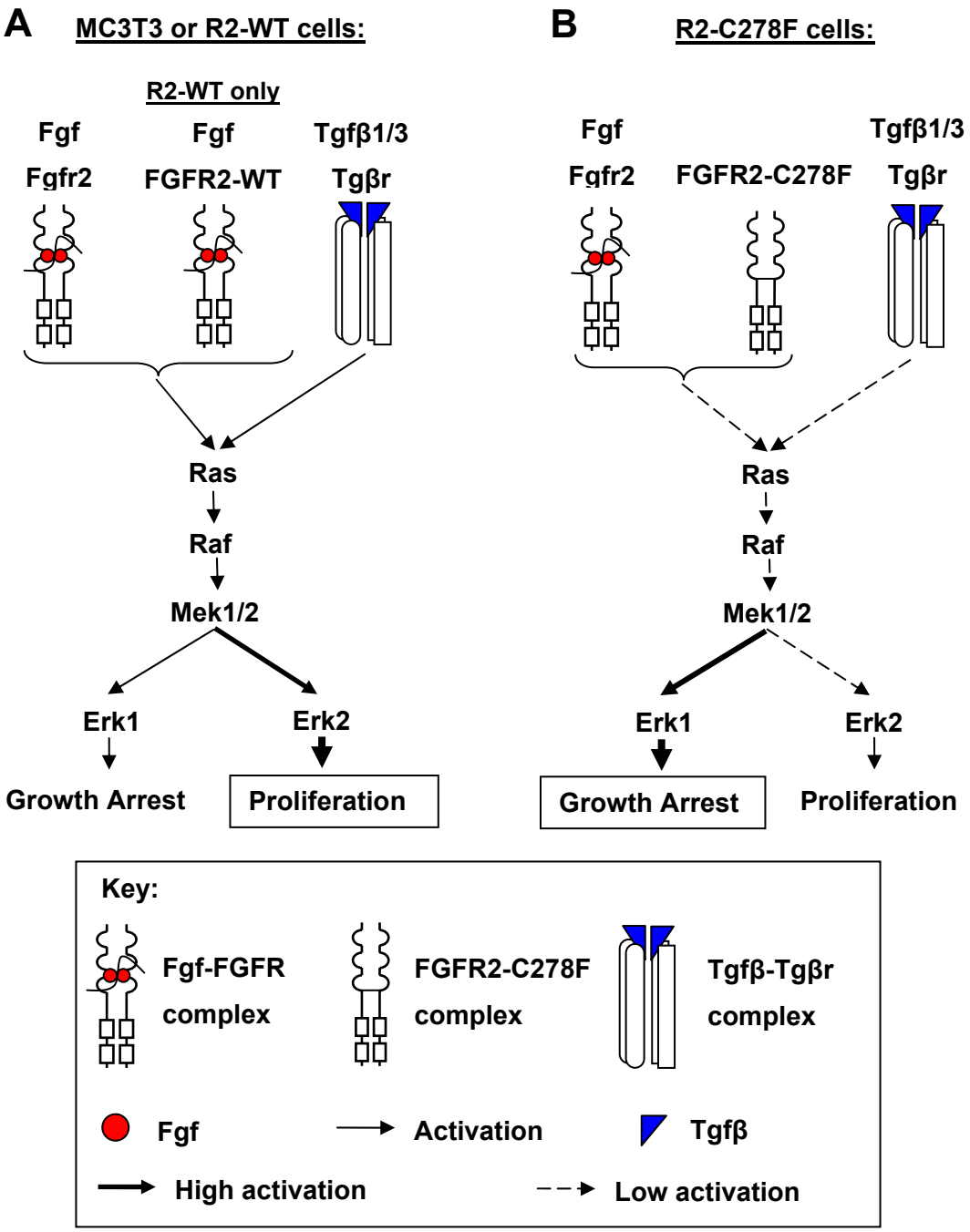

Figure 7.7 Proposed regulation of ERK pathway and its relationship to the proliferation defects in R2-C278F cells

A: In MC3T3 and R2-WT cells, the mitogenic signal most strongly activates the ERK2, favouring a proliferative response rather than growth arrest. **B:** In R2-C278F cells, there is a reduction in FGFR2 signalling, limiting the proliferative stimulation of the ERK1/2 pathway. There is also an increased ERK1/ERK2 ratio, which causes a shift in the ERK activation to ERK1, thereby resulting in a smaller level of proliferative response and a greater amount of growth arrest.

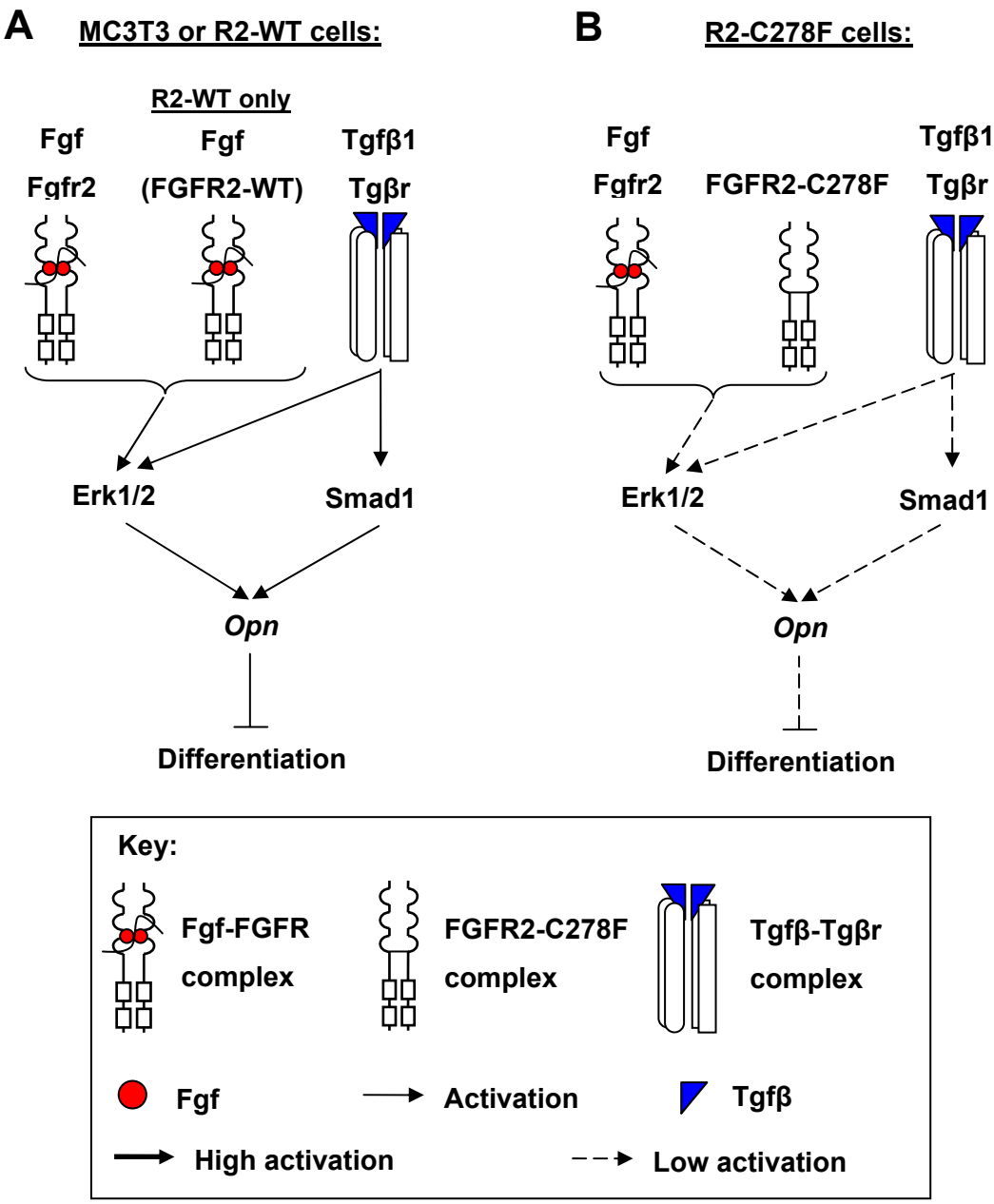

Figure 7.8 Hypothetical scheme of FGF and TGFbeta controlled differentiation via *Opn* expression
A: FGF activates Erk1/2; TGFbeta activates Erk1/2 and Smad1 signalling. Erk1/2 and Smad1 both upregulate *Opn* gene expression, which inhibits osteoblast differentiation. **B:** In R2-C278F cells the level of FGF and TGFbeta signalling is lower, which reduces Erk1/2 and Smad1 activation, thus reducing *Opn* expression, which reduces the level of inhibition on osteoblast differentiation. This results in increased osteoblast differentiation.

7.10 Further work

From the findings in this thesis, three main hypotheses have been created: One concerns the mechanisms of R2-C278F cell death and survival (Figure 7.6); another suggests a relationship between Fgf18 and osteoblast differentiation (Figure 7.2) and the third regarding the interaction between Fgf and Tgfbeta on osteoblast differentiation. The immediate future work will be to prove or disprove these hypotheses stated earlier in this chapter.

It is hypothesised that a low *Gapdh* expression is responsible for reduced R2-C278F cell survival, via a low level of glycolysis secondary to Gapdh (Figure 7.6). The level of glycolysis may be assessed by measuring the levels of ATP, which if low would support this hypothesis. Alternatively, Gapdh could be overexpressed in the R2-C278F mutant to observe for rescue of cell death. Caspase inhibitors may be used to determine whether cell death in R2-C278F cells occurs via a caspase independent mechanism.

Analysis of *Oc* expression in MC3T3, R2-WT and R2-C278F cells following exogenous FGF18 treatment would test the hypothesis that raised *Fgf18* expression found in R2-C278F cells positively regulates *Oc* expression, enhancing osteoblast differentiation (Figure 7.2).

For assessing the action of FGF and TGFbeta on Opn regulated differentiation, Erk1/2 should be inhibited with U0126 and *Opn* expression measured at confluence. If Erk1/2 inhibition reduces *Opn* expression, it would support the hypothesis that the reduction in Fgfr and Tgfbeta signalling leads to a reduced Erk1/2 signalling, which is responsible for regulating *Opn* expression (Figure 7.8). For TGFbeta and Smad1, it is necessary to confirm whether exogenous TGFbeta1 increases Smad1 activity in cells at confluence (as *Opn* expression was shown to increase in MC3T3 and R2-WT cells). If confirmed, the level of endogenous Smad1 activity should be determined. If Smad1 activity is low in R2-C278F cells, then this would support the hypothesis in Figure 7.8.

There are also several areas to investigate, which are discussed below.

7.10.1 The role of Erk1 in osteoblast differentiation

This study has correlated Erk2 with proliferation and implied that Erk1 may inhibit Erk2-induced proliferation and was involved in differentiation. To confirm these two suggestions, Erk1 could be overexpressed in MC3T3 cells and analysed for both proliferation and differentiation markers. Interestingly, alterations of the ratio between pERK1 and pERK2 are currently being researched and even patented (US 20070082366) for diagnosing pathological conditions such as Alzheimers disease (http://www.freshpatents.com/Alzheimer-s-disease-specific-alterations-of-the-erk1-erk2-phosphorylation-ratio-dt20070412ptan20070082366.php). Should modification of the Erk1/Erk2 prove useful in rescue of proliferation in craniosynostotic osteoblasts, this ratio could be of use in assessing the effectiveness of treatments. Alternatively in the future if osteoblast proliferation and differentiation are closely correlated to the Erk1/Erk2 ratio, this could be used as a simpler test to reflect the severity of disease or the prognosis to surgical or medical treatments.

To understand the mechanisms behind the change in Erk1/Erk2 ratio, it would be useful to investigate whether FGFR2 signalling can control Erk expression directly. This would also indicate that FGF signalling can modulate proliferative responses to other growth factors that signal via Erk1/2. One way of testing this would be to treat MC3T3, R2-WT and R2-C278F with cycloheximide to reduce the basal levels of Erk1 and Erk2 mRNA, followed by FGF2 treatment to observe whether the *Erk* expression is higher in treated cells compared to untreated cells. If Erk1 or Erk2 expression is upregulated, it will suggest that the ratio of Erk1 and Erk2 expression is directly regulated by FGF signalling.

7.10.2 Control of ERK ratios by FGF signalling

Explanations for the raised Erk1/Erk2 ratio in R2-C278F cells may lie in the stability of Erk protein or differences in gene expression. Both Erk1 and Erk2 are very similar in structure and sequence, however the 5' promoter sequences are notably different, indicating that there are different transcriptional controls for the Erk isoforms (Sugiura et al., 1997). The Erk2 promoter may be activated by NF-Y or Sp3 (Sugiura and Takishima, 2000). GC boxes are known targets of the Sp family of transcription factors, wheras CCAAT boxes are commonly targests of NF-Y transcription factors. Erk1 contains GC boxes in the promoter domain, whereas Erk2 contains both GC boxes and a CCAAT box, suggesting that Erk1 is targeted by Sp3, but not NF-Y (Sugiura and Takishima, 2000). FGF activates an Sp1-like transcription factor Spr2, thus it is possible that FGF signalling plays a role in the differential regulation of Erks as activation of Sp-like transcription factors has been reported to be downstream of FGF (Zhao et al., 2003). It

is possible that FGFR2 signals activate a member of the Sp family or similar proteins to change the Erk ratio. These molecules should be candidates for further investigation.

7.10.3 Investigating TGFbeta signalling

Both FGF and TGFbeta1 activate Erk1/2, however given that both produce different levels of cell growth, they are likely to activate this pathway in a different manner, such as signal intensity, time-course and cross talk between the downstream pathways. In this thesis, low TGFbeta signalling was suggested on the basis that SB431542 at low dose inhibited TβRI activation. It is also possible that low TβRI or TβRII expression could give a low and saturated TGFbeta signalling, assuming the ligand was in excess. The expression level of both receptors and the endogenous level of TGFbeta1 and -3 protein will need to be assessed in order to exclude for this effect.

7.10.4 Control of Fgf18 expression

In R2-C278F exogenous TGFbeta1 can increase *Fgf18* expression; however the low level of *Tgfbeta1* expression in these cells suggests that TGFbeta1 indirectly causes the increase in *Fgf18* expression observed at 2 days in culture. The underlying mechanisms for *Fgf18* regulation by FGFR2 signalling were not investigated in this thesis, but in the brain Fgf8b has been shown to positively regulate *Fgf18* expression (Liu et al., 2003). Interestingly, Fgf18 expression has been linked to FGF signalling in conjunction with Wnt signalling (Reinhold and Naski, 2007). Further study of the state of Wnt signalling may be necessary to determine how FGFR2 can control Fgf18 expression.

7.10.5 Control of Gapdh expression by Fgf

It is not clear whether Gapdh is a direct target of FGF signalling as changes in *Gapdh* expression may be secondary to other effects such as hypoxia (Lu et al., 2002). To determine this, protein synthesis could be inhibited using cyclohexamide and measuring *Gapdh* gene expression in response to FGF stimulation. Increased *Gapdh* expression would indicate this gene to be a direct target for FGF signalling.

7.10.6 Negative feedback of FGF signalling in R2-C278F cells

As mentioned in Chapter 4, there is decreased proliferation in R2-C278F cells instead of increased, implying a negative feedback response, supported in chapter 5 by observing a decreased level of mitogenic FGFR signalling and changes to *Fgfr2IIIc* expression.

However there are many other established negative feedback pathways associated with FGFR signalling, which may also be overactive in R2-C278F cells. The FGFR2 signalling expected from FGFR2-C278F may induce many feedback responses from the FGFR signalling pathway. Some ideas include the inhibitors Spred and Sprouty, which are transcriptionally activated upon FGF induced Erk1/2 activation (Yang et al., 2006). However the current literature suggests that the action of Spreds and Sproutys are at the level of Ras and Raf, not the receptor, therefore it is unlikely that a reduced level of FGFR signalling is wholly due to these inhibitors. Sef on the other hand, has been shown to inhibit FGFR tyrosine phosphorylation (Eblaghie et al., 2003; Kovalenko et al., 2003). It is interesting that the Erk1/2 expression levels had increased, but its level of signalling had not been shown to increase in R2-C278F cells. Activated Erk1/2 can negatively regulate further Erk1/2 activation by binding to FRS2 (Wu et al., 2003). It is possible that the level of pErk1/2 bound FRS may be involved with the observed negative feedback effect. It is not known whether there is also a difference the effectiveness of pErk1 and pErk2 in binding FRS to inhibit FGFR activation, which may be of interest for future studies due to the change in pErk1/pErk2 ratio reported in this thesis. These possiblities are laid out in Figure 7.9.

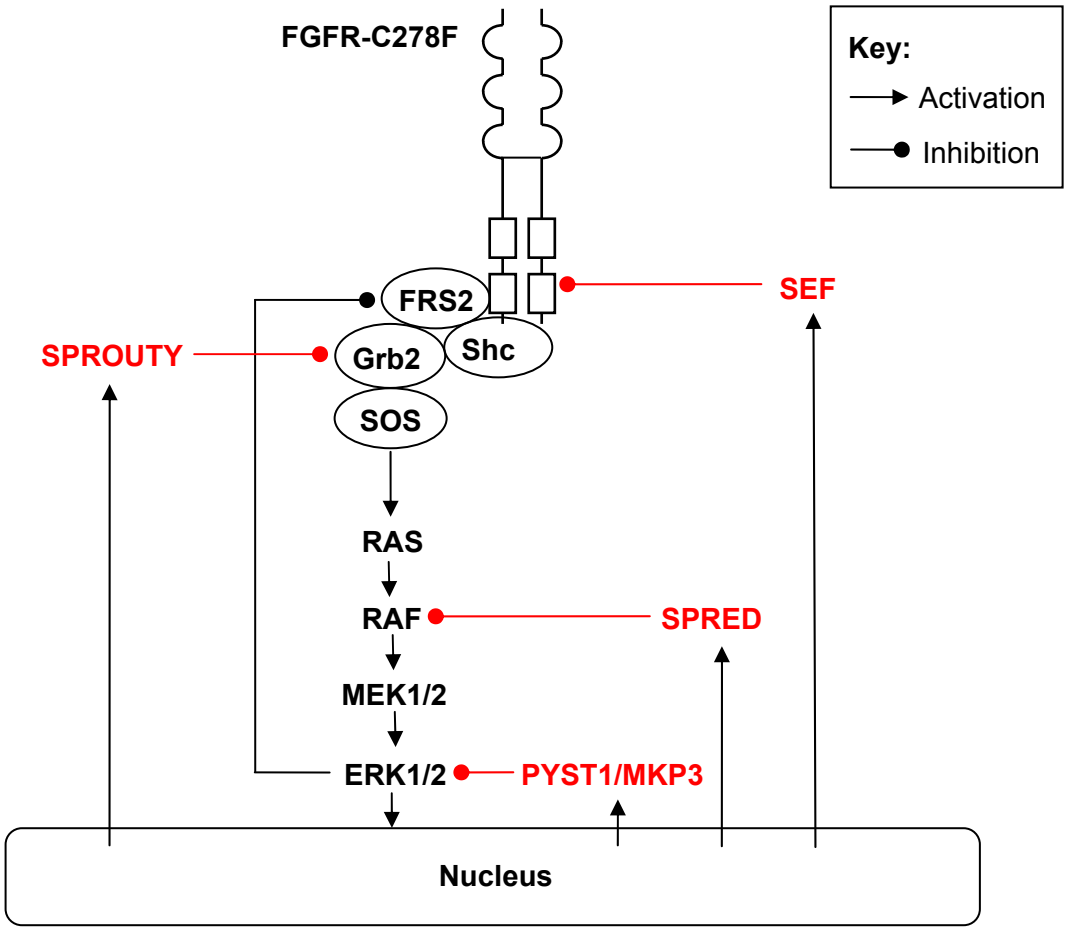

Figure 7.9 Possible negative feedback mechanisms for FGFR signalling

PYST1/MKP3, SEF, SPRED and SPROUTY are transcriptionally upregulated following FGFR MAPK signalling and inhibit FGFR and the ERK1/2 pathway as indicated in red. The activated form of ERK1/2 binds and inhibits FRS2 from further activating the ERK1/2 pathway. Adapted from Eblaghie 2003, Wu 2003 and Yang 2006.

7.11 Implications for patient treatment

Patient treatment may be divided into avoidance, prevention or reduction of the impact of craniosynostosis and post-surgical therapies.

Genetic counselling and preimplantation genetic diagnosis (PGD) with *in-vitro* fertilization (IVF) may be useful to avoid selection of affected embryos for couples with familial craniosynostoses, for example in Crouzon syndrome (Abou-Sleiman et al., 2002).

Although prenatal screening is a possible diagnostic tool, prenatal intrauterine treatment is both invasive and complicated with risks to both mother and foetus. Limiting the impacts of craniosynostosis may be an option if the suture fusion occurs after birth. Mouse studies have shown that treating sutures with reagents such as cytokines (e.g. TGFbeta) or antibodies to cytokines may help to block or delay suture fusion (Opperman et al., 1999; Eswarakumar et al., 2006; Wan et al., 2008).

Another area of treatment is post surgical. It has been shown that in osteoblasts with Apert or Crouzon syndrome craniosynostosis that cell proliferation is reduced (Fragale et al., 1999). Following craniotomies, it may be useful to increase osteoblast proliferation for faster healing and repair for which growth factors and other reagents may be used.

The work in this thesis have suggested that in osteoblasts carrying LICA FGFR mutations such as FGFR2-C278F, TGFbeta treatments may not be as effective as in normal osteoblasts because the aberrant FGFR signalling that impairs normal cellular responses to TGFbeta. This indicates that the role of TGFbeta may be limited in the delay of suture fusion and post-surgical treatment strategies. Furthermore the increased Erk1/Erk2 ratio observed in osteoblasts with FGFR2-C278F may have a role in affecting the proliferative responses to growth factors. It is possible that decreasing this ratio, for example by Erk1 siRNA may improve cellular responses to growth factor treatment such as TGFbeta and subsequently increase osteoblast proliferation. The findings in this thesis may therefore contribute to finding appropriate biological treatments of sutures pre- and post-surgery.

Chapter 8 Appendix

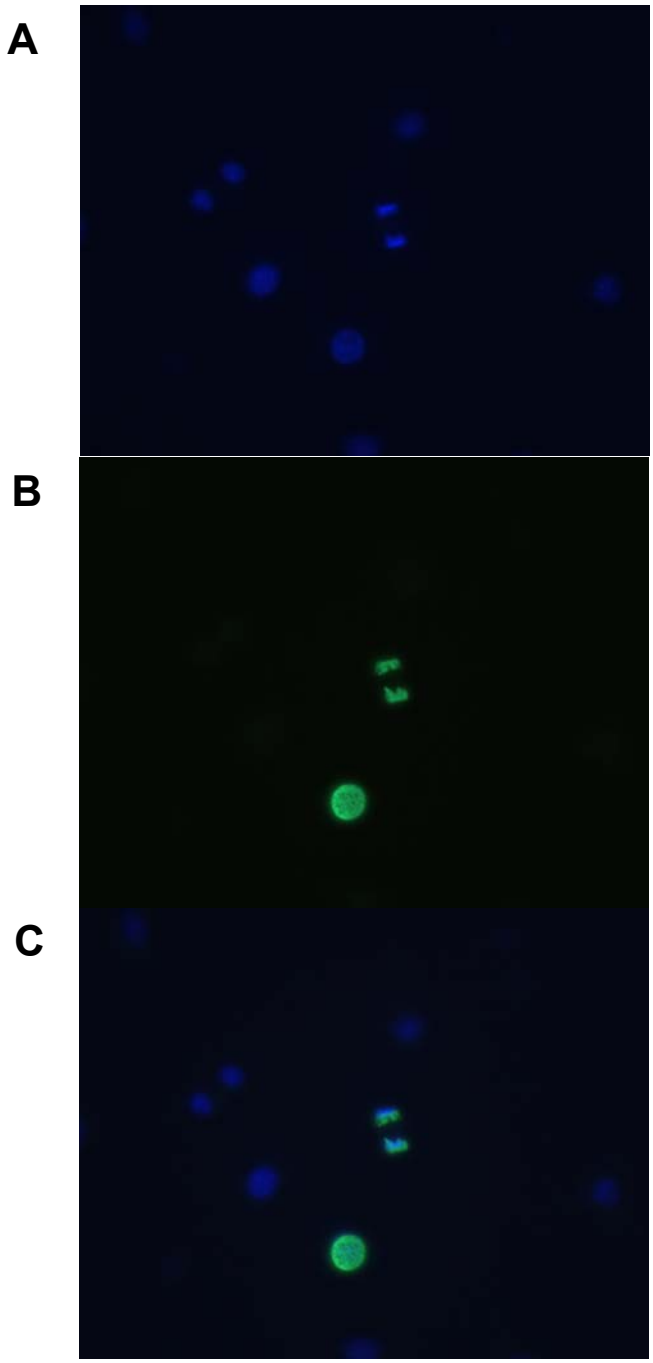

Figure 8.1 Immunocytochemistry staining of Phosphorylated Histone 3

The pH3 antibody supplied was tested and confirmed to bind in MC3T3. **A:** Hoescht counterstain for cell nuclei. **B:** Positive pH3 staining using Alexa 488 conjugated antibodies. **C:** Merged image demonstrating the distinction between M-phase and non-M-phase cells.

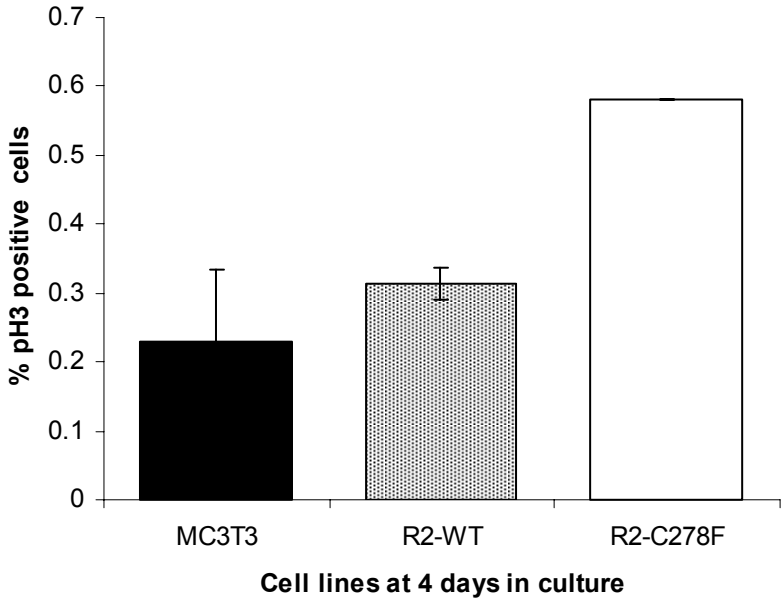

Figure 8.2 FACS M-phase analysis of MC3T3, R2-WT and R2-C278F cells at 4 days in culture
The level of pH3 staining is higher in R2-C278F cells at confluence than MC3T3 and R2-WT cells.

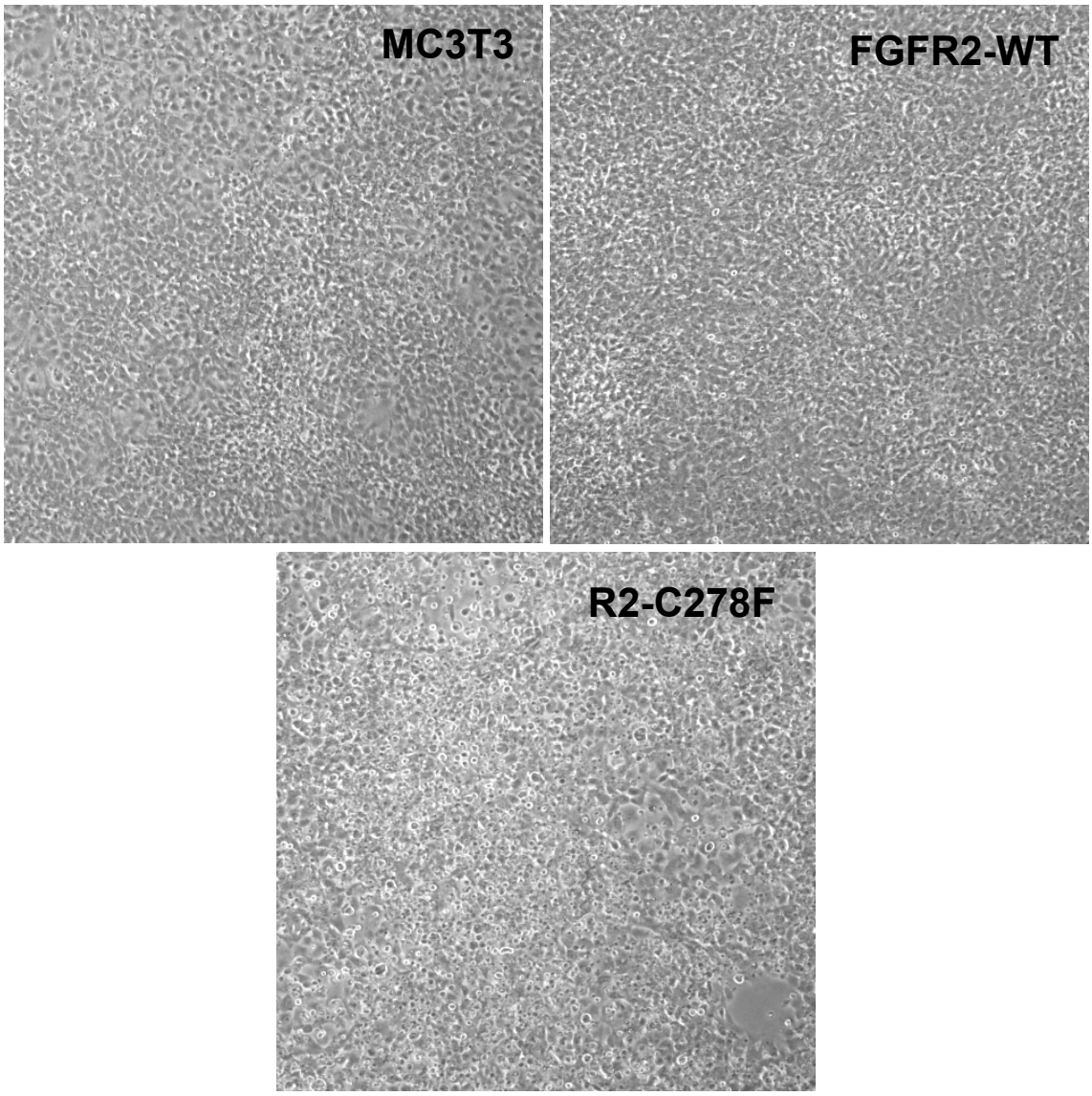

Figure 8.3 Photographs of cells at 6 days in culture without a change of culture medium.
Cells were grown for 6 days in culture and photographed.

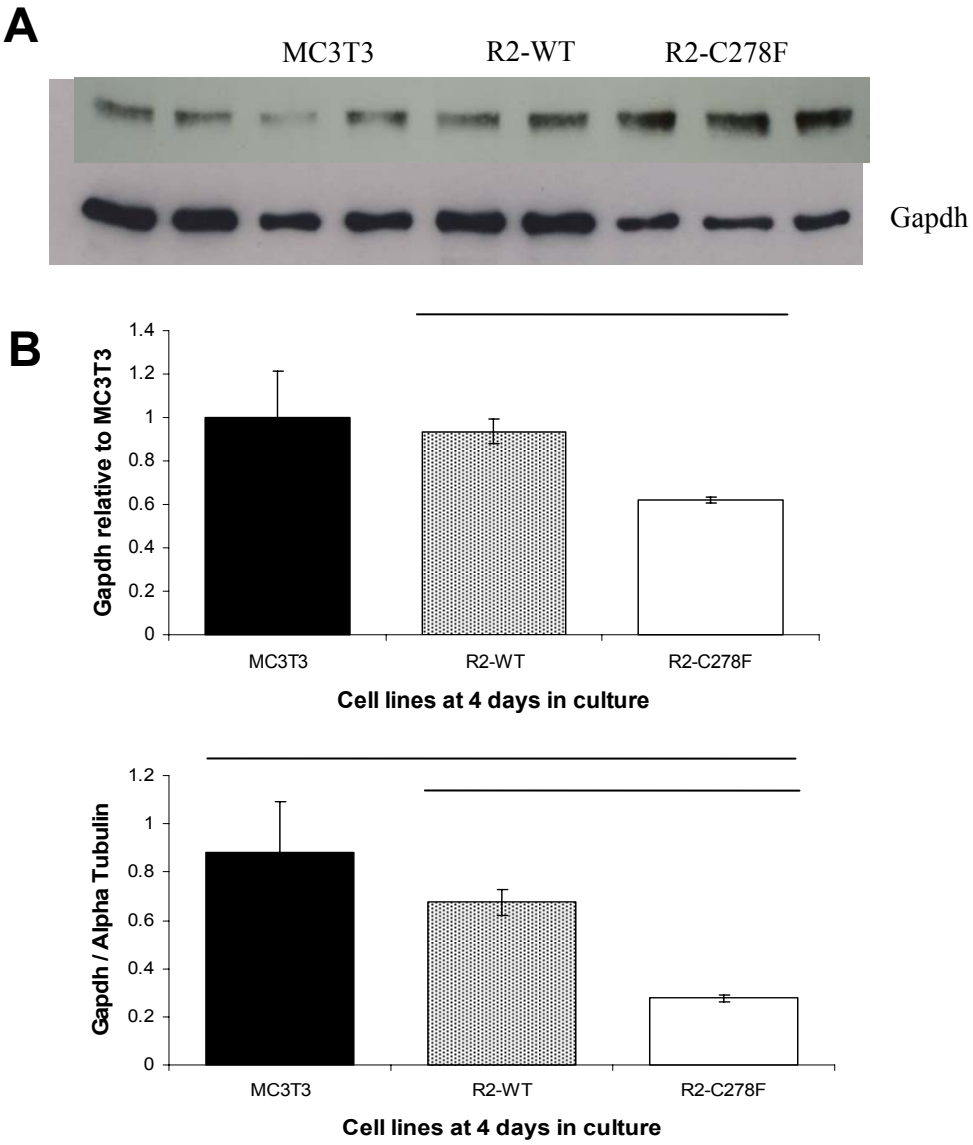

Figure 8.4 Gapdh protein expression at 4 days in culture

An initial study of Gapdh protein expression was performed using western blotting and normalised with Alpha Tubulin (n = 3).

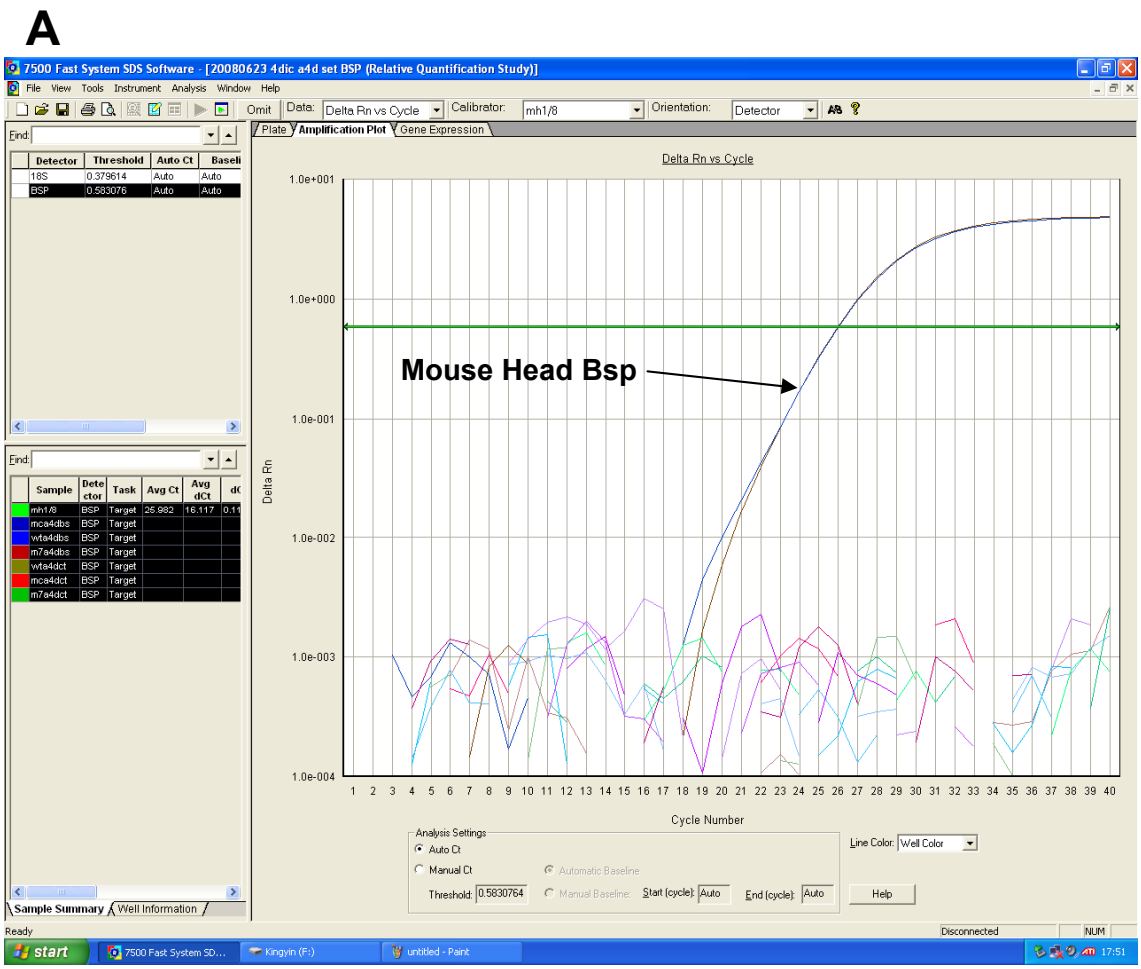

Figure 8.5 Real time PCR analysis of Bsp in MC3T3, R2-WT and R2-C278F cells at 4 DIC

A: Bsp expression amplification is found in Mouse Head at E13.5, but not in MC3T3, R2-WT and R2-C278F cells. **B:** The cDNA viability was confirmed using the endogenous control 18S. cDNA was present in all samples.

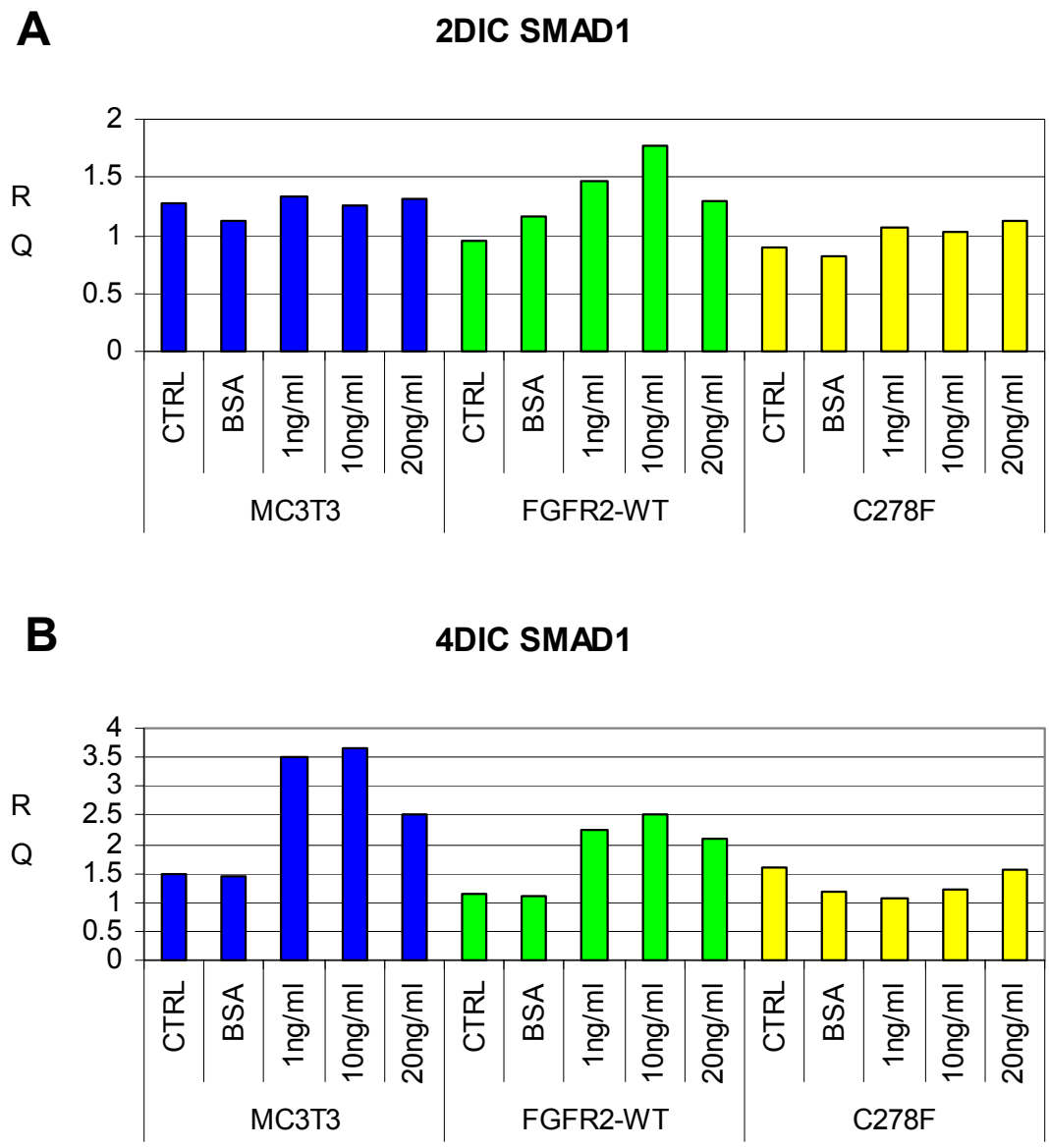

Figure 8.6 Real time PCR of *Smad1* expression in MC3T3, R2-WT and R2-C278F cells

Cells were seeded for 3 hours then treated with 1, 10 and 20, ng/ml of TGFbeta1 for 2 and 4 days in culture before relative quantification (RQ) of gene expression by real time PCR. **A**: *Smad1* increases in FGFR2-WT with TGFBeta1 treatment at 2 DIC, but not MC3T3 and R2-C278F cells **B**: TGFbeta1 treatment increases expression in MC3T3 at 4 DIC and FGFR2-WT, ($n = 2$, $p < *0.05$).

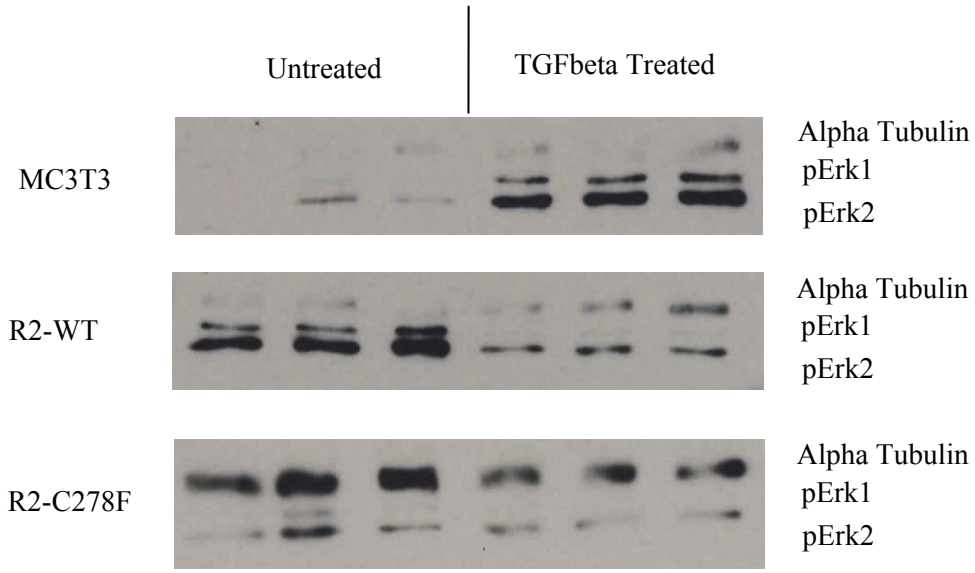

Figure 8.7 Western blot of TGFbeta1 treated MC3T3, R2-WT and R2-C278F cells

Western blot of TGFbeta1 treated MC3T3, R2-WT and R2-C278F cells at 2 days in culture. Cells were treated with TGFbeta1 for 10 minutes prior to Western blot analysis. Activation was seen in MC3T3, in R2-WT cells this was the opposite and in R2-C278F activation was not detected (n = 1).

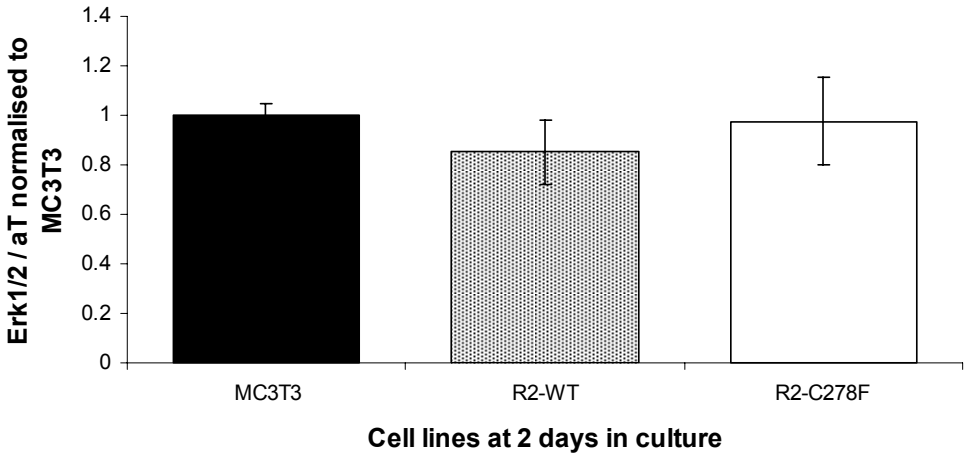

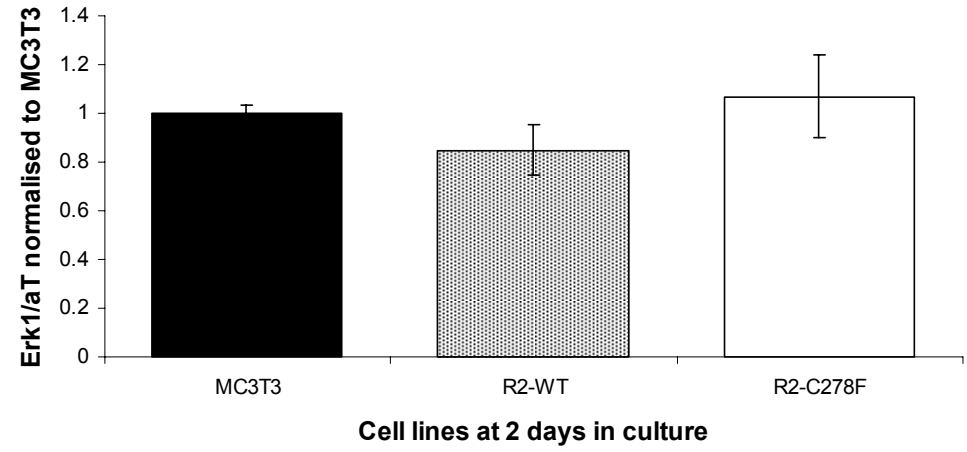

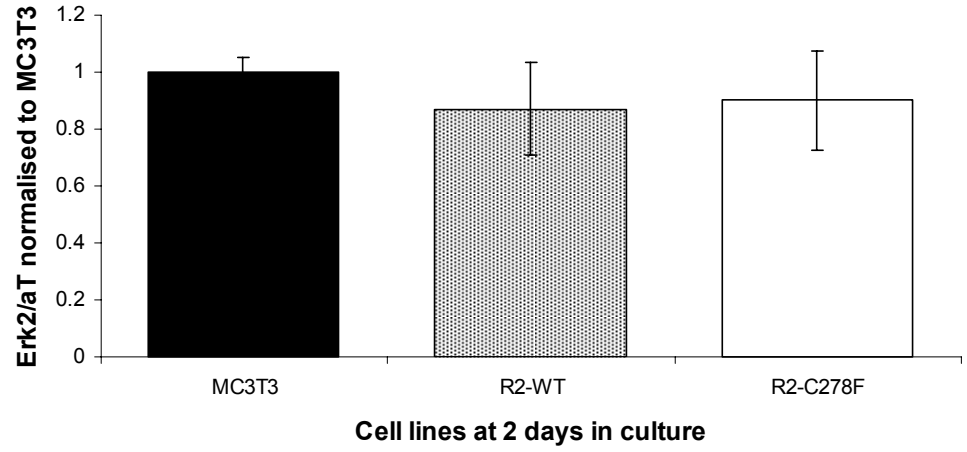

Figure 8.8 Analysis of Erk1/2 expression in MC3T3, R2-WT and R2-C278F cells by WB

Erk1/2 expressions were normalised to α-Tubulin.

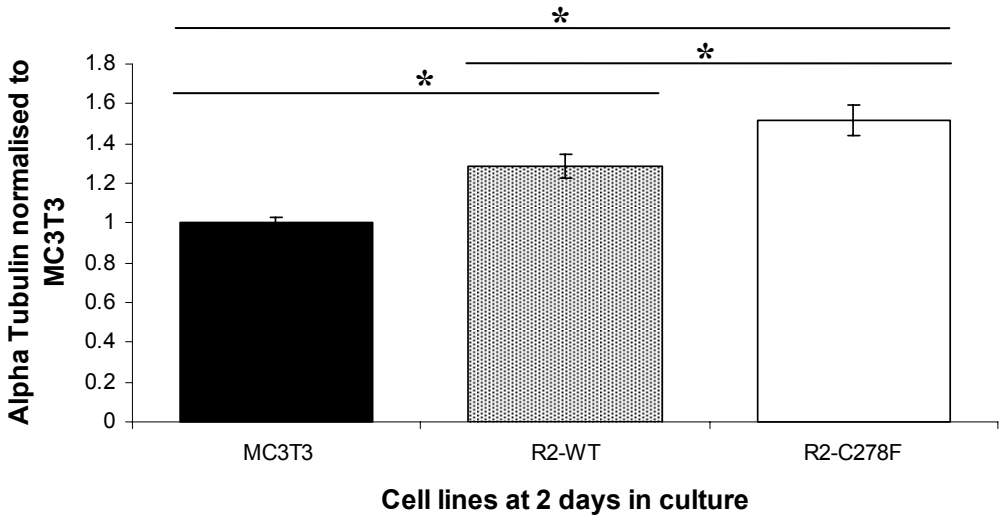

Figure 8.9 Semi-quantification of Alpha Tubulin in MC3T3, R2-WT and R2-C278F by WB

Alpha Tubulin was analysed at 2 days in culture by Western blotting. The band intensities alpha tubulin was normalised to the average for MC3T3 within 3 experiments to analyse together ($n = 3$, * $p < 0.05$).

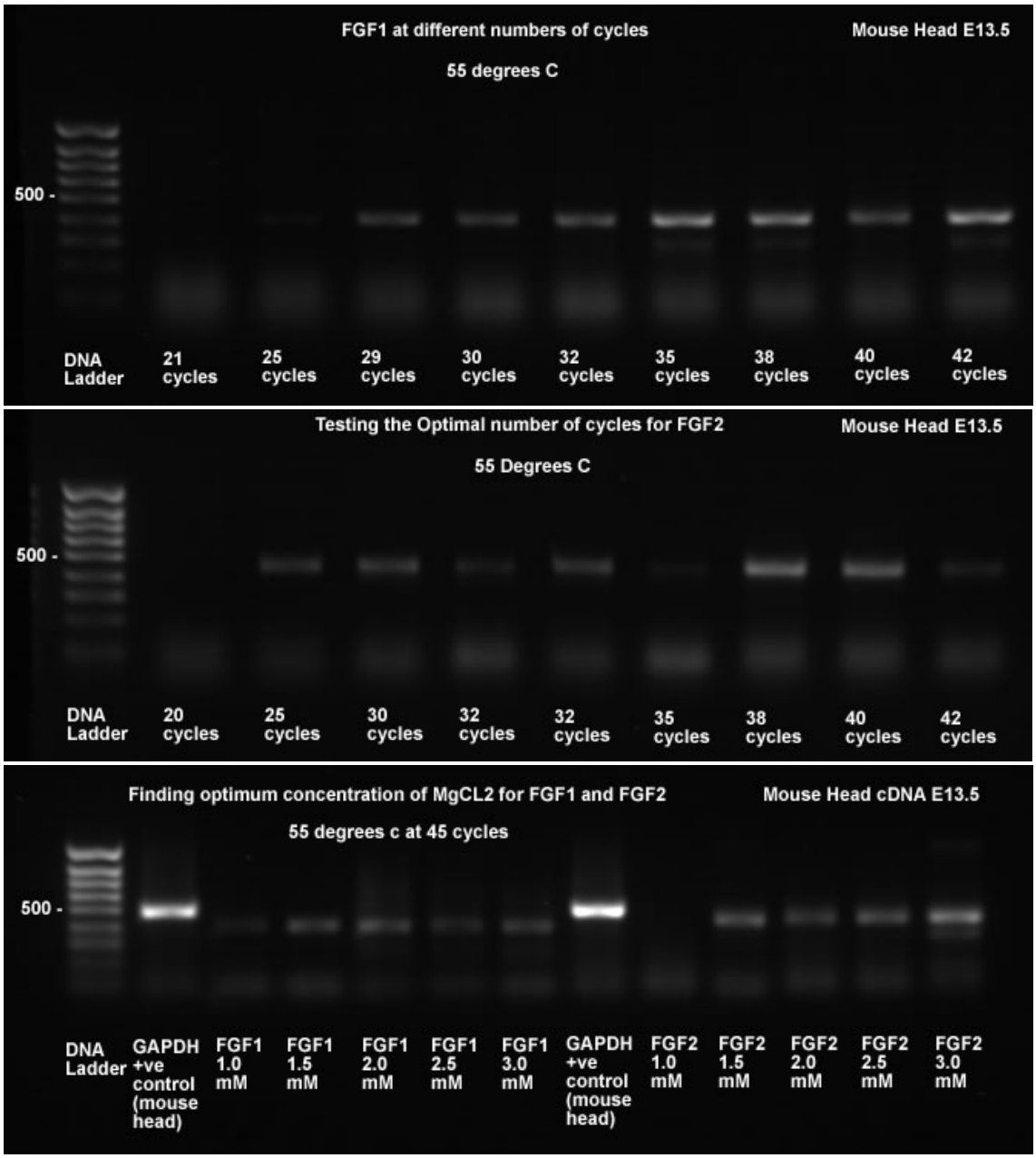

Figure 8.10 Optimization of Fgf1 and -2 RT-PCR products

PCR products of Fgf1 and Fgf2 were present in Mouse Head cDNA. It was confirmed that the optimal number of cycles was 35 cycles and the optimal concentration was 2 mM of Magnesium Chloride.

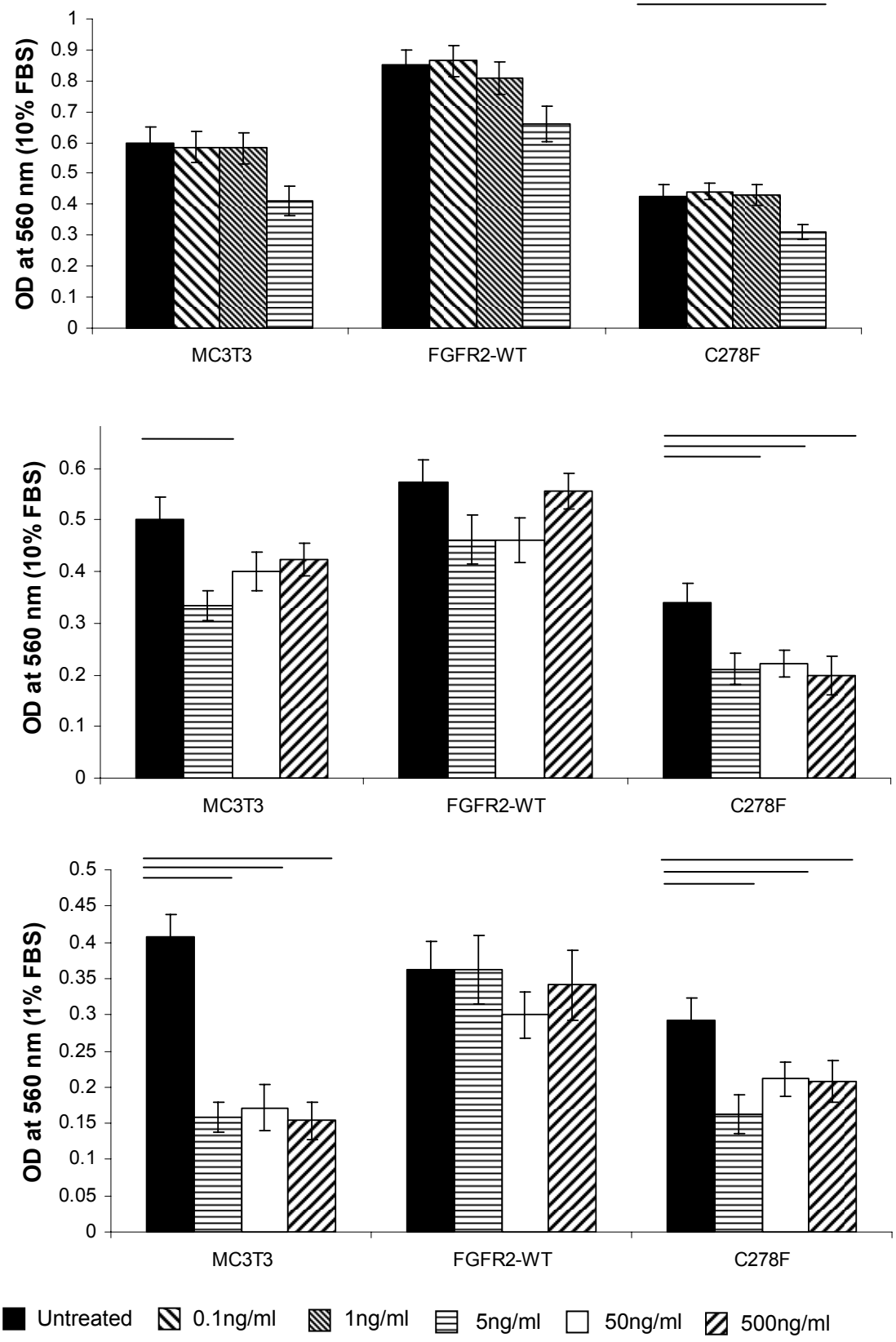

Figure 8.11 Cells treated with PMA for 2 days in culture

Cells were seeded for three hours before treating with PMA in titration range from 0.1 ng/ml to 500ng/ml ($n = 8$, line $p < 0.05$).

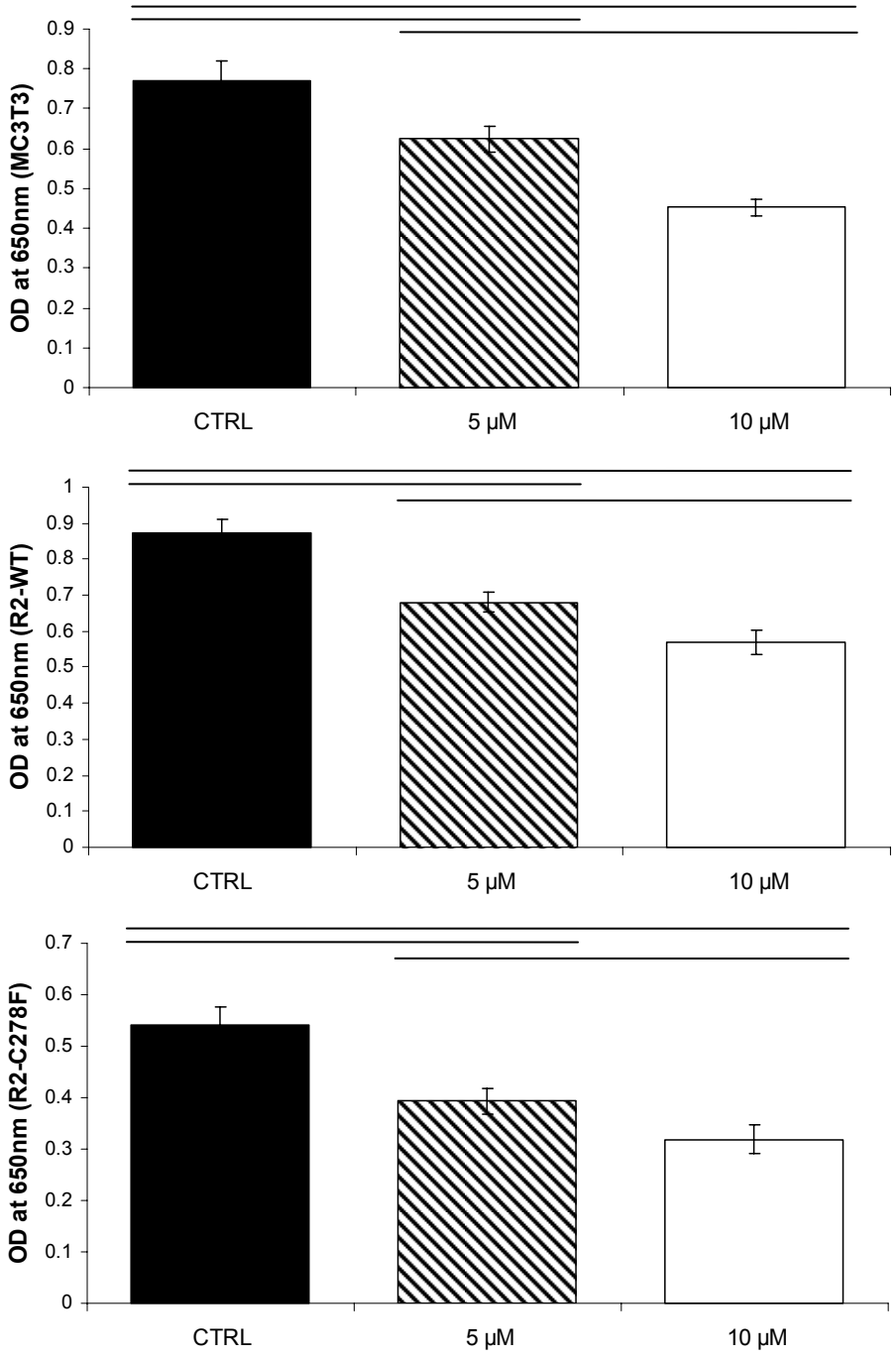

Figure 8.12 Treatment of cells with SU5402 at 10% serum

Cell growth in MC3T3, R2-WT and R2-C278F cells decrease with SU5402 treatment with a dose dependent effect. ($n = 8$, line $p < 0.05$).

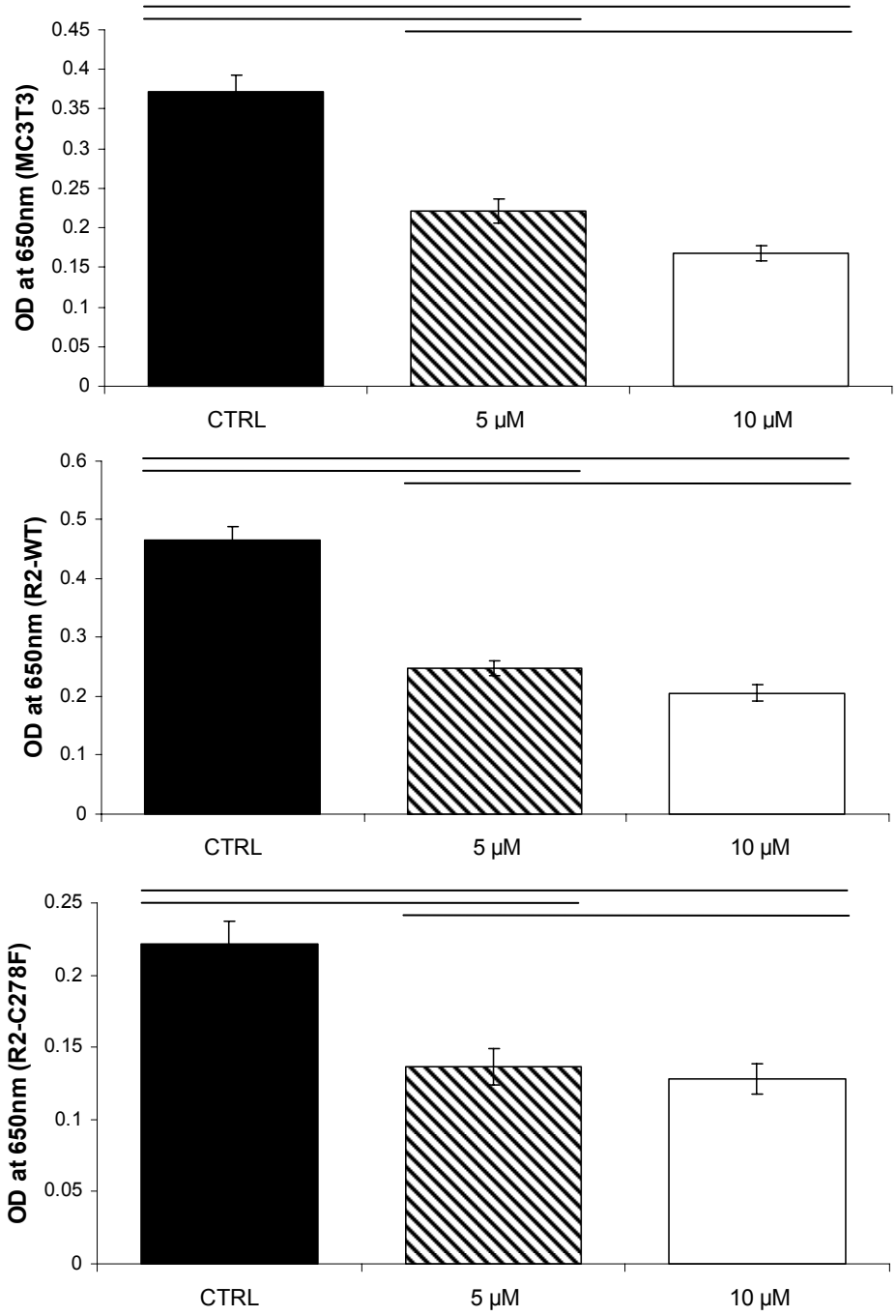

Figure 8.13 Treatment of cells with SU5402 at 1% serum

Cell growth in MC3T3, R2-WT and R2-C278F cells decrease with SU5402 treatment with a dose dependent effect ($n = 8$, line $p < 0.05$).

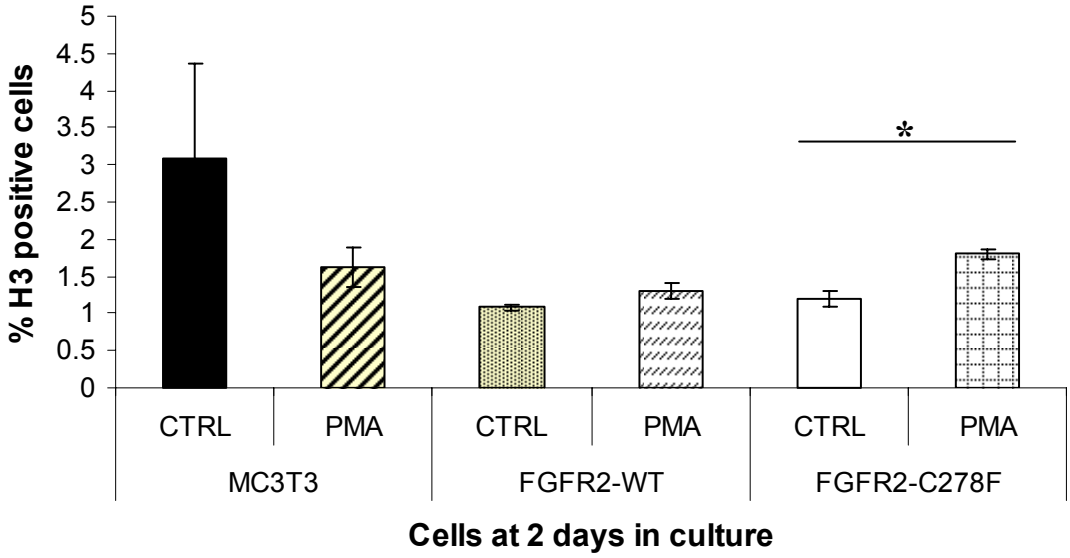

Figure 8.14 FACS analysis of pH3 in PMA treated MC3T3, R2-WT and R2-C278F cells

Cells were seeded for 3 hours and treated with PMA every 24 hours for 2 days in culture in 10% FBS containing cell medium. Treatment with PMA did not significantly change the percentage pH3 in MC3T3 and R2-WT cells, however in R2-C278F cells the H3 percentage was increased. ($n = 1$, $*p < 0.05$).

References

(2004). Clinical Management of Craniosynostosis., R.Hayward, B.Jones, D.Dunaway, R.Evans, and P.Tessier, eds. Mac Keith Press).

Abou-Sleiman,P.M., Apessos,A., Harper,J.C., Serhal,P., and Delhanty,J.D. (2002). Pregnancy following preimplantation genetic diagnosis for Crouzon syndrome. Mol. Hum. Reprod. *8*, 304-309.

Agur,A.M. and Lee,M.J. (1999). Grant's Atlas of Anatomy. Lippincott Williams & Wilkins).

Albuisson,J., Pecheux,C., Carel,J.C., Lacombe,D., Leheup,B., Lapuzina,P., Bouchard,P., Legius,E., Matthijs,G., Wasniewska,M., Delpech,M., Young,J., Hardelin,J.P., and Dode,C. (2005). Kallmann syndrome: 14 novel mutations in KAL1 and FGFR1 (KAL2). Hum. Mutat. *25*, 98-99.

Alliston,T., Choy,L., Ducy,P., Karsenty,G., and Derynck,R. (2001). TGF-beta-induced repression of CBFA1 by Smad3 decreases cbfa1 and osteocalcin expression and inhibits osteoblast differentiation. EMBO J. *20*, 2254-2272.

Arnaud,E., Touriol,C., Boutonnet,C., Gensac,M.C., Vagner,S., Prats,H., and Prats,A.C. (1999). A new 34-kilodalton isoform of human fibroblast growth factor 2 is cap dependently synthesized by using a non-AUG start codon and behaves as a survival factor. Mol. Cell Biol. *19*, 505-514.

Aubin,J.E. (2001). Regulation of osteoblast formation and function. Rev. Endocr. Metab Disord. *2*, 81-94.

Bae,J.S., Gutierrez,S., Narla,R., Pratap,J., Devados,R., van Wijnen,A.J., Stein,J.L., Stein,G.S., Lian,J.B., and Javed,A. (2007). Reconstitution of Runx2/Cbfa1-null cells identifies a requirement for BMP2 signaling through a Runx2 functional domain during osteoblast differentiation. J Cell Biochem. *100*, 434-449.

Bannink,N., Joosten,K.F., van Veelen,M.L., Bartels,M.C., Tasker,R.C., van Adrichem,L.N., van der Meulen,J.J., Vaandrager,J.M., de Jong,T.H., and Mathijssen,I.M. (2008). Papilledema in patients with Apert, Crouzon, and Pfeiffer syndrome: prevalence, efficacy of treatment, and risk factors. J Craniofac. Surg. *19*, 121-127.

Beck,G.R., Jr. and Knecht,N. (2003). Osteopontin regulation by inorganic phosphate is ERK1/2-, protein kinase C-, and proteasome-dependent. J Biol. Chem. *278*, 41921-41929.

Beck,L.S., Deguzman,L., Lee,W.P., Xu,Y., McFatridge,L.A., Gillett,N.A., and Amento,E.P. (1991). Rapid publication. TGF-beta 1 induces bone closure of skull defects. J Bone Miner. Res. *6*, 1257-1265.

Bernard-Pierrot,I., Ricol,D., Cassidy,A., Graham,A., Elvin,P., Caillault,A., Lair,S., Broet,P., Thiery,J.P., and Radvanyi,F. (2004). Inhibition of human bladder tumour cell growth by fibroblast growth factor receptor 2b is independent of its kinase activity. Involvement of the carboxy-terminal region of the receptor. Oncogene *23*, 9201-9211.

Bialek,P., Kern,B., Yang,X., Schrock,M., Sosic,D., Hong,N., Wu,H., Yu,K., Ornitz,D.M., Olson,E.N., Justice,M.J., and Karsenty,G. (2004). A twist code determines the onset of osteoblast differentiation. Dev. Cell *6*, 423-435.

Boguslawski,G., Hale,L.V., Yu,X.P., Miles,R.R., Onyia,J.E., Santerre,R.F., and Chandrasekhar,S. (2000). Activation of osteocalcin transcription involves interaction of protein kinase A- and protein kinase C-dependent pathways. J Biol. Chem. *275*, 999-1006.

Bosetti,M., Boccafoschi,F., Leigheb,M., and Cannas,M.F. (2007). Effect of different growth factors on human osteoblasts activities: a possible application in bone regeneration for tissue engineering. Biomol. Eng *24*, 613-618.

Boskey,A.L., Spevak,L., Paschalis,E., Doty,S.B., and McKee,M.D. (2002). Osteopontin deficiency increases mineral content and mineral crystallinity in mouse bone. Calcif. Tissue Int. *71*, 145-154.

Bradley,J.P., Levine,J.P., Roth,D.A., McCarthy,J.G., and Longaker,M.T. (1996). Studies in cranial suture biology: IV. Temporal sequence of posterior frontal cranial suture fusion in the mouse. Plast. Reconstr. Surg. *98*, 1039-1045.

Britto,J.A., Moore,R.L., Evans,R.D., Hayward,R.D., and Jones,B.M. (2001). Negative autoregulation of fibroblast growth factor receptor 2 expression characterizing cranial development in cases of Apert (P253R mutation) and Pfeiffer (C278F mutation) syndromes and suggesting a basis for differences in their cranial phenotypes. J. Neurosurg. *95*, 660-673.

Broker,L.E., Kruyt,F.A., and Giaccone,G. (2005). Cell death independent of caspases: a review. Clin. Cancer Res. *11*, 3155-3162.

Burgess,W.H. and Maciag,T. (1989). The heparin-binding (fibroblast) growth factor family of proteins. Annu. Rev. Biochem. *58*, 575-606.

Cabiling,D.S., Kim,E., Yan,D., Jacob,S., Nah,H.D., and Kirschner,R.E. (2007). Differential effects of TGF-beta isoforms on murine fetal dural cells and calvarial osteoblasts. Plast. Reconstr. Surg. *120*, 614-624.

Carinci,F., Pezzetti,F., Locci,P., Becchetti,E., Carls,F., Avantaggiato,A., Becchetti,A., Carinci,P., Baroni,T., and Bodo,M. (2005). Apert and Crouzon Syndromes: Clinical Findings, Genes and Extracellular Matrix. J. Craniofac. Surg. *16*, 361-368.

Centrella,M., Horowitz,M.C., Wozney,J.M., and McCarthy,T.L. (1994). Transforming growth factor-beta gene family members and bone. Endocr. Rev. *15*, 27-39.

Centrella,M., McCarthy,T.L., and Canalis,E. (1987). Transforming growth factor beta is a bifunctional regulator of replication and collagen synthesis in osteoblast-enriched cell cultures from fetal rat bone. J. Biol. Chem. *262*, 2869-2874.

Chai,Y., Ito,Y., and Han,J. (2003). TGF-beta signaling and its functional significance in regulating the fate of cranial neural crest cells. Crit Rev. Oral Biol. Med. *14*, 78-88.

Chambard,J.C., Lefloch,R., Pouyssegur,J., and Lenormand,P. (2007). ERK implication in cell cycle regulation. Biochim. Biophys. Acta *1773*, 1299-1310.

Chan,C.T. and Thorogood,P. (1999). Pleiotropic features of syndromic craniosynostoses correlate with differential expression of fibroblast growth factor receptors 1 and 2 during human craniofacial development. Pediatr. Res. *45*, 46-53.

Chang,E.J., Kim,H.H., Huh,J.E., Kim,I.A., Seung,K.J., Chung,C.P., and Kim,H.M. (2005). Low proliferation and high apoptosis of osteoblastic cells on hydrophobic surface are associated with defective Ras signaling. Exp. Cell Res. *303*, 197-206.

Chaudhary,L.R. and Hruska,K.A. (2001). The cell survival signal Akt is differentially activated by PDGF-BB, EGF, and FGF-2 in osteoblastic cells. J. Cell Biochem. *81*, 304-311.

Chen,J., McKee,M.D., Nanci,A., and Sodek,J. (1994). Bone sialoprotein mRNA expression and ultrastructural localization in fetal porcine calvarial bone: comparisons with osteopontin. Histochem. J *26*, 67-78.

Chen,J., Shapiro,H.S., and Sodek,J. (1992). Development expression of bone sialoprotein mRNA in rat mineralized connective tissues. J Bone Miner. Res. *7*, 987-997.

Cheung,W.M., Ng,W.W., and Kung,A.W. (2006). Dimethyl sulfoxide as an inducer of differentiation in preosteoblast MC3T3-E1 cells. FEBS Lett. *580*, 121-126.

Choi,K.Y., Kim,H.J., Lee,M.H., Kwon,T.G., Nah,H.D., Furuichi,T., Komori,T., Nam,S.H., Kim,Y.J., Kim,H.J., and Ryoo,H.M. (2005). Runx2 regulates FGF2-induced Bmp2 expression during cranial bone development. Dev. Dyn.

Chung,C.Y., Iida-Klein,A., Wyatt,L.E., Rudkin,G.H., Ishida,K., Yamaguchi,D.T., and Miller,T.A. (1999). Serial passage of MC3T3-E1 cells alters osteoblastic function and responsiveness to transforming growth factor-beta1 and bone morphogenetic protein-2. Biochem. Biophys. Res. Commun. *265*, 246-251.

Chung,H.A., Hyodo-Miura,J., Nagamune,T., and Ueno,N. (2005). FGF signal regulates gastrulation cell movements and morphology through its target NRH. Dev. Biol. *282*, 95-110.

Clarke,D.C. and Liu,X. (2008). Decoding the quantitative nature of TGF-beta/Smad signaling. Trends Cell Biol. *18*, 430-442.

Cohen,M.M., Jr. (1993). Sutural biology and the correlates of craniosynostosis. Am. J. Med. Genet. *47*, 581-616.

Cohen,M.M.J. (1986). Craniosynostosis: diagnosis, evaluation and management., M.M.J.Cohen, ed. New York: Raven Press), pp. 81-103.

Colell,A., Ricci,J.E., Tait,S., Milasta,S., Maurer,U., Bouchier-Hayes,L., Fitzgerald,P., Guio-Carrion,A., Waterhouse,N.J., Li,C.W., Mari,B., Barbry,P., Newmeyer,D.D., Beere,H.M., and Green,D.R. (2007). GAPDH and autophagy preserve survival after apoptotic cytochrome c release in the absence of caspase activation. Cell *129*, 983-997.

Conery,A.R., Cao,Y., Thompson,E.A., Townsend,C.M., Jr., Ko,T.C., and Luo,K. (2004). Akt interacts directly with Smad3 to regulate the sensitivity to TGF-beta induced apoptosis. Nat. Cell Biol. *6*, 366-372.

Cool,S., Jackson,R., Pincus,P., Dickinson,I., and Nurcombe,V. (2002). Fibroblast growth factor receptor 4 (FGFR4) expression in newborn murine calvaria and primary osteoblast cultures. Int. J Dev. Biol. *46*, 519-523.

Cooper,G.M., Singhal,V.K., Barbano,T., Wigginton,W., Rabold,T., Losken,H.W., Siegel,M.I., and Mooney,M.P. (2006). Intracranial volume changes in craniosynostotic rabbits: effects of age and surgical correction. Plast. Reconstr. Surg. *117*, 1886-1890.

Crane,N.J., Morris,M.D., Ignelzi,M.A., and Yu,G. (2005). Raman imaging demonstrates FGF2-induced craniosynostosis in mouse calvaria. J Biomed. Opt. *10*, 031119.

Cui,X.M., Shiomi,N., Chen,J., Saito,T., Yamamoto,T., Ito,Y., Bringas,P., Chai,Y., and Shuler,C.F. (2005). Overexpression of Smad2 in Tgf-beta3-null mutant mice rescues cleft palate. Dev. Biol. *278*, 193-202.

Dabovic,B., Levasseur,R., Zambuto,L., Chen,Y., Karsenty,G., and Rifkin,D.B. (2005). Osteopetrosis-like phenotype in latent TGF-beta binding protein 3 deficient mice. Bone.

Dailey,L., Ambrosetti,D., Mansukhani,A., and Basilico,C. (2005). Mechanisms underlying differential responses to FGF signaling. Cytokine Growth Factor Rev. *16*, 233-247.

Dastoor,Z. and Dreyer,J.L. (2001). Potential role of nuclear translocation of glyceraldehyde-3-phosphate dehydrogenase in apoptosis and oxidative stress. J Cell Sci. *114*, 1643-1653.

de Heer,I.M., de Klein,A., van den Ouweland,A.M., Vermeij-Keers,C., Wouters,C.H., Vaandrager,J.M., Hovius,S.E., and Hoogeboom,J.M. (2005). Clinical and genetic analysis of patients with Saethre-Chotzen syndrome. Plast. Reconstr. Surg. *115*, 1894-1902.

Dean,P.N. and Jett,J.H. (1974). Mathematical analysis of DNA distributions derived from flow microfluorometry. J Cell Biol. *60*, 523-527.

Debiais,F., Hott,M., Graulet,A.M., and Marie,P.J. (1998). The effects of fibroblast growth factor-2 on human neonatal calvaria osteoblastic cells are differentiation stage specific. J. Bone Miner. Res. *13*, 645-654.

Debiais,F., Lefevre,G., Lemonnier,J., Le Mee,S., Lasmoles,F., Mascarelli,F., and Marie,P.J. (2004). Fibroblast growth factor-2 induces osteoblast survival through a phosphatidylinositol 3-kinase-dependent, -beta-catenin-independent signaling pathway. Exp. Cell Res. *297*, 235-246.

Dubrovska,A., Kanamoto,T., Lomnytska,M., Heldin,C.H., Volodko,N., and Souchelnytskyi,S. (2005). TGFbeta1/Smad3 counteracts BRCA1-dependent repair of DNA damage. Oncogene *24*, 2289-2297.

Ducy,P., Zhang,R., Geoffroy,V., Ridall,A.L., and Karsenty,G. (1997). Osf2/Cbfa1: a transcriptional activator of osteoblast differentiation. Cell *89*, 747-754.

Dufour,C., Holy,X., and Marie,P.J. (2008). Transforming growth factor-beta prevents osteoblast apoptosis induced by skeletal unloading via PI3K/Akt, Bcl-2, and phospho-Bad signaling. Am. J Physiol Endocrinol. Metab *294*, E794-E801.

Dunlop,L.L. and Hall,B.K. (1995). Relationships between cellular condensation, preosteoblast formation and epithelial-mesenchymal interactions in initiation of osteogenesis. Int. J Dev. Biol. *39*, 357-371.

Eblaghie,M.C., Lunn,J.S., Dickinson,R.J., Munsterberg,A.E., Sanz-Ezquerro,J.J., Farrell,E.R., Mathers,J., Keyse,S.M., Storey,K., and Tickle,C. (2003). Negative feedback regulation of FGF signaling levels by Pyst1/MKP3 in chick embryos. Curr. Biol. *13*, 1009-1018.

Elberg,G., Elberg,D., Logan,C.J., Chen,L., and Turman,M.A. (2006). Limitations of commonly used internal controls for real-time RT-PCR analysis of renal epithelial-mesenchymal cell transition. Nephron Exp. Nephrol. *102*, e113-e122.

Erlebacher,A. and Derynck,R. (1996). Increased expression of TGF-beta 2 in osteoblasts results in an osteoporosis-like phenotype. J Cell Biol. *132*, 195-210.

Erlebacher,A., Filvaroff,E.H., Ye,J.Q., and Derynck,R. (1998). Osteoblastic responses to TGF-beta during bone remodeling. Mol. Biol. Cell *9*, 1903-1918.

Eswarakumar,V.P., Horowitz,M.C., Locklin,R., Morriss-Kay,G.M., and Lonai,P. (2004). A gain-of-function mutation of Fgfr2c demonstrates the roles of this receptor variant in osteogenesis. Proc. Natl. Acad. Sci. U. S. A *101*, 12555-12560.

Eswarakumar,V.P., Lax,I., and Schlessinger,J. (2005). Cellular signaling by fibroblast growth factor receptors. Cytokine Growth Factor Rev. *16*, 139-149.

Eswarakumar,V.P., Monsonego-Ornan,E., Pines,M., Antonopoulou,I., Morriss-Kay,G.M., and Lonai,P. (2002). The IIIc alternative of Fgfr2 is a positive regulator of bone formation. Development *129*, 3783-3793.

Eswarakumar,V.P., Ozcan,F., Lew,E.D., Bae,J.H., Tome,F., Booth,C.J., Adams,D.J., Lax,I., and Schlessinger,J. (2006). Attenuation of signaling pathways stimulated by pathologically activated FGF-receptor 2 mutants prevents craniosynostosis. Proc. Natl. Acad. Sci. U. S. A *103*, 18603-18608.

Filvaroff,E., Erlebacher,A., Ye,J., Gitelman,S.E., Lotz,J., Heillman,M., and Derynck,R. (1999). Inhibition of TGF-beta receptor signaling in osteoblasts leads to decreased bone remodeling and increased trabecular bone mass. Development *126*, 4267-4279.

Fragale,A., Tartaglia,M., Bernardini,S., Di Stasi,A.M., Di Rocco,C., Velardi,F., Teti,A., Battaglia,P.A., and Migliaccio,S. (1999). Decreased proliferation and altered differentiation in osteoblasts from genetically and clinically distinct craniosynostotic disorders. Am. J Pathol. *154*, 1465-1477.

Fremin,C., Ezan,F., Boisselier,P., Bessard,A., Pages,G., Pouyssegur,J., and Baffet,G. (2007). ERK2 but not ERK1 plays a key role in hepatocyte replication: An RNAi-mediated ERK2 knockdown approach in wild-type and ERK1 null hepatocytes. Hepatology *45*, 1035-1045.

Fromigue,O., Modrowski,D., and Marie,P.J. (2005). Apoptosis in membranous bone formation: role of fibroblast growth factor and bone morphogenetic protein signaling. Crit Rev. Eukaryot. Gene Expr. *15*, 75-92.

Fujita,T., Azuma,Y., Fukuyama,R., Hattori,Y., Yoshida,C., Koida,M., Ogita,K., and Komori,T. (2004). Runx2 induces osteoblast and chondrocyte differentiation and enhances their migration by coupling with PI3K-Akt signaling. J. Cell Biol. *166*, 85-95.

Funato,N., Ohtani,K., Ohyama,K., Kuroda,T., and Nakamura,M. (2001). Common regulation of growth arrest and differentiation of osteoblasts by helix-loop-helix factors. Mol. Cell Biol. *21*, 7416-7428.

Gaudenz,K., Roessler,E., Vainikka,S., Alitalo,K., and Muenke,M. (1998). Analysis of patients with craniosynostosis syndromes for a pro246Arg mutation of FGFR4. Mol. Genet. Metab *64*, 76-79.

Ghayor,C., Rey,A., and Caverzasio,J. (2005). Prostaglandin-dependent activation of ERK mediates cell proliferation induced by transforming growth factor beta in mouse osteoblastic cells. Bone *36*, 93-100.

Gong,Y., Cui,L., and Minuk,G.Y. (1996). Comparison of glyceraldehyde-3-phosphate dehydrogenase and 28s-ribosomal RNA gene expression in human hepatocellular carcinoma. Hepatology *23*, 734-737.

Goriely,A., McVean,G.A., Rojmyr,M., Ingemarsson,B., and Wilkie,A.O. (2003). Evidence for selective advantage of pathogenic FGFR2 mutations in the male germ line. Science *301*, 643-646.

Gosain,A.K., Recinos,R.F., Agresti,M., and Khanna,A.K. (2004). TGF-beta1, FGF-2, and receptor mRNA expression in suture mesenchyme and dura versus underlying brain in fusing and nonfusing mouse cranial sutures. Plast. Reconstr. Surg. *113*, 1675-1684.

Govindarajan,V. and Overbeek,P.A. (2006). FGF9 can induce endochondral ossification in cranial mesenchyme. BMC. Dev. Biol. *6*, 7.

Grammer,T.C. and Blenis,J. (1997). Evidence for MEK-independent pathways regulating the prolonged activation of the ERK-MAP kinases. Oncogene *14*, 1635-1642.

Grothe,C. and Timmer,M. (2007). The physiological and pharmacological role of basic fibroblast growth factor in the dopaminergic nigrostriatal system. Brain Res. Rev. *54*, 80-91.

Guimond,S.E. and Turnbull,J.E. (1999). Fibroblast growth factor receptor signalling is dictated by specific heparan sulphate saccharides. Curr. Biol. *9*, 1343-1346.

Hadari,Y.R., Gotoh,N., Kouhara,H., Lax,I., and Schlessinger,J. (2001). Critical role for the docking-protein FRS2 alpha in FGF receptor-mediated signal transduction pathways. Proc. Natl. Acad. Sci. U. S. A *98*, 8578-8583.

Hajihosseini,M.K., Duarte,R., Pegrum,J., Donjacour,A., Lana-Elola,E., Rice,D.P., Sharpe,J., and Dickson,C. (2008). Evidence that Fgf10 contributes to the skeletal and visceral defects of an apert syndrome mouse model. Dev. Dyn.

Hall,B.K. (1981). The induction of neural crest-derived cartilage and bone by embryonic epithelia: an analysis of the mode of action of an epithelial-mesenchymal interaction. J Embryol. Exp. Morphol. *64*, 305-320.

Hara,M.R. and Snyder,S.H. (2006). Nitric Oxide-GAPDH-Siah: A Novel Cell Death Cascade. Cell Mol. Neurobiol.

Harada,H., Tagashira,S., Fujiwara,M., Ogawa,S., Katsumata,T., Yamaguchi,A., Komori,T., and Nakatsuka,M. (1999). Cbfa1 isoforms exert functional differences in osteoblast differentiation. J. Biol. Chem. *274*, 6972-6978.

Harmer,N.J. (2006). Insights into the role of heparan sulphate in fibroblast growth factor signalling. Biochem. Soc. Trans. *34*, 442-445.

Hatch,N.E., Hudson,M., Seto,M.L., Cunningham,M.C., and Bothwell,M. (2006). Intracellular retention, degradation and signaling of glycosylation deficient FGFR2 and craniosynostosis syndrome associated FGFR2C278F. J. Biol. Chem.

Hoefkens,M.F., Vermeij-Keers,C., and Vaandrager,J.M. (2004). Crouzon syndrome: phenotypic signs and symptoms of the postnatally expressed subtype. J. Craniofac. Surg. *15*, 233-240.

Hollway,G.E., Phillips,H.A., Ades,L.C., Haan,E.A., and Mulley,J.C. (1995). Localization of craniosynostosis Adelaide type to 4p16. Hum. Mol. Genet. *4*, 681-683.

Horowitz,J.C., Lee,D.Y., Waghray,M., Keshamouni,V.G., Thomas,P.E., Zhang,H., Cui,Z., and Thannickal,V.J. (2004). Activation of the pro-survival phosphatidylinositol 3-kinase/AKT pathway by transforming growth factor-beta1 in mesenchymal cells is mediated by p38 MAPK-dependent induction of an autocrine growth factor. J Biol. Chem. *279*, 1359-1367.

Hosokawa,R., Urata,M., Han,J., Zehnaly,A., Bringas,P., Jr., Nonaka,K., and Chai,Y. (2007). TGF-beta mediated Msx2 expression controls occipital somites-derived caudal region of skull development. Dev. Biol. *310*, 140-153.

Huang,W., Carlsen,B., Rudkin,G., Berry,M., Ishida,K., Yamaguchi,D.T., and Miller,T.A. (2004). Osteopontin is a negative regulator of proliferation and differentiation in MC3T3-E1 pre-osteoblastic cells. Bone *34*, 799-808.

Ignelzi,M.A., Jr., Wang,W., and Young,A.T. (2003). Fibroblast growth factors lead to increased Msx2 expression and fusion in calvarial sutures. J. Bone Miner. Res. *18*, 751-759.

Inman,G.J., Nicolas,F.J., Callahan,J.F., Harling,J.D., Gaster,L.M., Reith,A.D., Laping,N.J., and Hill,C.S. (2002). SB-431542 is a potent and specific inhibitor of transforming growth factor-beta superfamily type I activin receptor-like kinase (ALK) receptors ALK4, ALK5, and ALK7. Mol. Pharmacol. *62*, 65-74.

Iseki,S., Wilkie,A.O., Heath,J.K., Ishimaru,T., Eto,K., and Morriss-Kay,G.M. (1997). Fgfr2 and osteopontin domains in the developing skull vault are mutually exclusive and can be altered by locally applied FGF2. Development *124*, 3375-3384.

Iseki,S., Wilkie,A.O., and Morriss-Kay,G.M. (1999). Fgfr1 and Fgfr2 have distinct differentiation- and proliferation-related roles in the developing mouse skull vault. Development *126*, 5611-5620.

Ito,Y. and Miyazono,K. (2003). RUNX transcription factors as key targets of TGF-beta superfamily signaling. Curr. Opin. Genet. Dev. *13*, 43-47.

Itoh,N. and Ornitz,D.M. (2004). Evolution of the Fgf and Fgfr gene families. Trends Genet. *20*, 563-569.

Jabs,E.W., Li,X., Scott,A.F., Meyers,G., Chen,W., Eccles,M., Mao,J.I., Charnas,L.R., Jackson,C.E., and Jaye,M. (1994). Jackson-Weiss and Crouzon syndromes are allelic with mutations in fibroblast growth factor receptor 2. Nat. Genet. *8*, 275-279.

Jabs,E.W., Muller,U., Li,X., Ma,L., Luo,W., Haworth,I.S., Klisak,I., Sparkes,R., Warman,M.L., Mulliken,J.B., and . (1993). A mutation in the homeodomain of the human MSX2 gene in a family affected with autosomal dominant craniosynostosis. Cell *75*, 443-450.

Jackson,A., Friedman,S., Zhan,X., Engleka,K.A., Forough,R., and Maciag,T. (1992). Heat shock induces the release of fibroblast growth factor 1 from NIH 3T3 cells. Proc. Natl. Acad. Sci. U. S. A *89*, 10691-10695.

Jackson,R.A., Nurcombe,V., and Cool,S.M. (2006). Coordinated fibroblast growth factor and heparan sulfate regulation of osteogenesis. Gene *379*, 79-91.

Janssens,K., ten Dijke,P., Janssens,S., and Van Hul,W. (2005). TGF-{beta}1 to the bone. Endocr. Rev.

Jenkins,D., Seelow,D., Jehee,F.S., Perlyn,C.A., Alonso,L.G., Bueno,D.F., Donnai,D., Josifova,D., Mathijssen,I.M., Morton,J.E., Orstavik,K.H., Sweeney,E., Wall,S.A., Marsh,J.L., Nurnberg,P., Passos-Bueno,M.R., and Wilkie,A.O. (2007). RAB23 mutations in Carpenter syndrome imply an unexpected role for hedgehog signaling in cranial-suture development and obesity. Am. J Hum. Genet. *80*, 1162-1170.

Jiang,X., Iseki,S., Maxson,R.E., Sucov,H.M., and Morriss-Kay,G.M. (2002). Tissue origins and interactions in the mammalian skull vault. Dev. Biol. *241*, 106-116.

Johnson,D., Iseki,S., Wilkie,A.O., and Morriss-Kay,G.M. (2000). Expression patterns of Twist and Fgfr1, -2 and -3 in the developing mouse coronal suture suggest a key role for twist in suture initiation and biogenesis. Mech. Dev. *91*, 341-345.

Johnson,P.T., Chen,J.K., Loeys,B.L., Dietz,H.C., and Fishman,E.K. (2007). Loeys-Dietz syndrome: MDCT angiography findings. AJR Am. J Roentgenol. *189*, W29-W35.

Kapur,S., Baylink,D.J., and Lau,K.H. (2003). Fluid flow shear stress stimulates human osteoblast proliferation and differentiation through multiple interacting and competing signal transduction pathways. Bone *32*, 241-251.

Karsdal,M.A., Fjording,M.S., Foged,N.T., Delaisse,J.M., and Lochter,A. (2001). Transforming growth factor-beta-induced osteoblast elongation regulates osteoclastic bone resorption through a p38 mitogen-activated protein kinase- and matrix metalloproteinase-dependent pathway. J Biol. Chem. *276*, 39350-39358.

Karsenty,G., Ducy,P., Starbuck,M., Priemel,M., Shen,J., Geoffroy,V., and Amling,M. (1999). Cbfa1 as a regulator of osteoblast differentiation and function. Bone *25*, 107-108.

Katoh,Y. and Katoh,M. (2005). Comparative genomics on FGF7, FGF10, FGF22 orthologs, and identification of fgf25. Int. J. Mol. Med. *16*, 767-770.

Kawamura,N., Kugimiya,F., Oshima,Y., Ohba,S., Ikeda,T., Saito,T., Shinoda,Y., Kawasaki,Y., Ogata,N., Hoshi,K., Akiyama,T., Chen,W.S., Hay,N., Tobe,K., Kadowaki,T., Azuma,Y., Tanaka,S., Nakamura,K., Chung,U.I., and Kawaguchi,H. (2007). Akt1 in osteoblasts and osteoclasts controls bone remodeling. PLoS. ONE. *2*, e1058.

Kiefer,P., Acland,P., Pappin,D., Peters,G., and Dickson,C. (1994). Competition between nuclear localization and secretory signals determines the subcellular fate of a single CUG-initiated form of FGF3. EMBO J *13*, 4126-4136.

Kim,B.G., Kim,H.J., Park,H.J., Kim,Y.J., Yoon,W.J., Lee,S.J., Ryoo,H.M., and Cho,J.Y. (2006). Runx2 phosphorylation induced by fibroblast growth factor-2/protein kinase C pathways. Proteomics. *6*, 1166-1174.

Kim,H.J., Kim,J.H., Bae,S.C., Choi,J.Y., Kim,H.J., and Ryoo,H.M. (2003). The protein kinase C pathway plays a central role in the fibroblast growth factor-stimulated expression and transactivation activity of Runx2. J. Biol. Chem. *278*, 319-326.

Kim,H.J., Rice,D.P., Kettunen,P.J., and Thesleff,I. (1998). FGF-, BMP- and Shh-mediated signalling pathways in the regulation of cranial suture morphogenesis and calvarial bone development. Development *125*, 1241-1251.

Kitching,R., Qi,S., Li,V., Raouf,A., Vary,C.P., and Seth,A. (2002). Coordinate gene expression patterns during osteoblast maturation and retinoic acid treatment of MC3T3-E1 cells. J. Bone Miner. Metab *20*, 269-280.

Klint,P. and Claesson-Welsh,L. (1999). Signal transduction by fibroblast growth factor receptors. Front Biosci. *4*, D165-D177.

Kodama,H.A., Amagai,Y., Sudo,H., Kasai,S., and Yamamoto,S. (1981). Establishment of a clonal osteogenic cell line from newborn mouse calvaria. Japanese Journal of Oral Biology *23*, 899-901.

Kono,S.J., Oshima,Y., Hoshi,K., Bonewald,L.F., Oda,H., Nakamura,K., Kawaguchi,H., and Tanaka,S. (2006). Erk pathways negatively regulate matrix mineralization. Bone.

Kovalenko,D., Yang,X., Nadeau,R.J., Harkins,L.K., and Friesel,R. (2003). Sef inhibits fibroblast growth factor signaling by inhibiting FGFR1 tyrosine phosphorylation and subsequent ERK activation. J Biol. Chem. *278*, 14087-14091.

Kozawa,O., Takatsuki,K., Kotake,K., Yoneda,M., Oiso,Y., and Saito,H. (1989). Possible involvement of protein kinase C in proliferation and differentiation of osteoblast-like cells. FEBS Lett. *243*, 183-185.

Lai,C.F., Chaudhary,L., Fausto,A., Halstead,L.R., Ory,D.S., Avioli,L.V., and Cheng,S.L. (2001). Erk is essential for growth, differentiation, integrin expression, and cell function in human osteoblastic cells. J. Biol. Chem. *276*, 14443-14450.

Lai,C.F. and Cheng,S.L. (2002). Signal transductions induced by bone morphogenetic protein-2 and transforming growth factor-beta in normal human osteoblastic cells. J. Biol. Chem. *277*, 15514-15522.

Lajeunie,E., Heuertz,S., El,G., V, Martinovic,J., Renier,D., Le Merrer,M., and Bonaventure,J. (2006). Mutation screening in patients with syndromic craniosynostoses indicates that a limited number of recurrent FGFR2 mutations accounts for severe forms of Pfeiffer syndrome. Eur. J Hum. Genet. *14*, 289-298.

Lampasso,J.D., Chen,W., and Marzec,N. (2006). The expression profile of PKC isoforms during MC3T3-E1 differentiation. Int. J. Mol. Med. *17*, 1125-1131.

Lana-Elola,E., Rice,R., Grigoriadis,A.E., and Rice,D.P. (2007). Cell fate specification during calvarial bone and suture development. Dev. Biol. *311*, 335-346.

Laping,N.J., Grygielko,E., Mathur,A., Butter,S., Bomberger,J., Tweed,C., Martin,W., Fornwald,J., Lehr,R., Harling,J., Gaster,L., Callahan,J.F., and Olson,B.A. (2002). Inhibition of transforming growth factor (TGF)-beta1-induced extracellular matrix with a novel inhibitor of the TGF-beta type I receptor kinase activity: SB-431542. Mol. Pharmacol. *62*, 58-64.

Lee,K.S., Hong,S.H., and Bae,S.C. (2002). Both the Smad and p38 MAPK pathways play a crucial role in Runx2 expression following induction by transforming growth factor-beta and bone morphogenetic protein. Oncogene *21*, 7156-7163.

Lee,M.K., Pardoux,C., Hall,M.C., Lee,P.S., Warburton,D., Qing,J., Smith,S.M., and Derynck,R. (2007). TGF-beta activates Erk MAP kinase signalling through direct phosphorylation of ShcA. EMBO J *26*, 3957-3967.

Lee,M.S., Lowe,G.N., Strong,D.D., Wergedal,J.E., and Glackin,C.A. (1999). TWIST, a basic helix-loop-helix transcription factor, can regulate the human osteogenic lineage. J. Cell Biochem. *75*, 566-577.

Lee,S.W., Choi,K.Y., Cho,J.Y., Jung,S.H., Song,K.B., Park,E.K., Choi,J.Y., Shin,H.I., Kim,S.Y., Woo,K.M., Baek,J.H., Nam,S.H., Kim,Y.J., Kim,H.J., and Ryoo,H.M. (2006). TGF-beta2 stimulates cranial suture closure through activation of the Erk-MAPK pathway. J. Cell Biochem. *98*, 981-991.

Lefloch,R., Pouyssegur,J., and Lenormand,P. (2008). Single and combined silencing of ERK1 and ERK2 reveals their positive contribution to growth signaling depending on their expression levels. Mol. Cell Biol. *28*, 511-527.

Lemonnier,J., Hay,E., Delannoy,P., Fromigue,O., Lomri,A., Modrowski,D., and Marie,P.J. (2001). Increased osteoblast apoptosis in apert craniosynostosis: role of protein kinase C and interleukin-1. Am. J Pathol. *158*, 1833-1842.

Levine,J.P., Bradley,J.P., Roth,D.A., McCarthy,J.G., and Longaker,M.T. (1998). Studies in cranial suture biology: regional dura mater determines overlying suture biology. Plast. Reconstr. Surg. *101*, 1441-1447.

Li,J., Tan,J.Z., Chen,L.L., Zhang,J., Shen,X., Mei,C.L., Fu,L.L., Lin,L.P., Ding,J., Xiong,B., Xiong,X.S., Liu,H., Luo,X.M., and Jiang,H.L. (2006). Design, synthesis and antitumor evaluation of a new series of N-substituted-thiourea derivatives. Acta Pharmacol. Sin. *27*, 1259-1271.

Li,J., Tsuji,K., Komori,T., Miyazono,K., Wrana,J.L., Ito,Y., Nifuji,A., and Noda,M. (1998). Smad2 overexpression enhances Smad4 gene expression and suppresses CBFA1 gene expression in osteoblastic osteosarcoma ROS17/2.8 cells and primary rat calvaria cells. J Biol. Chem. *273*, 31009-31015.

Li,S., Quarto,N., and Longaker,M.T. (2007). Dura mater-derived FGF-2 mediates mitogenic signaling in calvarial osteoblasts. Am. J Physiol Cell Physiol *293*, C1834-C1842.

Liu,A., Li,J.Y., Bromleigh,C., Lao,Z., Niswander,L.A., and Joyner,A.L. (2003). FGF17b and FGF18 have different midbrain regulatory properties from FGF8b or activated FGF receptors. Development *130*, 6175-6185.

Liu,Z., Xu,J., Colvin,J.S., and Ornitz,D.M. (2002). Coordination of chondrogenesis and osteogenesis by fibroblast growth factor 18. Genes Dev. *16*, 859-869.

Loeys,B.L., Chen,J., Neptune,E.R., Judge,D.P., Podowski,M., Holm,T., Meyers,J., Leitch,C.C., Katsanis,N., Sharifi,N., Xu,F.L., Myers,L.A., Spevak,P.J., Cameron,D.E., De Backer,J., Hellemans,J., Chen,Y., Davis,E.C., Webb,C.L., Kress,W., Coucke,P., Rifkin,D.B., De Paepe,A.M., and Dietz,H.C. (2005). A syndrome of altered cardiovascular, craniofacial, neurocognitive and skeletal development caused by mutations in TGFBR1 or TGFBR2. Nat. Genet. *37*, 275-281.

Lou,Y., Javed,A., Hussain,S., Colby,J., Frederick,D., Pratap,J., Xie,R., Gaur,T., van Wijnen,A.J., Jones,S.N., Stein,G.S., Lian,J.B., and Stein,J.L. (2008). A Runx2 Threshold for the Cleidocranial Dysplasia Phenotype. Hum. Mol. Genet.

Lu,S., Gu,X., Hoestje,S., and Epner,D.E. (2002). Identification of an additional hypoxia responsive element in the glyceraldehyde-3-phosphate dehydrogenase gene promoter. Biochim. Biophys. Acta *1574*, 152-156.

MacArthur,C.A., Lawshe,A., Xu,J., Santos-Ocampo,S., Heikinheimo,M., Chellaiah,A.T., and Ornitz,D.M. (1995). FGF-8 isoforms activate receptor splice forms that are expressed in mesenchymal regions of mouse development. Development *121*, 3603-3613.

Mangasarian,K., Li,Y., Mansukhani,A., and Basilico,C. (1997). Mutation associated with Crouzon syndrome causes ligand-independent dimerization and activation of FGF receptor-2. J. Cell Physiol *172*, 117-125.

Mansukhani,A., Bellosta,P., Sahni,M., and Basilico,C. (2000). Signaling by fibroblast growth factors (FGF) and fibroblast growth factor receptor 2 (FGFR2)-activating mutations blocks mineralization and induces apoptosis in osteoblasts. J. Cell Biol. *149*, 1297-1308.

Mansur,N.R., Meyer-Siegler,K., Wurzer,J.C., and Sirover,M.A. (1993). Cell cycle regulation of the glyceraldehyde-3-phosphate dehydrogenase/uracil DNA glycosylase gene in normal human cells. Nucleic Acids Res. *21*, 993-998.

Marie,P.J., Coffin,J.D., and Hurley,M.M. (2005). FGF and FGFR signaling in chondrodysplasias and craniosynostosis. J. Cell Biochem. *96*, 888-896.

Mark,M.P., Butler,W.T., Prince,C.W., Finkelman,R.D., and Ruch,J.V. (1988). Developmental expression of 44-kDa bone phosphoprotein (osteopontin) and bone gamma-carboxyglutamic acid (Gla)-containing protein (osteocalcin) in calcifying tissues of rat. Differentiation *37*, 123-136.

Marucci,D.D., Dunaway,D.J., Jones,B.M., and Hayward,R.D. (2008). Raised intracranial pressure in Apert syndrome. Plast. Reconstr. Surg. *122*, 1162-1168.

Mathy,J.A., Lenton,K., Nacamuli,R.P., Fong,K.D., Song,H.M., Fang,T.D., Yang,G.P., and Longaker,M.T. (2003). FGF-2 stimulation affects calvarial osteoblast biology: quantitative analysis of nine genes important for cranial suture biology by real-time reverse transcription polymerase chain reaction. Plast. Reconstr. Surg. *112*, 528-539.

Mehrara,B.J., Most,D., Chang,J., Bresnick,S., Turk,A., Schendel,S.A., Gittes,G.K., and Longaker,M.T. (1999). Basic fibroblast growth factor and transforming growth factor beta-1 expression in the developing dura mater correlates with calvarial bone formation. Plast. Reconstr. Surg. *104*, 435-444.

Meran,S., Thomas,D.W., Stephens,P., Enoch,S., Martin,J., Steadman,R., and Phillips,A.O. (2008). Hyaluronan facilitates transforming growth factor-beta1-mediated fibroblast proliferation. J Biol. Chem. *283*, 6530-6545.

Meyer-Siegler,K., Rahman-Mansur,N., Wurzer,J.C., and Sirover,M.A. (1992). Proliferative dependent regulation of the glyceraldehyde-3-phosphate dehydrogenase/uracil DNA glycosylase gene in human cells. Carcinogenesis *13*, 2127-2132.

Meyers,G.A., Orlow,S.J., Munro,I.R., Przylepa,K.A., and Jabs,E.W. (1995). Fibroblast growth factor receptor 3 (FGFR3) transmembrane mutation in Crouzon syndrome with acanthosis nigricans. Nat. Genet. *11*, 462-464.

Migliaccio,S., Wetsel,W.C., Fox,W.M., Washburn,T.F., and Korach,K.S. (1993). Endogenous protein kinase-C activation in osteoblast-like cells modulates responsiveness to estrogen and estrogen receptor levels. Mol. Endocrinol. *7*, 1133-1143.

Mignatti,P., Morimoto,T., and Rifkin,D.B. (1992). Basic fibroblast growth factor, a protein devoid of secretory signal sequence, is released by cells via a pathway independent of the endoplasmic reticulum-Golgi complex. J Cell Physiol *151*, 81-93.

Miyazawa,K., Shinozaki,M., Hara,T., Furuya,T., and Miyazono,K. (2002). Two major Smad pathways in TGF-beta superfamily signalling. Genes Cells *7*, 1191-1204.

Mohammadi,M., McMahon,G., Sun,L., Tang,C., Hirth,P., Yeh,B.K., Hubbard,S.R., and Schlessinger,J. (1997). Structures of the tyrosine kinase domain of fibroblast growth factor receptor in complex with inhibitors. Science *276*, 955-960.

Moore,R., Ferretti,P., Copp,A., and Thorogood,P. (2002). Blocking endogenous FGF-2 activity prevents cranial osteogenesis. Dev. Biol. *243*, 99-114.

Morriss-Kay,G.M. and Wilkie,A.O. (2005). Growth of the normal skull vault and its alteration in craniosynostosis: insights from human genetics and experimental studies. J. Anat. *207*, 637-653.

Moss,M.L. (1958). Fusion of the frontal suture in the rat. Am. J. Anat. *102*, 141-165.

Moursi,A.M., Winnard,P.L., Winnard,A.V., Rubenstrunk,J.M., and Mooney,M.P. (2002). Fibroblast growth factor 2 induces increased calvarial osteoblast proliferation and cranial suture fusion. Cleft Palate Craniofac. J. *39*, 487-496.

Muenke,M., Gripp,K.W., McDonald-McGinn,D.M., Gaudenz,K., Whitaker,L.A., Bartlett,S.P., Markowitz,R.I., Robin,N.H., Nwokoro,N., Mulvihill,J.J., Losken,H.W., Mulliken,J.B., Guttmacher,A.E., Wilroy,R.S., Clarke,L.A., Hollway,G., Ades,L.C., Haan,E.A., Mulley,J.C., Cohen,M.M., Jr., Bellus,G.A., Francomano,C.A., Moloney,D.M., Wall,S.A., Wilkie,A.O., and . (1997). A unique point mutation in the fibroblast growth factor receptor 3 gene (FGFR3) defines a new craniosynostosis syndrome. Am. J. Hum. Genet. *60*, 555-564.

Mukherjee,A., Dong,S.S., Clemens,T., Alvarez,J., and Serra,R. (2005). Co-ordination of TGF-beta and FGF signaling pathways in bone organ cultures. Mech. Dev. *122*, 557-571.

Nakayama,K., Satoh,T., Igari,A., Kageyama,R., and Nishida,E. (2008). FGF induces oscillations of Hes1 expression and Ras/ERK activation. Curr. Biol. *18*, R332-R334.

Noda,M. (1989). Transcriptional regulation of osteocalcin production by transforming growth factor-beta in rat osteoblast-like cells. Endocrinology *124*, 612-617.

Noda,M. and Vogel,R. (1989). Fibroblast growth factor enhances type beta 1 transforming growth factor gene expression in osteoblast-like cells. J Cell Biol. *109*, 2529-2535.

Noda,M., Yoon,K., Prince,C.W., Butler,W.T., and Rodan,G.A. (1988). Transcriptional regulation of osteopontin production in rat osteosarcoma cells by type beta transforming growth factor. J Biol. Chem. *263*, 13916-13921.

Ogle,R.C., Tholpady,S.S., McGlynn,K.A., and Ogle,R.A. (2004). Regulation of cranial suture morphogenesis. Cells Tissues. Organs *176*, 54-66.

Ohbayashi,N., Shibayama,M., Kurotaki,Y., Imanishi,M., Fujimori,T., Itoh,N., and Takada,S. (2002). FGF18 is required for normal cell proliferation and differentiation during osteogenesis and chondrogenesis. Genes Dev. *16*, 870-879.

Olsen,S.K., Garbi,M., Zampieri,N., Eliseenkova,A.V., Ornitz,D.M., Goldfarb,M., and Mohammadi,M. (2003). Fibroblast growth factor (FGF) homologous factors share structural but not functional homology with FGFs. J Biol. Chem. *278*, 34226-34236.

Opperman,L.A. (2000). Cranial sutures as intramembranous bone growth sites. Dev. Dyn. *219*, 472-485.

Opperman,L.A., Adab,K., and Gakunga,P.T. (2000). Transforming growth factor-beta 2 and TGF-beta 3 regulate fetal rat cranial suture morphogenesis by regulating rates of cell proliferation and apoptosis. Dev. Dyn. *219*, 237-247.

Opperman,L.A., Chhabra,A., Cho,R.W., and Ogle,R.C. (1999). Cranial suture obliteration is induced by removal of transforming growth factor (TGF)-beta 3 activity and prevented by removal of TGF-beta 2 activity from fetal rat calvaria in vitro. J. Craniofac. Genet. Dev. Biol. *19*, 164-173.

Opperman,L.A., Fernandez,C.R., So,S., and Rawlins,J.T. (2006). Erk1/2 signaling is required for Tgf-beta2-induced suture closure. Dev. Dyn. *235*, 1292-1299.

Opperman,L.A., Galanis,V., Williams,A.R., and Adab,K. (2002a). Transforming growth factor-beta3 (Tgf-beta3) down-regulates Tgf-beta3 receptor type I (Tbetar-I) during rescue of cranial sutures from osseous obliteration. Orthod. Craniofac. Res. *5*, 5-16.

Opperman,L.A., Moursi,A.M., Sayne,J.R., and Wintergerst,A.M. (2002b). Transforming growth factor-beta 3(Tgf-beta3) in a collagen gel delays fusion of the rat posterior interfrontal suture in vivo. Anat. Rec. *267*, 120-130.

Opperman,L.A., Nolen,A.A., and Ogle,R.C. (1997). TGF-beta 1, TGF-beta 2, and TGF-beta 3 exhibit distinct patterns of expression during cranial suture formation and obliteration in vivo and in vitro. J. Bone Miner. Res. *12*, 301-310.

Opperman,L.A., Sweeney,T.M., Redmon,J., Persing,J.A., and Ogle,R.C. (1993). Tissue interactions with underlying dura mater inhibit osseous obliteration of developing cranial sutures. Dev. Dyn. *198*, 312-322.

Ornitz,D.M. and Itoh,N. (2001). Fibroblast growth factors. Genome Biol. *2*, REVIEWS3005.

Ornitz,D.M. and Marie,P.J. (2002). FGF signaling pathways in endochondral and intramembranous bone development and human genetic disease. Genes Dev. *16*, 1446-1465.

Ornitz,D.M., Xu,J., Colvin,J.S., McEwen,D.G., MacArthur,C.A., Coulier,F., Gao,G., and Goldfarb,M. (1996). Receptor specificity of the fibroblast growth factor family. J. Biol. Chem. *271*, 15292-15297.

Orr-Urtreger,A., Bedford,M.T., Burakova,T., Arman,E., Zimmer,Y., Yayon,A., Givol,D., and Lonai,P. (1993). Developmental localization of the splicing alternatives of fibroblast growth factor receptor-2 (FGFR2). Dev. Biol. *158*, 475-486.

Ortiz,J., Harris,H.W., Guitart,X., Terwilliger,R.Z., Haycock,J.W., and Nestler,E.J. (1995). Extracellular signal-regulated protein kinases (ERKs) and ERK kinase (MEK) in brain: regional distribution and regulation by chronic morphine. J Neurosci. *15*, 1285-1297.

Otto,F., Thornell,A.P., Crompton,T., Denzel,A., Gilmour,K.C., Rosewell,I.R., Stamp,G.W., Beddington,R.S., Mundlos,S., Olsen,B.R., Selby,P.B., and Owen,M.J. (1997). Cbfa1, a candidate gene for cleidocranial dysplasia syndrome, is essential for osteoblast differentiation and bone development. Cell *89*, 765-771.

Park,E.R., Eblen,S.T., and Catling,A.D. (2007). MEK1 activation by PAK: A novel mechanism. Cell Signal. *19*, 1488-1496.

Partanen,J. (2007). FGF signalling pathways in development of the midbrain and anterior hindbrain. J Neurochem. *101*, 1185-1193.

Passos-Bueno,M.R., Serti Eacute,A.E., Jehee,F.S., Fanganiello,R., and Yeh,E. (2008). Genetics of craniosynostosis: genes, syndromes, mutations and genotype-phenotype correlations. Front Oral Biol. *12*, 107-143.

Passos-Bueno,M.R., Sertie,A.L., Richieri-Costa,A., Alonso,L.G., Zatz,M., Alonso,N., Brunoni,D., and Ribeiro,S.F. (1998). Description of a new mutation and characterization of FGFR1, FGFR2, and FGFR3 mutations among Brazilian patients with syndromic craniosynostoses. Am. J Med Genet. *78*, 237-241.

Paterson,J.L., Li,Z., Wen,X.Y., Masih-Khan,E., Chang,H., Pollett,J.B., Trudel,S., and Stewart,A.K. (2004). Preclinical studies of fibroblast growth factor receptor 3 as a therapeutic target in multiple myeloma. Br. J Haematol. *124*, 595-603.

Perizonius,W.R.K. (1984). Closing and non-closing sutures in 256 crania of known age and sex from Amsterdam. Journal of Human Evolution *13*, 201-216.

Perlyn,C.A., Morriss-Kay,G., Darvann,T., Tenenbaum,M., and Ornitz,D.M. (2006). A model for the pharmacological treatment of crouzon syndrome. Neurosurgery *59*, 210-215.

Peterson,W.J., Tachiki,K.H., and Yamaguchi,D.T. (2004). Serial passage of MC3T3-E1 cells down-regulates proliferation during osteogenesis in vitro. Cell Prolif. *37*, 325-336.

Petiot, A. Fibroblast growth factors and skeletogenesis. 2001.
Ref Type: Thesis/Dissertation

Petiot,A., Ferretti,P., Copp,A.J., and Chan,C.T. (2002). Induction of chondrogenesis in neural crest cells by mutant fibroblast growth factor receptors. Dev. Dyn. *224*, 210-221.

Pfeiffer,R.A. (1964). [DOMINANT HEREDITARY ACROCEPHALOSYNDACTYLIA.]. Z. Kinderheilkd. *90*, 301-320.

Piotrowicz,R.S., Martin,J.L., Dillman,W.H., and Levin,E.G. (1997). The 27-kDa heat shock protein facilitates basic fibroblast growth factor release from endothelial cells. J Biol. Chem. *272*, 7042-7047.

Poisson,E., Sciote,J.J., Koepsel,R., Cooper,G.M., Opperman,L.A., and Mooney,M.P. (2004). Transforming growth factor-beta isoform expression in the perisutural tissues of craniosynostotic rabbits. Cleft Palate Craniofac. J *41*, 392-402.

Pouyssegur,J. and Lenormand,P. (2003). Fidelity and spatio-temporal control in MAP kinase (ERKs) signalling. Eur. J Biochem. *270*, 3291-3299.

Powers,C.J., McLeskey,S.W., and Wellstein,A. (2000). Fibroblast growth factors, their receptors and signaling. Endocr. Relat Cancer *7*, 165-197.

Prince,M., Banerjee,C., Javed,A., Green,J., Lian,J.B., Stein,G.S., Bodine,P.V., and Komm,B.S. (2001). Expression and regulation of Runx2/Cbfa1 and osteoblast phenotypic markers during the growth and differentiation of human osteoblasts. J. Cell Biochem. *80*, 424-440.

Przylepa,K.A., Paznekas,W., Zhang,M., Golabi,M., Bias,W., Bamshad,M.J., Carey,J.C., Hall,B.D., Stevenson,R., Orlow,S., Cohen,M.M., Jr., and Jabs,E.W. (1996). Fibroblast growth factor receptor 2 mutations in Beare-Stevenson cutis gyrata syndrome. Nat. Genet. *13*, 492-494.

Pungchanchaikul, P. Palatal bone formation is regulated by palatal shelf fusion. 2008.
Ref Type: Thesis/Dissertation

Ratisoontorn,C., Fan,G.F., McEntee,K., and Nah,H.D. (2003). Activating (P253R, C278F) and dominant negative mutations of FGFR2: differential effects on calvarial bone cell proliferation, differentiation, and mineralization. Connect. Tissue Res. *44 Suppl 1*, 292-297.

Raucci,A., Bellosta,P., Grassi,R., Basilico,C., and Mansukhani,A. (2008). Osteoblast proliferation or differentiation is regulated by relative strengths of opposing signaling pathways. J Cell Physiol *215*, 442-451.

Rawlins,J.T. and Opperman,L.A. (2008). Tgf-beta regulation of suture morphogenesis and growth. Front Oral Biol. *12*, 178-196.

Raybaud,C. and Di Rocco,C. (2007). Brain malformation in syndromic craniosynostoses, a primary disorder of white matter: a review. Childs Nerv. Syst. *23*, 1379-1388.

Reardon,W., Winter,R.M., Rutland,P., Pulleyn,L.J., Jones,B.M., and Malcolm,S. (1994). Mutations in the fibroblast growth factor receptor 2 gene cause Crouzon syndrome. Nat. Genet. *8*, 98-103.

Reilly,J.F., Mizukoshi,E., and Maher,P.A. (2004). Ligand dependent and independent internalization and nuclear translocation of fibroblast growth factor (FGF) receptor 1. DNA Cell Biol. *23*, 538-548.

Reinhold,M.I. and Naski,M.C. (2007). Direct interactions of Runx2 and canonical Wnt signaling induce FGF18. J Biol. Chem. *282*, 3653-3663.

Renier,D., Lajeunie,E., Arnaud,E., and Marchac,D. (2000). Management of craniosynostoses. Childs Nerv. Syst. *16*, 645-658.

Reuss,B. and Bohlen und,H.O. (2003). Fibroblast growth factors and their receptors in the central nervous system. Cell Tissue Res. *313*, 139-157.

Reyes-Botella,C., Vallecillo-Capilla,M.F., and Ruiz,C. (2002). Effect of different growth factors on human cultured osteoblast-like cells. Cell Physiol Biochem. *12*, 353-358.

Rice,D.P., Aberg,T., Chan,Y., Tang,Z., Kettunen,P.J., Pakarinen,L., Maxson,R.E., and Thesleff,I. (2000). Integration of FGF and TWIST in calvarial bone and suture development. Development *127*, 1845-1855.

Rice,D.P., Rice,R., and Thesleff,I. (2003). Fgfr mRNA isoforms in craniofacial bone development. Bone *33*, 14-27.

Roberts,E.C., Hammond,K., Traish,A.M., Resing,K.A., and Ahn,N.G. (2006). Identification of G2/M targets for the MAP kinase pathway by functional proteomics. Proteomics. *6*, 4541-4553.

Robertson,S.C., Meyer,A.N., Hart,K.C., Galvin,B.D., Webster,M.K., and Donoghue,D.J. (1998). Activating mutations in the extracellular domain of the fibroblast growth factor receptor 2 function by disruption of the disulfide bond in the third immunoglobulin-like domain. Proc. Natl. Acad. Sci. U. S. A *95*, 4567-4572.

Roth,D.A., Bradley,J.P., Levine,J.P., McMullen,H.F., McCarthy,J.G., and Longaker,M.T. (1996). Studies in cranial suture biology: part II. Role of the dura in cranial suture fusion. Plast. Reconstr. Surg. *97*, 693-699.

Sabatini,M., Lesur,C., Pacherie,M., Pastoureau,P., Kucharczyk,N., Fauchere,J.L., and Bonnet,J. (1996). Effects of parathyroid hormone and agonists of the adenylyl cyclase and protein kinase C pathways on bone cell proliferation. Bone *18*, 59-65.

Sadler,T.W. (2004). Langman's Medical Embryology. Lippincott Williams & Wilkins).

Sahni,D., Jit,I., Neelam, and Sanjeev (2005). Time of closure of cranial sutures in northwest Indian adults. Forensic Sci. Int. *148*, 199-205.

Sahni,M., Ambrosetti,D.C., Mansukhani,A., Gertner,R., Levy,D., and Basilico,C. (1999). FGF signaling inhibits chondrocyte proliferation and regulates bone development through the STAT-1 pathway. Genes Dev. *13*, 1361-1366.

Sanford,L.P., Ormsby,I., Gittenberger-de Groot,A.C., Sariola,H., Friedman,R., Boivin,G.P., Cardell,E.L., and Doetschman,T. (1997). TGFbeta2 knockout mice have multiple developmental defects that are non-overlapping with other TGFbeta knockout phenotypes. Development *124*, 2659-2670.

Santos-Ruiz,L., Mowatt,D.J., Marguerie,A., Tukiainen,D., Kellomaki,M., Tormala,P., Suokas,E., Arstila,H., Ashammakhi,N., and Ferretti,P. (2007). Potential use of craniosynostotic osteoprogenitors and bioactive scaffolds for bone engineering. J Tissue Eng Regen Med *1*, 199-210.

Sasaki,T., Ito,Y., Bringas,P., Jr., Chou,S., Urata,M.M., Slavkin,H., and Chai,Y. (2006). TGF{beta}-mediated FGF signaling is crucial for regulating cranial neural crest cell proliferation during frontal bone development. Development *133*, 371-381.

Savage,C., Das,P., Finelli,A.L., Townsend,S.R., Sun,C.Y., Baird,S.E., and Padgett,R.W. (1996). Caenorhabditis elegans genes sma-2, sma-3, and sma-4 define a conserved family of transforming growth factor beta pathway components. Proc. Natl. Acad. Sci. U. S. A *93*, 790-794.

Schmierer,B. and Hill,C.S. (2007). TGFbeta-SMAD signal transduction: molecular specificity and functional flexibility. Nat. Rev. Mol. Cell Biol. *8*, 970-982.

Schoorlemmer,J. and Goldfarb,M. (2001). Fibroblast growth factor homologous factors are intracellular signaling proteins. Curr. Biol. *11*, 793-797.

Sekelsky,J.J., Newfeld,S.J., Raftery,L.A., Chartoff,E.H., and Gelbart,W.M. (1995). Genetic characterization and cloning of mothers against dpp, a gene required for decapentaplegic function in Drosophila melanogaster. Genetics *139*, 1347-1358.

Selvamurugan,N., Kwok,S., Alliston,T., Reiss,M., and Partridge,N.C. (2004). Transforming growth factor-beta 1 regulation of collagenase-3 expression in osteoblastic cells by cross-talk between the Smad and MAPK signaling pathways and their components, Smad2 and Runx2. J. Biol. Chem. *279*, 19327-19334.

Shapiro,H.S., Chen,J., Wrana,J.L., Zhang,Q., Blum,M., and Sodek,J. (1993). Characterization of porcine bone sialoprotein: primary structure and cellular expression. Matrix *13*, 431-440.

Sher,S., Cole,P., Kaufman,Y., Hatef,D.A., and Hollier,L. (2008). Craniosynostotic variations in syndromic, identical twins. Ann. Plast. Surg. *61*, 290-293.

Shi,Y. and Massague,J. (2003). Mechanisms of TGF-beta signaling from cell membrane to the nucleus. Cell *113*, 685-700.

Shotelersuk,V., Mahatumarat,C., Ittiwut,C., Rojvachiranonda,N., Srivuthana,S., Wacharasindhu,S., and Tongkobpetch,S. (2003). FGFR2 mutations among Thai children with Crouzon and Apert syndromes. J. Craniofac. Surg. *14*, 101-104.

Sirover,M.A. (1997). Role of the glycolytic protein, glyceraldehyde-3-phosphate dehydrogenase, in normal cell function and in cell pathology. J. Cell Biochem. *66*, 133-140.

Sodek,J., Chen,J., Nagata,T., Kasugai,S., Todescan,R., Jr., Li,I.W., and Kim,R.H. (1995). Regulation of osteopontin expression in osteoblasts. Ann. N. Y. Acad. Sci. *760*, 223-241.

Song,K., Wang,H., Krebs,T.L., and Danielpour,D. (2006). Novel roles of Akt and mTOR in suppressing TGF-beta/ALK5-mediated Smad3 activation. EMBO J. *25*, 58-69.

Sood,S., Eldadah,Z.A., Krause,W.L., McIntosh,I., and Dietz,H.C. (1996). Mutation in fibrillin-1 and the Marfanoid-craniosynostosis (Shprintzen-Goldberg) syndrome. Nat. Genet. *12*, 209-211.

Sorensen,V., Nilsen,T., and Wiedlocha,A. (2006a). Functional diversity of FGF-2 isoforms by intracellular sorting. Bioessays *28*, 504-514.

Sorensen,V., Wiedlocha,A., Haugsten,E.M., Khnykin,D., Wesche,J., and Olsnes,S. (2006b). Different abilities of the four FGFRs to mediate FGF-1 translocation are linked to differences in the receptor C-terminal tail. J Cell Sci. *119*, 4332-4341.

Sowa,H., Kaji,H., Yamaguchi,T., Sugimoto,T., and Chihara,K. (2002). Activations of ERK1/2 and JNK by transforming growth factor beta negatively regulate Smad3-induced alkaline phosphatase activity and mineralization in mouse osteoblastic cells. J. Biol. Chem. *277*, 36024-36031.

Spector,J.A., Mathy,J.A., Warren,S.M., Nacamuli,R.P., Song,H.M., Lenton,K., Fong,K.D., Fang,D.T., and Longaker,M.T. (2005). FGF-2 acts through an ERK1/2 intracellular pathway to affect osteoblast differentiation. Plast. Reconstr. Surg. *115*, 838-852.

Spinella-Jaegle,S., Roman-Roman,S., Faucheu,C., Dunn,F.W., Kawai,S., Gallea,S., Stiot,V., Blanchet,A.M., Courtois,B., Baron,R., and Rawadi,G. (2001). Opposite effects of bone morphogenetic protein-2 and transforming growth factor-beta1 on osteoblast differentiation. Bone *29*, 323-330.

Spivak-Kroizman,T., Lemmon,M.A., Dikic,I., Ladbury,J.E., Pinchasi,D., Huang,J., Jaye,M., Crumley,G., Schlessinger,J., and Lax,I. (1994). Heparin-induced oligomerization of FGF molecules is responsible for FGF receptor dimerization, activation, and cell proliferation. Cell *79*, 1015-1024.

Stachowiak,M.K., Fang,X., Myers,J.M., Dunham,S.M., Berezney,R., Maher,P.A., and Stachowiak,E.K. (2003). Integrative nuclear FGFR1 signaling (INFS) as a part of a universal "feed-forward-and-gate" signaling module that controls cell growth and differentiation. J Cell Biochem. *90*, 662-691.

Stein,G.S., Lian,J.B., and Owen,T.A. (1990). Relationship of cell growth to the regulation of tissue-specific gene expression during osteoblast differentiation. FASEB J *4*, 3111-3123.

Sudo,H., Kodama,H.A., Amagai,Y., Yamamoto,S., and Kasai,S. (1983). In vitro differentiation and calcification in a new clonal osteogenic cell line derived from newborn mouse calvaria. J. Cell Biol. *96*, 191-198.

Sugiura,N., Suga,T., Ozeki,Y., Mamiya,G., and Takishima,K. (1997). The mouse extracellular signal-regulated kinase 2 gene. Gene structure and characterization of the promoter. J Biol. Chem. *272*, 21575-21581.

Sugiura,N. and Takishima,K. (2000). Regulation of the gene promoter for extracellular signal-regulated protein kinase 2 by transcription factors NF-Y and Sp3. Biochem. J *347 Pt 1*, 155-161.

Suzuki,A., Guicheux,J., Palmer,G., Miura,Y., Oiso,Y., Bonjour,J.P., and Caverzasio,J. (2002a). Evidence for a role of p38 MAP kinase in expression of alkaline phosphatase during osteoblastic cell differentiation. Bone *30*, 91-98.

Suzuki,A., Palmer,G., Bonjour,J.P., and Caverzasio,J. (1999). Regulation of alkaline phosphatase activity by p38 MAP kinase in response to activation of Gi protein-coupled receptors by epinephrine in osteoblast-like cells. Endocrinology *140*, 3177-3182.

Suzuki,T., Tsuzuku,J., Ajima,R., Nakamura,T., Yoshida,Y., and Yamamoto,T. (2002b). Phosphorylation of three regulatory serines of Tob by Erk1 and Erk2 is required for Ras-mediated cell proliferation and transformation. Genes Dev. *16*, 1356-1370.

Tamburrini,G., Caldarelli,M., Massimi,L., Santini,P., and Di Rocco,C. (2005). Intracranial pressure monitoring in children with single suture and complex craniosynostosis: a review. Childs Nerv. Syst.

Tang,C.H., Yang,R.S., Chen,Y.F., and Fu,W.M. (2007). Basic fibroblast growth factor stimulates fibronectin expression through phospholipase C gamma, protein kinase C alpha, c-Src, NF-kappaB, and p300 pathway in osteoblasts. J Cell Physiol *211*, 45-55.

Tavormina,P.L., Shiang,R., Thompson,L.M., Zhu,Y.Z., Wilkin,D.J., Lachman,R.S., Wilcox,W.R., Rimoin,D.L., Cohn,D.H., and Wasmuth,J.J. (1995). Thanatophoric dysplasia (types I and II) caused by distinct mutations in fibroblast growth factor receptor 3. Nat. Genet. *9*, 321-328.

ten Dijke,P. and Hill,C.S. (2004). New insights into TGF-beta-Smad signalling. Trends Biochem. Sci. *29*, 265-273.

Todaro,G.J. and Green,H. (1963). Quantitative studies of the growth of mouse embryo cells in culture and their development into established lines. J Cell Biol. *17*, 299-313.

Tokuda,H., Hirade,K., Wang,X., Oiso,Y., and Kozawa,O. (2003). Involvement of SAPK/JNK in basic fibroblast growth factor-induced vascular endothelial growth factor release in osteoblasts. J Endocrinol. *177*, 101-107.

Trainor,P.A. (2005). Specification of neural crest cell formation and migration in mouse embryos. Semin. Cell Dev. Biol. *16*, 683-693.

Tuite,G.F., Chong,W.K., Evanson,J., Narita,A., Taylor,D., Harkness,W.F., Jones,B.M., and Hayward,R.D. (1996). The effectiveness of papilledema as an indicator of raised intracranial pressure in children with craniosynostosis. Neurosurgery *38*, 272-278.

Twigg,S.R., Matsumoto,K., Kidd,A.M., Goriely,A., Taylor,I.B., Fisher,R.B., Hoogeboom,A.J., Mathijssen,I.M., Lourenco,M.T., Morton,J.E., Sweeney,E., Wilson,L.C., Brunner,H.G., Mulliken,J.B., Wall,S.A., and Wilkie,A.O. (2006). The origin of EFNB1 mutations in craniofrontonasal syndrome: frequent somatic mosaicism and explanation of the paucity of carrier males. Am. J Hum. Genet. *78*, 999-1010.

Tyler,M.S. (1983). Development of the frontal bone and cranial meninges in the embryonic chick: an experimental study of tissue interactions. Anat. Rec. *206*, 61-70.

Tyler,M.S. and McCobb,D.P. (1980). The genesis of membrane bone in the embryonic chick maxilla: epithelial-mesenchymal tissue recombination studies. J Embryol. Exp. Morphol. *56*, 269-281.

Uht,R.M., Amos,S., Martin,P.M., Riggan,A.E., and Hussaini,I.M. (2006). The protein kinase C-eta isoform induces proliferation in glioblastoma cell lines through an ERK/Elk-1 pathway. Oncogene.

Valta,M.P., Hentunen,T., Qu,Q., Valve,E.M., Harjula,A., Seppanen,J.A., Vaananen,H.K., and Harkonen,P.L. (2006). Regulation of osteoblast differentiation: a novel function for fibroblast growth factor 8. Endocrinology *147*, 2171-2182.

Valverde-Franco,G., Liu,H., Davidson,D., Chai,S., Valderrama-Carvajal,H., Goltzman,D., Ornitz,D.M., and Henderson,J.E. (2004). Defective bone mineralization and osteopenia in young adult FGFR3-/- mice. Hum. Mol. Genet. *13*, 271-284.

Van den,B.L., Laurell,H., Huez,I., Zanibellato,C., Prats,H., and Bugler,B. (2000). FIF [fibroblast growth factor-2 (FGF-2)-interacting-factor], a nuclear putatively antiapoptotic factor, interacts specifically with FGF-2. Mol. Endocrinol. *14*, 1709-1724.

Vantaggiato,C., Formentini,I., Bondanza,A., Bonini,C., Naldini,L., and Brambilla,R. (2006). ERK1 and ERK2 mitogen-activated protein kinases affect Ras-dependent cell signaling differentially. J Biol. *5*, 14.

Viereck,V., Siggelkow,H., Tauber,S., Raddatz,D., Schutze,N., and Hufner,M. (2002). Differential regulation of Cbfa1/Runx2 and osteocalcin gene expression by vitamin-D3, dexamethasone, and local growth factors in primary human osteoblasts. J Cell Biochem. *86*, 348-356.

Villa,I., Dal Fiume,C., Maestroni,A., Rubinacci,A., Ravasi,F., and Guidobono,F. (2003). Human osteoblast-like cell proliferation induced by calcitonin-related peptides involves PKC activity. Am. J Physiol Endocrinol. Metab *284*, E627-E633.

Vogels,A. and Fryns,J.P. (2006). Pfeiffer syndrome. Orphanet. J Rare. Dis. *1*, 19.

Wan,D.C., Kwan,M.D., Lorenz,H.P., and Longaker,M.T. (2008). Current treatment of craniosynostosis and future therapeutic directions. Front Oral Biol. *12*, 209-230.

Wang,Q.P., Xie,H., Yuan,L.Q., Luo,X.H., Li,H., Wang,D., Meng,P., and Liao,E.Y. (2008). Effect of progesterone on apoptosis of murine MC3T3-E1 osteoblastic cells. Amino. Acids.

Webster,M.K. and Donoghue,D.J. (1997). FGFR activation in skeletal disorders: too much of a good thing. Trends Genet. *13*, 178-182.

Wieland,I., Jakubiczka,S., Muschke,P., Cohen,M., Thiele,H., Gerlach,K.L., Adams,R.H., and Wieacker,P. (2004). Mutations of the ephrin-B1 gene cause craniofrontonasal syndrome. Am. J Hum. Genet. *74*, 1209-1215.

Wilkie,A.O. (2005). Bad bones, absent smell, selfish testes: the pleiotropic consequences of human FGF receptor mutations. Cytokine Growth Factor Rev. *16*, 187-203.

Wilkie,A.O., Slaney,S.F., Oldridge,M., Poole,M.D., Ashworth,G.J., Hockley,A.D., Hayward,R.D., David,D.J., Pulleyn,L.J., Rutland,P., and . (1995). Apert syndrome results from localized mutations of FGFR2 and is allelic with Crouzon syndrome. Nat. Genet. *9*, 165-172.

Wu,D., Chen,B., Parihar,K., He,L., Fan,C., Zhang,J., Liu,L., Gillis,A., Bruce,A., Kapoor,A., and Tang,D. (2006). ERK activity facilitates activation of the S-phase DNA damage checkpoint by modulating ATR function. Oncogene *25*, 1153-1164.

Wu,Y., Chen,Z., and Ullrich,A. (2003). EGFR and FGFR signaling through FRS2 is subject to negative feedback control by ERK1/2. Biol. Chem. *384*, 1215-1226.

Xu,J., Lawshe,A., MacArthur,C.A., and Ornitz,D.M. (1999). Genomic structure, mapping, activity and expression of fibroblast growth factor 17. Mech. Dev. *83*, 165-178.

Yang,X., Ji,X., Shi,X., and Cao,X. (2000). Smad1 domains interacting with Hoxc-8 induce osteoblast differentiation. J Biol. Chem. *275*, 1065-1072.

Yang,X., Webster,J.B., Kovalenko,D., Nadeau,R.J., Zubanova,O., Chen,P.Y., and Friesel,R. (2006). Sprouty genes are expressed in osteoblasts and inhibit fibroblast growth factor-mediated osteoblast responses. Calcif. Tissue Int. *78*, 233-240.

Yoon,K., Buenaga,R., and Rodan,G.A. (1987). Tissue specificity and developmental expression of rat osteopontin. Biochem. Biophys. Res. Commun. *148*, 1129-1136.

Yu,K., Herr,A.B., Waksman,G., and Ornitz,D.M. (2000). Loss of fibroblast growth factor receptor 2 ligand-binding specificity in Apert syndrome. Proc. Natl. Acad. Sci. U. S. A *97*, 14536-14541.

Yu,K., Xu,J., Liu,Z., Sosic,D., Shao,J., Olson,E.N., Towler,D.A., and Ornitz,D.M. (2003). Conditional inactivation of FGF receptor 2 reveals an essential role for FGF signaling in the regulation of osteoblast function and bone growth. Development *130*, 3063-3074.

Yu,P.J., Ferrari,G., Galloway,A.C., Mignatti,P., and Pintucci,G. (2007). Basic fibroblast growth factor (FGF-2): the high molecular weight forms come of age. J Cell Biochem. *100*, 1100-1108.

Zhang,Y., Sawada,T., Jing,X., Yokote,H., Yan,X., and Sakaguchi,K. (2007). Regulation of ephexin1, a guanine nucleotide exchange factor of Rho family GTPases, by fibroblast growth factor receptor-mediated tyrosine phosphorylation. J Biol. Chem. *282*, 31103-31112.

Zhao,J., Cao,Y., Zhao,C., Postlethwait,J., and Meng,A. (2003). An SP1-like transcription factor Spr2 acts downstream of Fgf signaling to mediate mesoderm induction. EMBO J *22*, 6078-6088.

Zuniga,J.E., Groppe,J.C., Cui,Y., Hinck,C.S., Contreras-Shannon,V., Pakhomova,O.N., Yang,J., Tang,Y., Mendoza,V., Lopez-Casillas,F., Sun,L., and Hinck,A.P. (2005). Assembly of TbetaRI:TbetaRII:TGFbeta ternary complex in vitro with receptor extracellular domains is cooperative and isoform-dependent. J Mol. Biol. *354*, 1052-1068.